7-16-2015

Transition Metal-Olefin Bonding Interactions: A Density Functional Theory Study [M(CO) x (Æ? 2 - C 2 H 3 - C 6 H 4 - Y)]

Michael John Berninger
Illinois State University, michael_berninger@ilstu.edu

TRANSITION METAL-OLEFIN BONDING INTERACTIONS:

A DENSITY FUNCTIONAL THEORY STUDY

$[M(CO)_x(\eta^2\text{-}C_2H_3\text{-}C_6H_4\text{-}Y)]$

Michael J. Berninger

129 Pages

Metal-olefin equilibrium geometries, bond formation energies (ΔE), enthalpies (ΔH), and free energies (ΔG) for a select series of transition metal (M = Ni, Fe, Cr, Mo and W) -olefin carbonyl complexes $[M(CO)_x(\eta^2\text{-}C_2H_3\text{-}C_6H_4\text{-}Y)]$ have been calculated and compared using density functional theory (DFT), with the BP86 functional under standard state conditions (1 atm, 298.15 K) for the general gas phase formation reaction:

$$M(CO)_x + (C_2H_3\text{-}C_6H_4\text{-}Y) \rightarrow [M(CO)_x(\eta^2\text{-}C_2H_3\text{-}C_6H_4\text{-}Y)] \quad (1)$$

Computations were completed on η^2 bonded complexes. In regards to the electronic modification of the substituent (Y) on styrene at the para position, this study quantitatively investigated the effect of electron-withdrawing and electron-donating influence on transition metal-olefin coordination; namely using the substituent series Y = NO_2, CN, COOH, H, OH, NH_2, and $N(CH_3)_2$. For bond formation reaction (1), $[M(CO)_x(\eta^2\text{-}C_2H_3\text{-}C_6H_4\text{-}Y)]$: x = 5 for the group six triad transition metal (M = Cr, Mo, W) carbonyl complex series; x = 4 for the $[Fe(CO)_4(\eta^2\text{-}C_2H_3\text{-}C_6H_4\text{-}Y)]$ complex series; and x = 3 for the $[Ni(CO)_3(\eta^2\text{-}C_2H_3\text{-}C_6H_4\text{-}Y)]$ complex series.

All complex geometries were optimized to minimum energy conformations using the Spartan molecular modeling software package. Geometric results show evidence of sp^2 to sp^3 rehybridization of the olefin carbon atoms. Metal-olefin bond energies were further evaluated using a bond energy decomposition analysis (BEDA) scheme. The key attractive and repulsive interactions contributing to the bond formation energies were obtained. The trends were compared with those expected from the traditional Dewar-Chatt-Duncanson (DCD) frontier orbital bonding model. The DCD model was not always predictive of the bond energy strengths, since it does not consider thermodynamic costs from geometrical changes. An energy decomposition analysis of the bonding interactions demonstrate that, contrary to the DCD bonding model, as electron-withdrawing nature of the para substituent increase, strength of the metal-olefin interaction diminishes.

DFT has also been applied to describe electronic substituent effects, especially in the pursuit of linear relationships similar to those observed from the Hammett Correlations based on *Linear Free Energy Relationships* (LFERs). Plots of $\text{Log}(K_Y/K_H)$ vs. Hammett substituent constants (σ_p) indicate that metal-olefin bond formation occurs more favorably in complexes with more electron-donating capacity for the $[M(CO)_5L\text{-}Y]$ complex series, whereas formation for the $[Fe(CO)_4L\text{-}Y]$ and$[Ni(CO)_3L\text{-}Y]$ complex series were much less sensitive to substituent effects based on reactivity constants ρ.

KEYWORDS: Amsterdam Density Functional (ADF), Bond Energy Decomposition Analysis (BEDA), π-Complexes, Dewar–Chatt–Duncanson (DCD), Density Functional Theory (DFT), Hammett Linear Free Energy Relationships (LFERs), Metal-Olefin, Styrene.

TRANSITION METAL-OLEFIN BONDING INTERACTIONS:

A DENSITY FUNCTIONAL THEORY STUDY

$[M(CO)_x(\eta^2\text{-}C_2H_3\text{-}C_6H_4\text{-}Y)]$

MICHAEL J. BERNINGER

A Thesis Submitted in Partial
Fulfillment of the Requirements
for the Degree of

MASTER OF SCIENCE

Department of Chemistry

ILLINOIS STATE UNIVERSITY

2015

TRANSITION METAL-OLEFIN BONDING INTERACTIONS:

A DENSITY FUNCTIONAL THEORY STUDY

$[M(CO)_x(\eta^2\text{-}C_2H_3\text{-}C_6H_4\text{-}Y)]$

MICHAEL J. BERNINGER

COMMITTEE MEMBERS:

David L. Cedeño, Chair

Jean M. Standard

Jon A. Friesen

ACKNOWLEDGMENTS

I would like to first and foremost extend my deepest gratitude to my adviser, Dr. David Cedeño, whose expertise, knowledge, generous guidance, and inspirational support made it possible for me to acquire the computational intuition and experience necessary for the extensive investigation of the topics discussed herein this thesis. He has been a magnificent mentor over the years and I am forever grateful to have had the opportunity to study under his supervision.

In addition, I would like to thankfully acknowledge Dr. Jon Friesen for all his kind words of advice and encouragement over the course of my academic career. I most definitely enjoyed his charisma and stamina for teaching Biochemistry! Any time I had a question of quantum mechanical nature, I knew I could always call on Dr. Jean Standard for help. She is a phenomenal instructor as well, captivating, motivational and exciting!

I would also like to recognize with gratitude the support and love of my family and friends, as well as pay special homage to Dr. Johll, Dr. Nagorski, Dr. Kim, and Dr. Zona, for the motivational guidance and wisdom they have passed on to me throughout my academic experience. Lastly, I would like to thank my former chemistry professors for their devout commitment to education and enthusiasm for awakening the bliss within creative expression and understanding. If it were not for you all, I would not be the chemist I am today.

M. J. B.

CONTENTS

TABLES

FIGURES

CHAPTER I

ORGANOMETALLIC CHEMISTRY

Transition Metal-Olefin Catalysis

The transition metal-olefin bond has been a topic of special interest to chemist for over a century now due to its rising prevalence in application of organometallic catalysis. A number of important chemical processes such as olefin (alkene) hydrogenation, metathesis, polymerization, and oxidation among others are driven by the presence of a transition metal catalyst and involve the formation and or cleavage of a metal-olefin bond.[1-11] Thus, because the occurrence of olefin and olefin-related products in industry has become more prevalent, a more complete understanding of the factors that influence the strength of this bonding interaction must be developed in order to establish a more rational design of suitable catalysts for such processes.

Despite continuous advancements in our understanding of the transition metal-olefin interaction, there still exists a need to explore deeper into the chemical nature of coordination.[12-15] Characteristics often related to metal oxidation state, ligand influence, and substituent effects often leaves open room for inquisition. Contributing to a level of understanding that would allow for an accurate estimate of the metal-olefin bond strength is the primary goal of our research. One current bonding description used to qualitatively describe and rationalize the bond strength between a metal complex and an olefin is the *Dewar-Chatt-Duncanson* (DCD) model of metal-olefin coordinate bonding.

The Dewar-Chatt-Duncanson (DCD) Model

The nature of the transition metal-olefin coordinate bonding has been the subject of much discussion. It is quite generally accepted that the σ, π bonding description originally suggested by **D**ewar,[16] later complemented by **C**hatt and **D**uncanson[17] holds for most of the transition metal series. According to this bonding formulism, the metal-olefin interaction can be viewed as a two-way synergistic electron exchange in which the ***H**ighest **O**ccupied **M**olecular **O**rbital* (HOMO, π) of the olefin donates electron density through a σ interaction to the ***L**owest **U**noccupied **M**olecular **O**rbital* (LUMO, d_σ) of the metal complex. In addition, there is a π back bonding interaction in which the metal donates electron density back to the olefin from an occupied d_π orbital (HOMO, d_π symmetry orbitals: d_{xy}, d_{yz}, d_{xz}) to the antibonding π* LUMO of the olefin, Figure 1.

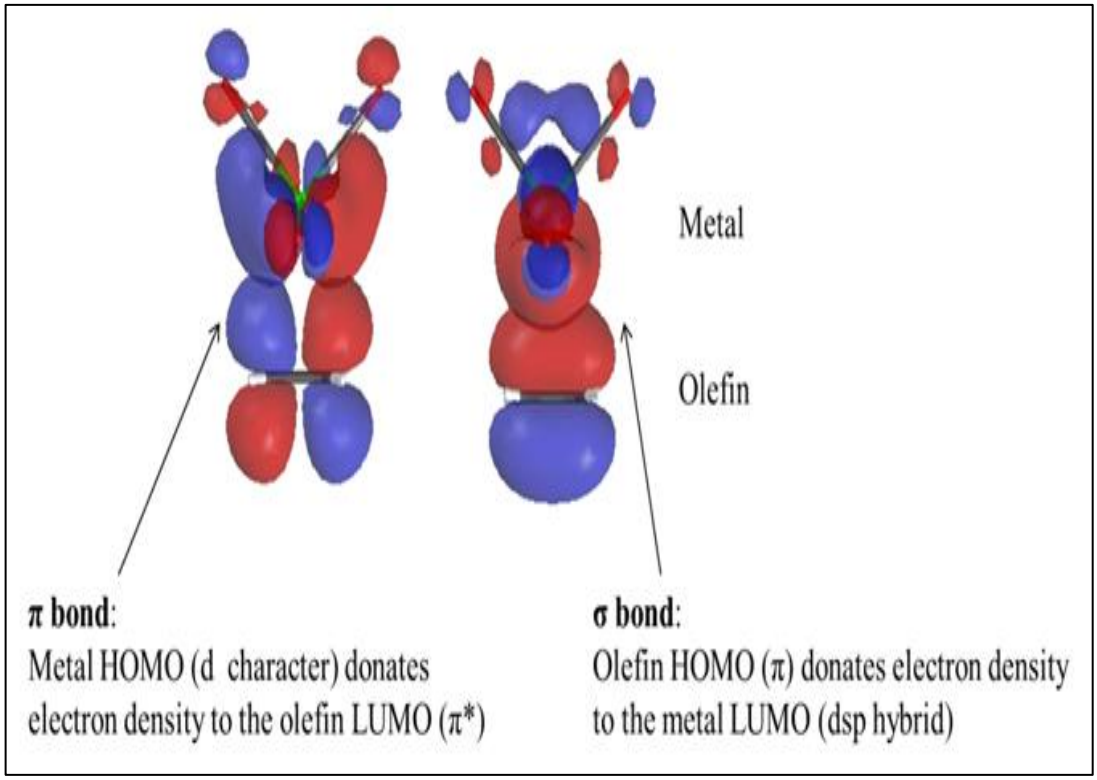

Figure 1. Schematic representation of the DCD metal-olefin bonding model.

Since 1953, the contributions and implications of the DCD model have been used to describe and rationalize the nature of transition metal-olefin bond strength, as well as molecular geometry.[13-14] Based on statements made in Dewar's original paper, widespread interpretation of the model suggests that for some metals the π-back bonding interaction take precedence over the σ interaction in the overall stabilization of the metal-olefin complex.[18] The DCD model also predicts an increase in the olefin C=C bond length in proportion to electron withdrawing ability of the olefin due to a shift in the hybridization of the olefin carbon atoms from sp^2 towards more sp^3 character upon complex formation. Based on this rationalization, the DCD model would anticipate that if the hydrogen atoms in ethylene were to be replaced with a more electron-withdrawing substituent such as a halogen (X = F, Cl), then the back bonding potential would increase because a halogenated ethylene is a better π acceptor than ethylene.[19, 20] Experimental[21] and computational[22-23] evidence, however, seems to indicate that such predictions are not always fulfilled.[24] According to Schlappi and Cedeño,[23] an in-depth analysis of the metal-olefin interaction using a bond energy decomposition scheme suggests that the interaction between a transition metal and a given olefin is not solely influenced by the ability to accept and donate electron density. Steric contribution due to the electronic repulsion between the olefin substituents and other ligands in the metal complex must also be considered, not to mention the reorganizational energy lost due to geometrical changes experienced by the olefin and the metal complex during the bonding interaction. Although experimental metal-olefin bond energies are difficult to obtain, there is clear evidence that indicates that trends in stability and bond strengths of metal-olefin complexes cannot always be rationalized in the context of the DCD model.

Experimental Bond Dissociation Enthalpies

Time-resolved infrared spectroscopy is a powerful tool for probing the reactivity of intermediates which may be formed during metal-olefin catalysis.[25] Metal complexes containing carbonyl ligands, in particular, have been shown to serve as appropriate models for investigating metal-olefin coordination as the photolytic loss of CO often occurs selectively in solution and with high quantum efficiency.[26] The production of metal-olefin complexation following photodissociation can then be monitored using FTIR spectroscopy since remaining CO ligands attached to the metal center are ideal infrared tags for probing the transient profile of the resulting intermediates.[25-27]

One method for experimentally measuring metal-olefin bond dissociation enthalpy consists of tracking the rate of chemical decomposition using FTIR spectroscopy over a range of time scales. Typically, a competitive reaction scheme will be set up between the olefin and a ligand that is expected to coordinate more strongly. Considering the Arrhenius relationship between rate constant and temperature, pertinent kinetic detail for the dissociation reaction can then be extrapolated from the temperature dependence of the competitive ligand substitution. Assuming that the decomposition occurs via a dissociative mechanism, the difference in activation energies between a series of similar metal-olefin complexes reflects their difference in bond energies. This value should not be very different from the bond enthalpy measured using laser photoacoustic calorimetry or the bond energy difference calculated using ***D****ensity* ***F****unctional* ***T****heory* (DFT).[28] The DFT algorithms complement experimental methodology by providing an in depth analysis of the thermodynamic factors which contribute to metal-olefin bond strength.

Computational Chemistry

In recent years, the use of computational chemistry has become common practice in all fields of chemical research.[29] The availability of both sophisticated methods and capable hardware has definitively contributed to the increased popularity of computational chemistry. Among the different methodologies available, DFT has gained popularity because of its reliable estimate of molecular geometries, energies, and frequencies at a relatively low computational price.[30] Quantum mechanics is the mathematical description for rationalizing the behavior of matter and its interactions with energy at the subatomic level. In its original formulation, DFT was designed as a means to compute the quantum state properties of atoms, molecules and solids using quantum mechanical functionals. According to the Hohnberg-Kohn theorem, it is asserted that the electron density of any system determines all the ground-state properties of that system; that is, the energy of that system can be described in terms of the electron density, i.e. $E = E[\rho]$, where ρ is the ground-state density of the system.[31]

DFT is regarded as a powerful tool for providing quantitative insights into metal-olefin interactions that are difficult to study using experiments, as it allows for the fairly accurate calculation of bond energies.[1] As such, these calculations can be used to explain trends in bond dissociation enthalpy, to test available models for bonding, and to attempt to formulate more quantitative models of bonding.[24] A ***B****ond* ***E****nergy* ***D****ecomposition* ***A****nalysis (*BEDA) scheme included in the ***A****msterdam* ***D****ensity* ***F****unctional* (ADF) chemistry software was used to quantify electronic, steric, and reorganizational interactions.[32] Bond energy decomposition analyses have shown to be extremely valuable in our understanding of metal-olefin bonding interactions.[33-34]

Employed in this study was the BEDA scheme of Ziegler and Rauk, as implemented by Baerends et al. in ADF.[34-37] In this computational algorithm, the bond formation energy (ΔE) is broken down into the summation of two key components, the interaction energy (ΔE_{int}) and reorganization energy (ΔE_{reorg}). The interaction energy (ΔE_{int}) can then be further delineated as the sum of attractive ($\Delta E_{oi} + \Delta E_{elst}$) and repulsive ($\Delta E_{pauli}$) terms. The orbital interaction energy (ΔE_{oi}) value forms the basis for the DCD model predictions. ΔE_{elst} represents the Coulombic energy contribution resulting from electrostatic attractive interactions, thus reflecting the ionic nature of the bond. ΔE_{pauli} is the repulsive energy due to interaction between occupied orbitals and consequently reflects the extent of steric repulsion. The reorganization energy (ΔE_{reorg}) term represents the energy loss involved in deforming the geometries of the reactants in their ground states to the geometries they adopt in the final bound complex state. The ΔE_{reorg} costs are not considered by the DCD bonding model.

One major drawback to DFT is that a given molecular system may yield significantly different bond energies if different DFT functionals are used. The traditional approach to overcome this is to carry out benchmarking calculations using a few of the most commonly used DFT functional (such as B3LYP, and PBE) and compare the results to experimental values. Previous literature has already established that the BP86 functional is appropriate for olefin complexes of the transition (M = Ni, Fe, Cr, Mo, W) metal carbonyls.[1, 22-23] To our knowledge there are no structural experimental data for the complex series $[M(CO)_x(\eta^2\text{-}C_2H_3\text{-}C_6H_4\text{-}Y)]$, but previous work employing the BP86 functional on metal-olefin complexes have shown good structural agreement between DFT calculations and experimental data.[1, 22, 38]

In this thesis, metal-olefin equilibrium geometries, bond formation energies (ΔE), enthalpies (ΔH), and free energies (ΔG) for a select series of transition (M = Ni, Fe, Cr, Mo and W) metal carbonyl complexes $[M(CO)_x(\eta^2\text{-}C_2H_3\text{-}C_6H_4\text{-}Y)]$ have been determined in the gas phase using DFT, with the BP86 functional under standard state conditions (1 atm, 298.15 K) for the general bond formation reaction:

$$M(CO)_x + (C_2H_3\text{-}C_6H_4\text{-}Y) \rightarrow [M(CO)_x(\eta^2\text{-}C_2H_3\text{-}C_6H_4\text{-}Y)] \qquad (1)$$

In regards to the electronic modification of the substituent (Y) on styrene at the *para* position, this study aims to quantitatively investigate the effect of electron withdrawing and electron donating influence on metal-styrene coordination; namely using the substituent series Y = NO_2, CN, COOH, H, OH, NH_2, and $N(CH_3)_2$. For bond formation reaction (1), $[M(CO)_x(\eta^2\text{-}C_2H_3\text{-}C_6H_4\text{-}Y)]$: x = 5 for the group six triad transition (M = Cr, Mo, W) metal carbonyl complex series; x = 4 for the $[Fe(CO)_4(\eta^2\text{-}C_2H_3\text{-}C_6H_4\text{-}Y)]$ complex series; and x = 3 for the $[Ni(CO)_3(\eta^2\text{-}C_2H_3\text{-}C_6H_4\text{-}Y)]$ complex series. Computations were completed on η^2 bonded complexes, where η represents the number of atoms in the ligand bonded to the metal. All complexes were geometrically optimized to minimum energy conformations using crystal structures from the Cambridge Structural Database (CSD) as the starting points, if available.[39] Metal-olefin bond energies were further evaluated with ADF using a bond energy decomposition analysis (BEDA) scheme. The DCD model was not always predictive of the bond energy strengths, since it does not thermodynamically consider costs from geometrical changes. An energy decomposition analysis of the bonding interactions demonstrate that, contrary to the DCD bonding model, as electron-withdrawing nature of the para substituent increase, strength of the metal-olefin interaction *diminishes*.

CHAPTER II

LITERATURE SURVEY

Transition Metal-Olefin Coordination Chemistry

Organometallic Chemistry is the study of compounds containing transition metal-carbon bonds. Olefin ligands are typically found bound to transition metal centers. The oldest organometallic compound isolated in pure form, Zeise's salt ($K[PtCl_3(\eta^2\text{-}C_2H_4)]$), is a platinum-olefin complex.[40] The report in 1825 by William Zeise on the synthesis and purification of Potassium trichloro(η^2-ethene)platinate(II) was a topic of controversy for nearly a century due to the unresolved nature of chemical bonding in Zeise's salt structure.[41] The first proposed model for metal-olefin bonding was published in 1951 by Michael Dewar which described it as a normal dative bond via overlap between the filled π-orbitals of ethylene and the empty orbitals of silver(I) or copper(I) complexes.[12, 16] In Dewar's original description it was suggested that, in addition to σ-donation of olefin π-bonding electrons to the metal, d_π electrons on the metal would also interact with antibonding orbitals of π-symmetry on the olefin. No structural evidence was provided, however, to support this proposal at the time; nor was mention made of Zeise's salt. The bonding depiction for Zeise's salt was further expanded upon by Joseph Chatt and L.A. Duncanson in 1953 and what became as the first published bonding diagram of this classical bonding description; referred to as the DCD model.[42] Recent reviews of the DCD model and its impact are widely available in the literature.[12-17]

The DCD Bonding Description in Review

Since 1953, the Dewar-Chatt-Duncanson model has been utilized to rationalize and explain the nature of chemical bonding between an olefin ligand and a metal forming a π complex, as well as molecular geometry.[1] In 1953, an X-ray crystallographic analysis of Zeise's salt was collected and the structure of Zeise's salt was published.[43-44] Evidence for σ donation and the π-backbonding interaction was supported by the facts that the hydrogens on the ethylene are bent away from the normal C=C-H plane by a dihedral angle of 32.5°,[45] and that the C=C bond length of coordinated ethylene (1.375 Å)[46] is longer than that of free ethylene (1.337 Å).[47] By 1975, a neutron diffraction study of Zeise's salt structure had surfaced,[47] further confirming earlier suggestions by the DCD description of η^2 bonding character. Since its original discovery, Zeise's salt has become one of the most cited to examples of the Dewar-Chatt-Duncanson (DCD) model for describing and rationalizing metal-olefin complexation.[47]

According to the DCD description, η^2 –alkenes are considered to be two electron neutral ligands which normally bond side-on to a metal atom with both carbon atoms of the double bond equidistant from the metal with the other groups on the alkene approximately perpendicular to the plane of the metal atom and the two carbon atoms. In this arrangement, the electron density of the C=C bond can be donated to an empty orbital on the metal atom to form a σ bond. In parallel with this interaction, a filled metal d orbital can donate electron density back to the empty π* antibonding orbital on the alkene to form a π bond. Electron donor and acceptor character appear to be evenly balanced in most ethene complexes of the d metals,[48] but the degree of donation and backdonation can be altered by substituents on the metal atom and on the alkene.

Although this description is correct, it does not provide a complete quantitative understanding of metal-olefin bond strengths. Qualitative interpretations of the model suggest that π-bonding dominates the interaction between electron-rich metals and olefins implying, for example, that halogenated olefins would bind to metals stronger than ethylene because they are better π acceptors of electron density.[1, 48-49] Experimental data on the homologous series $Cr(CO)_5(C_2X_4)$ (X= H, F, Cl) indicates, however, that the perhalogenated ethylenes bind weaker than ethylene.[24] Further evidence is demonstrated in the study performed by Tolman in 1974, where it was found that fluorinated olefins coordinating to a nickel(0) bis(tri-o-tolyl phosphate) complex are thermodynamically less stable than the ethylene complex.[50] A few years later, a study by Ittel also found that the fluorinated ethylene complexes $Ni(PPh_3)_2(\eta^2\text{-}C_2F_4)$ and $Ni(PPh_3)_2(\textit{trans}\text{-}C_2H_2F_2)$ are less stable than the corresponding ethylene complex.[51]

While experimental techniques were developing in the field of organometallics, so were computational approaches. Ziegler published several papers including a 1994 review article discussing DFT "as a practical tool in studies of organometallic energetics and kinetics.[52]" In 2001, Cedeño and Weitz applied DFT computational methods to quantify metal-olefin bonding interactions for the complex series $[Cr(CO)_5(\eta^2\text{-}C_2X_4)]$ and $[Fe(CO)_4(\eta^2\text{-}C_2X_4)]$ (X = H, F, Cl), which provide a rational for the inadequacy of the DCD description.[22, 24] Further studies by Schlappi and Cedeño also found that the bonding of the perhalogenated olefins to $Ni(PH_3)_2(CO)$ follow a trend very similar to the one shown in Tolman's study and confirmed his presumption that the reason for the inadequacy of the DCD picture of metal-olefin bonding was due to the reorganization that occurs in the olefin due to rehybridization from sp^2 to sp^3 upon complex formation.[23]

More recently, our laboratory found that the bond energies between carbonyl transition metals complexes in the group 6 triad ($Cr(CO)_5$, $Mo(CO)_5$, $W(CO)_5$) and chlorinated ethylenes (C_2Cl_4, C_2HCl_3, and *iso*-$C_2H_2Cl_2$) follow a trend that is opposite to the electron withdrawing ability of the olefin based on predictions made by the traditional DCD metal-olefin bonding model.[1] The results demonstrated that as the number of electron-withdrawing substituents on the olefin increased, the overall bond energies decreased. DFT calculations and a BEDA scheme were employed to understand the paradoxic behavior of the halogenated olefins. From the studies, it is evident that the interaction between a transition metal and an olefin is not exclusively influenced by the ability to accept and donate electron density. Steric contribution due to the electronic repulsion between the olefin substituents and other ligands in the metal complex must also be considered, not to mention the reorganizational energy lost due to geometrical changes experienced by the olefin and metal complex during bonding formation.[53]

The DCD model also qualitatively predicts an increase in the olefin C=C bond length in proportion to the electron withdrawing ability of the olefin.[1] Electron population changes in the π and π^* orbitals of the olefin often result in a decrease in olefinic bond order. This is equivalent to the partial sp^2 to sp^3 rehybridization of the olefinic carbons that causes the lengthening of the C=C bond distance and a lowering of its vibration frequency, in addition to the back-bending of the substituents around the C=C bond away from the metal complex and outside of the plane of the C=C bond.[53] One of the implications of the DCD model is that the metal-olefin bond strength is determined by the extent of π-backbonding and that back-donation increases with the metal principal quantum number of the outermost electrons.

The importance of the π component for stability of the complexes may be indicated by the very few known complexes of the metals with fewer d-electrons, i.e., group IIIB-VB metals. The energy levels of the metal orbitals will depend upon its oxidation state, which will often define the d-electron density, and upon the number and nature of other ligands, while the energy levels of the olefin will be affected by the substituent groups at the double bond. The strength of a given metal-olefin bond is dependent on the number of d-electrons available in the metal for back bonding donation and the availability of empty orbitals to accept electrons from the olefin. It is also well known that the bond strength is different for metals that belong to the same group even though they have same count of d-electrons and empty orbitals.[54]

In this thesis, we quantify the relative effect of the influence of the group 6 triad transition metal (M= Cr, Mo, W) down a group for the olefin complex series, $[M(CO)_5(\eta^2\text{-}C_2H_3\text{-}C_6H_4\text{-}Y)]$. We also measure and compare metal-olefin bond energies for the $[Fe(CO)_4(\eta^2\text{-}C_2H_3\text{-}C_6H_4\text{-}Y)]$ and $[Ni(CO)_3(\eta^2\text{-}C_2H_3\text{-}C_6H_4\text{-}Y)]$ complex series. Nickel(0) is a d^8 electron metal, which can be compared with the d^5 group 6 triad. The iron complexes are d^6 and will provide a direct comparison to the nickel styrene complexes. Ultimately, the research in this thesis aims to further our understanding of transition metal-olefin bonding by computationally investigating how the modification of electron withdrawing and electron donating functionality at the para position of styrene contributes to the overall metal-olefin bond strength. In this series steric and reorganizational energy effects should in principle be similar because the effector group is well far from the bonding site. Our findings suggest that the DCD model may not adequately account for all of the variables involved in metal-olefin bonding.

CHAPTER III

COMPUTATIONAL METHODOLOGY

Density Functional Theory (DFT)

Application of the ***D****ensity* ***F****unctional* ***T****heory* (DFT) model allows for the accurate computation of an optimized equilibrium or lowest energy geometry for each molecule in the net complex bond formation reaction (reaction (1)). According to the literature, DFT has shown to be a powerful tool for estimating bond energies.[55-57] In this study, transition meta-olefin equilibrium geometries (bond lengths and angles), bond formation energies (ΔE), enthalpies (ΔH), and free energies (ΔG) were calculated using Local Density Approximation (LDA), under the BP86 functional from DFT optimized molecular geometries of both the complexes and starting molecular fragments using the computational chemistry software package Spartan (2014,Wavefunction Inc.).[58]

Traditionally, the BP86 functional has provided optimized transition-metal complex structures which have shown good agreement with experimental results and is the common method of choice.[1,22-24, 28, 30] The DFT methodology employed is based upon Slater's[59] and Vosko, Wilk, and Nusair (VWN)'s[60] models for electron exchange Xα potential and electron correlation, respectively. BP86 is a gradient-corrected functional which employs Becke's 1988[61] function for electron exchange, and Perdew's 1986[62] and VWN's functionals[60] for non-local electron correlation. The basis set used to define the orbitals in this study was LACV3P**.

Calculations involving transition metals can be simplified by considering only the valence electrons, while replacing the core by some form of pseudopotential using a relativistic zero order regular approximation (ZORA) STO-TZP available in the ADF program. LACV3P** is a triple ζ basis set which employs Hay and Wadt's effective core potential (ECP)[63] to fix core transition-metal electron orbitals and Gaussian basis functions to define the outermost core and valence electron interactions of other atoms. In particular, LACV3P** uses the 6-31G Gaussian basis set to describe metal atoms, and the 6-311$_{++}$G** basis set for other nonmetal atoms (H, C, N, O, and F).[64]

From the optimized geometries, measureable quantitative changes in transition-metal-olefin bond angles and bond lengths between their free states and their bound coordinated states could be obtained. In addition, graphical comparisons resulting from differences in central transition metal (M = Ni, Fe, Cr, Mo, and W) and electronic effects due to substituent modification (Y = NO_2, CN, COOH, H, OH, NH_2, $N(CH_3)_2$) on styrene and para substituted styrene analog (η^2-C_2H_3-C_6H_4-Y) coordination were generated. Geometrical measurements of the complexes were examined to correlate reorganization energy expenditures to the geometrical changes of the molecules. Specifically, the bond length and angle parameters measured in this study included: 1) Olefin C=C bond length; 2) changes in C=C bond length (Δ C=C) relative to the unbound (free) state; 3) changes in the Δ (OC-M-CO) bond angle for the group six transition metal triad (M = Cr, Mo, and W); 4) *Trans* carbonyl M-C≡O_{Trans} bond length; and 5) Transition metal to olefin C=C bond distance, M-C_{Olefin}. Deviations from planarity Θ, which is defined as the difference between 180 and the R-C=C-H (R = C_6H_4-Y) dihedral angle in the bound olefin, were acquired as well; Θ is defined as zero for the free olefin.

Geometrical measurements of the complexes were examined also to correlate reorganization energy expenditures to the conformational changes parameters of the molecules. DFT geometry optimizations were executed for the unbound or free reactants and after complex formation. Geometric optimization tolerance was set at $1x10^{-6}$ a.u. Resulting changes Δ (between the unbound and bound states) in the bond lengths and angles were acquired, as well as the loss of planarity values or ΔdhΘ (change in the dihedral angles relative to free ethylene). In particular, all dihedral dhΘ measurements were obtained for the X-C=C-H torsional angle. In addition, angle measurements on the pentacarbonyl metal fragment M-$(CO)_5$ were acquired before and after bonding to the olefin ligand. The ΔΘ measurements were also obtained for these angles. These ΔΘ values quantitatively demonstrate how the metal fragment angularly deforms from its free of the olefin state to its final bound state (to metal). There is convincing evidence that metal-olefins bond strengths are influenced at great extent by the deformation of the olefin. This energetic cost must be overcome as the metal binds to the olefin and is accountable for the discrepancy between the DCD picture and experimental results.[1]

Gas phase metal-olefin bond formation energies ΔE were obtained for the following transition metal (M = Cr, Mo, W) –olefin bond formation reactions from the calculated energies of the optimized ground-state geometries:

$$M(CO)_5 + (C_2H_3\text{-}C_6H_4\text{-}Y) \rightarrow [M(CO)_5(\eta^2\text{-}C_2H_3\text{-}C_6H_4\text{-}Y)] \quad (2)$$

$$^3Fe(CO)_4 + (C_2H_3\text{-}C_6H_4\text{-}Y) \rightarrow [Fe(CO)_4(\eta^2\text{-}C_2H_3\text{-}C_6H_4\text{-}Y)] \quad (3)$$

$$Ni(CO)_3 + (C_2H_3\text{-}C_6H_4\text{-}Y) \rightarrow [Ni(CO)_3(\eta^2\text{-}C_2H_3\text{-}C_6H_4\text{-}Y)] \quad (4)$$

namely using the substituent series, Y = NO_2, CN, CF_3, COOH, COH, $OCOCH_3$, H, CH_3, $C(CH_3)_3$, OH, OCH_3, $OC(CH_3)_3$, NH_2, and $N(CH_3)_2$. ΔE was calculated using Eq. (5):

$$\Delta E = E[M(CO)_x(\eta^2\text{-}C_2H_3\text{-}C_6H_4\text{-}Y)] - E[(C_2H_3\text{-}C_6H_4\text{-}Y)] - E[M(CO)_x] \quad (5)$$

For the $[Fe(CO)_4(\eta^2\text{-}C_2H_3\text{-}C_6H_4\text{-}Y)]$ complex series, bond energies were calculated relative to the triplet state of $Fe(CO)_4$ because this is the experimentally determined ground state.[51] ΔE is a measure of the reaction energy for transition metal-olefin bond formation relative to the minimum in the potential energy surface. By thermodynamic convention, in terms of Eqs. (1) and (5), factors that lead to an increase in bonding are negative and those unfavorable for bonding are positive. Equation (5) represents the metal-olefin gas phase bond formation energy ΔE, where E is the total internal energy of the molecule, and is calculated as the summation of the electronic energy ($E_{electronic}$), the zero point vibrational energy (ZPE), and the thermal contributions of motion (E_{th}). The zero point energy (ZPE) is the quantum mechanical vibrational ground state energy. The thermal energy ($E_{thermal}$) results from the contributions of vibrations, rotations, and translations obtained at 298 K and 1 atm. The metal-olefin bond enthalpy of reaction ΔH (298 K) was calculated[65] via the following relationship:

$$\Delta H_{298} = \Delta E + \Delta ZPE + \Delta E_{th} + \Delta(PV) \quad (6)$$

where ΔZPE is the zero point energy difference obtained from the vibrational frequency calculations, ΔE_{th} is the change in thermal energy for rotations, vibrations, and translations in going from 0 to 298 K, and $\Delta(PV)$ is the molar work, equal to ΔnRT. Inclusive in the study were also bond energy decomposition analyses (BEDA) using the Amsterdam Density Functional (SCM),[32-34]which employs an extended transition-metal state method for calculatons.[66- 67] The BEDA differentiates the relative contributions from the interaction (ΔE_{int}) energy including electronic, steric, electrostatic, and reorganizational (ΔE_{reorg}) effects to the computed bond formation energies (ΔE).

Bond Energy Decomposition Analysis (BEDA)

The second computational investigation employed in this study included a bond energy decomposition analysis (BEDA) using the Amsterdam Density Functional (ADF) computational quantum chemistry program. Bond energy decomposition analyses have shown to provide reliable quantitative values of the effect of halogen substitution and ring strain and aliphatic length chain in various studies previously published by Cedeño et al.[1,22- 24, 28] For instance, it has been established that in the case of the chloroethylene complexes of $M(CO)_5$, (M = Cr, Mo, W) there is an almost linear relationship between the bond energy, the reorganizational energy and the number of chlorine atoms around the double bond. Intriguingly, the summation of ΔE_{oi}, ΔE_{elect} and ΔE_{pauli}, which represents the net interaction energy (ΔE_{int}) between the olefin and metal complex fragment without including reorganization, does not show a lot of variation with the number of chlorine atoms. Similarities are also found in the case of the calculations carried out for halogenated olefins (F, Cl) bonded to $Ni(CO)(PH_3)_2$, although differences due to the nickel and its environment are also evident. For example, ΔE_{int} increases linearly with the number of fluorine or chlorine atoms in the olefin, but such an increase is offset by the reorganizational energy in such a way that the bond energies are almost independent of the number of halogen atoms, which is similar to the stability trend observed by Tolman in his study with fluroolefin complexes of $Ni[P(O\text{-}o\text{-}tolyl)_3]_2$. In the case of the cycloolefin complexes of the $M(CO)_5$ complexes Cedeño et al. also establish almost linear correlations between ΔE_{int} and olefin ring strain, and linear relationships between the reorganizational energies and changes in geometrical parameters such as C=C bond elongation and pyramidalization angle.[28]

All energy decomposition analyses were performed using the same BP86 functional used for energy minimization, and the equilibrium geometries obtained with Spartan. The distribution of the key contributors to the metal to olefin bonding interactions was obtained computationally for each transition metal (M = Ni, Fe, Cr, Mo, W) and styrene combination (C_2H_3-C_6H_4-Y). This study investigated the probable effects of electron withdrawing and electron donating functionality on metal to styrene bond strength. The key variables (within the complexes) that affect the bonding energy ΔE, such as orbital interactions (ΔE_{oi}), electrostatic attractive (ΔE_{elect}), Pauli repulsive (ΔE_{pauli}), and reorganizational costs (ΔE_{reorg}) were determined. Bond energy decomposition analyses were made using ADF, which incorporates the decomposition scheme of Ziegler and Rauk as implemented by Baerends and co-workers.[34-37] In this analysis, the bond energy (ΔE) is initially broken into contributions from two terms:

$$\Delta E = \Delta E_{int} + \Delta E_{reorg} \quad (7)$$

The first term in Eq. (7) is the interaction energy (ΔE_{int}) due to the electronic bonding interactions between the styrene and the metal carbonyl $M(CO)_x$ fragments. Because interactions that lead to an increase in the metal-styrene bond strength are taken to be positive, the opposite of ΔE_{int} represents the energy required to break the bond, yielding the free olefin and metal carbonyl $M(CO)_x$ in a state in which their geometries are those that they have in the bound complex. This quantity is sometimes referred to as the "bond-snap" energy.[1] The interaction energy ΔE_{int} can be further broken down into energy components for both the attractive ($\Delta E_{oi} + \Delta E_{elect}$) and the repulsive ($\Delta E_{pauli}$) electronic interactions of the molecular orbitals involved in the metal-styrene bond:

$$\Delta E_{int} = \Delta E_{oi} + \Delta E_{elect} + \Delta E_{pauli} \quad (8)$$

The calculated values of ΔE_{oi}, ΔE_{elect}, and ΔE_{pauli} were directly acquired from a BEDA calculation. ΔE_{oi} serves as a measure of the attractive energy due to the interactions between occupied orbitals of one fragment and empty orbitals of the other fragment as well as between the occupied and empty orbitals within a given fragment (polarization). In Eq. (7), ΔE_{reorg} represents the reorganizational energy, which is the energy required to deform the fragments from the geometries they have as isolated ground-state entities to the geometries they possess in the final complex state; by convention, this is a positive number. The reorganization energy may then be determined by subtracting the interaction energy from the bond energy (ΔE) in accord with Eq. (9):

$$\Delta E_{reorg} = \Delta E - \Delta E_{int} = \Delta E - (\Delta E_{oi} + \Delta E_{elect} + \Delta E_{pauli}) \qquad (9)$$

Herein this thesis DFT calculated metal-olefin bond energies are compared for a select series of para substituted styrene complexes, $[M(CO)_x(C_2H_3\text{-}C_6H_4\text{-}Y)]$ (M = Ni, Fe, Cr, Mo and W). A BEDA is carried out that breaks down the bond formation energy of a metal and olefin into its component contributions to compare overall changes in relation to one another in terms of their contribution to total bond energy. Additionally, for each system, a Mulliken population analysis[68] was performed to evaluate the electron population changes occurring when the ligand and metal fragment interact. When one complex is compared to another, some of the calculated energy differences may be within the error limits of experimental methods and the level of theory used. However, we focus on *trends* in bond energies and the contributions of various factors to these bond energies. The lack of an extended database of experimental and its related computational data has precluded the extension of some of the correlations presented here into a more generalized form that may allow us to make predictions of bond strengths.

Hammett Correlations on Linear Free Energy Relationships (LFERs)

The correlation between reaction equilibria and rates with changes in molecular structure is a major goal of interest in the field of physical organic chemistry. In chemical kinetics, the change in an equilibrium constant, *K*, or a rate constant, *k*, which results from the substitution of a specific group for hydrogen, the so-called *substituent effect*, is of particular interest.[69] Louis P. Hammett standardized much of the research in this area as of 1937 with a publication entitled "The Effect of Structure upon the Reactions of Organic Compounds. Benzene Derivatives," which defined a quantitative measurement σ (*the substituent constant*) to summarize the effects of meta- or para-substituents on the rate constants or equilibrium constants of side-chain reactions of benzene derivatives[70]:

$$\log(K_Y/K_H) = \Delta\, pK_a = \sigma \qquad (10)$$

where K_H was the acid dissociation constant for the ionization of benzoic acid and K_Y is the acid dissociation constant for the ionization of a substituted benzoic acid with a given substituent Y at a given position on the aromatic ring.[71] The key principle in Hammett's correlations is that a structural modification will produce a proportional change in free energy differences $\Delta G^{\ddagger}$ based on the overall behavior of σ. Since $\log K_H$ is directly related to the standard free energy change accompanying the ionization of benzoic acid ($\Delta G_H = -RT \ln K_H = -2.303RT \log K_H$), and $\log K_Y$ is directly related to the standard free energy change accompanying the ionization of substituted benzoic acid ($\Delta G_Y = -2.303RT \log K_Y$), the substituent constant is then actually related to the difference in the free energy changes for the two ionization processes $\Delta G^{\ddagger}$[72] and serves as a measure of the substituent effect expressed in terms of a free energy quantity:

$$\Delta G^{\ddagger} = \Delta G_Y - \Delta G_H = -2.303\ RT\ \rho\ \sigma \rightarrow \Delta G_Y = \Delta G_H - 2.303\ RT\ \rho\ \sigma \qquad (11)$$

Hammett's postulate was that the electronic effects (both the inductive and resonance effects) of a set of substituents should be similar for different organic reactions. Therefore, if values could be assigned to substituents in a standard organic reaction, these same values could be used to estimate rates in a new organic reaction.[73-74] In essence, Hammett was able to demonstrate a direct relationship between acid dissociation constants for a related series of ionization processes using para and meta substituted benzoic acids (R = C_6H_4-Y): RCOOH + OH^- ⇌ $RCOO^-$ + H_2O. This was the very first approach that allowed for the prediction of related reaction rates using *linear free energy relationships* (LFERs). Intuitively, it seems reasonable that as the *electron-withdrawing* (EWD) capacity of Y increases (relative to benzoic acid), the reaction constant (K_a) should increase commensurately (the reaction should be favored to the right) because Y is inductively pulling electron density from the carboxylic acid group, making it more acidic (a reactant argument); it is also stabilizing the negative charge on the carboxylate group in the transition state (a product argument). A similar relationship should exist for a rate constant (k) where charge develop in the transition state (consider ground-state and transition-state stabilizations). If the same series of changes in conditions affects a second reaction in exactly the same way as it affected the first reaction, then there exists a linear free energy relationship between the two sets of effects; LFERs have been observed for a wide variety of organic reactions. The relationship between the two reactions can then be expressed by Eq. (13):

$$\log K_Y = \rho \log k_Y + C \qquad (13)$$

where the two variables are, k_Y and K_Y. The slope of the line is ρ, and the intercept is C. When there is no measurable substituent effect, i.e., Y = H, then Eq. (14) applies:

$$\log K_H = \rho \log k_H + C \quad (14)$$

Subtraction of Eq. (14) from Eq. (13) gives Eq. (15), where k and K_0 are the rate and equilibrium constants, respectively, for compounds with a para modified substituent Y:

$$\log(K_Y/K_H) = \rho \log(k_Y/k_H) \quad (15)$$

and k_H and K_H are the rate and equilibrium constants, respectively, for the formation of the parent compound, (Y = H). If $\log(k_Y/k_H)$ is defined as σ, then Eq. (15) reduces to Eq. (16), the *Hammett Equation*:

$$\text{Log}\,(K_Y/K_H) = \rho\,\sigma \quad (16)$$

The *electronic parameter* σ depends on the electronic properties and position of the substituent on the ring and therefore, is also called the *substituent constant*; σ is defined specifically for benzoic acid dissociation in water at 25 ^{o}C. Also, since the magnitude of the substituent effect depends upon the position of the substituent upon the aromatic ring, there are different substituent constants for *para*, *meta*, and *ortho* substituents. Typically, these are distinguished as σ_p, σ_m, and σ_o. The more electron withdrawing a substituent, the more positive is its σ value (relative to H, which is set at 0.0); conversely, the more electron donating, the more negative is its σ value. The σ_m constants result from inductive effects, but the σ_p constants correspond to the net inductive and resonance effects. Therefore, σ_m and σ_p for the same substituent may generally vary. The ρ values (the slope) depend on the particular type of reaction and the reaction conditions (e.g., temperature and solvent) and, therefore, are called *reaction constants*. The significance of ρ is that it serves as a measure of the sensitivity of a reaction to the electronic influence of substituent effects. If ρ > 1, this indicates a reaction that is sensitive to substituent effects relative to that of standard benzoic acid ionization, ρ = 1.

Linear Free Energy Relationships (LFERs) are attempts to develop quantitative relationships between the effects that electron- donating or withdrawing groups have on the transition state or intermediate during the course of a chemical reaction.[74] If the ratio (K_Y/K_0) >1, the substituent has increased the acidity of the benzoic acid, and the behavior of σ is described as positive. Such a substituent is considered to be an *electron-withdrawing group* (EWG), because electron density is increased at the reaction site in the product benzoate anion, and an EWG will favor this change by withdrawing electron density away from the reaction site. On the other end of the spectrum, *electron-donating groups* (EDG) (which tend to increase the electron density near the reaction site electron donating groups) disfavor the ionization to a negatively charged ion and have (K_Y/K_0) < 1.[75] The linear trend obtained from the plot indicates that the nature of the reaction mechanism and that the coordination of the transition states do not change upon the variation of the substituent. The sign and absolute magnitude of the ρ value determined from a Hammett plot provide information about charge development at the transition state. The sign of ρ tells whether a positive or negative charge is being developed in the activated complex relative to the reactants. A positive ρ value means that electron density is increased (negative charge is being produced) in the activated complex; ρ = 1 for standard benzoate ionization at 25^{o}C. A negative ρ value means that electron deficiency is being produced (often a positive charge) in the activated complex. Generally ρ values have absolute magnitudes between 0 and 3, but values as high as 10 or 12 are known.[76] The use of Hammett correlations on LFER complement our DFT studies by providing an in depth quantitative analysis of how substituent modification at the para position Y on styrene and styrene analogs affects the overall rate for metal-olefin bond formation.

CHAPTER IV

RESULTS AND DISCUSSION

DFT Geometry Optimization Trends

The olefin ligand (L = η^2-C_2H_3-C_6H_4-Y) system of study in this thesis consists of styrene and styrene analogs, electronically modified at the para position, Y. DFT geometry optimizations were completed for the ground state of every molecular structure including the unbound olefin and metal carbonyl fragments. To our knowledge there are no experimental structural data for the complex series [$M(CO)_xL$-Y], but preceding work employing the BP86 functional on metal-olefin complexes have shown good structural agreement between DFT calculations and available experimental data for other metal-olefin complexes.[21-24, 77] Nineteen unbound fragment structures and seventy metal-olefin structures of the [$M(CO)_xL$-Y] complex series were geometrically optimized for a combined total of eighty-nine molecular structures analyzed in this study:

$Cr(CO)_5$; $Mo(CO)_5$; $W(CO)_5$; $^3Fe(CO)_4$; $Ni(CO)_3$	$M(CO)_x$ Fragments
C_2H_3-C_6H_4-Y	Olefin Ligand Fragments
[$M(CO)_xL$-Y]	[$M(CO)_xL$-Y] Complex Series

Optimized representations of the molecular structures used in this study are shown in Figures 2-6. Selected DFT optimal geometrical parameters are provided in Tables 1-8. Provided in Table 1 are the optimized geometrical parameters obtained for the group six transition metal (M = Cr, Mo, W) pentacarbonyl fragment series, $M(CO)_5$, prior to metal- olefin complexation; Figure 2 depicts optimized fragment representations.

TABLE 1: Optimized Geometry Parameters for the $M(CO)_5$ Fragments.

$M(CO)_5$	$Cr(CO)_5$	$Mo(CO)_5$	$W(CO)_5$
C_{eq}-M-C_{eq}	178.69	179.97	178.42
C_{eq}-M-C_{ax}	90.66	89.93	90.77
O-C_{eq}-M	178.45	178.41	179.19
M-C_{eq}	1.896	2.064	2.054
M-C_{ax}	1.819	1.948	1.948
C-O_{eq}	1.166	1.165	1.167
C-O_{ax}	1.172	1.172	1.174

Bond lengths in angstroms and angles in degrees.

It has been established that the ground state for the unsaturated transition metal pentacarbonyl $M(CO)_5$ fragments are singlet state with a square pyramidal geometry (C_{4v} symmetry).[78] Optimized geometries were similar amongst complexes in the group six triad. Provided in Table 2 are the selected geometrical parameters obtained following the optimization of the $^3Fe(CO)_4$ fragment prior to metal-olefin bond formation. Recall that bond formation energies for the $[Fe(CO)_4(\eta^2\text{-}C_2H_3\text{-}C_6H_4\text{-}Y)]$ complex series were calculated relative to the triplet state of $Fe(CO)_4$ because this is the experimentally determined ground state.[45] Table 3 contains the select geometry parameters acquired based on optimization of the $Ni(CO)_3$fragment prior to metal-olefin bond formation. Geometry optimizations were also carried out against a series of 14 para substituted styrene ligand fragments ($L = \eta^2\text{-}C_2H_3\text{-}C_6H_4\text{-}Y$). Table 4 shows the most relevant geometric calculations obtained following the structural optimization of the unbound olefin ligand fragments; Refer to Figure 3.

TABLE 2: Optimized Geometry Parameters for the $^3Fe(CO)_4$ Fragment.

Fe-C_{ax}	Fe-C_{eq}	C_{ax}-Fe-C_{ax}	C_{eq}-Fe-C_{eq}	Fe-CO_{ax}	Fe-C-O_{eq}
1.827	1.787	150.98	98.01	176.93	178.80

Bond lengths in angstroms and angles in degrees.

TABLE 3: Optimized Geometry Parameters for the $Ni(CO)_3$ Fragment.

C_1-Ni-C_2	C_1-Ni-C_3	Ni-C_1	Ni-C_3	O-C_1	O-C_3
116.69	117.16	1.764	1.766	167.49	168.07

Bond lengths in angstroms and angles in degrees.

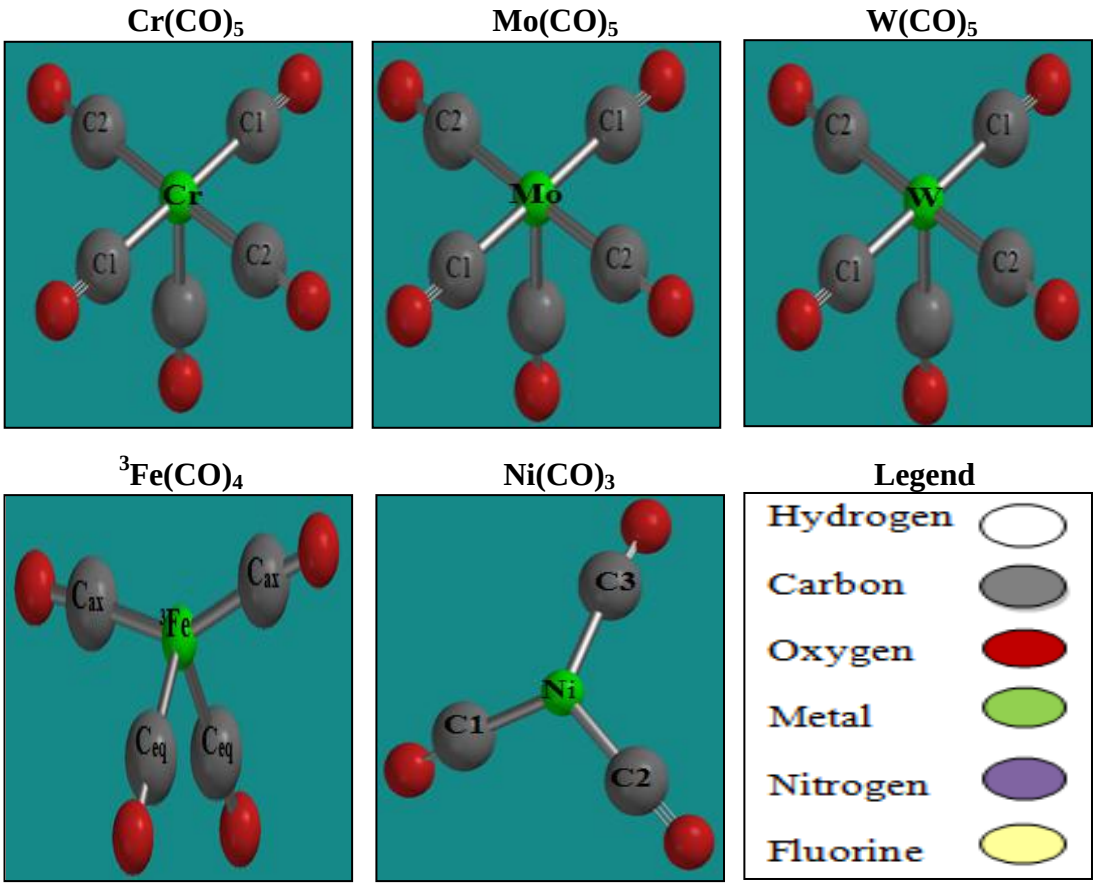

Figure 2. Depiction of the $M(CO)_x$ fragments following geometry optimization.

TABLE 4: Optimized Geometry Parameters for Unbound Olefin Fragments.

Name	Olefin	C=C	Θ
Ethylene	C_2H_4	1.340	0
4-Nitrostyrene	C_2H_3-C_6H_4-NO_2	1.349	0
4-Cyanostyrene	C_2H_3-C_6H_4-CN	1.349	0
4-Vinylcarboxyllic acid	C_2H_3-C_6H_4-COOH	1.349	0
4-Vinylaldehyde	C_2H_3-C_6H_4-COH	1.349	0
4-Trifluoromethylstyrene	C_2H_3-C_6H_4-COH	1.349	0
4-Acetoxystyrene	C_2H_3-C_6H_4-COH	1.349	0
Styrene	C_2H_3-C_6H_5	1.349	0
4-Methylstyrene	C_2H_3-C_6H_4-CH_3	1.349	0
4-t-butylstyrene	C_2H_3-C_6H_4-CCH_3	1.349	0
4-Hydroxystyrene	C_2H_3-C_6H_4-OH	1.350	0
4-Methoxystyrene	C_2H_3-C_6H_4-OCH_3	1.350	0
4-t-butoxystyrene	C_2H_3-C_6H_4-$OCCH_3$	1.350	0
4-Aminostyrene	C_2H_3-C_6H_4-NH_3	1.351	0
4-Dimethylaminostyrene	C_2H_3-C_6H_4-$N(CH)_2$	1.351	0

Bond lengths in angstroms and angles in degrees.

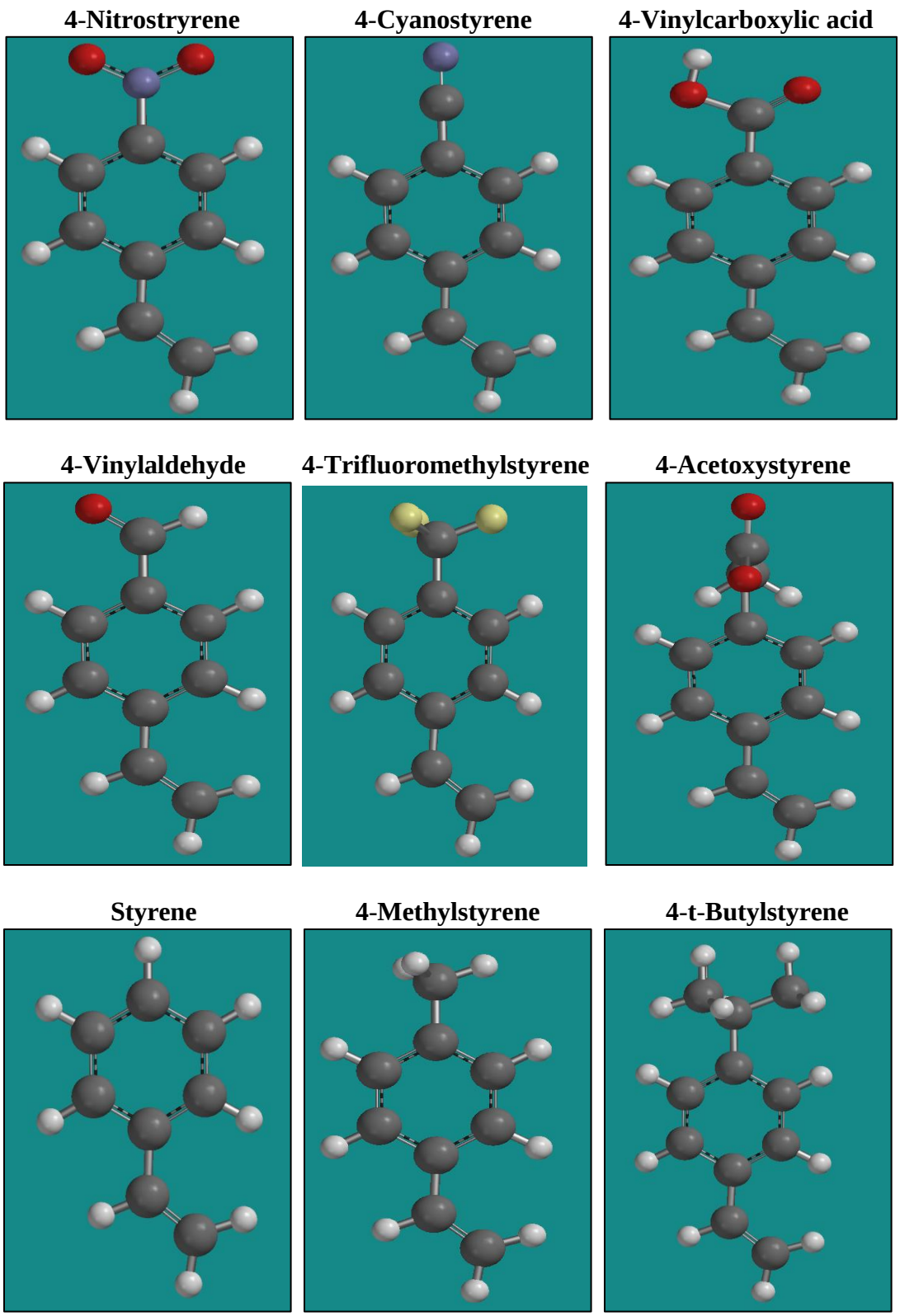

Figure 3. Depiction of free olefins following geometry optimization (Figure Continues).

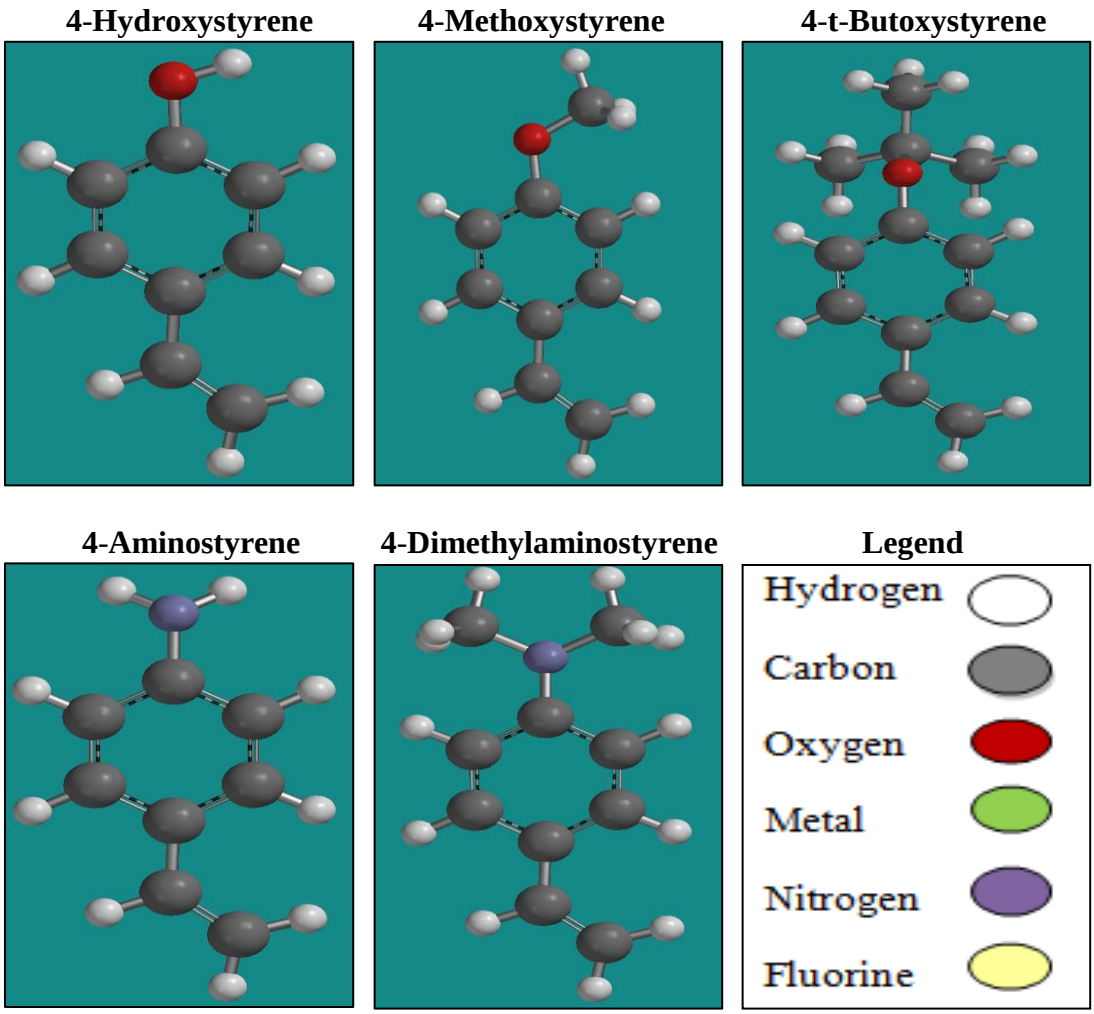

Figure 3. Depiction of the free olefins following geometry optimization.

The $^{1}M(CO)_5$ fragments are square pyramidal in shape with the two sets of *trans* CO ligands oriented approximately 180° opposite each other. A structural optimization of $^{3}Fe(CO)_4$ results in a distorted tetrahedral geometry, with a C_{ax}-Fe-C_{ax} angle of 150.98°. The $^{3}Fe(CO)_4$ fragment deforms by bending the axial CO ligands away from the olefin. Structural optimization of the singlet state nickel tricarbonyl fragment $^{1}Ni(CO)_3$ resulted in a trigonal planar geometry, with a C-Ni-C angle separation of 117.16°. Combination of the $^{1}Cr(CO)_5$ and unbound styrene fragment lead to the overall formation of the net $[Cr(CO)_5(\eta^2\text{-}C_2H_3\text{-}C_6H_5)]$ metal-olefin complex; Refer to Figure 4.

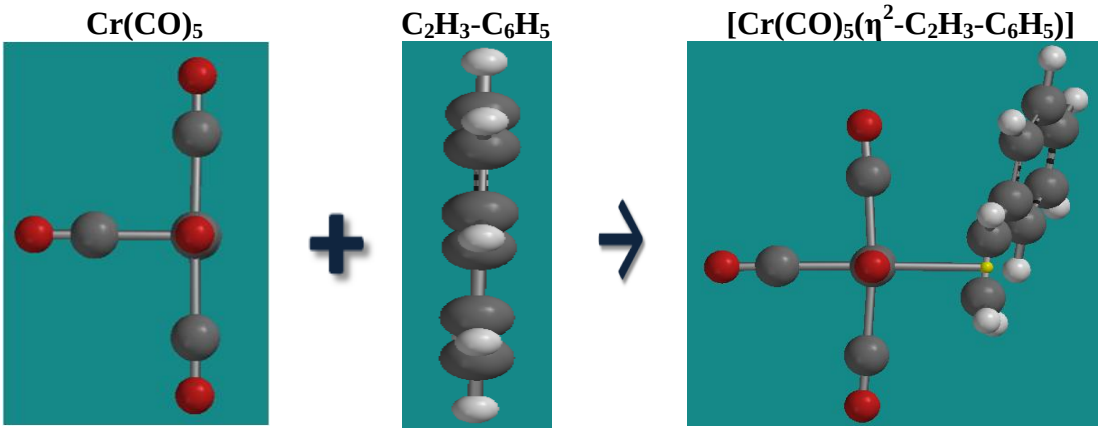

Figure 4. Net complex formation reaction for $[Cr(CO)_5(\eta^2\text{-}C_2H_3\text{-}C_6H_5)]$complex.

All unbound olefin ligands are planar and the C=C bond distance varies with respect to the electronic nature of the para substituent. Upon binding to an olefin, the C=C double bond of the olefin is aligned approximately parallel to one set of equatorial carbonyl groups, forcing these equatorial carbonyls of the $M(CO)_5$ complex to bend back away from the olefin, as shown in Figure 4. This flexing is accounted for in the C-M-C angle and represents the largest geometrical change in the unbound $M(CO)_5$ fragment relative to the $M(CO)_5$ complex. The substituents around the olefinic double bond bend away from the $M(CO)_5$ fragment as accounted for in the pyramidalization angle Θ (180 degrees minus the dihedral angle between trans substituents). Finally, as the bond is formed, the double bond of the olefin increases in length relative to its unbound state.

Table 5 contains the most relevant calculated geometrical parameters obtained following the structural optimization of the transition metal-olefin pentacarbonyl complex series $[M(CO)_5L\text{-}Y]$, (M = Cr, Mo, W; where, Y = NO_2, CN, COOH, COH, CF_3, $OCOCH_3$, H, CH_3, $C(CH_3)_3$, OH, OCH_3, $OC(CH_3)_3$, NH_2, $N(CH_3)_2$). Optimized geometrical representations of the chromium-olefin complex $[Cr(CO)_5(\eta^2\text{-}C_2H_3\text{-}C_6H_4\text{-}Y)]$ series are shown in Figure 5.

TABLE 5: Optimized Geometry Parameters; [$M(CO)_5L$-Y] Complex Series.

$M(CO)_5L$- Y	M-C_{Olef} [a]	C=C [a]	Δ(C=C) [a]	Θ[b] (HC=CR)
$Cr(CO)_5L$- NO_2	2.236	1.403	0.054	30.35
$Cr(CO)_5L$- CN	2.241	1.403	0.054	30.30
$Cr(CO)_5L$- COOH	2.245	1.403	0.054	30.06
$Cr(CO)_5L$- COH	2.247	1.403	0.054	29.94
$Cr(CO)_5L$- CF_3	2.247	1.402	0.053	29.90
$Cr(CO)_5L$- $OCOCH_3$	2.253	1.402	0.053	30.22
$Cr(CO)_5L$- H	2.259	1.401	0.052	29.87
$Cr(CO)_5L$- CH_3	2.264	1.401	0.052	29.71
$Cr(CO)_5L$- $C(CH_3)_3$	2.265	1.401	0.052	29.68
$Cr(CO)_5L$- OH	2.276	1.401	0.051	29.66
$Cr(CO)_5L$- OCH_3	2.285	1.401	0.051	29.57
$Cr(CO)_5L$- $OC(CH_3)_3$	2.289	1.401	0.051	29.25
$Cr(CO)_5L$- NH_3	2.294	1.402	0.051	29.27
$Cr(CO)_5L$- $N(CH_3)_2$	2.309	1.402	0.051	28.39
$Mo(CO)_5L$- NO_2	2.425	1.393	0.044	23.01
$Mo(CO)_5L$- CN	2.431	1.393	0.044	23.30
$Mo(CO)_5L$- COOH	2.437	1.392	0.043	22.67
$Mo(CO)_5L$- COH	2.443	1.392	0.043	22.59
$Mo(CO)_5L$- CF_3	2.444	1.391	0.042	22.33
$Mo(CO)_5L$- $OCOCH_3$	2.443	1.392	0.043	22.94
$Mo(CO)_5L$- H	2.455	1.391	0.042	22.84
$Mo(CO)_5L$- CH_3	2.459	1.391	0.042	22.63
$Mo(CO)_5L$- $C(CH_3)_3$	2.462	1.391	0.042	22.10
$Mo(CO)_5L$- OH	2.469	1.391	0.041	22.15
$Mo(CO)_5L$- OCH_3	2.476	1.391	0.041	22.14
$Mo(CO)_5L$- $OC(CH_3)_3$	2.482	1.391	0.041	22.17
$Mo(CO)_5L$- NH_3	2.488	1.392	0.041	21.97
$Mo(CO)_5L$- $N(CH_3)_2$	2.497	1.392	0.041	21.41
$W(CO)_5L$- NO_2	2.382	1.403	0.054	26.93
$W(CO)_5L$- CN	2.390	1.403	0.053	26.93
$W(CO)_5L$- COOH	2.396	1.399	0.052	26.09
$W(CO)_5L$- COH	2.399	1.400	0.052	26.21
$W(CO)_5L$- CF_3	2.402	1.401	0.052	25.96
$W(CO)_5L$- $OCOCH_3$	2.402	1.401	0.052	26.65
$W(CO)_5L$- H	2.407	1.400	0.051	26.11
$W(CO)_5L$- CH_3	2.414	1.400	0.051	26.24
$W(CO)_5L$- $C(CH_3)_3$	2.417	1.399	0.050	25.09
$W(CO)_5L$- OH	2.427	1.400	0.050	26.00
$W(CO)_5L$- OCH_3	2.432	1.400	0.050	25.29
$W(CO)_5L$- $OC(CH_3)_3$	2.436	1.399	0.049	25.50
$W(CO)_5L$- NH_3	2.443	1.400	0.049	25.70
$W(CO)_5L$- $N(CH_3)_2$	2.456	1.400	0.049	24.78

a) Bond lengths in angstroms, angles in degrees. *b)* Θ is the difference between 180° and dihedral angle around C=C.

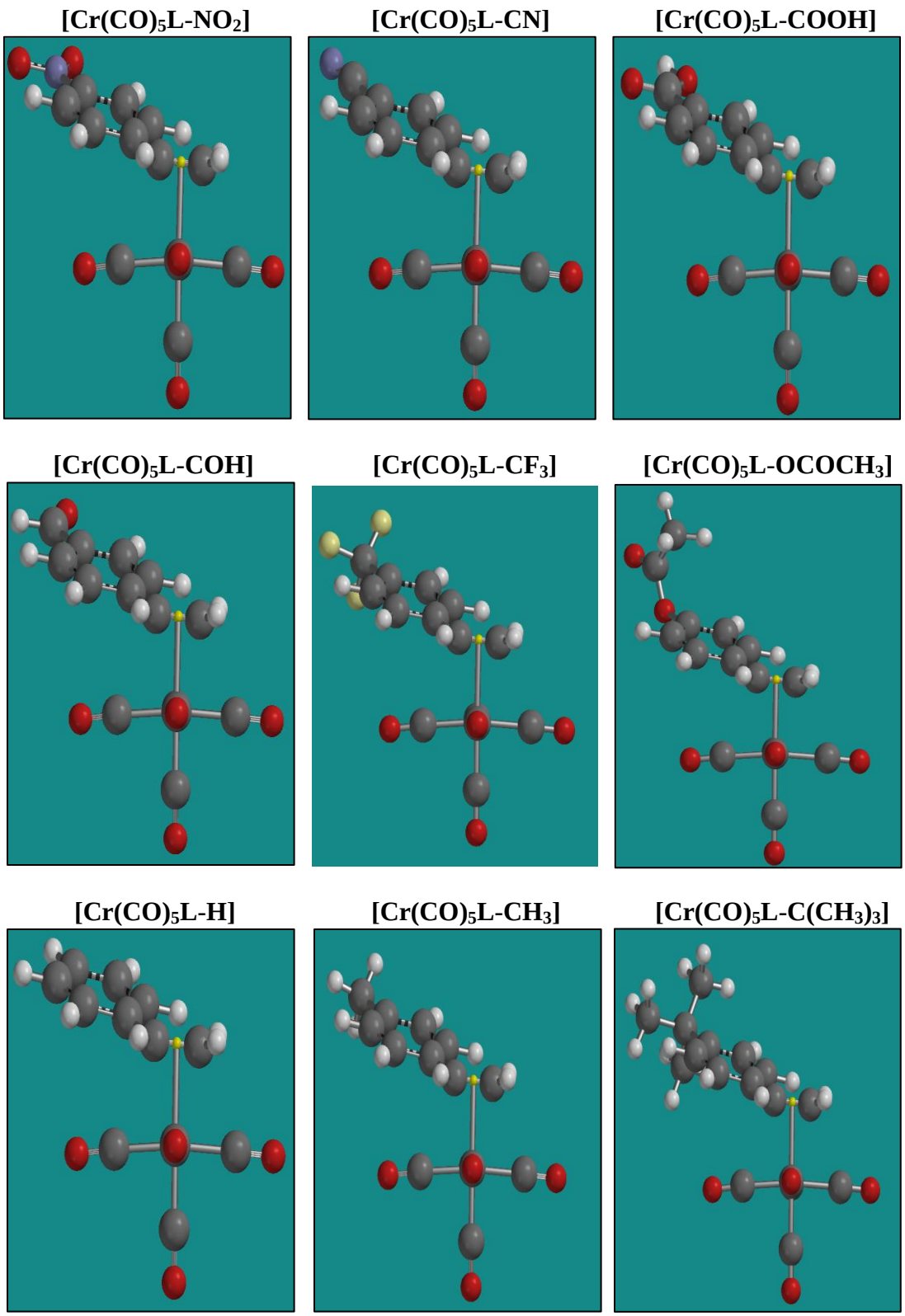

Figure 5. Depiction of the [$Cr(CO)_5$L-Y] metal-olefin interactions (Figure Continues).

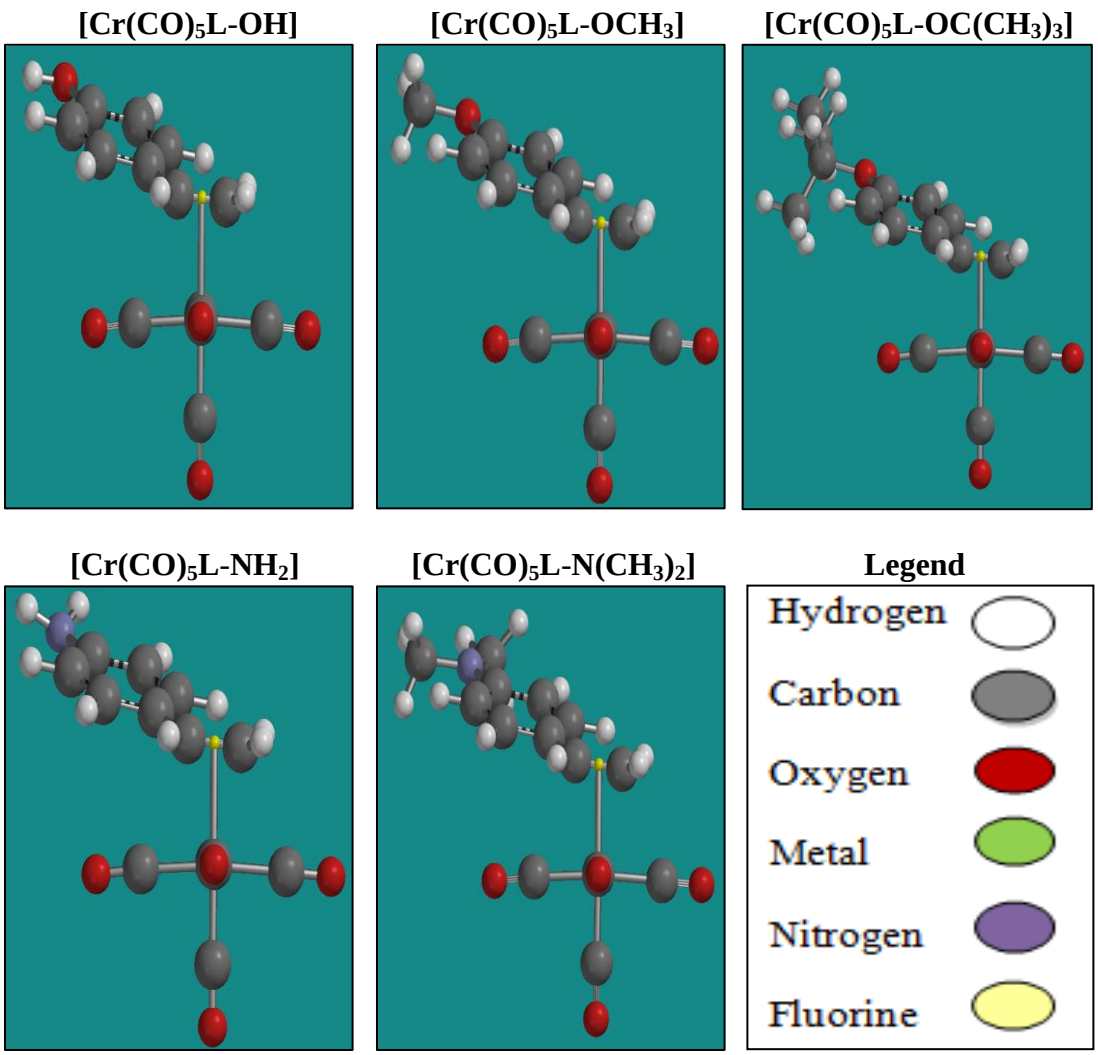

Figure 5. Depiction of the [$Cr(CO)_5$L-Y] metal-olefin interactions.

The transition metal-olefin pentacarbonyl [$M(CO)_5(\eta^2\text{-}C_2H_3\text{-}C_6H_4\text{-}Y)$] complexes are octahedral in shape with the two sets of trans CO ligands oriented approximately 180° opposite each other. As anticipated, all olefins deviate from a planar geometry upon metal-olefin bond formation. This is both supported by the elongation of the C=C bond (Δ(C=C) in Table 5) and the so-called pyramidalization angle of the olefin (Θ Table 5). Figure 6 illustrates the optimized net complex reaction for the formation of the singlet state iron-styrene tetracarbonyl [$Fe(CO)_4(\eta^2\text{-}C_2H_3\text{-}C_6H_5)$] complex.

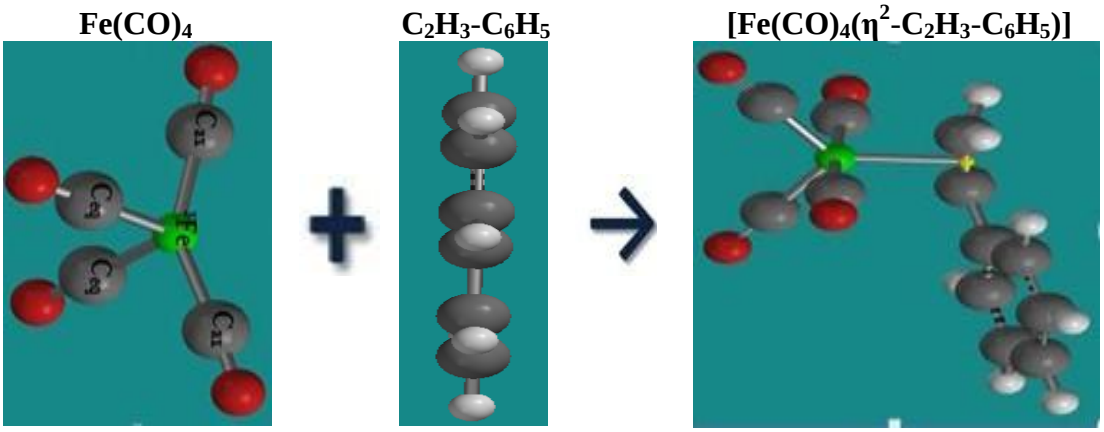

Figure 6. Net complex formation reaction for the $[Fe(CO)_4(\eta^2\text{-}C_2H_3\text{-}C_6H_5)]$ complex.

Optimized structural representations regarding the formation of the iron-olefin tetracarbonyl $[Fe(CO)_4(\eta^2\text{-}C_2H_3\text{-}C_6H_4\text{-}Y)]$ complex series are provided in Figure 7. Only the equatorial (C_{2V} symmetry) isomer of the complexes has been considered since it is well documented from both experiment[79-82] and theory[83] that this isomer is expected to be lowest in energy. Table 6 contains the most relevant parameters obtained following geometrical optimization of the iron-olefin complex series $[Fe(CO)_4L\text{-}Y]$.

TABLE 6: Optimized Geometry Parameters; $[Fe(CO)_4L\text{-}Y]$ Complex Series.

Y	$Fe\text{-}C_{Olef}$ [a]	C=C [a]	ΔC=C	Θ[b] (HC=CR)	$C_{ax}\text{-}Fe\text{-}C_{ax}$ [a]	$C_{eq}\text{-}Fe\text{-}C_{eq}$ [a]
NO_2	2.002	1.430	0.081	34.99	177.39	110.25
CN	2.002	1.430	0.081	35.24	177.03	110.10
COOH	2.007	1.429	0.080	34.93	177.20	110.49
COH	2.007	1.430	0.081	35.14	177.00	110.34
CF_3	2.004	1.429	0.080	35.04	177.12	110.44
$OCOCH_3$	2.008	1.429	0.080	35.52	176.18	110.14
H	2.012	1.429	0.080	35.22	176.62	110.04
CH_3	2.016	1.429	0.080	35.04	176.01	110.46
CCH_3	2.014	1.429	0.080	35.59	175.32	110.01
OH	2.023	1.428	0.078	35.37	175.53	110.53
OCH_3	2.025	1.428	0.078	35.56	176.22	110.88
$OCCH_3$	2.028	1.428	0.078	34.96	175.64	110.58
NH_2	2.033	1.428	0.077	35.30	175.14	110.48
$N(CH_3)_2$	2.037	1.428	0.077	35.34	175.64	110.84

a) Bond lengths in angstroms, angles in degrees. *b)* Θ is the difference between 180° and dihedral angle around C=C.

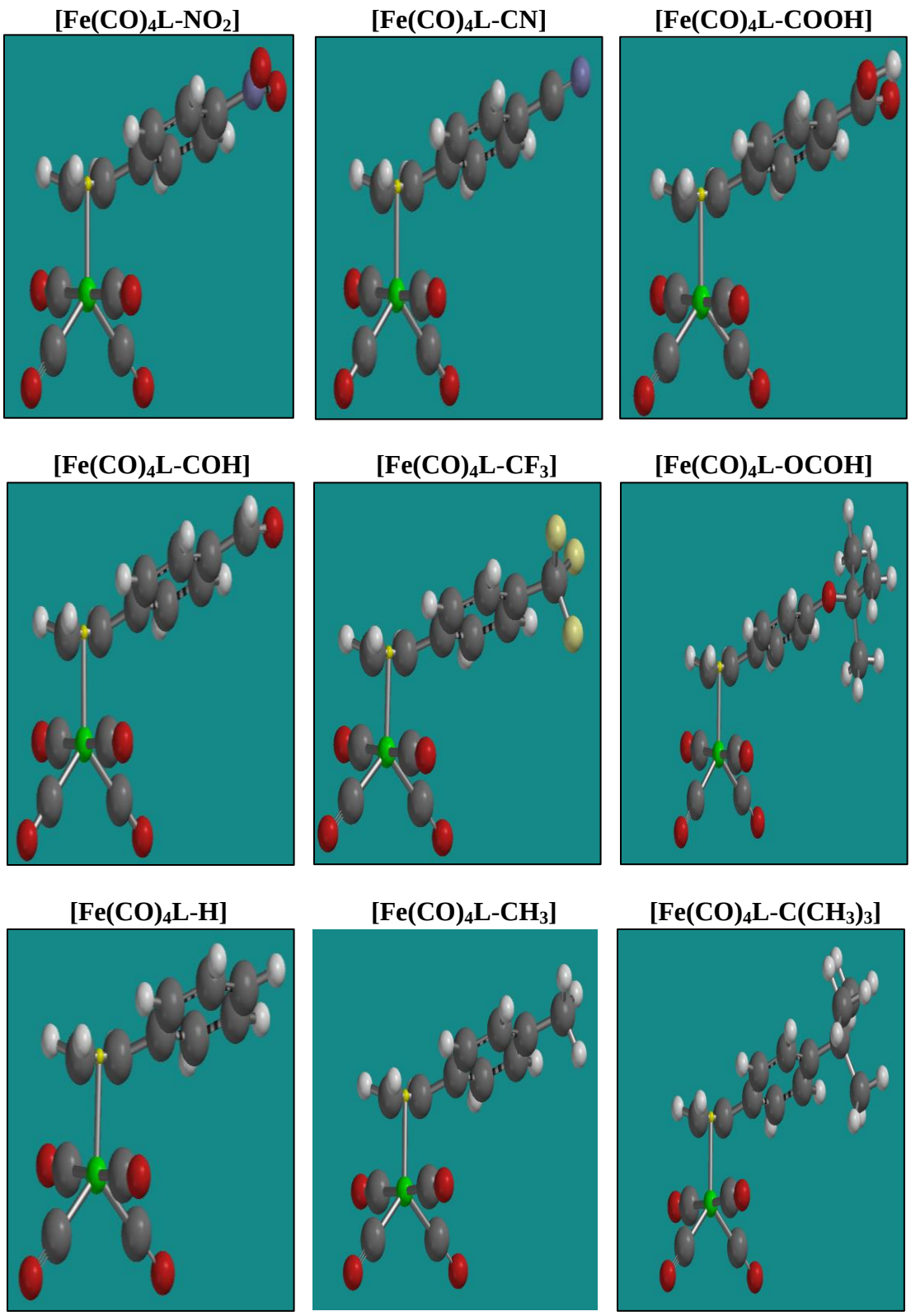

Figure 7. Depiction of the [Fe(CO)$_4$L-Y] metal-olefin interactions (Figure Continues).

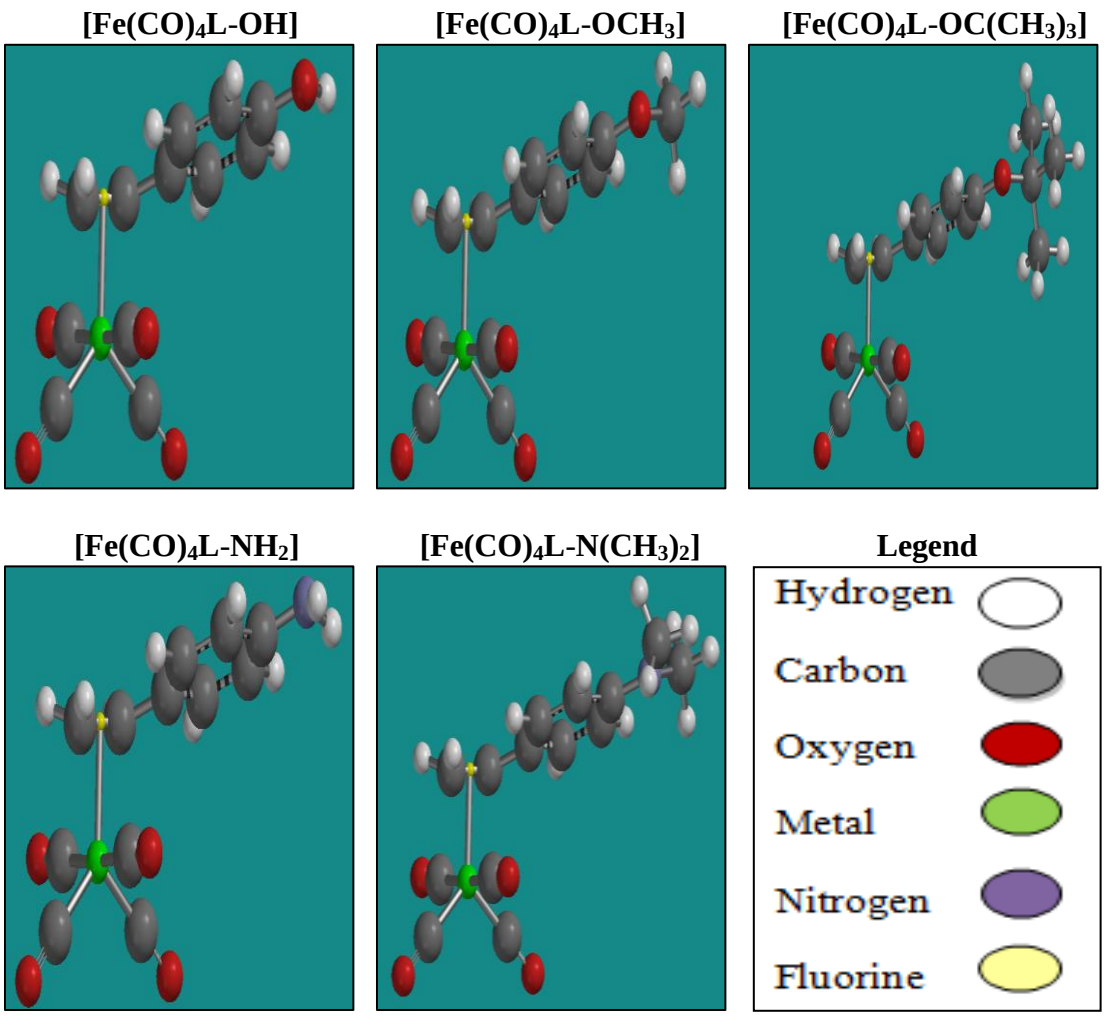

Figure 7. Depiction of the [$Fe(CO)_4$L-Y] metal-olefin interactions.

The iron-olefin tetracarbonyl [$Fe(CO)_4(\eta^2\text{-}C_2H_3\text{-}C_6H_4\text{-}Y)$] complexes are trigonal pyramidal in shape with the two sets of trans CO ligands oriented approximately 180° opposite each other. As seen in Figures 6-7, both the iron tetracarbonyl fragment and the olefin fragments deform moderately upon bond formation. The change in the C_{ax}-Fe-C_{ax} bending angle correlates with the identity of the para substituent, increasing with an increase in the electron-withdrawing capacity of the substituent. Figure 8 illustrates the optimized net complex reaction for the formation of the singlet state nickel-styrene tricarbonyl [$Ni(CO)_3(\eta^2\text{-}C_2H_3\text{-}C_6H_5)$] complex.

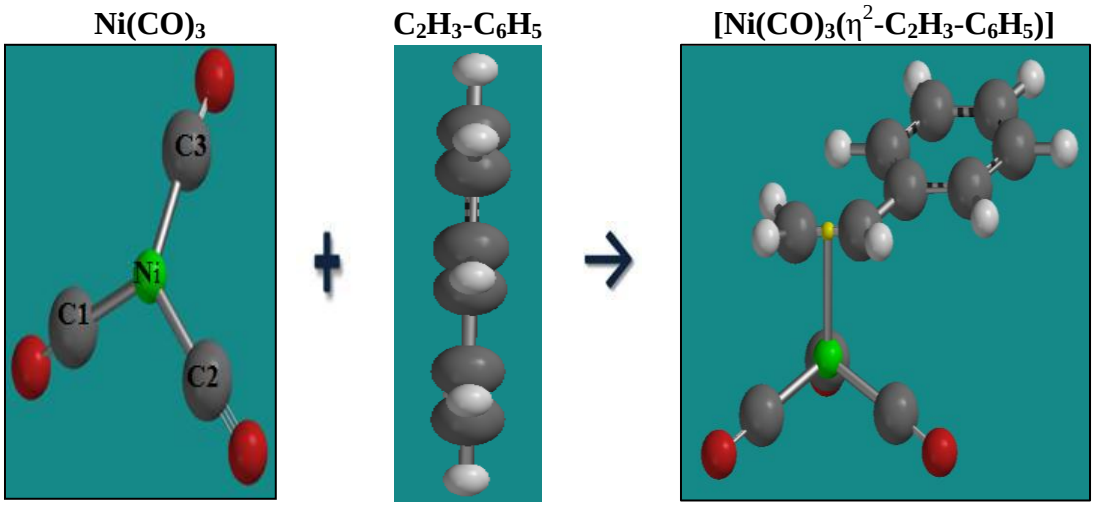

Figure 8. Net complex formation reaction for the $[Ni(CO)_3(\eta^2\text{-}C_2H_3\text{-}C_6H_5)]$ complex.

Optimized structural representations of the singlet state nickel-olefin tricarbonyl complexes $[Ni(CO)_3(\eta^2\text{-}C_2H_3\text{-}C_6H_4\text{-}Y)]$ are provided in Figure 9.Table 7 contains most relevant parameters obtained following geometrical optimization of the nickel-olefin tricarbonyl $[Ni(CO)_3L\text{-}Y]$ complex series.

TABLE 7: Optimized Geometry Parameters; $[Ni(CO)_3L\text{-}Y]$ Complex Series.

Y	Ni-C_{Olef} [a]	C=C [a]	ΔC=C	Θ[b] (HC=CR)	Ni-C_1 [a]	Ni-C_3 [a]
NO_2	2.000	1.401	0.052	25.89	1.786	1.804
CN	2.002	1.401	0.052	25.81	1.785	1.803
COOH	2.004	1.401	0.052	26.14	1.785	1.802
COH	2.007	1.401	0.052	25.23	1.786	1.801
CF_3	2.006	1.400	0.051	25.89	1.785	1.802
$OCOCH_3$	2.011	1.400	0.051	25.69	1.784	1.801
H	2.016	1.399	0.050	25.45	1.783	1.800
CH_3	2.019	1.400	0.051	25.49	1.783	1.799
CCH_3	2.018	1.400	0.051	26.00	1.784	1.797
OH	2.026	1.400	0.050	25.57	1.783	1.797
OCH_3	2.026	1.400	0.050	25.66	1.783	1.797
$OCCH_3$	2.031	1.400	0.050	24.74	1.782	1.796
NH_2	2.034	1.400	0.049	25.66	1.782	1.796
$N(CH_3)_2$	2.039	1.401	0.050	25.77	1.783	1.794

a) Bond lengths in angstroms, angles in degrees. *b)* Θ is the difference between 180° and dihedral angle around C=C.

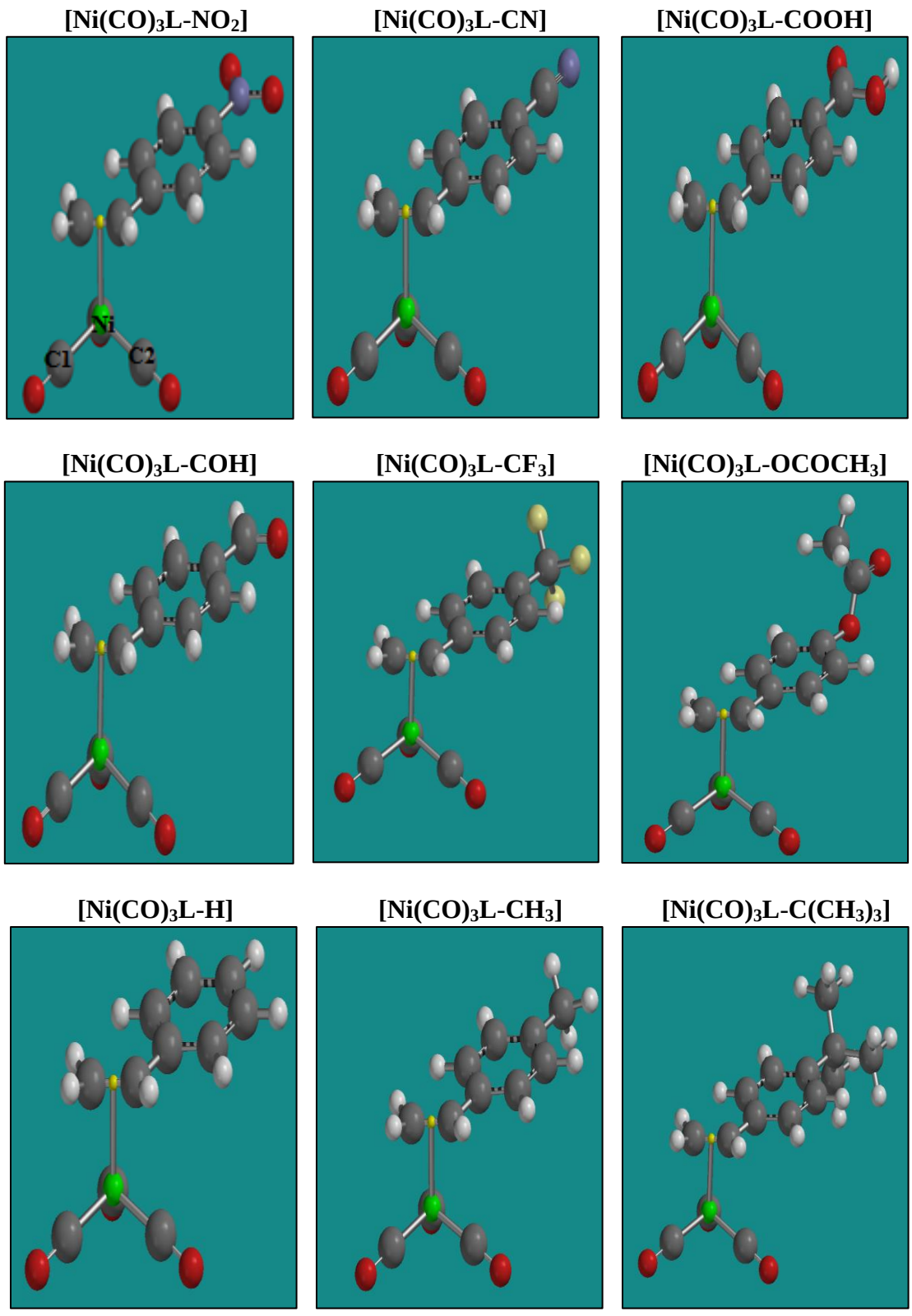

Figure 9. Depiction of the [Ni(CO)$_3$L-Y] metal-olefin interactions (Figure Continues).

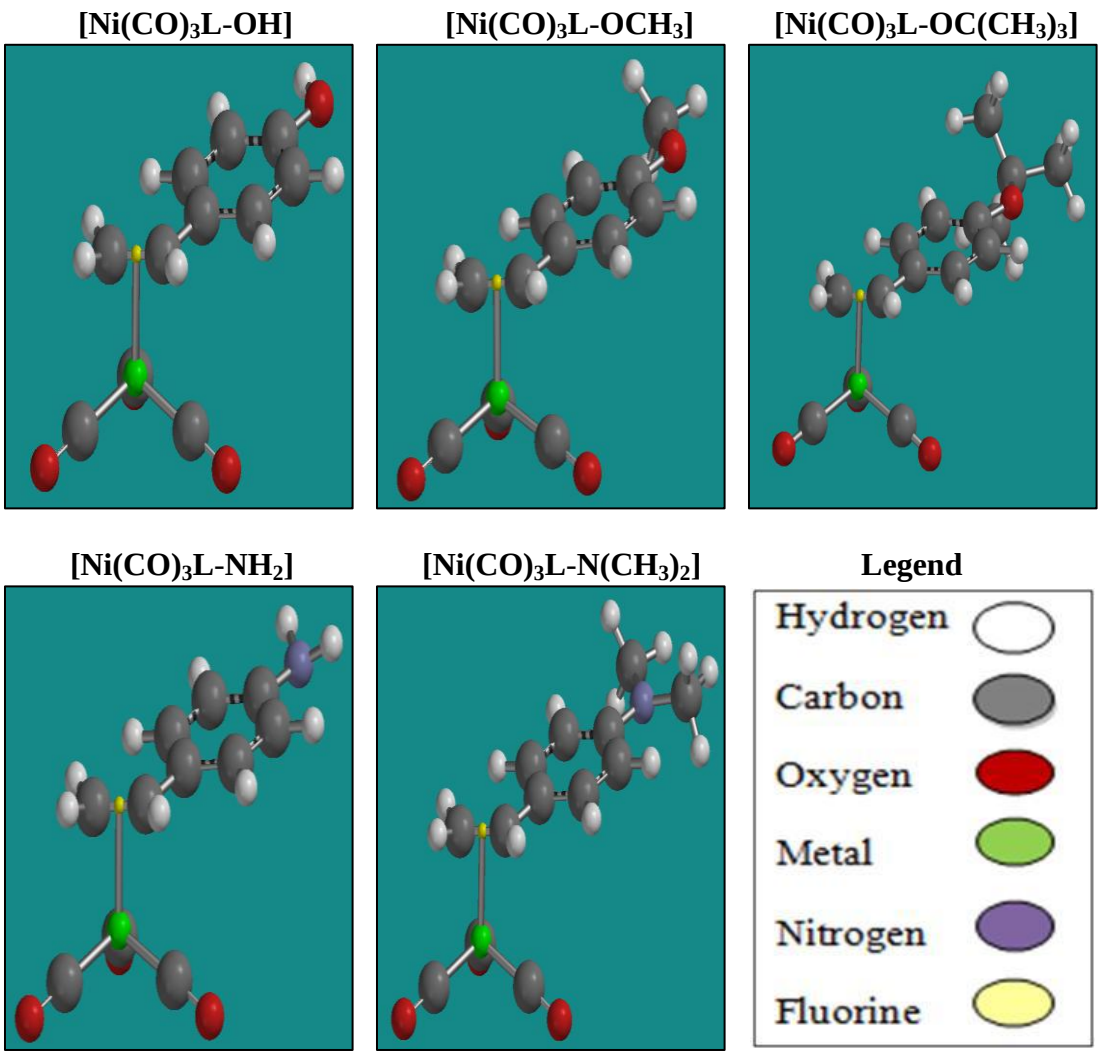

Figure 9. Depiction of the [$Ni(CO)_3L$-Y] metal-olefin interactions.

The nickel-olefin tricarbonyl [$Ni(CO)_3(\eta^2$-C_2H_3-C_6H_4-Y)] complexes are tetrahedral in geometry with the three sets of trans CO ligands oriented approximately 110° opposite each other. As seen in Figures 8-9, both the nickel tricarbonyl fragment and the olefin fragments deform moderately upon bond formation. Trends in selected geometrical parameters were plotted against substituent constants σ_p obtained from Reference 75 and are shown in Figures 10-23 for the [$M(CO)_x(\eta^2$-C_2H_3-C_6H_4-Y)] complex series; where Y = NO_2, CN, COOH, H, OH, NH_2, $N(CH_3)_2$.

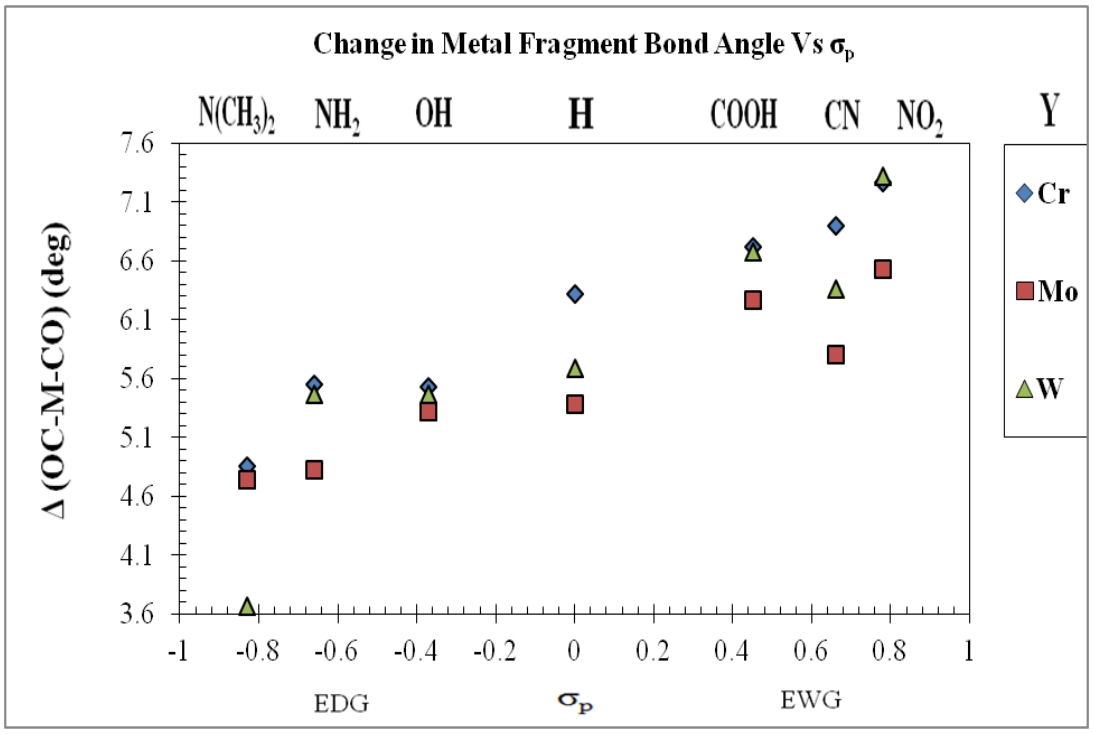

Figure 10. Graph of Δ (OC-M-CO) vs. σ_p for the $[M(CO)_5L\text{-}Y]$ complex series.

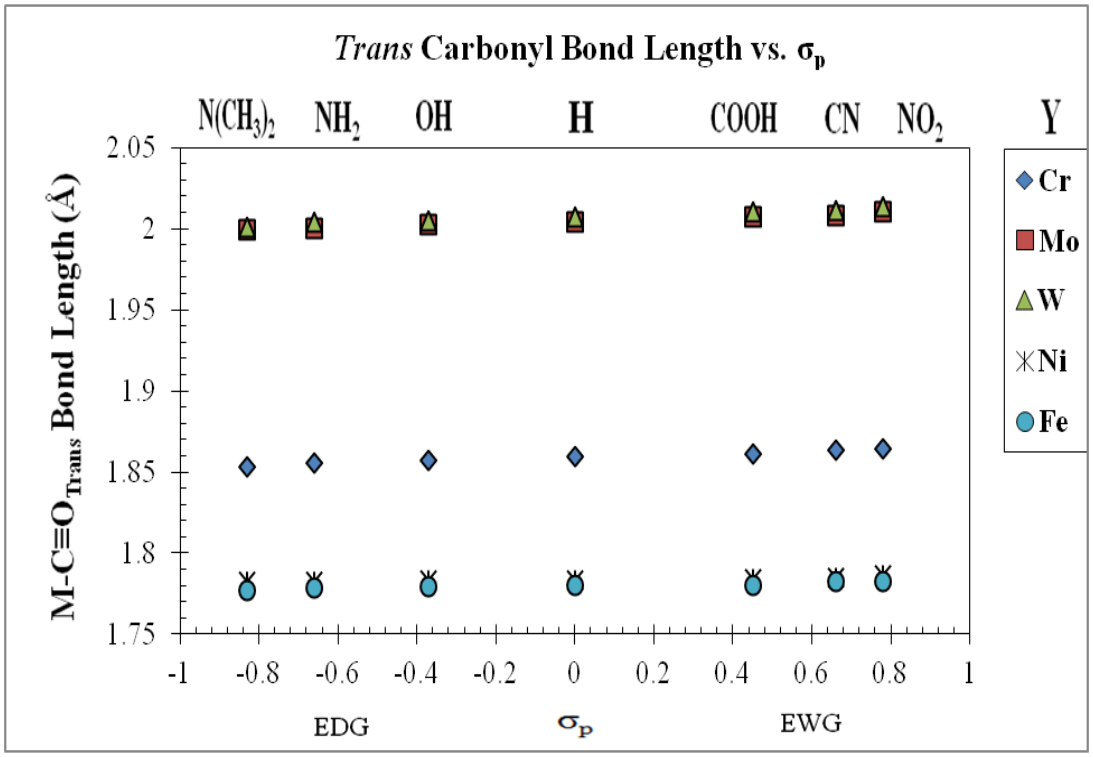

Figure 11. Graph of $M\text{-}C{\equiv}O_{Trans}$ vs. σ_p for the $[M(CO)_xL\text{-}Y]$ complex series.

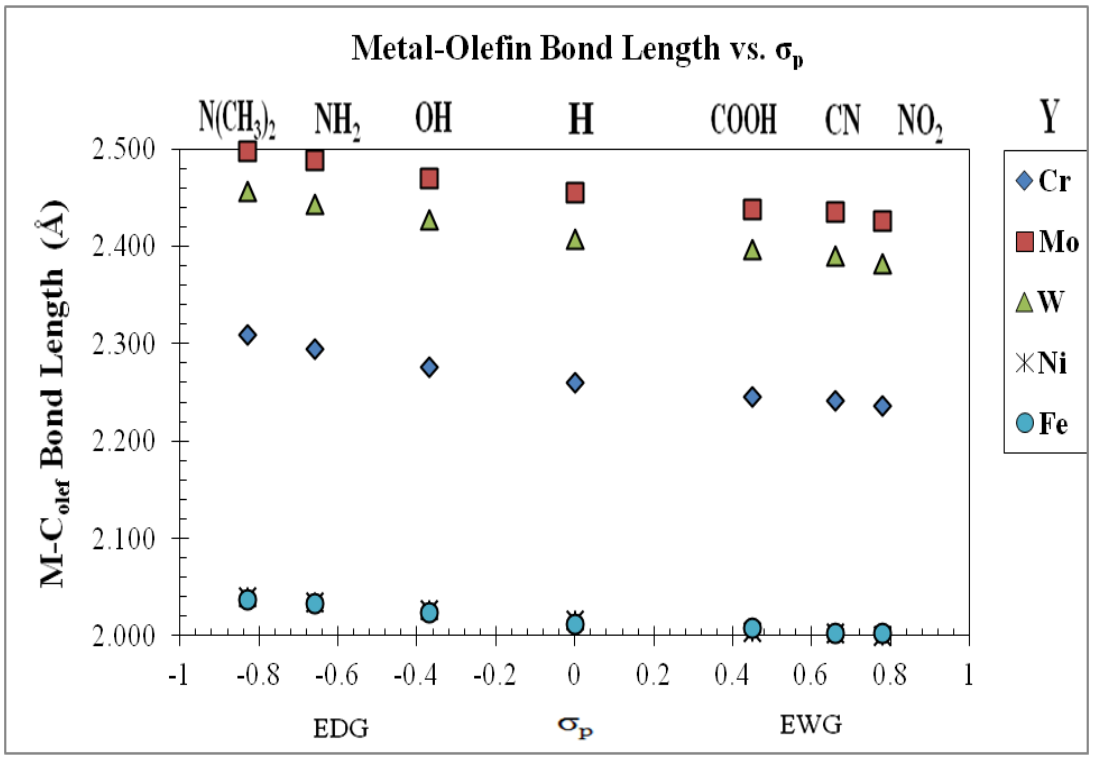

Figure 12. Graph of M-C_{olef} vs. σ_p for the [$M(CO)_xL$-Y] complex series.

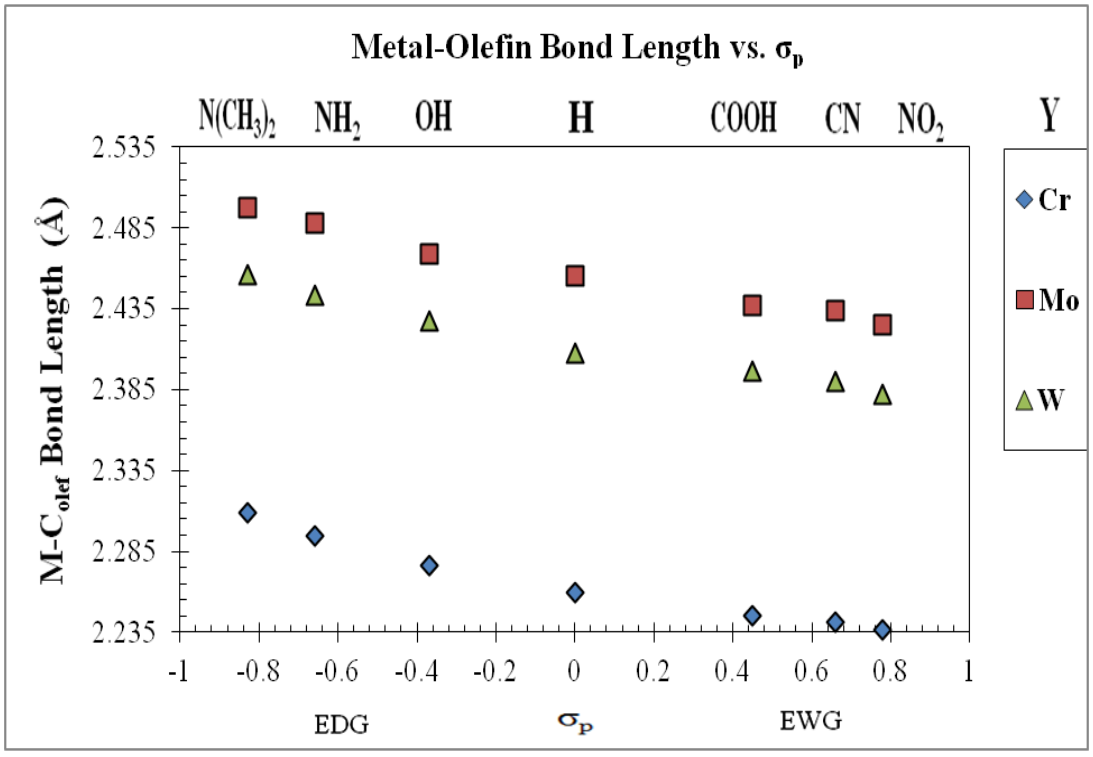

Figure 13. Graph of M-C_{olef} vs. σ_p for the [$M(CO)_5L$-Y] complex series.

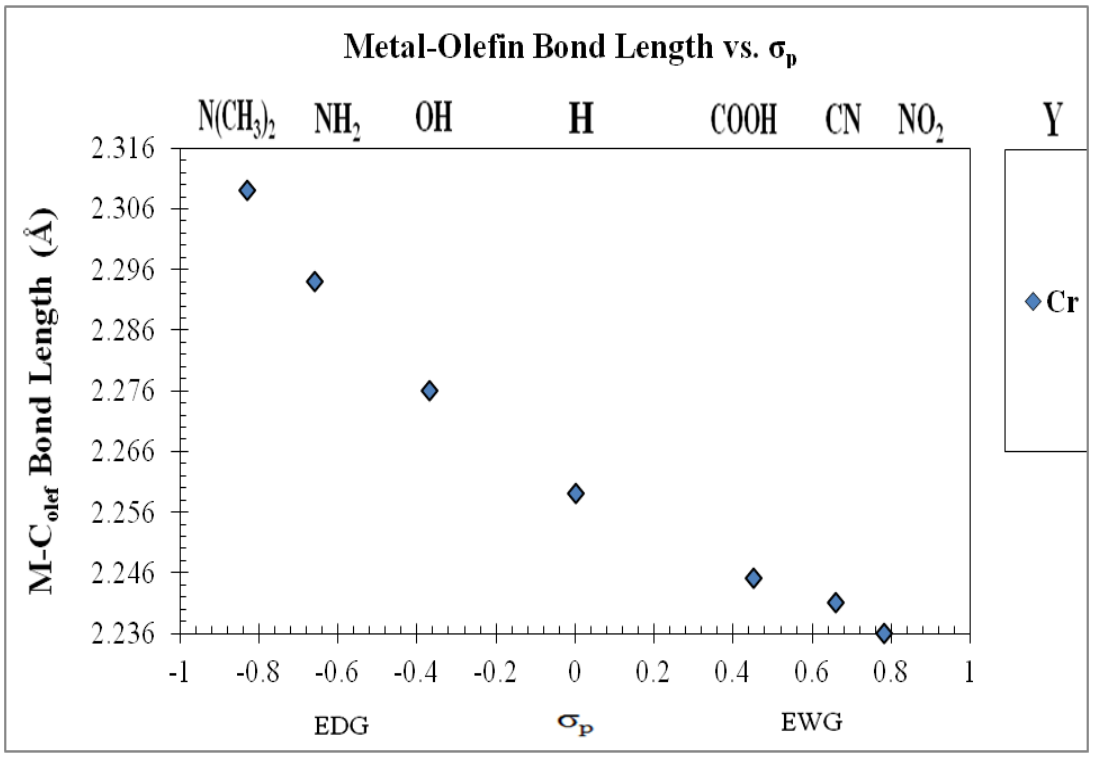

Figure 14. Graph of M-C_{olef} vs. σ_p for the [$Cr(CO)_5$L-Y] complex series.

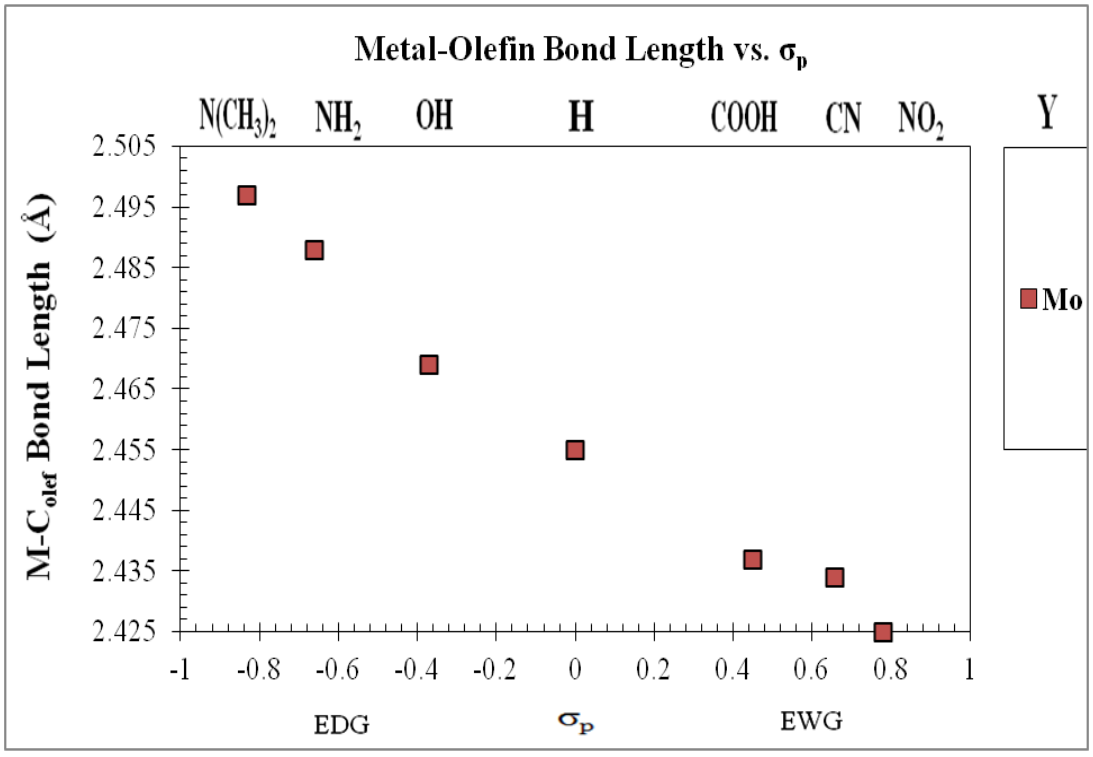

Figure 15. Graph of M-C_{olef} vs. σ_p for the [$Mo(CO)_5$L-Y] complex series.

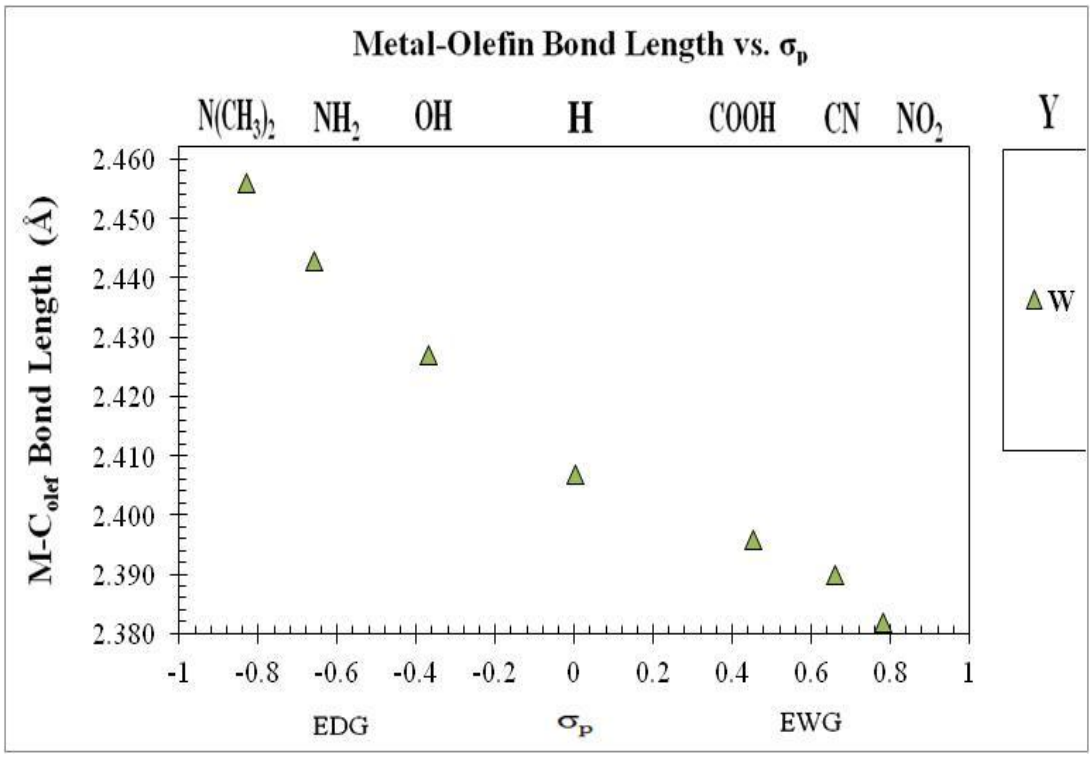

Figure 16. Graph of M-C_{olef} vs. σ_p for the [$W(CO)_5$L-Y] complex series.

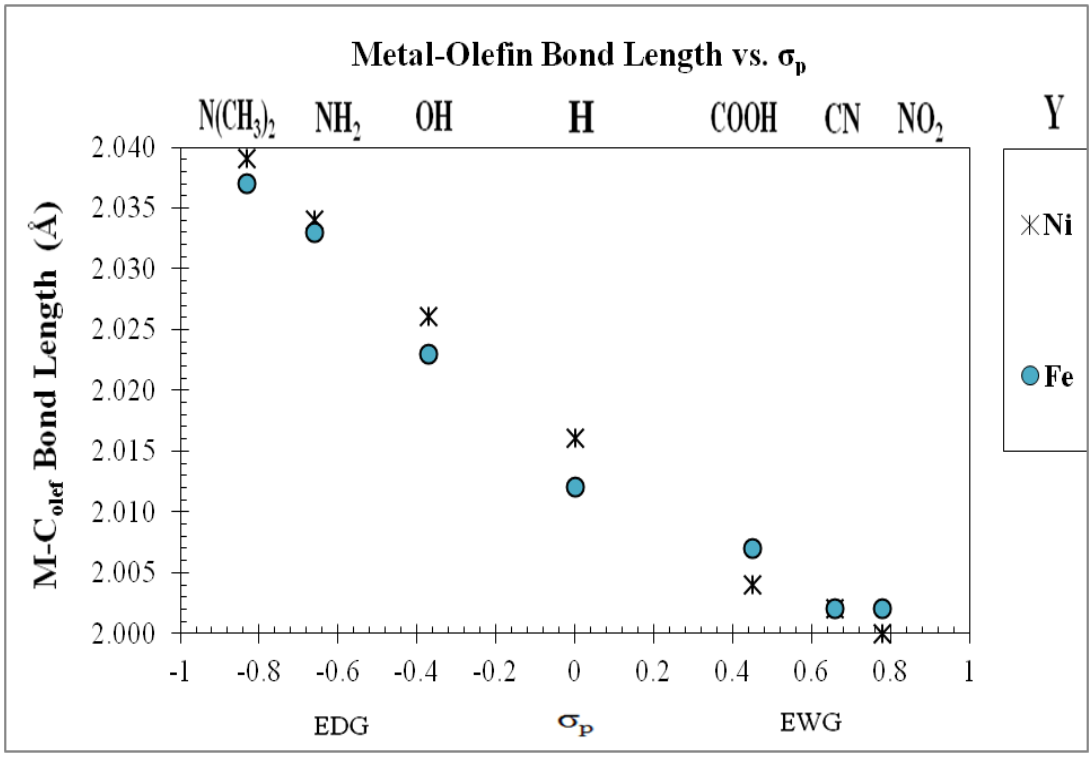

Figure 17. Graph of M-C_{olef} vs. σ_p for the [$M(CO)_x$L-Y] complex series.

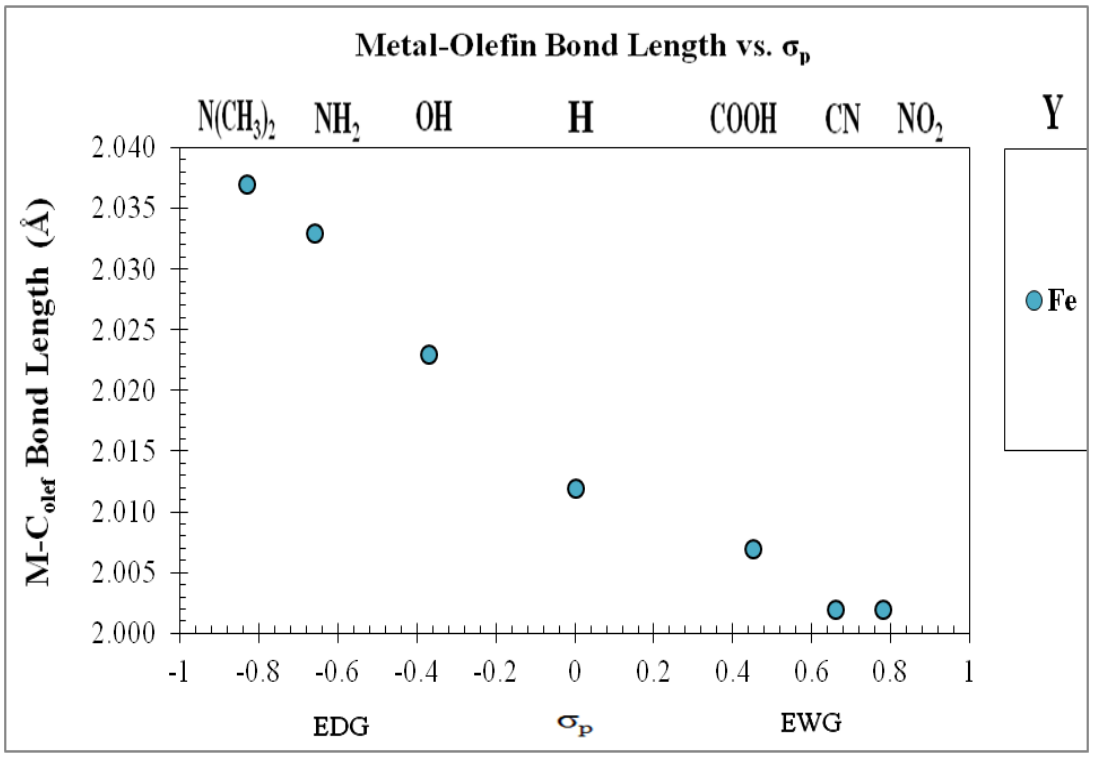

Figure 18. Graph of M-C_{olef} vs. σ_p for the [$Fe(CO)_4$L-Y] complex series.

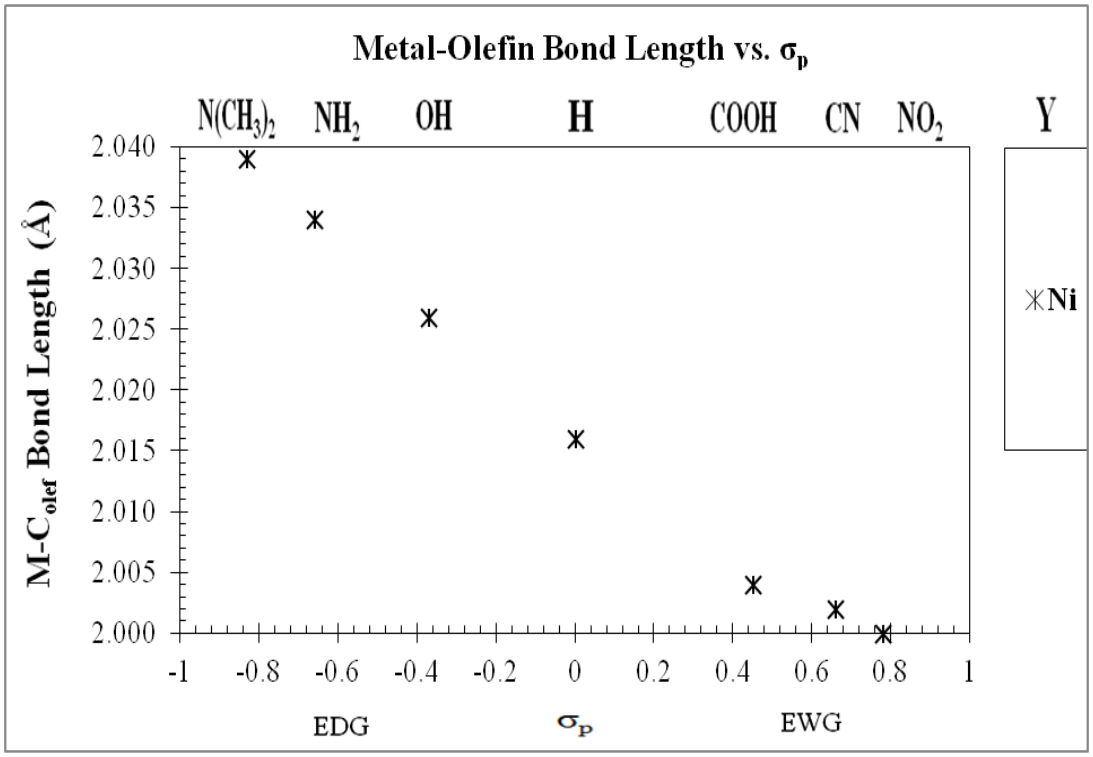

Figure 19. Graph of M-C_{olef} vs. σ_p for the [$Ni(CO)_3$L-Y] complex series.

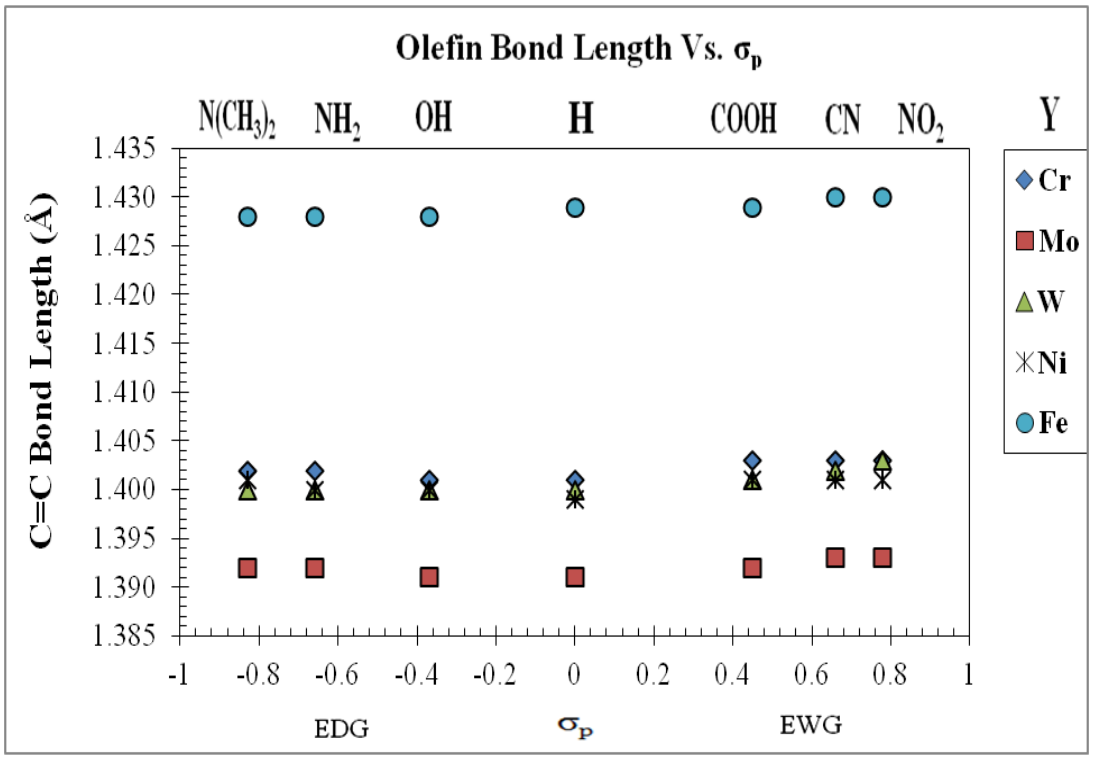

Figure 20. Graph of (C=C) vs. σ_p for the [$M(CO)_xL$-Y] complex series.

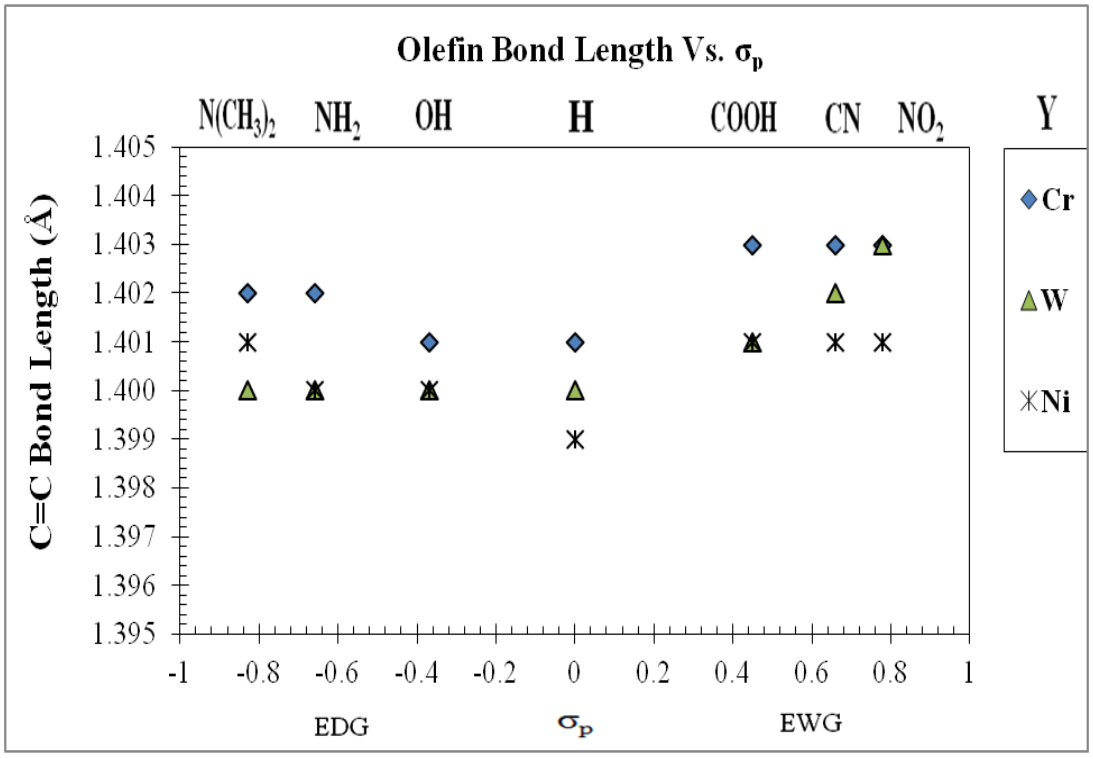

Figure 21. Graph of (C=C) vs. σ_p for the [$M(CO)_xL$-Y] complex series.

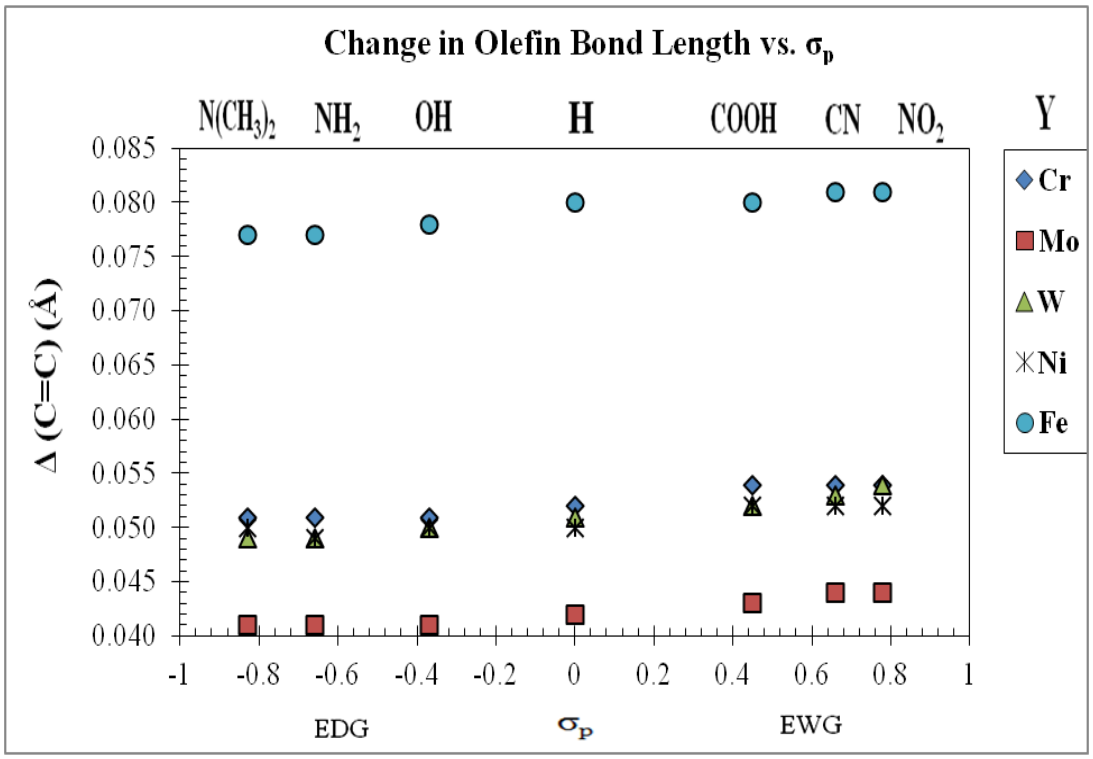

Figure 22. Graph of Δ(C=C) vs. σ_p for the [$M(CO)_xL$-Y] complex series.

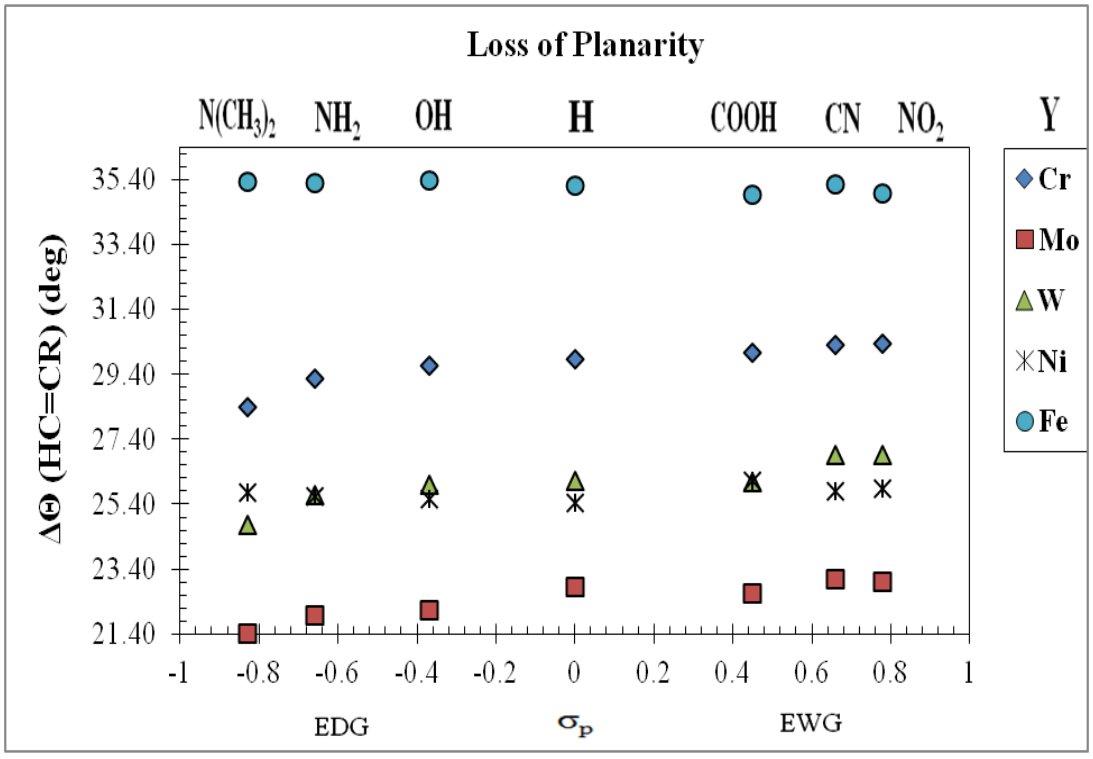

Figure 23. Graph of ΔΘ (HC=CR) vs. σ_p for the [$M(CO)_xL$-Y] complex series.

Upon formation of the metal-olefin bond, the equatorial carbonyls of the $M(CO)_5$ complex bend back away from the olefin. Geometrical changes in C-M-C angle as a function of substituent effects reflect an intrinsic relationship between structure and activity as manifested in Figure 10. As anticipated, the M-C(O) and C-O bond lengths correlate with the electronic nature of the para substituent on the olefin, especially for the CO *trans* to the olefin (Figure 11). When comparing the effects of transition metal influence, it is shown that the magnitude of the $M\text{-}C{\equiv}O_{Trans}$ bond length for the metal carbonyl *trans* to metal-olefin bond formation should follow in general order of $[Mo(CO)_5L\text{-}Y] \geq [W(CO)_5L\text{-}Y] > [Cr(CO)_5L\text{-}Y] > [Ni(CO)_3L\text{-}Y] \geq [Fe(CO)_4L\text{-}Y]$.

As expected, all olefins deviate from a planar geometry upon metal-olefin bond formation. This is both supported by the elongation of the C=C bond (Δ (C=C)) and the so-called *pyramidalization angle* of the olefin (Θ); as demonstrated through Figures 20-23. In general, it is shown that as the electron-withdrawing capacity of the para substituent increases, there is an observed increase in both the olefin C=C bond length and in deviations from olefin planarity, Θ, across the series; with Y = NO_2 placing the greatest demand on the change in olefinic bond length ΔC=C in each series. In all the results, one trend is obvious: As the *electron-withdrawing* nature of the olefin increases, the length of the transition metal-olefin $M\text{-}C_{olef}$ bond decreases. On the basis of the DCD model, an increase in the electron-withdrawing ability of the para substituent should lead to a decrease in the metal-olefin bond length do to an enhancement in the nature of the π back-bonding interaction. When comparing the effects of transition metal influence, it is shown that the magnitude of the $M\text{-}C_{olef}$ bond length should follow the *trend* of $[Mo(CO)_5L\text{-}Y] > [W(CO)_5L\text{-}Y] > [Cr(CO)_5L\text{-}Y] > [Ni(CO)_3L\text{-}Y] > [Fe(CO)_4L\text{-}Y]$.

DFT Bond Energy and Enthalpy Calculations

Gas phase transition metal (M = Ni, Fe, Cr, Mo, W) -olefin bond formation energies ΔE, enthalpies ΔH, and free energy changes ΔG were all calculated using DFT in conjunction with the Spartan quantum chemistry software package. All calculations were carried out using the BP86 functional with a 6-311^{++}G** basis set for geometry optimization and frequency calculations. Tables 8 and 9 compare the calculated metal to olefin ΔE, ΔH, and ΔG values for the metal complexes under study. Based on thermodynamic convention, factors favorable for bonding are listed as negative and those unfavorable for bonding will be positive. It must be taken into consideration that calculated DFT/BP86 values may be overestimated.[39] Based on substituent effects, the $[M(CO)_xL\text{-}N(CH_3)_2]$ complex series of substituted olefins makes for stronger bonds than do the $[M(CO)_xL\text{-}NO_2]$ complex series. In regards to transition metal influence, our calculations indicate that bond formation energy should follow in general trend order of: $Mo(CO)_5 < Ni(CO)_3 < Cr(CO)_5 < W(CO)_5 < Fe(CO)_4$.

In all the results, one trend is clear: As the electron withdrawing ability of the para substituent increased, the strength of the metal olefin bonds decreases. On the basis of the DCD model, an increase in the electron-withdrawing (EWD) capacity of the para substituent should lead to an increase in the overall olefinic EWD ability, leading to an increase in π back-bonding and a stronger bond between the metal and the olefin.[1] Figures 24-29, however, indicate that this anticipated trend is not observed. In fact, these results indicate that the opposite occurs. Clearly, the magnitude of the metal-olefin bond energy is dependent on more than just the covalent orbital interactions ΔE_{oi}, on which the DCD model is solely based.

TABLE 8: Calculated ΔE, ΔH, and ΔG Values; [$M(CO)_5L$-Y] Complex Series.

$M(CO)_5L$- Y	ΔE	ΔH	ΔG
$Cr(CO)_5L$- NO_2	-24.34	-22.84	-6.60
$Cr(CO)_5L$- CN	-23.75	-23.02	-6.94
$Cr(CO)_5L$- COOH	-24.99	-23.54	-7.28
$Cr(CO)_5L$- COH	-24.82	-23.36	-7.24
$Cr(CO)_5L$- CF_3	-24.34	-23.64	-7.18
$Cr(CO)_5L$- $OCOCH_3$	-24.42	-23.60	-7.21
$Cr(CO)_5L$- H	-25.77	-24.23	-8.40
$Cr(CO)_5L$- CH_3	-25.41	-24.63	-8.69
$Cr(CO)_5L$- $C(CH_3)_3$	-25.41	-25.01	-8.77
$Cr(CO)_5L$- OH	-26.29	-24.87	-8.95
$Cr(CO)_5L$- OCH_3	-25.63	-24.96	-8.83
$Cr(CO)_5L$- $OC(CH_3)_3$	-25.40	-25.14	-8.74
$Cr(CO)_5L$- NH_3	-26.99	-25.56	-9.61
$Cr(CO)_5L$- $N(CH_3)_2$	-26.84	-26.27	-10.01
$Mo(CO)_5L$- NO_2	-20.08	-19.68	-3.13
$Mo(CO)_5L$- CN	-19.97	-19.88	-3.51
$Mo(CO)_5L$- COOH	-20.27	-20.37	-3.81
$Mo(CO)_5L$- COH	-20.20	-20.23	-3.81
$Mo(CO)_5L$- CF_3	-20.58	-20.45	-3.68
$Mo(CO)_5L$- $OCOCH_3$	-20.64	-20.39	-3.68
$Mo(CO)_5L$- H	-21.64	-21.14	-5.05
$Mo(CO)_5L$- CH_3	-21.64	-21.43	-5.22
$Mo(CO)_5L$- $C(CH_3)_3$	-21.75	-21.59	-4.78
$Mo(CO)_5L$- OH	-22.12	-21.65	-5.41
$Mo(CO)_5L$- OCH_3	-22.32	-21.83	-5.40
$Mo(CO)_5L$- $OC(CH_3)_3$	-21.68	-22.27	-5.64
$Mo(CO)_5L$- NH_3	-22.75	-22.44	-6.26
$Mo(CO)_5L$- $N(CH_3)_2$	-23.12	-22.81	-6.18
$W(CO)_5L$- NO_2	-25.03	-24.87	-8.23
$W(CO)_5L$- CN	-25.38	-25.02	-8.54
$W(CO)_5L$- COOH	-25.69	-25.48	-8.82
$W(CO)_5L$- COH	-25.54	-25.28	-8.77
$W(CO)_5L$- CF_3	-25.95	-25.56	-8.69
$W(CO)_5L$- $OCOCH_3$	-26.15	-25.56	-8.74
$W(CO)_5L$- H	-26.60	-26.23	-10.05
$W(CO)_5L$- CH_3	-27.06	-26.57	-10.25
$W(CO)_5L$- $C(CH_3)_3$	-27.16	-26.59	-9.62
$W(CO)_5L$- OH	-27.17	-26.90	-10.56
$W(CO)_5L$- OCH_3	-27.26	-26.82	-10.24
$W(CO)_5L$- $OC(CH_3)_3$	-26.94	-26.98	-10.10
$W(CO)_5L$- NH_3	-28.03	-27.77	-11.43
$W(CO)_5L$- $N(CH_3)_2$	-28.49	-28.00	-11.27

All reported values are in kcal/mol.

TABLE 9: Calculated ΔE, ΔH, and ΔG Values; [$M(CO)_xL$-Y] Complex Series.

$M(CO)_x$-L- Y	ΔE	ΔH	ΔG
$Fe(CO)_4L$- NO_2	-36.48	-35.28	-18.04
$Fe(CO)_4L$- CN	-36.63	-35.22	-18.14
$Fe(CO)_4L$- COOH	-36.64	-35.48	-18.25
$Fe(CO)_4L$- COH	-36.68	-35.33	-18.21
$Fe(CO)_4L$- CF_3	-36.91	-35.52	-18.09
Fe $(CO)_4L$- $OCOCH_3$	-36.51	-34.99	-17.64
Fe $(CO)_4L$- H	-36.81	-35.42	-18.60
Fe $(CO)_4L$- CH_3	-36.88	-35.60	-18.66
Fe $(CO)_4L$- $C(CH_3)_3$	-37.16	-35.82	-18.47
Fe $(CO)_4L$- OH	-36.74	-35.46	-18.51
Fe $(CO)_4L$- OCH_3	-36.89	-35.42	-18.25
Fe $(CO)_4L$- $OC(CH_3)_3$	-36.30	-35.59	-18.30
Fe $(CO)_4L$- NH_3	-37.04	-35.80	-18.88
Fe $(CO)_4L$- $N(CH_3)_2$	-37.38	-35.90	-18.68
$Ni(CO)_3L$- NO_2	-23.84	-23.52	-7.21
$Ni(CO)_3L$- CN	-24.07	-23.53	-7.38
$Ni(CO)_3L$- COOH	-24.21	-23.83	-7.51
$Ni(CO)_3L$- COH	-24.04	-23.77	-7.58
$Ni(CO)_3L$- CF_3	-24.38	-23.87	-7.38
$Ni(CO)_3L$- $OCOCH_3$	-24.26	-23.71	-7.28
$Ni(CO)_3L$- H	-24.54	-24.11	-8.18
$Ni(CO)_3L$- CH_3	-24.75	-24.42	-8.36
$Ni(CO)_3L$- $C(CH_3)_3$	-24.87	-24.73	-8.45
$Ni(CO)_3L$- OH	-24.74	-24.41	-8.39
$Ni(CO)_3L$- OCH_3	-24.83	-24.34	-8.08
$Ni(CO)_3L$- $OC(CH_3)_3$	-24.30	-24.68	-8.29
$Ni(CO)_3L$- NH_3	-25.08	24.70	-8.62
$Ni(CO)_3L$- $N(CH_3)_2$	-25.53	-24.97	-8.63

All reported values are in kcal/mol.

Trends in metal-olefin bond enthalpy as a function of substituent effect for the optimized structures under study are demonstrated in Figures 24-29. Graphical analysis was completed on the [$M(CO)_x(\eta^2$-C_2H_3-C_6H_4-Y)] complex series; where Y = NO_2, CN, COOH, H, OH, NH_2, $N(CH_3)_2$. It must be noted that the magnitude of the slope was indicated on each graph to serve as a relative measure of the overall change in bond enthalpy as a function of substituent effect and should follow in the order of: [$Mo(CO)_5$L-Y] < [$Ni(CO)_3$L-Y] ≤ [$Cr(CO)_5$L-Y] < [$W(CO)_5$L-Y] < [$Fe(CO)_4$L-Y].

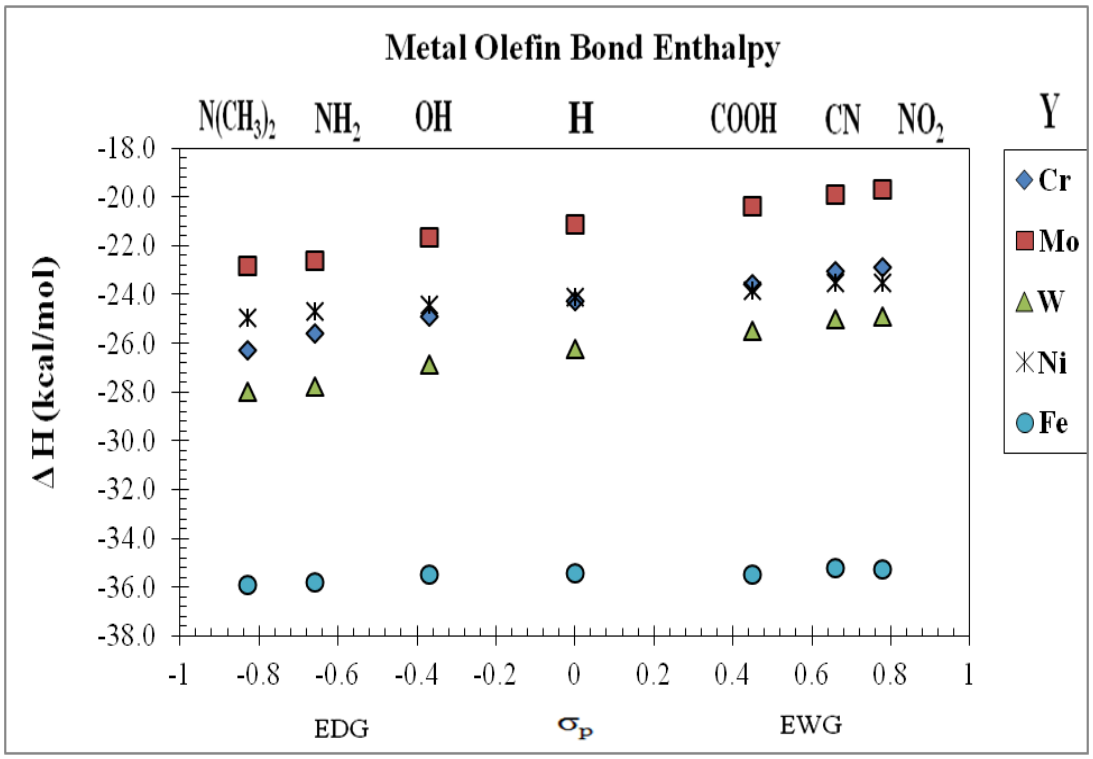

Figure 24. Graph of ΔH vs. σ_p for the [$M(CO)_xL$-Y] complex series.

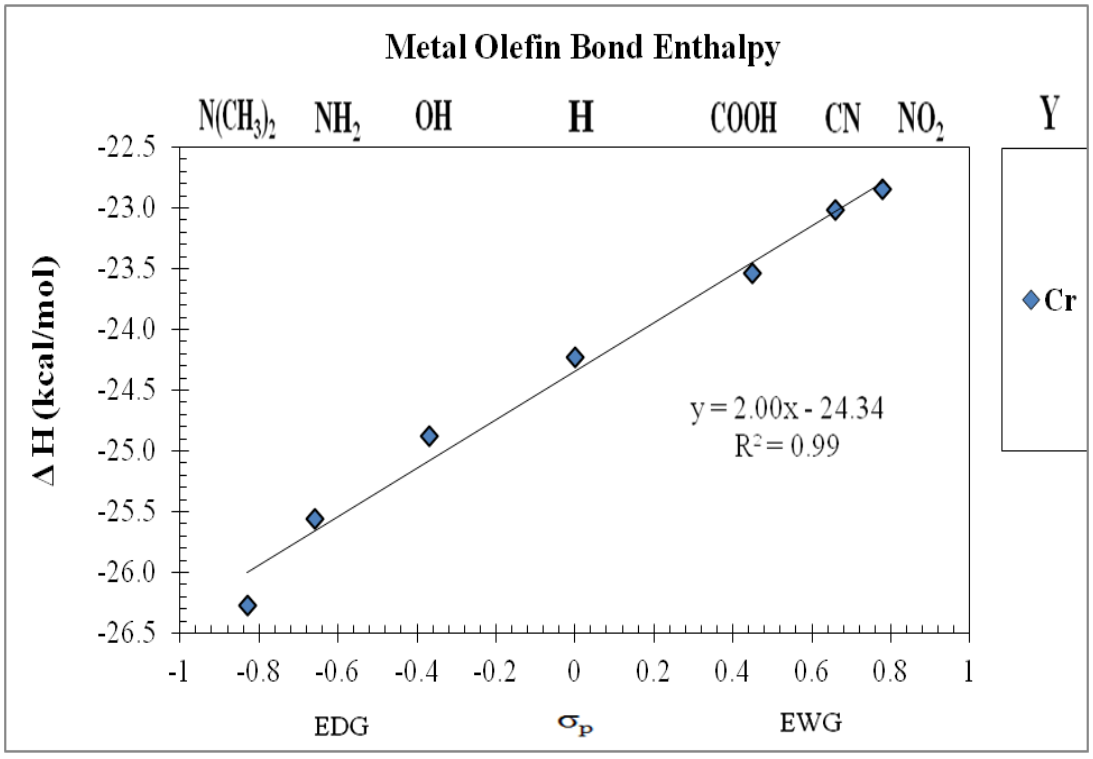

Figure 25. Graph of ΔH vs. σ_p for the [$Cr(CO)_5L$-Y] complex series.

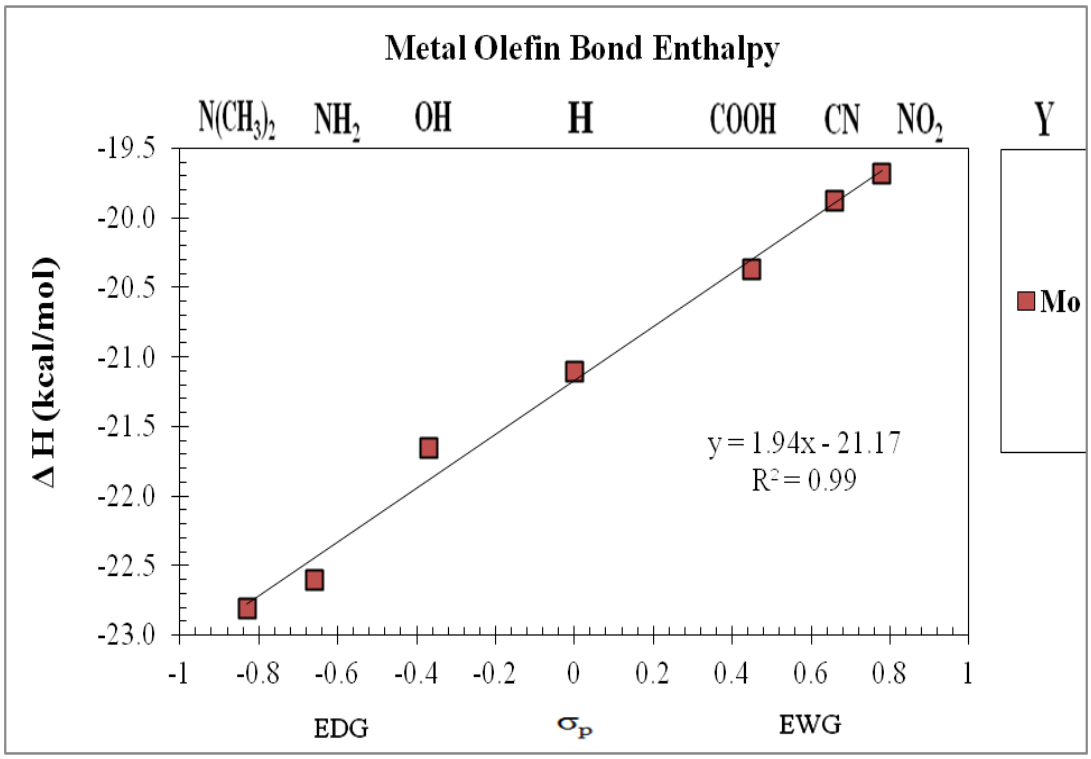

Figure 26. Graph of ΔH vs. σ_p for the $[Mo(CO)_5L\text{-}Y]$ complex series.

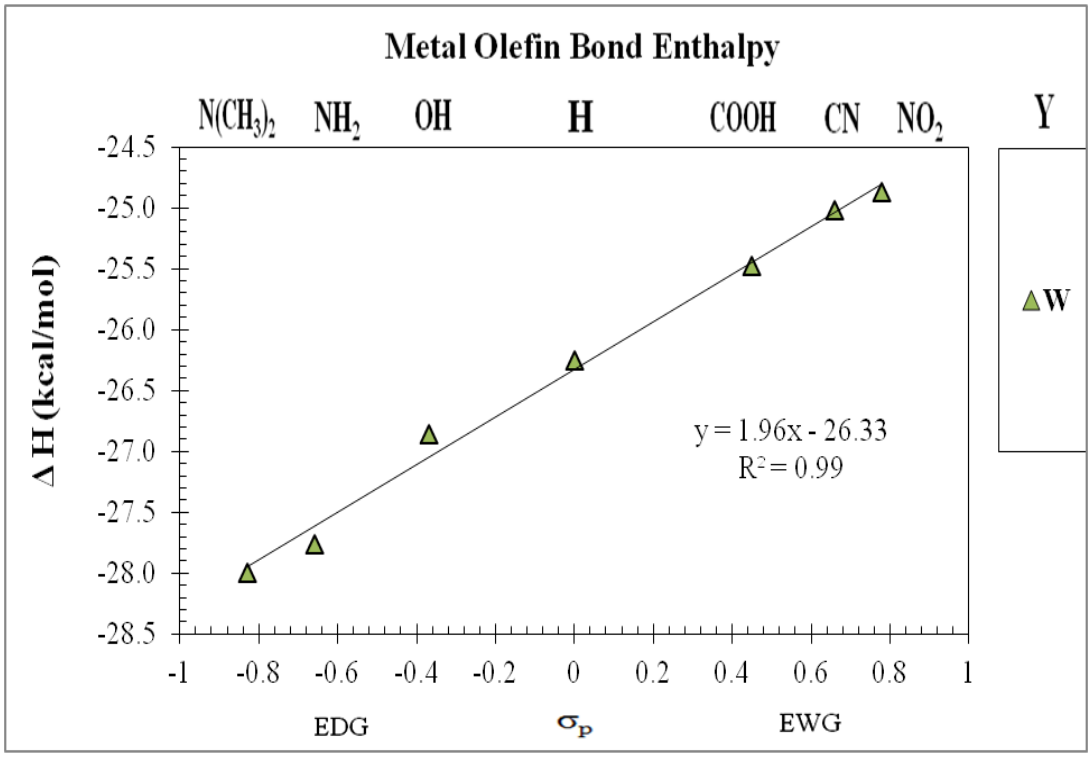

Figure 27. Graph of ΔH vs. σ_p for the $[W(CO)_5L\text{-}Y]$ complex series.

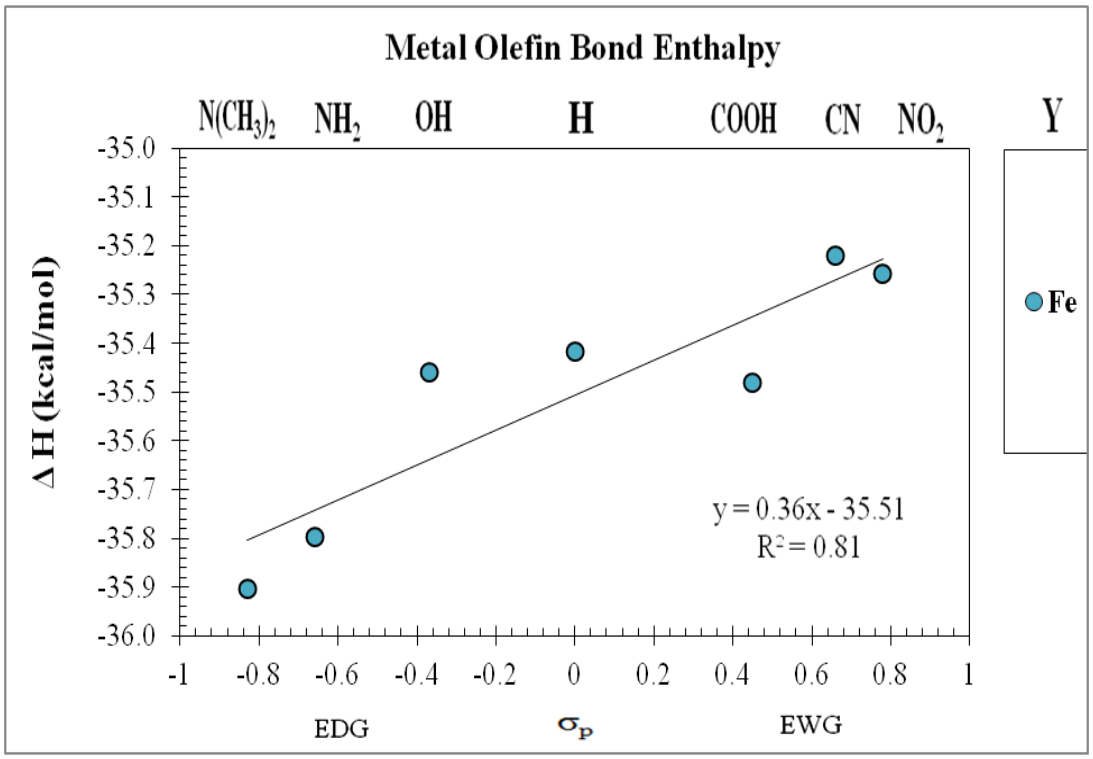

Figure 28. Graph of ΔH vs. σ_p for the [$Fe(CO)_4$L-Y] complex series.

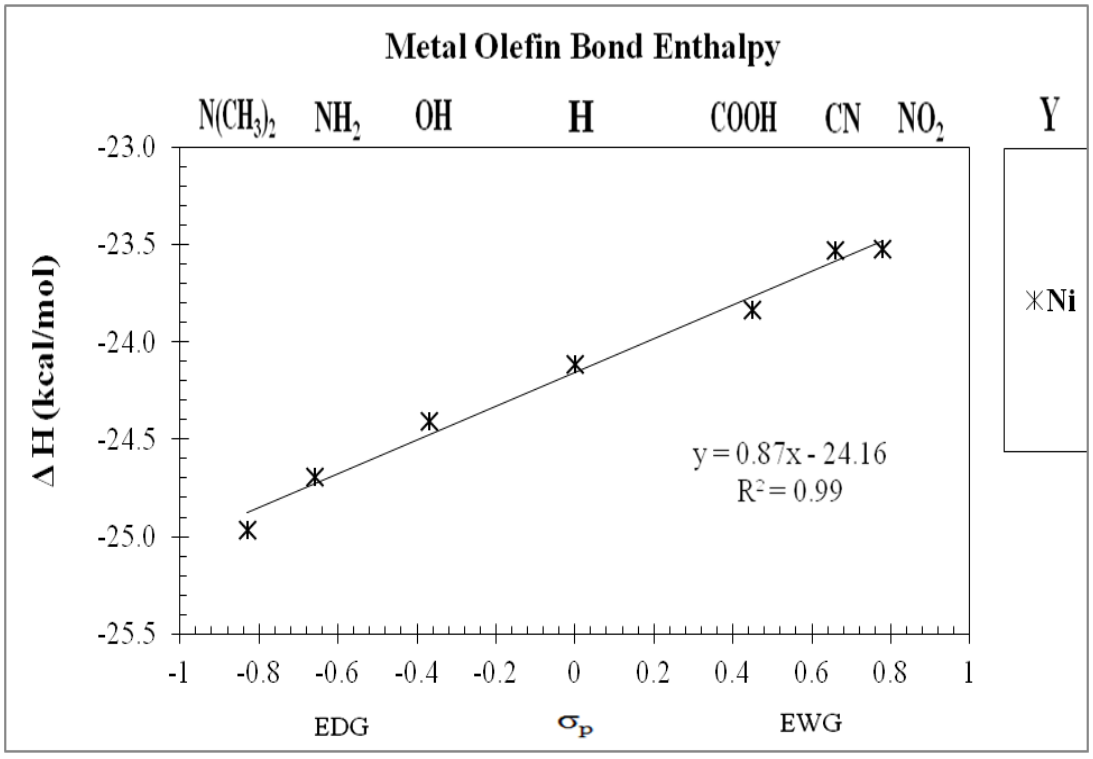

Figure 29. Graph of ΔH vs. σ_p for the [$Ni(CO)_3$L-Y] complex series.

The DCD Model from a Molecular Orbital Perspective

As mentioned in the Introduction, the DCD model provides a qualitative frontier molecular orbital description of the metal-olefin bonding interactions. We have carried out a *molecular orbital* (MO) analysis in order to describe such interactions quantitatively in terms of the DCD model implications. Plots showing the dependence of HOMO-LUMO energy gap, and the change in the electron population of the HOMO and LUMO of the olefin as a function of substituent modification are herein described. The MO analysis provides a view of frontier MO energies and electron populations in both the $M(CO)_x$ portion of the complex and the olefin. Figures 30-39 show calculated energy gaps and changes in electron populations for the frontier Mos involved in the σ and π interactions between both the $M(CO)_x$ complex and the olefin. The determination of the σ *Energy Gap* parameters listed in Table 12 was made by taking the difference between the LUMO of the transition metal and the HOMO of a given olefin; whereas, the energy gap for the π transition was made by taking the difference between the HOMO of a given metal and the LUMO of a select olefin. Figures 30-34 noticeably demonstrate that the energy difference between the HOMO of the olefin and the LUMO of the $M(CO)_x$ fragments are affected by modification of the para substituent, with electron-withdrawing substituents noticeably favoring π interaction as manifested by a reduction in the π energy gap and electron-donating substituents favoring the σ interaction as described by an observed decrease in the σ energy gap. Clearly, as the *electron-withdrawing* capacity diminishes, the π interaction between the two molecular orbitals becomes considerably less favorable and the σ interaction begins to predominate. This trend is observed for all metals and is in agreement with the foundations of the DCD bonding model.

The electron-accepting and –donating capabilities of a ligand can be quantitatively evaluated on the basis of how the populations of the ligand orbitals change in going from a free to a bound ligand. The changes in Mulliken electron orbital population in the HOMO and LUMO of the olefin (Figures 35-39) reflect the trends observed in orbital energy gaps described above. Tables 10-11 contain the results from the most relevant calculations. It is evident that there is a greater transfer of electron density as the electron-withdrawing effect increases, mostly as a result of the π back-bonding interaction. In terms of the σ interaction, the amount of electron density transferred decreases slightly as the electron-withdrawing effect increase as a result of the decrease in the orbital overlap imposed by steric constraints. Thus, from a molecular orbital perspective the back-bonding dominates the metal-olefin interaction, in good agreement with the DCD model that predicts that an olefin with more electron-withdrawing potential should be more favorable for bonding. The influence of the σ bonding is smaller and seems to have an opposite destabilizing effect as the electron-withdrawing capacity of the para substituent increases.

The molecular orbital analyses allow us to conclude that the olefins with more electron-withdrawing capacity are much better π bonders, although they are slightly worse as σ bonders. It also tells us that the metal-olefin interaction is dominated by the π interaction and thus an olefin would bond stronger to $M(CO)_x$ in direct proportion to the electron-withdrawing capacity of the para substituent. However, the calculated M-olefin bond enthalpies show a trend opposite to the expected trend from this molecular orbital perspective (on which the DCD model is based). How can then we explain such a contradiction?

TABLE 10: HOMO-LUMO Energy Levels for the [$M(CO)_xL$-Y] Complex Series.

$M(CO)_xL$- Y	$HOMO_{OLEFIN}$	$LUMO_{OLEFIN}$	$HOMO_{METAL}$	$LUMO_{METAL}$
$Cr(CO)_5L$- NO_2	-0.235	-0.140	-0.231	-0.166
$Cr(CO)_5L$- CN	-0.229	-0.118	-0.231	-0.166
$Cr(CO)_5L$- COOH	-0.222	-0.112	-0.232	-0.166
$Cr(CO)_5L$- H	-0.206	-0.085	-0.232	-0.167
$Cr(CO)_5L$- OH	-0.191	-0.077	-0.233	-0.167
$Cr(CO)_5L$- NH_2	-0.195	-0.083	-0.233	-0.168
$Cr(CO)_5L$- $N(CH_3)_2$	-0.163	-0.063	-0.233	-0.168
$Mo(CO)_5L$- NO_2	-0.236	-0.139	-0.231	-0.153
$Mo(CO)_5L$- CN	-0.229	-0.116	-0.231	-0.153
$Mo(CO)_5L$- COOH	-0.207	-0.092	-0.231	-0.153
$Mo(CO)_5L$- H	-0.206	-0.082	-0.232	-0.154
$Mo(CO)_5L$- OH	-0.191	-0.074	-0.232	-0.154
$Mo(CO)_5L$- NH_2	-0.175	-0.066	-0.232	-0.154
$Mo(CO)_5L$- $N(CH_3)_2$	-0.163	-0.060	-0.232	-0.155
$W(CO)_5L$- NO_2	-0.235	-0.140	-0.236	-0.156
$W(CO)_5L$- CN	-0.229	-0.118	-0.236	-0.156
$W(CO)_5L$- COOH	-0.222	-0.112	-0.237	-0.156
$W(CO)_5L$- H	-0.206	-0.084	-0.237	-0.157
$W(CO)_5L$- OH	-0.191	-0.076	-0.237	-0.157
$W(CO)_5L$- NH_2	-0.175	-0.068	-0.238	-0.158
$W(CO)_5L$- $N(CH_3)_2$	-0.164	-0.062	-0.238	-0.158
$Fe(CO)_4L$- NO_2	-0.236	-0.142	-0.198	-0.174
$Fe(CO)_4L$- CN	-0.230	-0.122	-0.198	-0.174
$Fe(CO)_4L$- COOH	-0.221	-0.112	-0.199	-0.175
Fe $(CO)_4L$- H	-0.207	-0.090	-0.199	-0.175
Fe $(CO)_4L$- OH	-0.193	-0.082	-0.200	-0.175
Fe $(CO)_4L$- NH_2	-0.178	-0.075	-0.200	-0.175
Fe $(CO)_4L$- $N(CH_3)_2$	-0.165	-0.069	-0.201	-0.175
$Ni(CO)_3L$- NO_2	-0.236	-0.14	-0.223	-0.139
$Ni(CO)_3L$- CN	-0.229	-0.118	-0.223	-0.139
$Ni(CO)_3L$- $COOCH_3$	-0.222	-0.112	-0.223	-0.139
$Ni(CO)_3L$- H	-0.207	-0.084	-0.223	-0.139
$Ni(CO)_3L$- OH	-0.191	-0.077	-0.225	-0.140
$Ni(CO)_3L$- NH_2	-0.176	-0.079	-0.225	-0.140
$Ni(CO)_3L$- $N(CH_3)_2$	-0.164	-0.063	-0.225	-0.140

All reported values are in atomic units (au).

The tables below summarize the results from the molecular orbital analysis. The energy gap (in atomic units) is between the HOMO and LUMO for each particular interaction (sigma or pi). The population change is the difference in HOMO or LUMO population in the olefin upon binding during metal-olefin bond formation.

TABLE 11: HOMO-LUMO Energy Gap for the [$M(CO)_xL$-Y] Complex Series.

$M(CO)_xL$- Y	σ Energy Gap	π Energy Gap	Bond Order
$Cr(CO)_5L$- NO_2	0.069	0.091	1.690
$Cr(CO)_5L$- CN	0.063	0.113	1.730
$Cr(CO)_5L$- COOH	0.056	0.120	1.695
$Cr(CO)_5L$- H	0.039	0.147	1.705
$Cr(CO)_5L$- OH	0.024	0.156	1.715
$Cr(CO)_5L$- NH_2	0.027	0.150	1.715
$Cr(CO)_5L$- $N(CH_3)_2$	0.000	0.170	1.730
$Mo(CO)_5L$- NO_2	0.083	0.092	1.775
$Mo(CO)_5L$- CN	0.076	0.115	1.775
$Mo(CO)_5L$- COOH	0.054	0.139	1.780
$Mo(CO)_5L$- H	0.052	0.150	1.795
$Mo(CO)_5L$- OH	0.037	0.158	1.800
$Mo(CO)_5L$- NH_2	0.021	0.166	1.805
$Mo(CO)_5L$- $N(CH_3)_2$	0.008	0.172	1.805
$W(CO)_5L$- NO_2	0.079	0.096	1.750
$W(CO)_5L$- CN	0.073	0.118	1.760
$W(CO)_5L$- COOH	0.066	0.125	1.760
$W(CO)_5L$- H	0.049	0.153	1.770
$W(CO)_5L$- OH	0.034	0.161	1.780
$W(CO)_5L$- NH_2	0.017	0.170	1.785
$W(CO)_5L$- $N(CH_3)_2$	0.006	0.176	1.800
$Fe(CO)_4L$- NO_2	0.062	0.056	1.705
$Fe(CO)_4L$- CN	0.056	0.076	1.710
$Fe(CO)_4L$- COOH	0.046	0.087	1.715
$Fe\ (CO)_4L$- H	0.032	0.109	1.715
$Fe\ (CO)_4L$- OH	0.018	0.118	1.725
$Fe\ (CO)_4L$- NH_2	0.003	0.125	1.725
$Fe\ (CO)_4L$- $N(CH_3)_2$	0.000	0.132	1.730
$Ni(CO)_3L$- NO_2	0.097	0.083	1.495
$Ni(CO)_3L$- CN	0.090	0.105	1.500
$Ni(CO)_3L$- COOH	0.083	0.111	1.505
$Ni(CO)_3L$- H	0.068	0.139	1.520
$Ni(CO)_3L$- OH	0.051	0.148	1.515
$Ni(CO)_3L$- NH_2	0.036	0.146	1.525
$Ni(CO)_3L$- $N(CH_3)_2$	0.024	0.162	1.525

All reported values are in atomic units (au).

Tables 12-15 show the general BEDA Energy Distribution for the [$M(CO)_xL$-Y] Complex Series. Figures 40-86 show the general trends obtained for the [$M(CO)_x(\eta^2$-C_2H_3-C_6H_4-Y)] complex series; where Y = NO_2, CN, COOH, H, OH, NH_2, $N(CH_3)_2$.

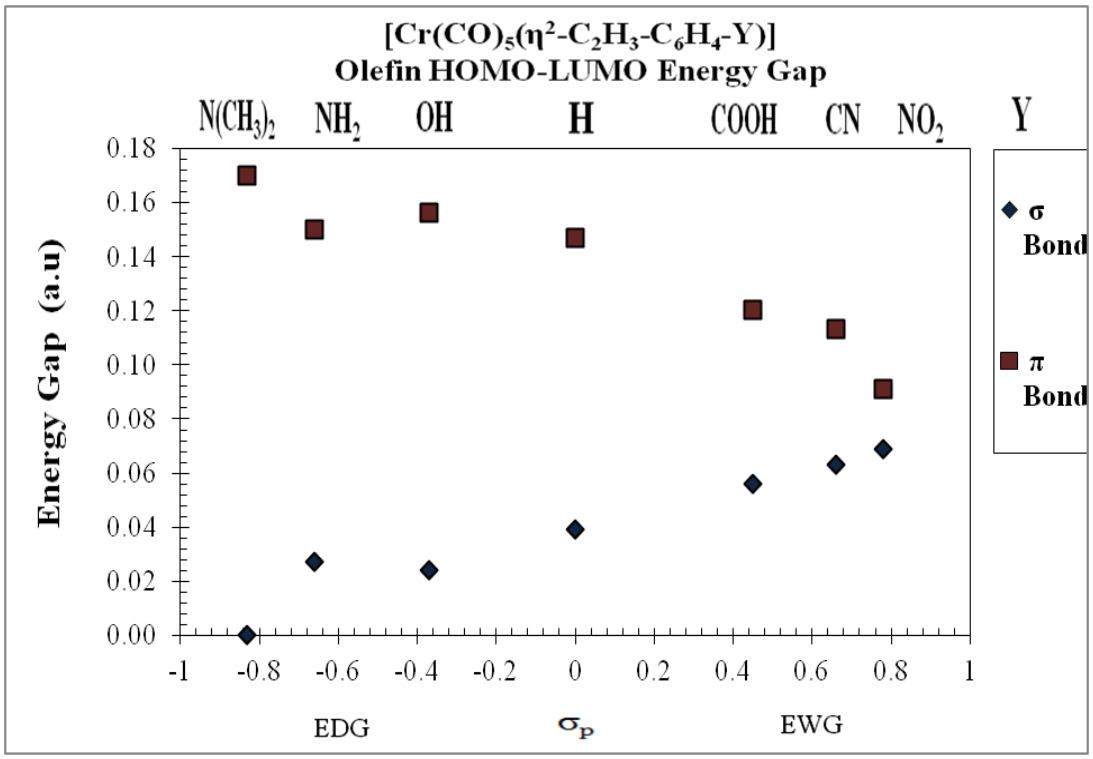

Figure 30. Graph of the Olefin Energy Gap for the $[Cr(CO)_5L\text{-}Y]$ complex series.

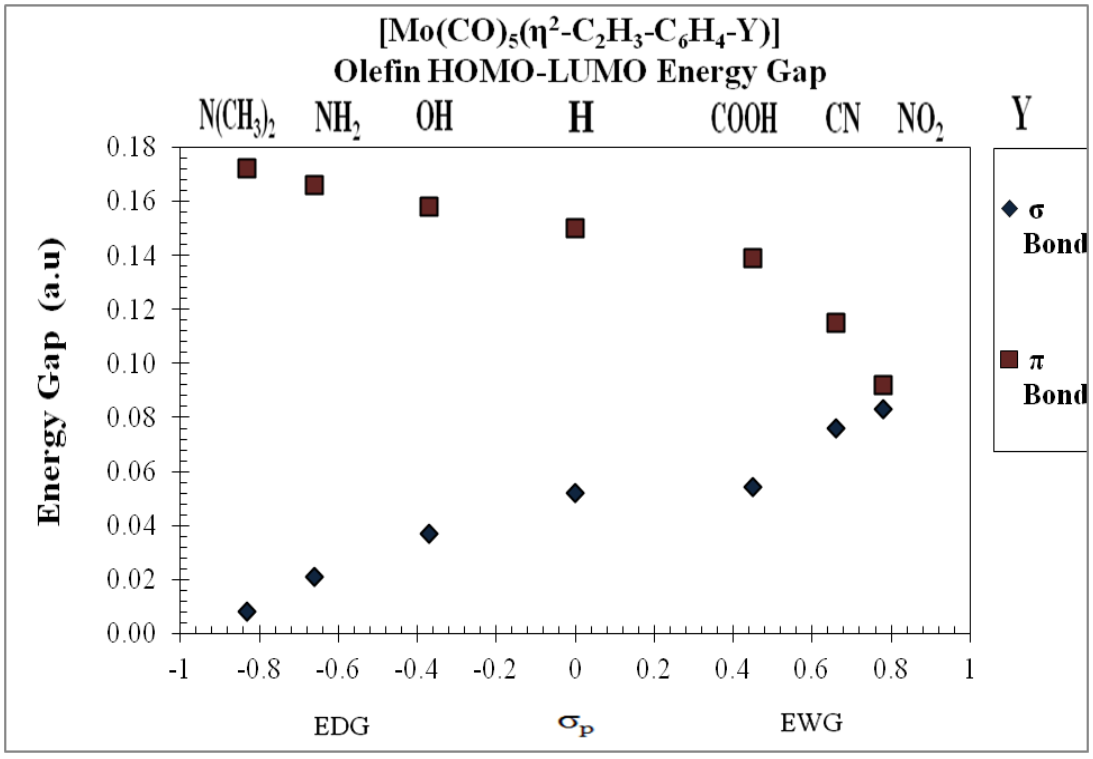

Figure 31. Graph of the Olefin Energy Gap for the $[Mo(CO)_5L\text{-}Y]$ complex series.

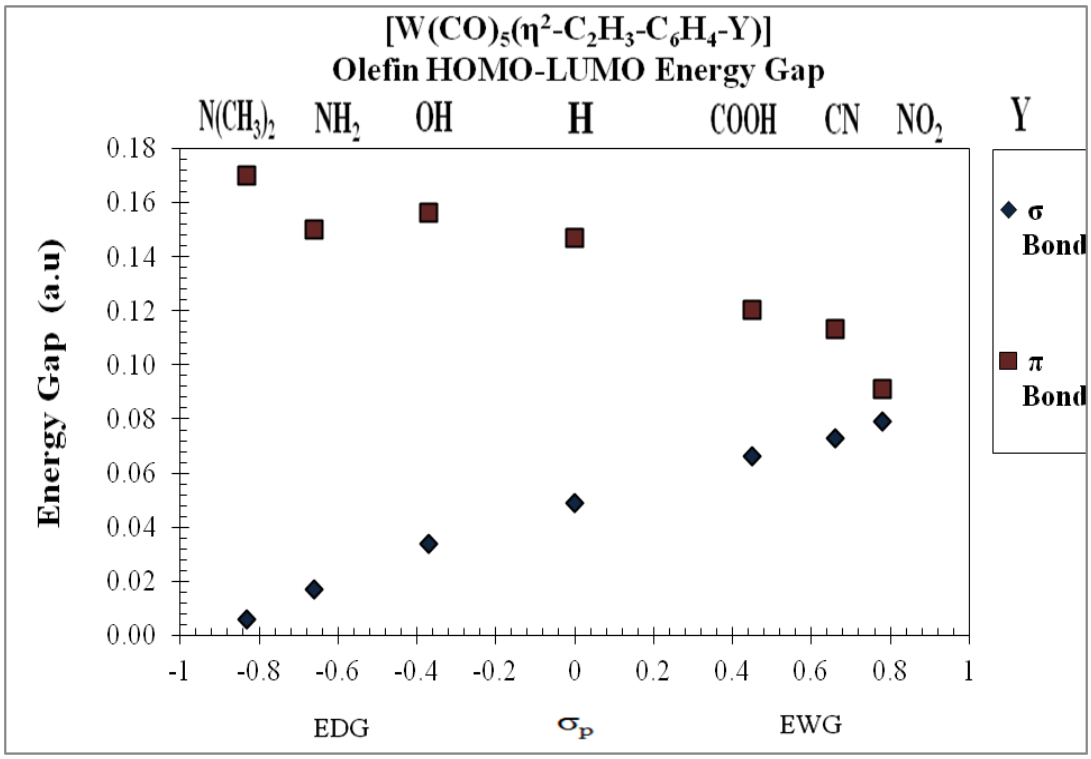

Figure 32. Graph of the Olefin Energy Gap for the $[W(CO)_5L\text{-}Y]$ complex series.

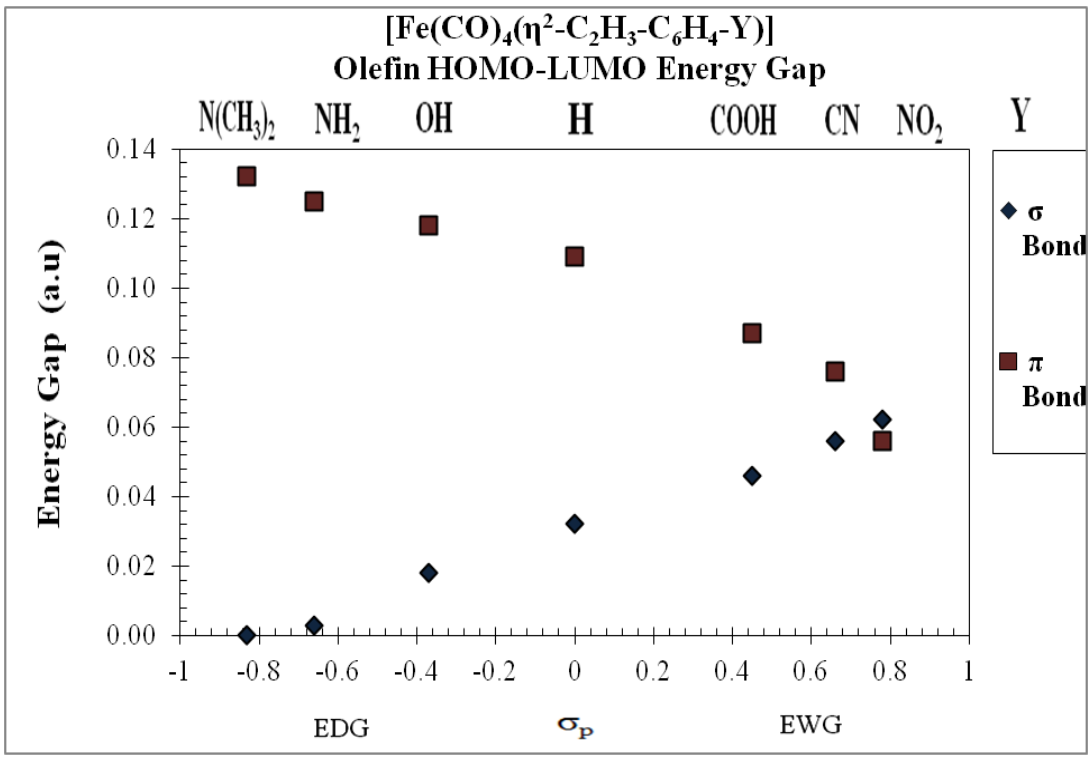

Figure 33. Graph of the Olefin Energy Gap for the $[Fe(CO)_4L\text{-}Y]$ complex series.

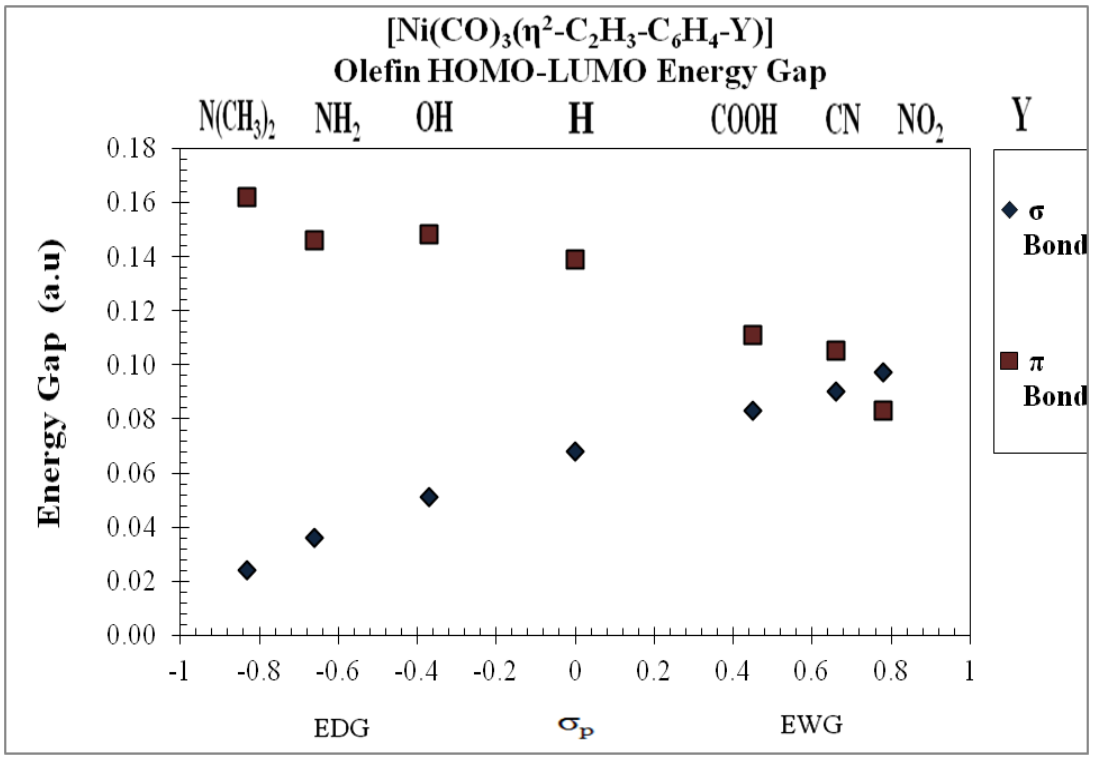

Figure 34. Graph of the Olefin Energy Gap for the [$Ni(CO)_3$L-Y] complex series.

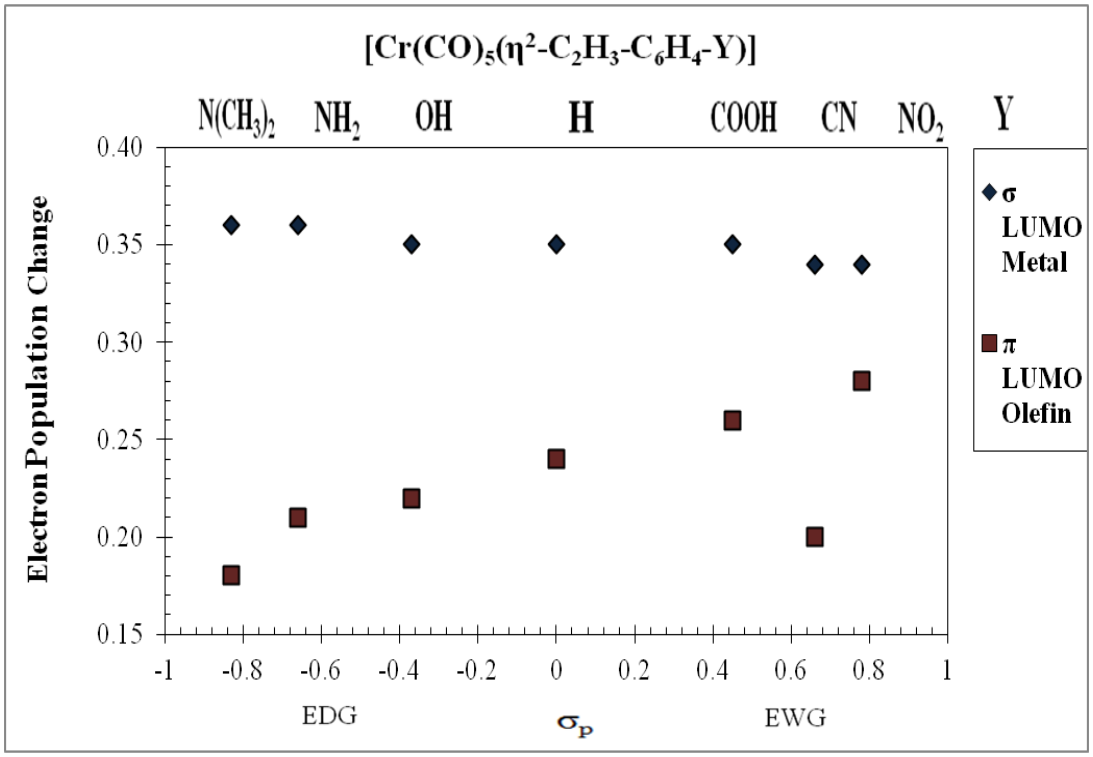

Figure 35. Mulliken Population Analysis for the [$Cr(CO)_5$L-Y] complex series.

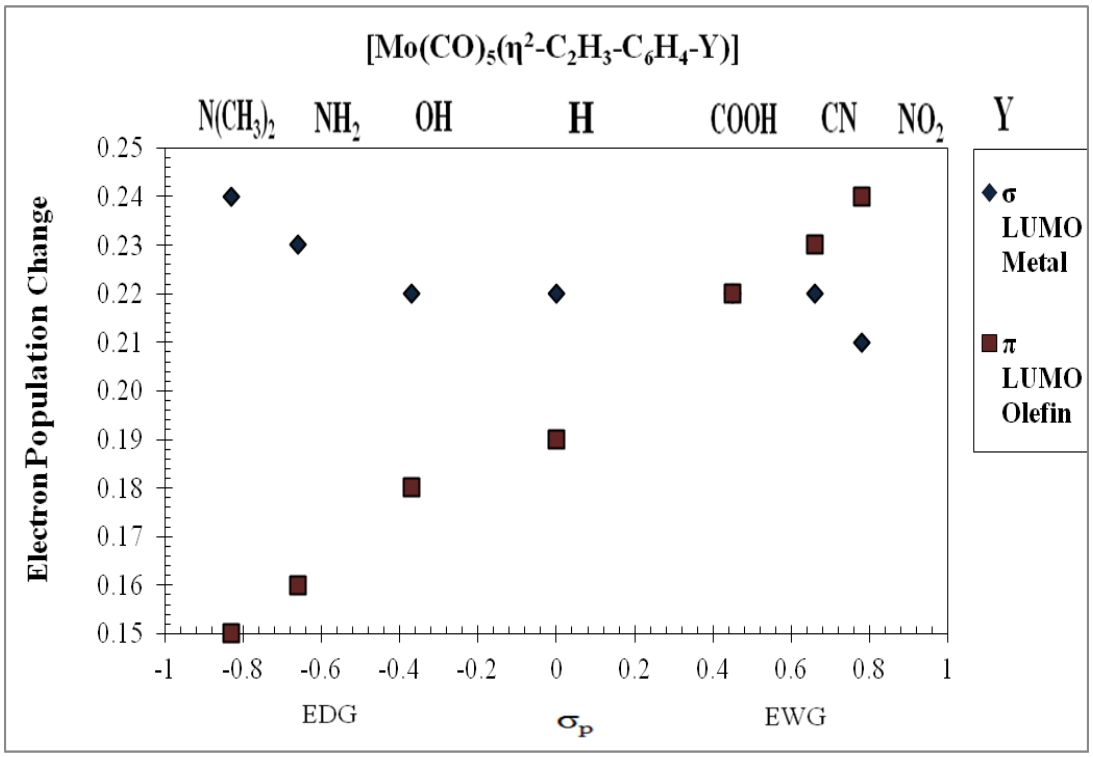

Figure 36. Mulliken Population Analysis for the $[Mo(CO)_5L\text{-}Y]$ complex series.

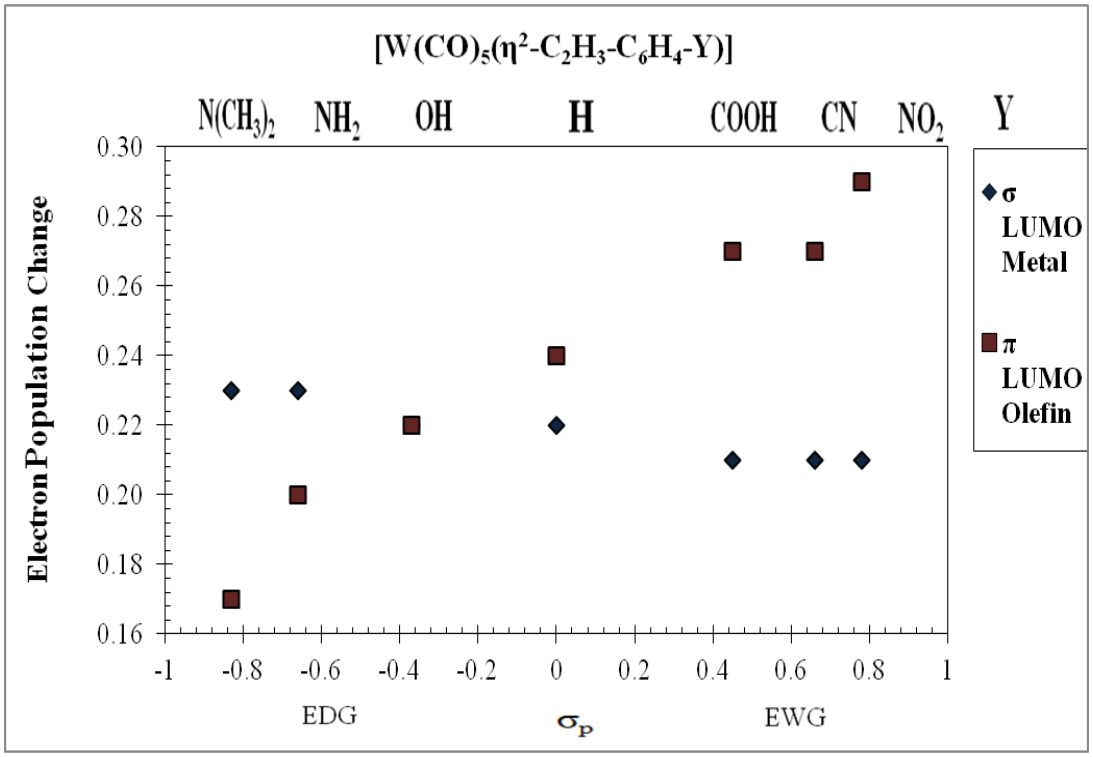

Figure 37. Mulliken Population Analysis for the $[W(CO)_5L\text{-}Y]$ complex series

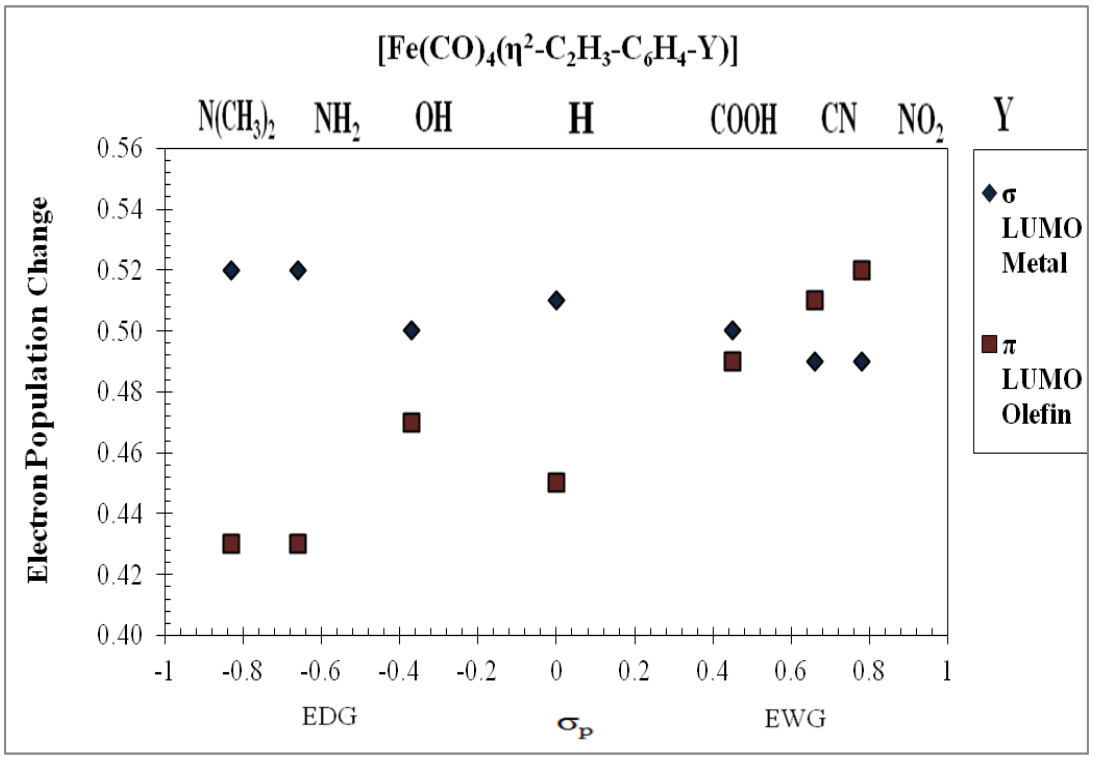

Figure 38. Mulliken Population Analysis for the $[Fe(CO)_4L\text{-}Y]$ complex series.

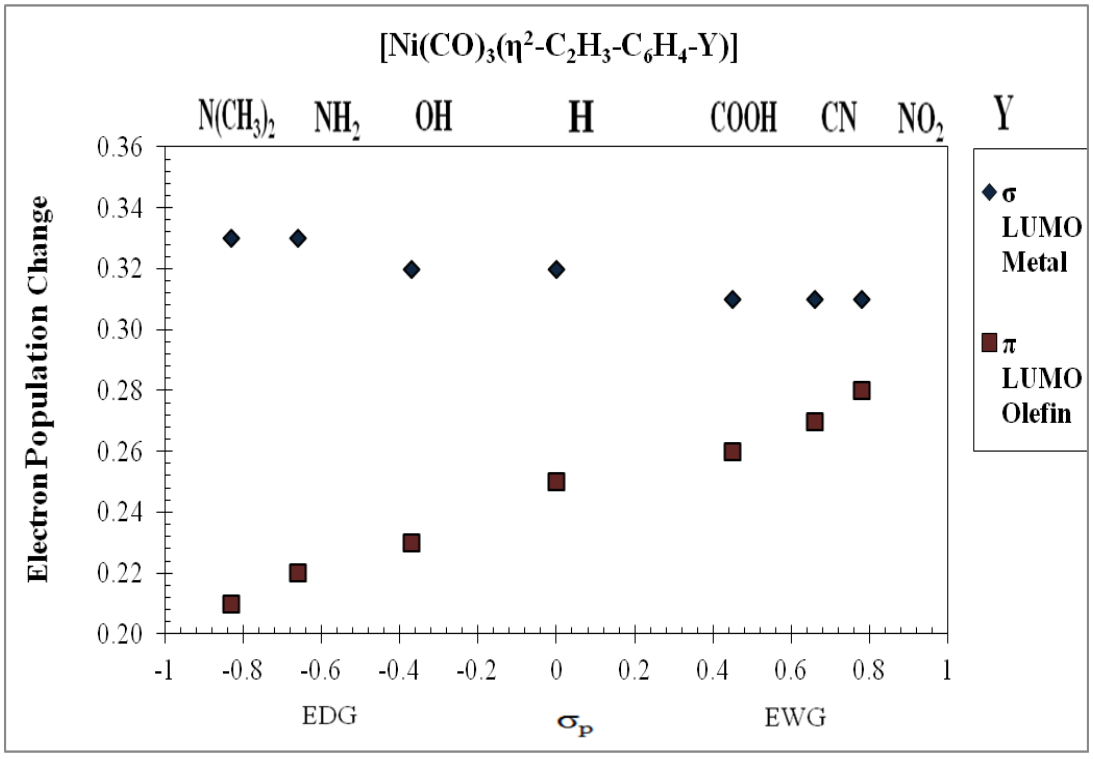

Figure 39. Mulliken Population Analysis for the $[Ni(CO)_3L\text{-}Y]$ complex series.

BEDA Energy Distribution: Extending the Scope of the DCD Model

Metal-olefin bond energy decomposition analyses provide an answer to the contradiction between the calculated bond energies and the expectation based on a MO analysis and the DCD model. A bond energy decomposition analysis is carried out that breaks down the net bonding formation energy of a metal and olefin into four component energy terms according to Eq. (8): $\Delta E_{int} = \Delta E_{elect} + \Delta E_{oi} + \Delta E_{pauli.}$ The changes that occur in all of these components were compared in relation to one another and in terms of their contribution to the total bond energy $\Delta E = \Delta E_{int} + \Delta E_{reorg}$.

In all the results, one trend is obvious: As the EWD capacity of the para substituent increases, the strength of the metal olefin bond decreases. On the basis of the Dewar-Chatt-Duncanson model, an increase in the EWD potential of the para substituent should increase its electron-withdrawing ability, leading to an increase in back-bonding and a stronger bond between the metal and the olefin.[1] Thus, the results indicate that this anticipated trend is not observed. In fact, the results indicate that the suggested trends run counter to predictions of the DCD bonding model interpretations. Some explanations of this discrepancy were found within the data set. Clearly, the magnitude of the metal-olefin bond energy is dependent on more than just the covalent frontier orbital interactions in which the DCD model is solely based. The computational data shows that the DCD model does not consider all the variables involved in metal-olefin bonding interactions. The bond energy ΔE calculations consider the sum of both reorganization costs ΔE_{reorg} and the interaction energy ΔE_{int} which accounts for both attractive (favorable to bonding: ΔE_{oi} and ΔE_{elect}) and repulsive (unfavorable to bonding: ΔE_{pauli}) contributions. Reorganization costs thermodynamically oppose bond formation.

TABLE 12: BEDA Energy Distribution for the [$M(CO)_5L$-Y] Complex Series.

$M(CO)_5L$- Y	ΔE_{oi}	ΔE_{elect}	ΔE_{pauli}
$Cr(CO)_5L$- NO_2	-55.80	-55.45	84.94
$Cr(CO)_5L$- CN	-55.69	-55.04	84.37
$Cr(CO)_5L$- COOH	-54.51	-56.20	84.13
$Cr(CO)_5L$- COH	-54.48	-55.36	83.50
$Cr(CO)_5L$- CF_3	-54.19	-55.95	83.66
$Cr(CO)_5L$- $OCOCH_3$	-53.43	-56.70	83.53
$Cr(CO)_5L$- H	-52.68	-57.10	82.73
$Cr(CO)_5L$- CH_3	-52.26	-57.49	82.58
$Cr(CO)_5L$- $C(CH_3)_3$	-52.11	-57.52	82.49
$Cr(CO)_5L$- OH	-51.23	-56.97	81.07
$Cr(CO)_5L$- OCH_3	-50.33	-56.19	79.35
$Cr(CO)_5L$- $OC(CH_3)_3$	-50.56	-57.26	80.35
$Cr(CO)_5L$- NH_3	-49.80	-56.51	78.83
$Cr(CO)_5L$- $N(CH_3)_2$	-48.50	-55.83	76.69
$Mo(CO)_5L$- NO_2	-44.20	-47.06	68.67
$Mo(CO)_5L$- CN	-43.19	-46.91	67.49
$Mo(CO)_5L$- COOH	-42.64	-47.37	67.15
$Mo(CO)_5L$- COH	-42.46	-46.24	66.26
$Mo(CO)_5L$- CF_3	-42.05	-46.67	66.20
$Mo(CO)_5L$- $OCOCH_3$	-41.87	-48.21	67.21
$Mo(CO)_5L$- H	-40.73	-47.94	65.36
$Mo(CO)_5L$- CH_3	-40.32	-48.34	65.13
$Mo(CO)_5L$- $C(CH_3)_3$	-40.08	-48.20	64.81
$Mo(CO)_5L$- OH	-39.44	-48.06	64.03
$Mo(CO)_5L$- OCH_3	-38.96	-47.70	63.25
$Mo(CO)_5L$- $OC(CH_3)_3$	-38.42	-47.76	62.47
$Mo(CO)_5L$- NH_3	-38.30	-47.81	62.04
$Mo(CO)_5L$- $N(CH_3)_2$	-37.67	-47.85	61.20
$W(CO)_5L$- NO_2	-57.65	-61.82	89.40
$W(CO)_5L$- CN	-56.52	-61.74	88.18
$W(CO)_5L$- COOH	-55.45	-61.73	87.07
$W(CO)_5L$- COH	-55.58	-60.73	86.43
$W(CO)_5L$- CF_3	-54.91	-60.96	85.97
$W(CO)_5L$- $OCOCH_3$	-54.53	-62.59	86.95
$W(CO)_5L$- H	-53.83	-63.26	86.60
$W(CO)_5L$- CH_3	-53.00	-63.13	85.35
$W(CO)_5L$- $C(CH_3)_3$	-52.47	-62.65	84.48
$W(CO)_5L$- OH	-52.47	-62.65	84.48
$W(CO)_5L$- OCH_3	-50.21	-60.45	80.26
$W(CO)_5L$- $OC(CH_3)_3$	-50.80	-62.34	82.14
$W(CO)_5L$- NH_3	-50.41	-62.26	81.41
$W(CO)_5L$- $N(CH_3)_2$	-49.32	-61.48	79.59

All reported values are in kcal/mol.

TABLE 13: BEDA Energy Distribution for the [$M(CO)_xL$-Y] Complex Series.

$M(CO)_xL$- Y	ΔE_{oi}	ΔE_{elect}	ΔE_{pauli}
$Fe(CO)_4L$- NO_2	-84.77	-89.45	128.10
$Fe(CO)_4L$- CN	-84.40	-90.71	128.99
$Fe(CO)_4L$- COOH	-83.23	-90.59	128.02
$Fe(CO)_4L$- COH	-83.74	-90.05	127.84
$Fe(CO)_4L$- CF_3	-83.57	-91.38	129.02
Fe $(CO)_4L$- $OCOCH_3$	-82.52	-91.79	128.70
Fe $(CO)_4L$- H	-81.71	-92.86	128.88
Fe $(CO)_4L$- CH_3	-80.65	-92.81	128.15
Fe $(CO)_4L$- $C(CH_3)_3$	-81.20	-93.47	126.01
Fe $(CO)_4L$- OH	-79.39	-92.29	126.83
Fe $(CO)_4L$- OCH_3	-79.03	-92.30	126.58
Fe $(CO)_4L$- $OC(CH_3)_3$	-78.33	-92.38	126.01
Fe $(CO)_4L$- NH_3	-77.78	-92.13	125.34
Fe $(CO)_4L$- $N(CH_3)_2$	-76.96	-92.28	124.79
$Ni(CO)_3L$- NO_2	-56.94	-79.00	109.95
$Ni(CO)_3L$- CN	-56.37	-79.58	110.03
$Ni(CO)_3L$- COOH	-55.66	-79.55	109.31
$Ni(CO)_3L$- COH	-55.90	-79.10	109.26
$Ni(CO)_3L$- CF_3	-55.69	-79.89	109.66
$Ni(CO)_3L$- $OCOCH_3$	-54.65	-80.19	109.18
$Ni(CO)_3L$- H	-53.84	-80.25	108.19
$Ni(CO)_3L$- CH_3	-53.35	-80.47	107.90
$Ni(CO)_3L$- $C(CH_3)_3$	-53.61	-81.02	108.64
$Ni(CO)_3L$- OH	-52.56	-80.18	106.97
$Ni(CO)_3L$- OCH_3	-52.53	-80.51	107.23
$Ni(CO)_3L$- $OC(CH_3)_3$	-51.82	-80.08	106.33
$Ni(CO)_3L$- NH_3	-51.53	-79.86	105.55
$Ni(CO)_3L$- $N(CH_3)_2$	-50.97	-80.06	105.05

All reported values are in kcal/mol.

Tables 12-13 contain a select list of BEDA Energy distribution parameters resulting from the ΔE_{oi}, ΔE_{elect}, and ΔE_{pauli} determinations based on calculations using Eq. (5) for the [$M(CO)_xL$-Y] complex series. Tables 14-15 provide select BEDA Energy distribution calculations resulting from ΔE_{int}, ΔE, and ΔE_{reorg} determinations for the [$M(CO)_xL$-Y] complex series. Figures 40-86 show graphical comparisons of the general trends obtained in metal-olefin bond energies calculated from Eq. (5), as well as the trends obtained resulting from the bond energy decomposition analysis.

TABLE 14: BEDA Energy Distribution for the [$M(CO)_5L$-Y] Complex Series.

$M(CO)_5L$- Y	ΔE_{int}	ΔE	ΔE_{reorg}
$Cr(CO)_5L$- NO_2	-26.31	-17.40	8.91
$Cr(CO)_5L$- CN	-26.36	-17.63	8.73
$Cr(CO)_5L$- COOH	-26.58	-17.94	8.64
$Cr(CO)_5L$- COH	-26.34	-17.90	8.44
$Cr(CO)_5L$- CF_3	-26.48	-17.97	8.51
$Cr(CO)_5L$- $OCOCH_3$	-26.61	-18.16	8.45
$Cr(CO)_5L$- H	-27.05	-18.79	8.26
$Cr(CO)_5L$- CH_3	-27.16	-19.36	7.80
$Cr(CO)_5L$- $C(CH_3)_3$	-27.14	-19.27	7.87
$Cr(CO)_5L$- OH	-27.13	-19.33	7.80
$Cr(CO)_5L$- OCH_3	-27.17	-19.64	7.53
$Cr(CO)_5L$- $OC(CH_3)_3$	-27.47	-19.76	7.71
$Cr(CO)_5L$- NH_3	-27.47	-19.93	7.54
$Cr(CO)_5L$- $N(CH_3)_2$	-27.65	-20.60	7.05
$Mo(CO)_5L$- NO_2	-22.59	-16.80	5.79
$Mo(CO)_5L$- CN	-22.61	-17.01	5.60
$Mo(CO)_5L$- COOH	-22.85	-17.32	5.53
$Mo(CO)_5L$- COH	-22.45	-17.25	5.20
$Mo(CO)_5L$- CF_3	-22.51	-17.27	5.24
$Mo(CO)_5L$- $OCOCH_3$	-22.87	-17.48	5.39
$Mo(CO)_5L$- H	-23.31	-18.04	5.27
$Mo(CO)_5L$- CH_3	-23.54	-18.61	4.93
$Mo(CO)_5L$- $C(CH_3)_3$	-23.47	-18.44	5.03
$Mo(CO)_5L$- OH	-23.48	-18.51	4.97
$Mo(CO)_5L$- OCH_3	-23.41	-18.79	4.62
$Mo(CO)_5L$- $OC(CH_3)_3$	-23.71	-19.00	4.71
$Mo(CO)_5L$- NH_3	-24.07	-19.22	4.85
$Mo(CO)_5L$- $N(CH_3)_2$	-24.32	-19.66	4.66
$W(CO)_5L$- NO_2	-30.07	-22.59	7.48
$W(CO)_5L$- CN	-30.08	-22.85	7.23
$W(CO)_5L$- COOH	-30.12	-23.06	7.06
$W(CO)_5L$- COH	-29.87	-23.09	6.78
$W(CO)_5L$- CF_3	-29.90	-23.13	6.77
$W(CO)_5L$- $OCOCH_3$	-30.17	-23.23	6.94
$W(CO)_5L$- H	-30.50	-23.81	6.69
$W(CO)_5L$- CH_3	-30.78	-24.38	6.40
$W(CO)_5L$- $C(CH_3)_3$	-30.64	-24.26	6.38
$W(CO)_5L$- OH	-30.64	-24.26	6.38
$W(CO)_5L$- OCH_3	-30.41	-24.52	5.89
$W(CO)_5L$- $OC(CH_3)_3$	-31.00	-24.61	6.39
$W(CO)_5L$- NH_3	-31.25	-24.93	6.32
$W(CO)_5L$- $N(CH_3)_2$	-31.21	-25.37	5.84

All reported values are in kcal/mol.

TABLE 15: BEDA Energy Distribution for the [$M(CO)_xL$-Y] Complex Series.

$M(CO)_xL$- Y	ΔE_{int}	ΔE	ΔE_{reorg}
$Fe(CO)_4L$- NO_2	-46.13	-33.77	12.36
$Fe(CO)_4L$- CN	-46.12	-33.66	12.46
$Fe(CO)_4L$- COOH	-45.80	-33.83	11.97
$Fe(CO)_4L$- COH	-45.95	-33.90	12.05
$Fe(CO)_4L$- CF_3	-45.92	-33.77	12.15
Fe $(CO)_4L$- $OCOCH_3$	-45.61	-33.55	12.06
Fe $(CO)_4L$- H	-45.69	-33.86	11.83
Fe $(CO)_4L$- CH_3	-45.30	-34.14	11.16
Fe $(CO)_4L$- $C(CH_3)_3$	-45.70	-34.01	11.69
Fe $(CO)_4L$- OH	-44.86	-33.84	11.02
Fe $(CO)_4L$- OCH_3	-44.75	-34.00	10.75
Fe $(CO)_4L$- $OC(CH_3)_3$	-44.69	-33.92	10.77
Fe $(CO)_4L$- NH_3	-44.58	-34.12	10.46
Fe $(CO)_4L$- $N(CH_3)_2$	-44.44	-34.27	10.17
$Ni(CO)_3L$- NO_2	-25.99	-22.65	3.34
$Ni(CO)_3L$- CN	-25.92	-22.72	3.20
$Ni(CO)_3L$- COOH	-25.92	-22.91	3.01
$Ni(CO)_3L$- COH	-25.74	-22.87	2.87
$Ni(CO)_3L$- CF_3	-25.92	-22.86	3.06
$Ni(CO)_3L$- $OCOCH_3$	-25.66	-22.85	2.81
$Ni(CO)_3L$- H	-25.57	-23.26	2.31
$Ni(CO)_3L$- CH_3	-25.92	-23.62	2.30
$Ni(CO)_3L$- $C(CH_3)_3$	-26.00	-23.49	2.51
$Ni(CO)_3L$- OH	-25.77	-23.43	2.34
$Ni(CO)_3L$- OCH_3	-25.81	-23.52	2.29
$Ni(CO)_3L$- $OC(CH_3)_3$	-25.57	-23.59	1.98
$Ni(CO)_3L$- NH_3	-25.84	-23.75	2.09
$Ni(CO)_3L$- $N(CH_3)_2$	-25.98	-24.04	1.94

All reported values are in kcal/mol.

Figures 40-46 show the general trends for the behavior of the orbital attractive terms ΔE_{oi} as a function of substituent effects, Y. Figures 47-53 illustrate the general trends for the behavior of the Coulombic attractive terms ΔE_{elect} as a function of substituent effects Y. Figures 54-60 demonstrate the general trends for the behavior of the repulsive steric energy ΔE_{pauli} contribution as a function of substituent effects Y. Figures 40, 47, and 54 in particular are used as a means to compare the overall ΔE_{oi}, ΔE_{elect}, and ΔE_{pauli} differences between each transition metal studied, respectively.

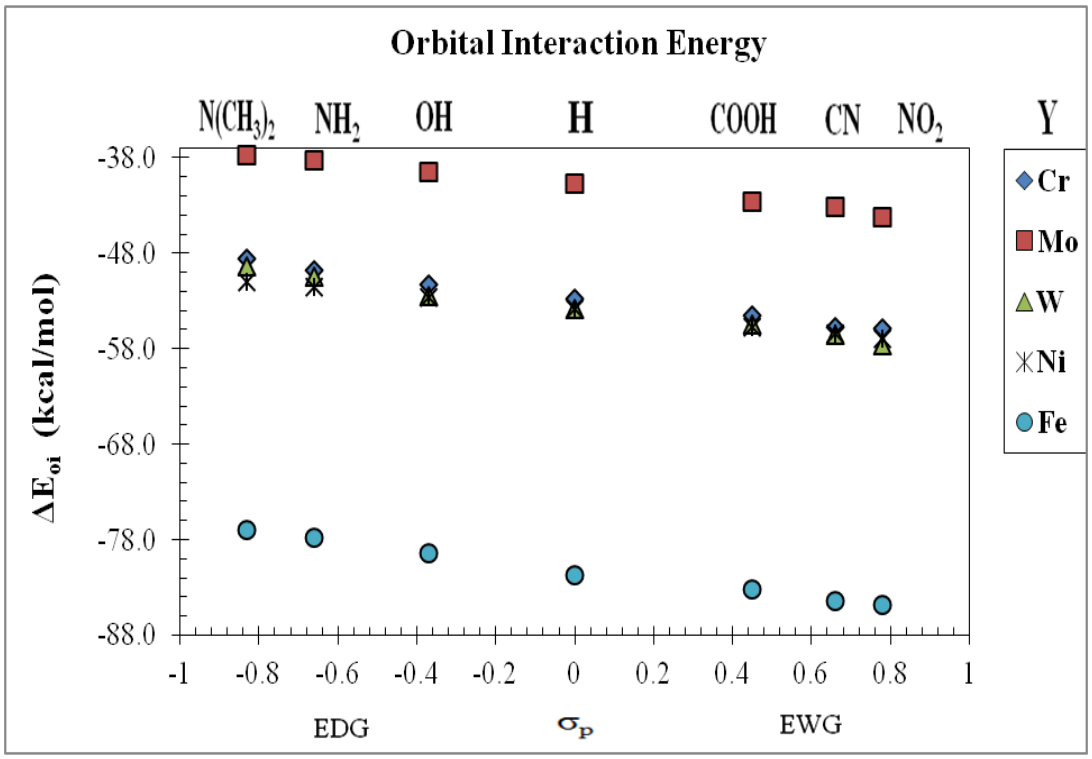

Figure 40. Graph of ΔE_{oi} vs. σ_p for the [$M(CO)_xL$-Y] complex series.

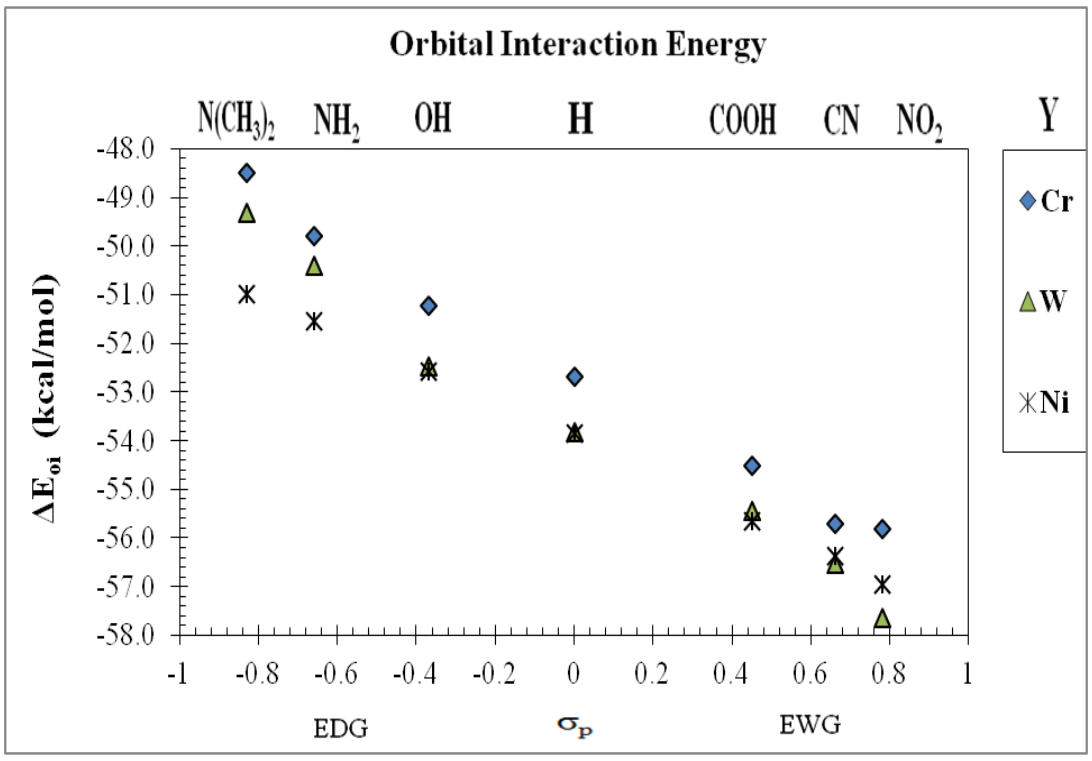

Figure 41. Graph of ΔE_{oi} vs. σ_p for the [$M(CO)_xL$-Y] complex series.

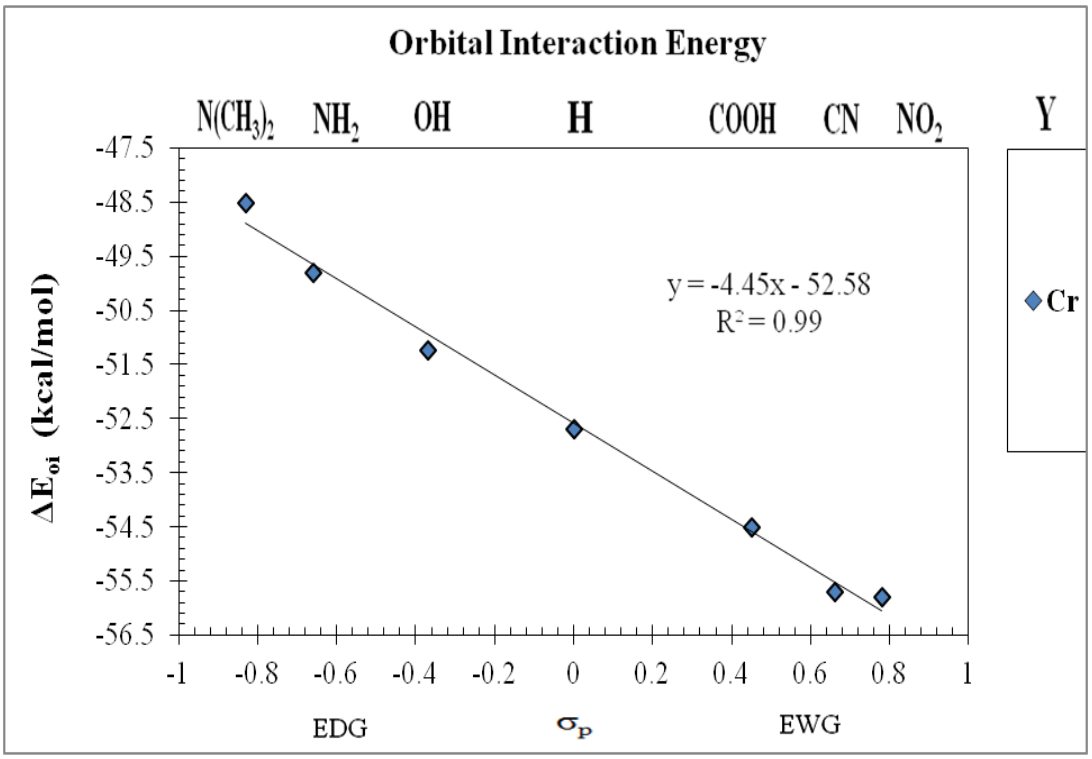

Figure 42. Graph of ΔE_{oi} vs. σ_p for the $[Cr(CO)_5L\text{-}Y]$ complex series.

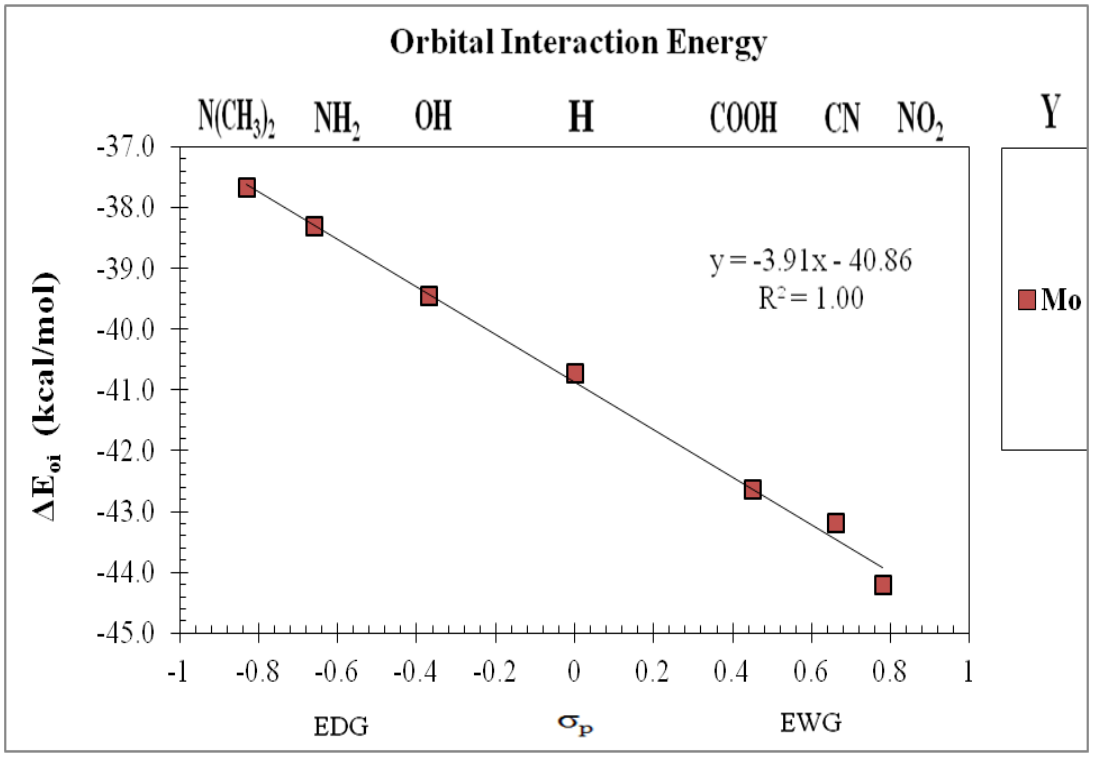

Figure 43. Graph of ΔE_{oi} vs. σ_p for the $[Mo(CO)_5L\text{-}Y]$ complex series.

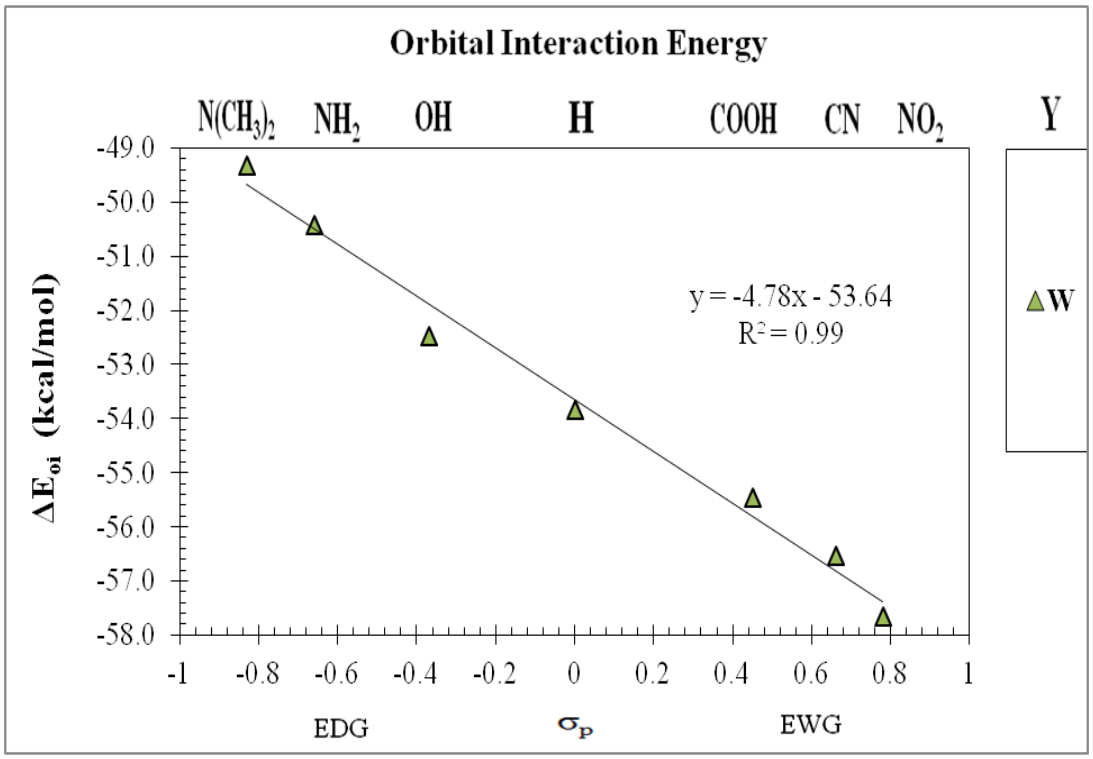

Figure 44. Graph of ΔE_{oi} vs. σ_p for the $[W(CO)_5L\text{-}Y]$ complex series.

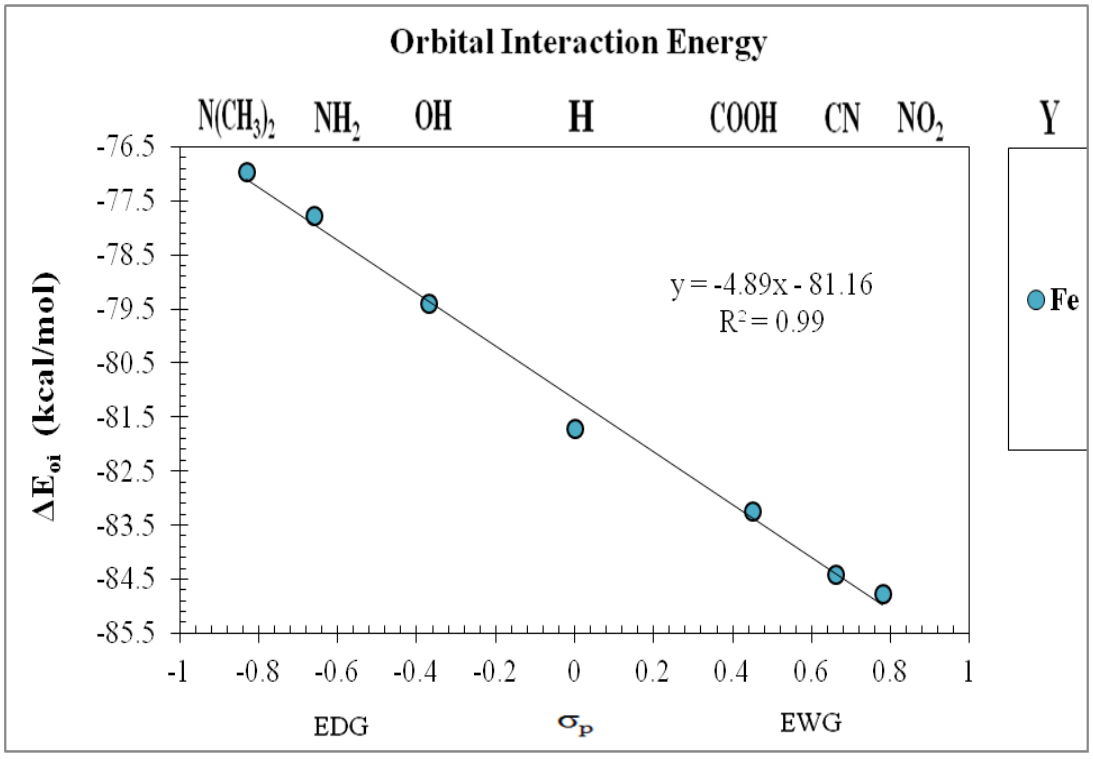

Figure 45. Graph of ΔE_{oi} vs. σ_p for the $[Fe(CO)_4L\text{-}Y]$ complex series.

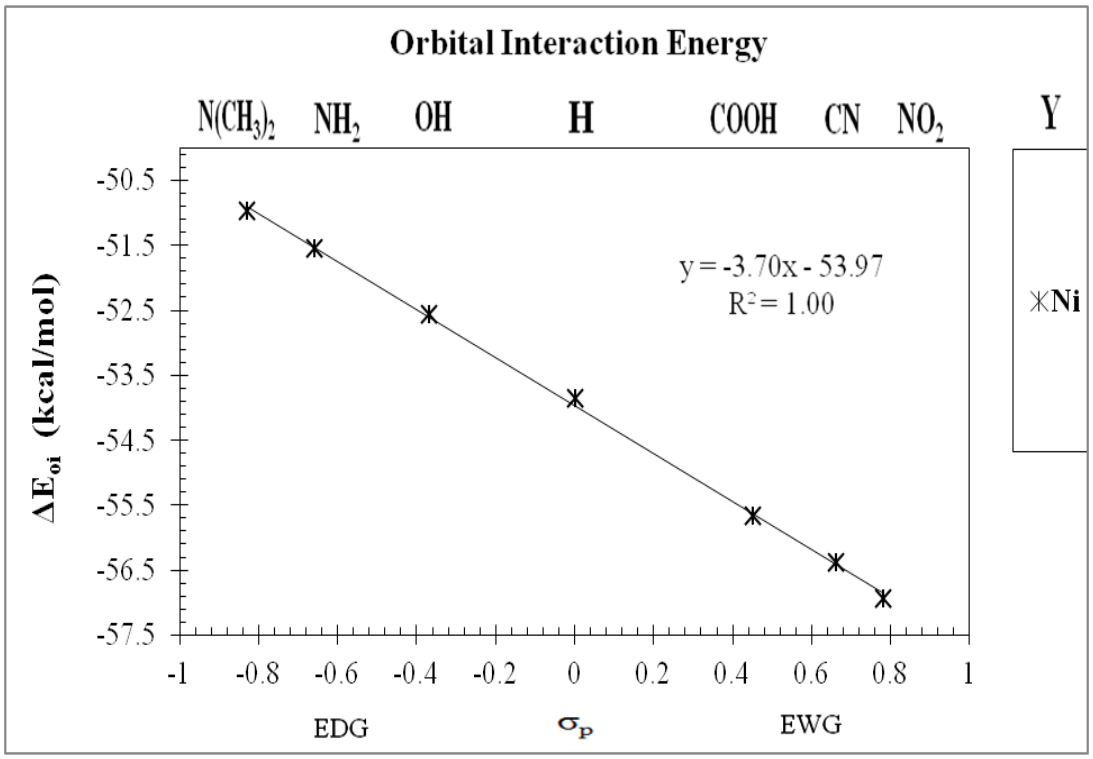

Figure 46. Graph of ΔE_{oi} vs. σ_p for the [Ni(CO)$_3$L-Y] complex series.

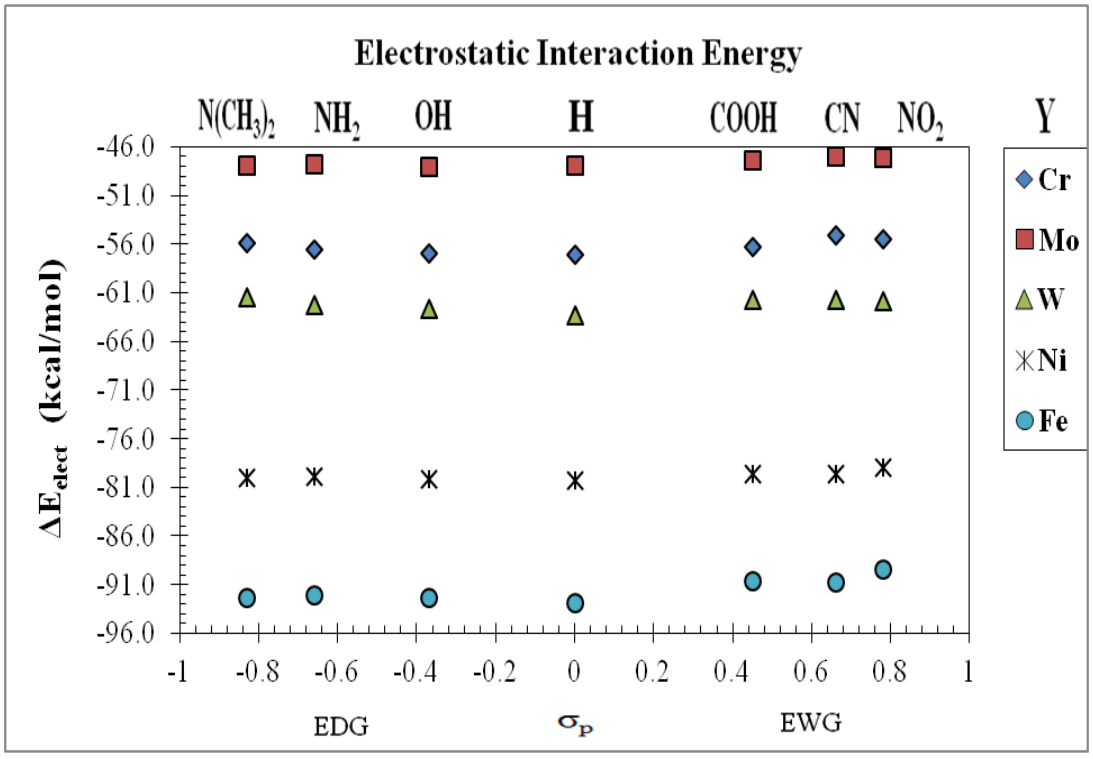

Figure 47. Graph of ΔE_{elect} vs. σ_p for the [M(CO)$_x$L-Y] complex series.

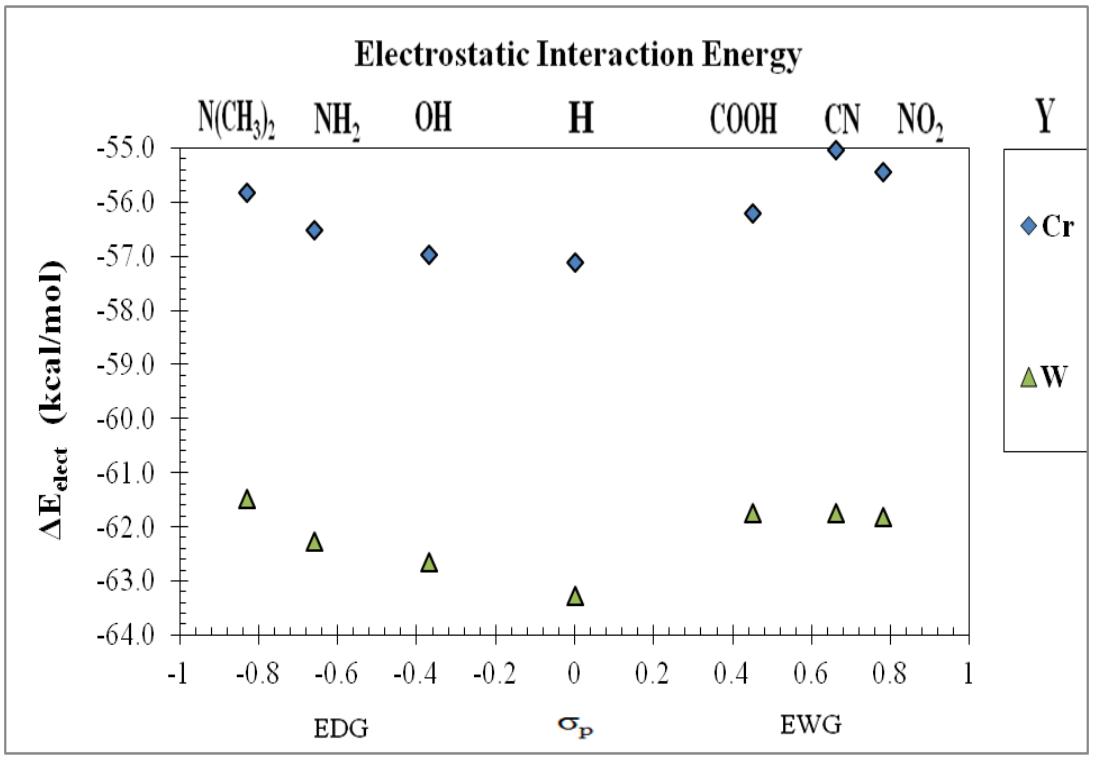

Figure 48. Graph of ΔE_{elect} vs. σ_p for the $[M(CO)_xL\text{-}Y]$ complex series.

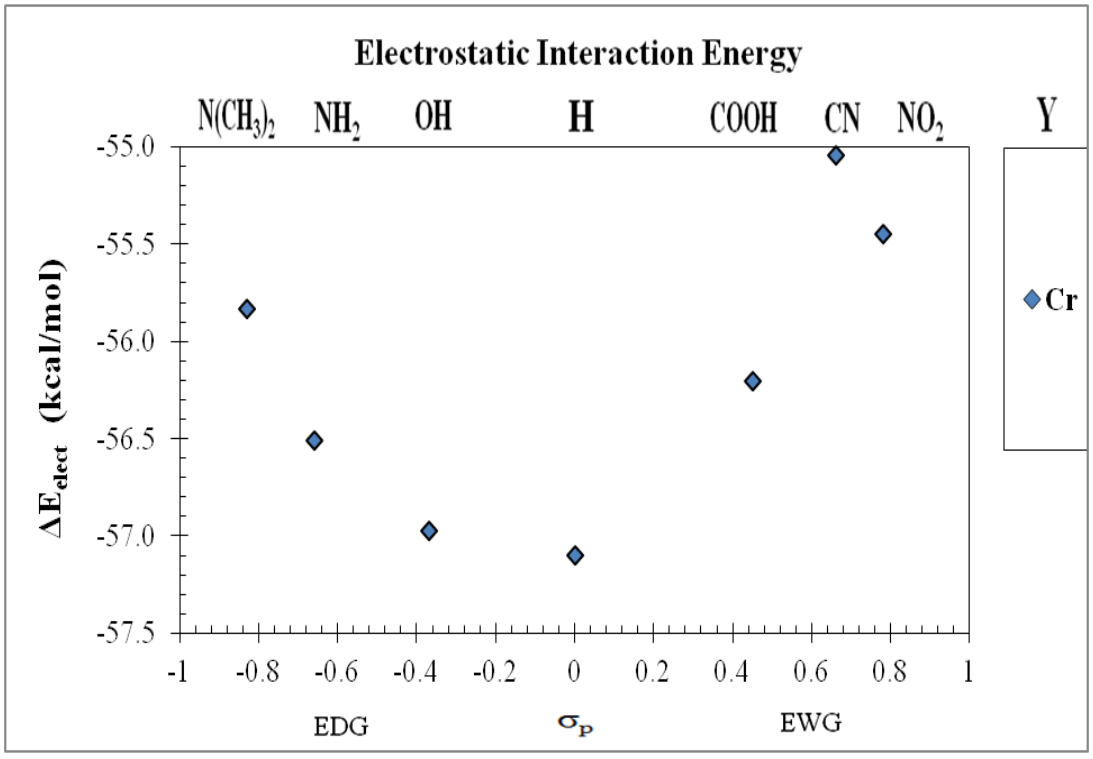

Figure 49: Graph of ΔE_{elect} vs. σ_p for the $[Cr(CO)_5L\text{-}Y]$ complex series.

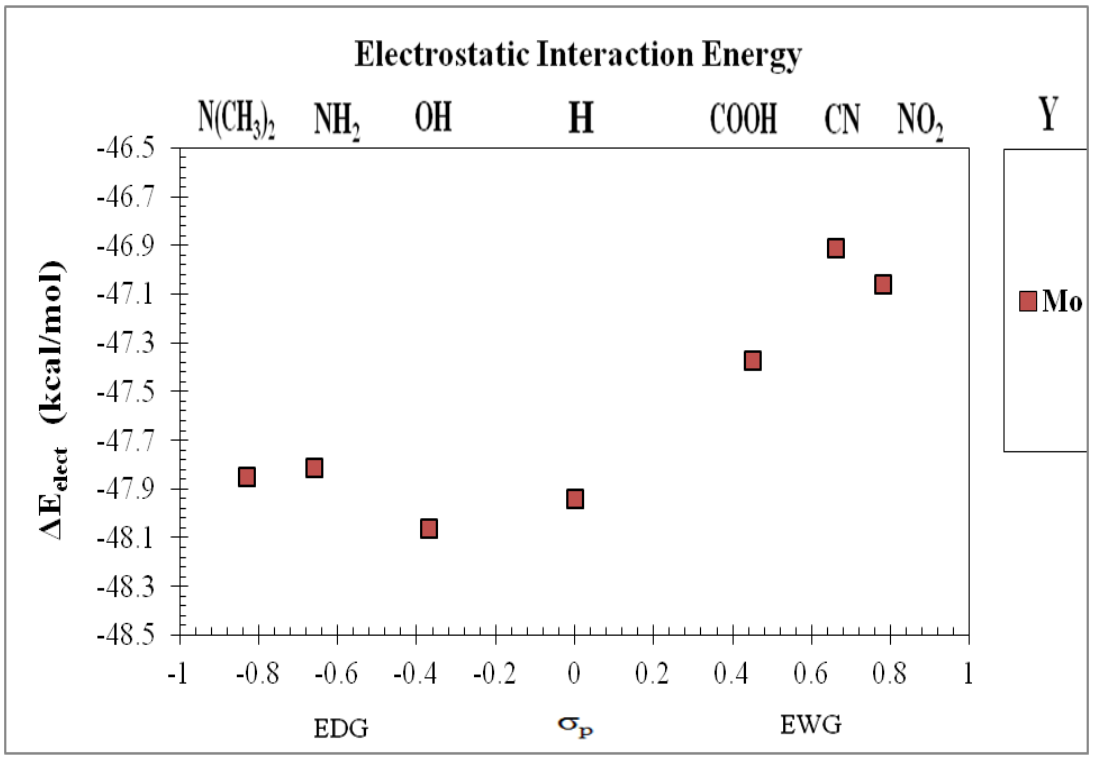

Figure 50. Graph of ΔE_{elect} vs. σ_p for the [$Mo(CO)_5$L-Y] complex series.

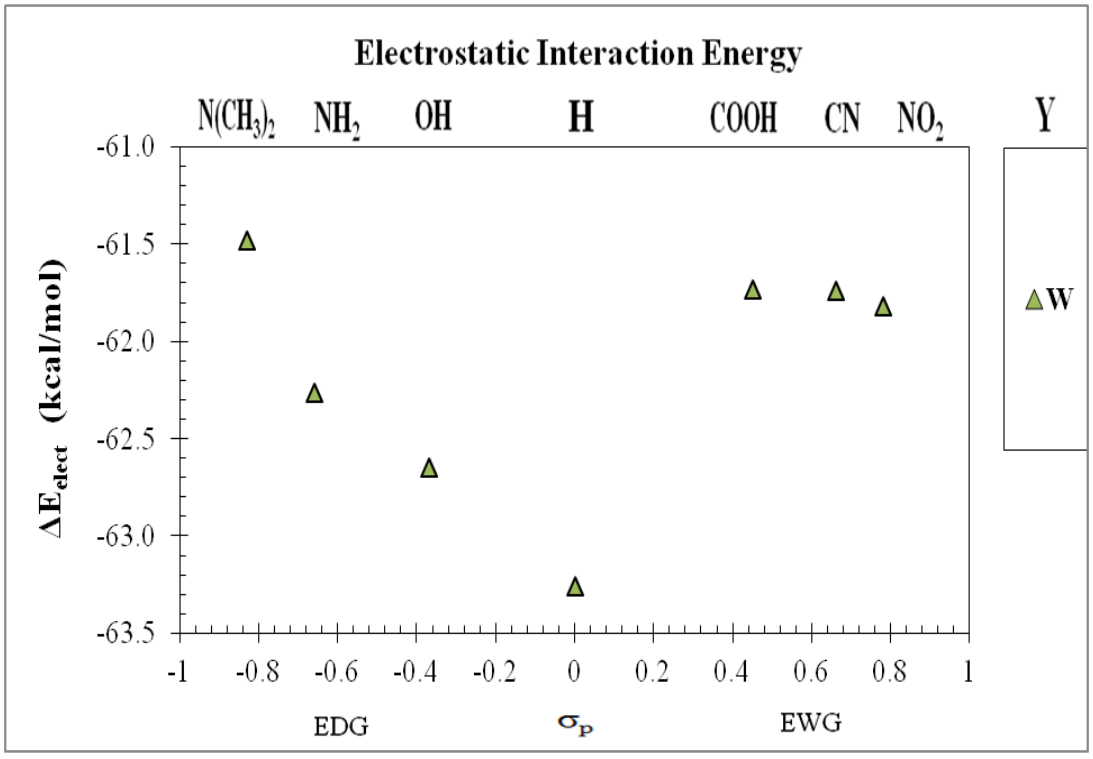

Figure 51. Graph of ΔE_{elect} vs. σ_p for the [$W(CO)_5$L-Y] complex series.

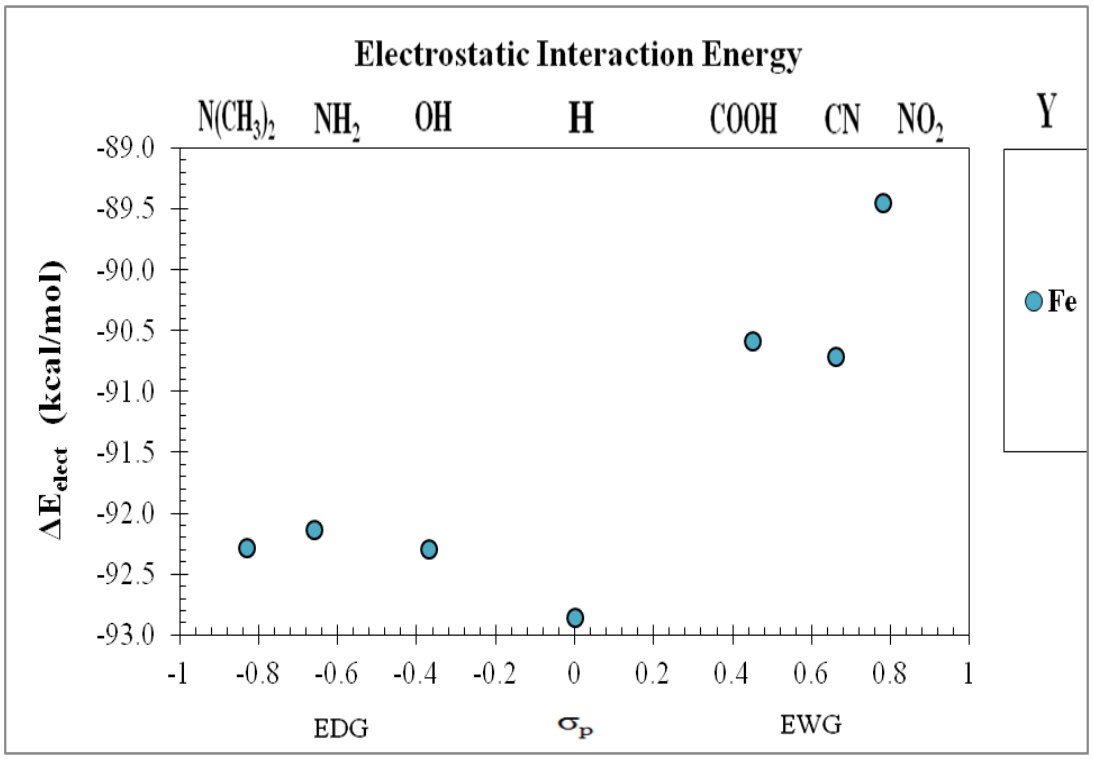

Figure 52. Graph of ΔE_{elect} vs. σ_p for the $[Fe(CO)_4L\text{-}Y]$ complex series.

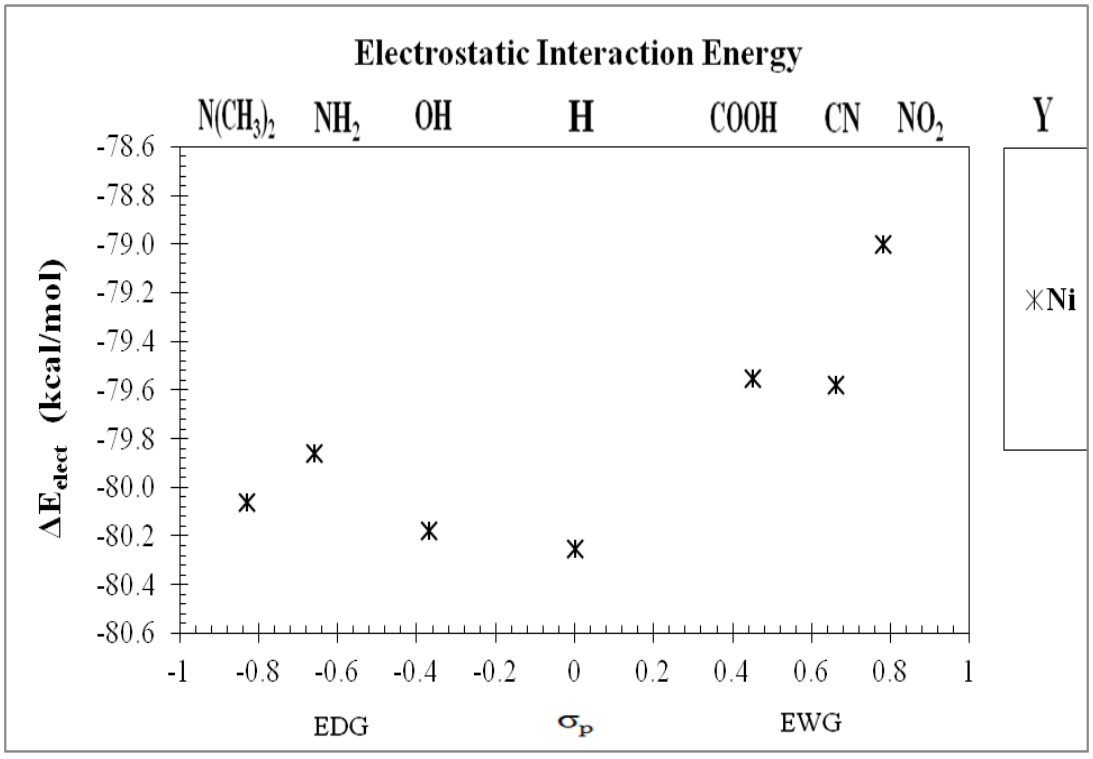

Figure 53. Graph of ΔE_{elect} vs. σ_p for the $[Ni(CO)_3L\text{-}Y]$ complex series.

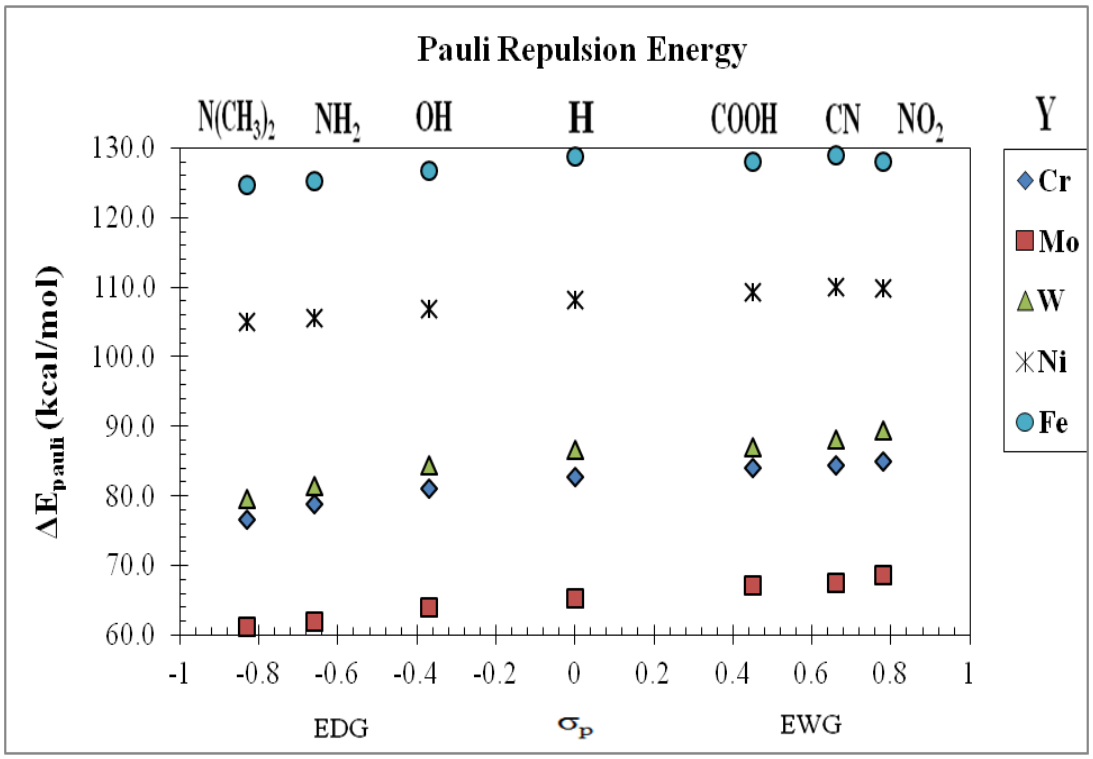

Figure 54. Graph of ΔE_{pauli} vs. σ_p for the $[M(CO)_xL\text{-}Y]$ complex series.

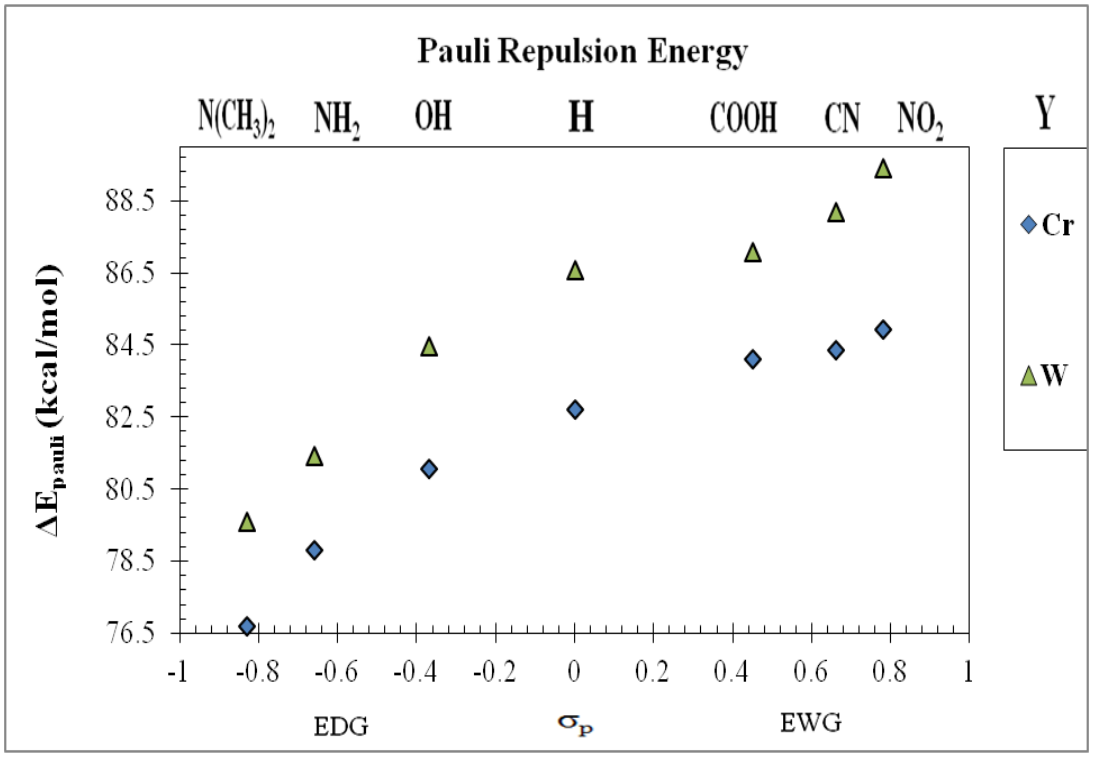

Figure 55. Graph of ΔE_{pauli} vs. σ_p for the $[M(CO)_5L\text{-}Y]$ complex series.

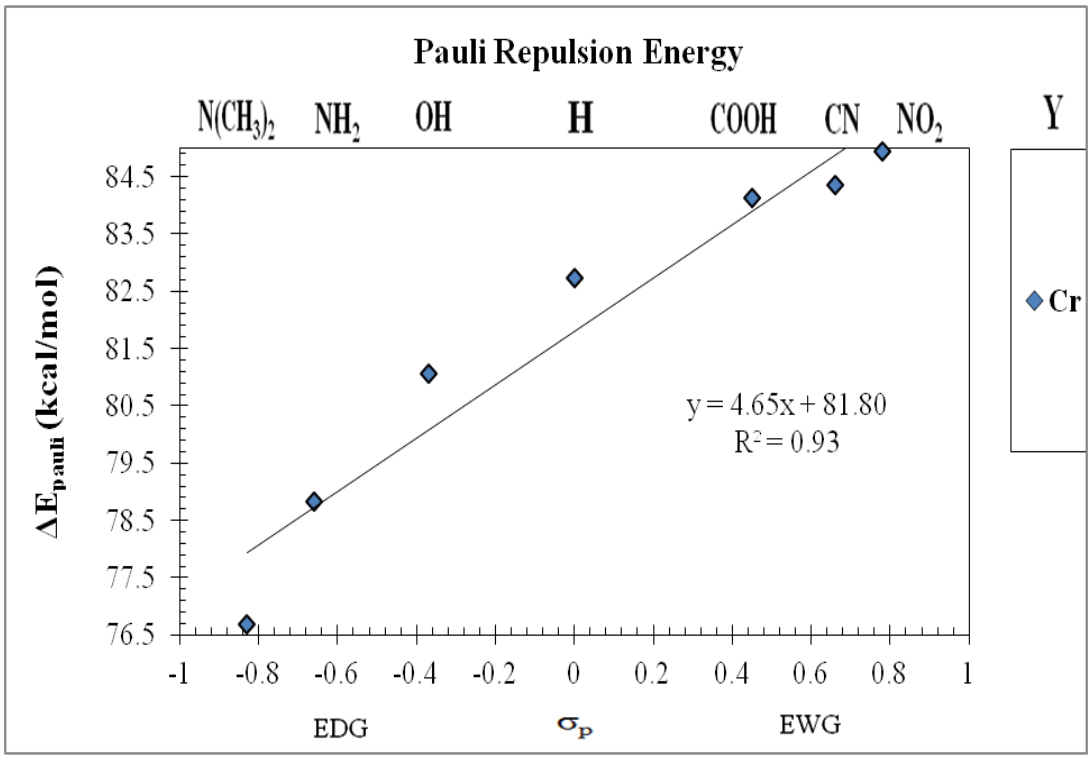

Figure 56. Graph of ΔE_{pauli} vs. σ_p for the $[Cr(CO)_5L\text{-}Y]$ complex series.

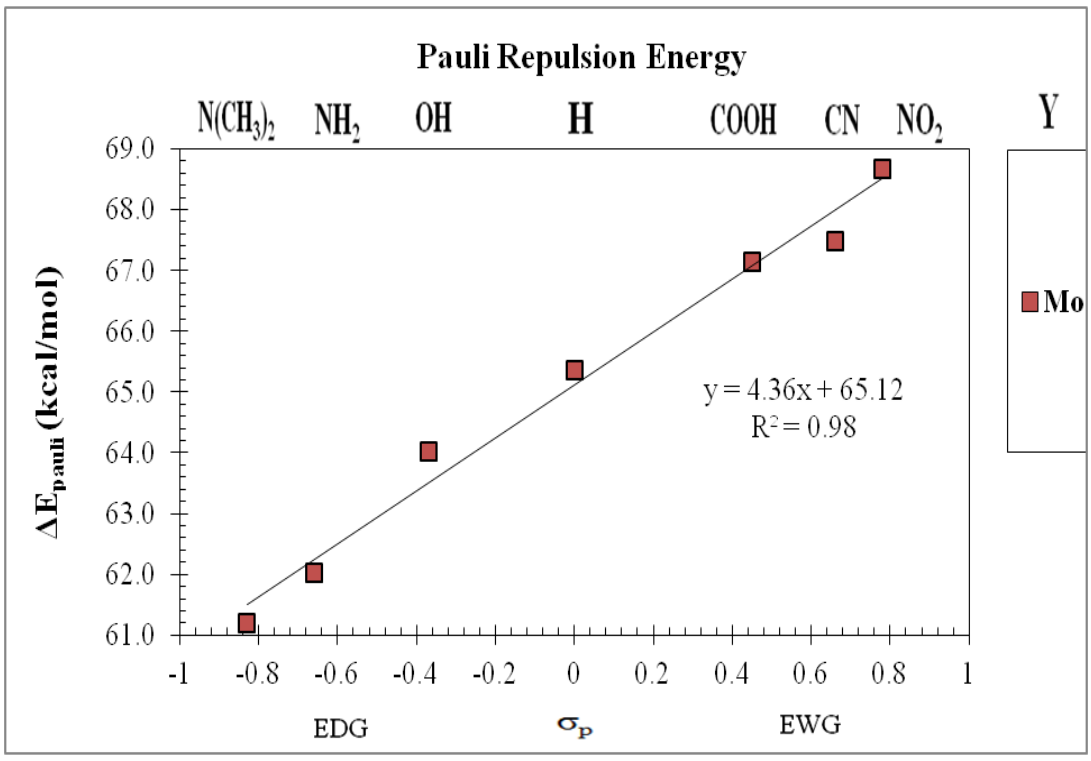

Figure 57. Graph of ΔE_{pauli} vs. σ_p for the $[Mo(CO)_5L\text{-}Y]$ complex series.

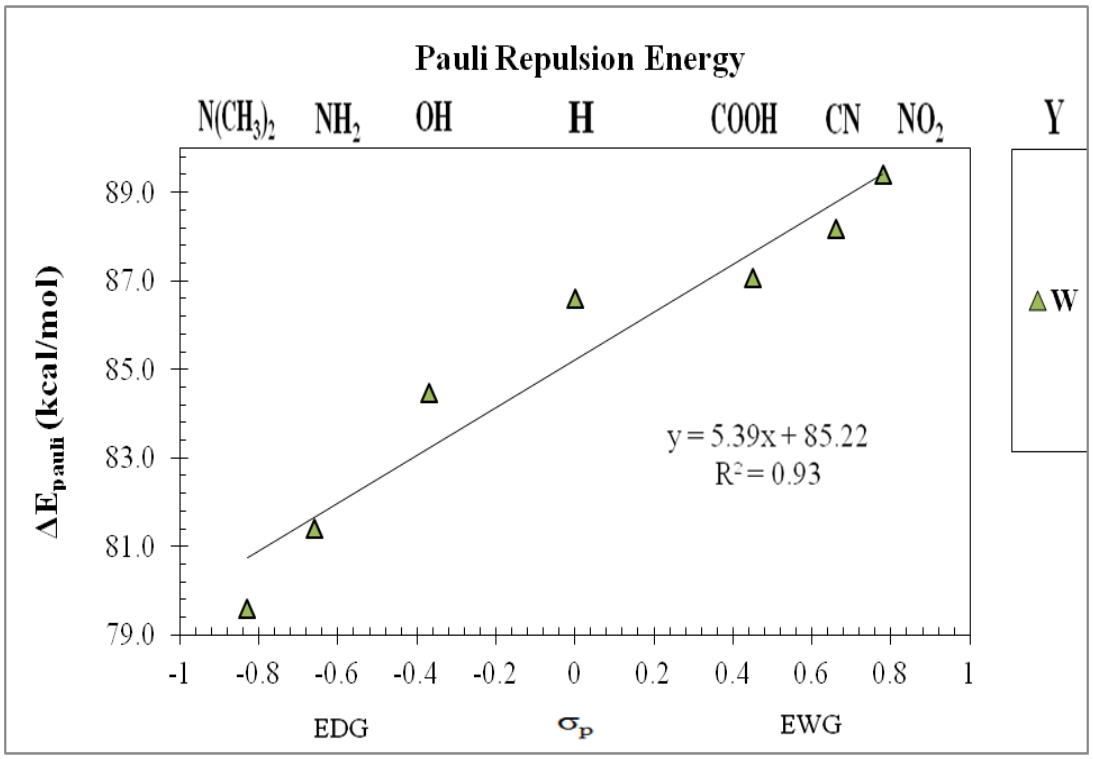

Figure 58. Graph of ΔE_{pauli} vs. σ_p for the $[W(CO)_5L\text{-}Y]$ complex series.

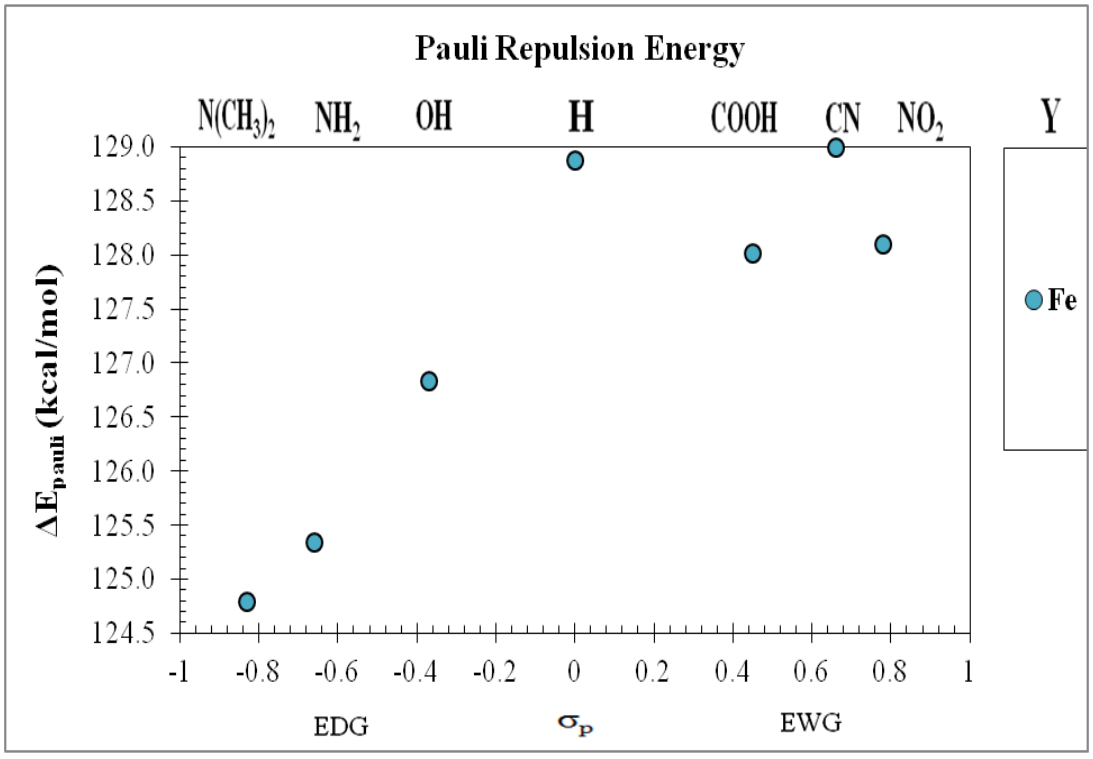

Figure 59. Graph of ΔE_{pauli} vs. σ_p for the $[Fe(CO)_4L\text{-}Y]$ complex series.

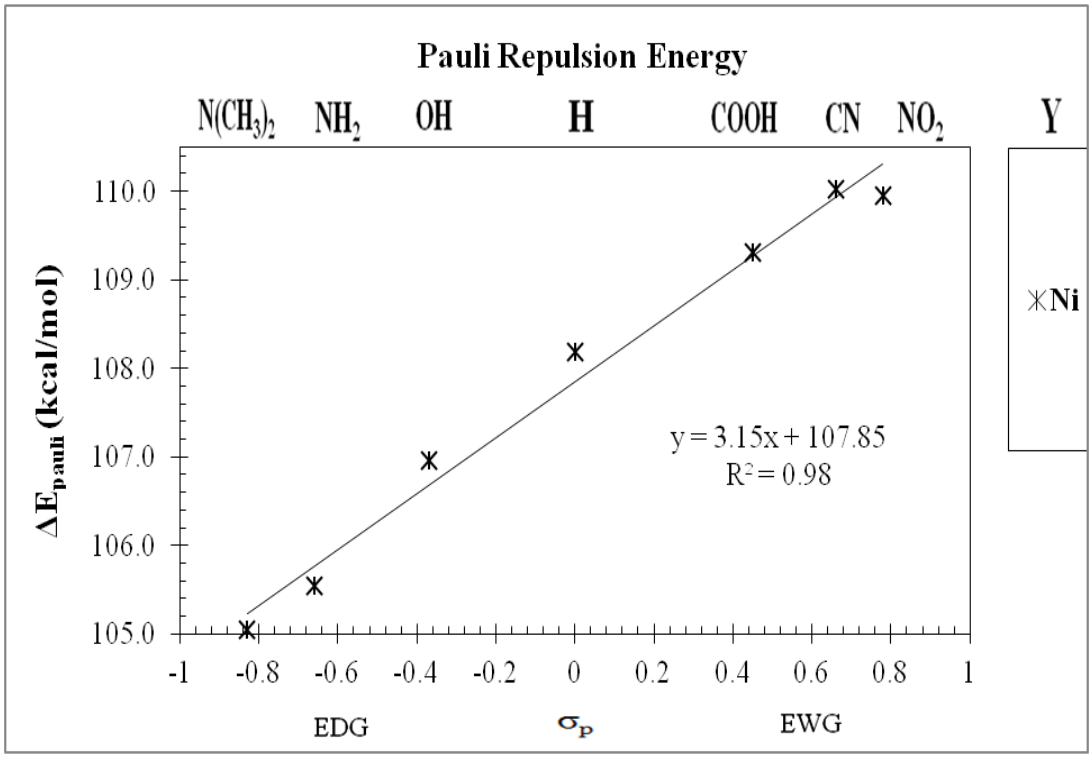

Figure 60. Graph of ΔE_{pauli} vs. σ_p for the [$Ni(CO)_3$L-Y] complex series.

Figures 40, 47, and 54 compare general bond energy trends between each transition metal studied based on the results of the bond energy decomposition analysis, $\Delta E_{int} = \Delta E_{elect} + \Delta E_{oi} + \Delta E_{pauli}$. Figure 40 in particular compares general covalent orbital interaction trends between each transition metal studied. The trend in (ΔE_{oi}, kcal/mol) based on transition metal order follows as: $Mo(CO)_5 < Cr(CO)_5 < Ni(CO)_3 < W(CO)_5 < Fe(CO)_4$. Figure 47 indicates that the overall trend in electrostatic energy (ΔE_{elect}, kcal/mol) based on transition metal order follows as: $Mo(CO)_5 < Cr(CO)_5 < W(CO)_5 < Ni(CO)_3 < Fe(CO)_4$. Figure 54 specifically compares general steric interaction trends based on transition metal influence. The overall trend in the Pauli repulsive contribution (ΔE_{pauli}, kcal/mol) based on transition metal order follows as: $Mo(CO)_5 < Cr(CO)_5 < W(CO)_5 < Ni(CO)_3 < Fe(CO)_4$.

It was found that the total magnitude of the covalent attraction term ΔE_{oi} increases in proportion to an increase in the EWD ability of the para substituent. Interestingly, the overall magnitudes of both the molecular orbital interaction (ΔE_{oi}) and steric repulsive energy terms (ΔE_{pauli}) seem to behave in opposition to one another with respect to an increase in the EWD capacity of the para substituent, whereas the electrostatic term ΔE_{elect} values are relatively constant across the series; refer to Figures 40-46, 54-60, and 47-53, respectively. This causes the trend in the interaction energy term to be rather flat. Take particular notice of the trends in slope for ΔE_{oi} or ΔE_{pauli} relative to the overall trend of ΔE_{elect} across the ligand series. The results from the energy decomposition analysis indicate that both the trends in the orbital interaction (ΔE_{oi}), and orbital repulsion energies (ΔE_{pauli}) should follow in the general order of: $N(CH_3)_2 > NH_2 > OH > H >$ $COOH > CN > NO_2$. The strong interaction between the EWD olefins and the metal carbonyl fragments is due to the large orbital interaction energy (ΔE_{oi}). As expected, EWD olefins will draw the olefins in closer, further giving rise to a greater deal of Pauli repulsion interaction as a result of the attraction; the greater the attraction between orbitals of bonding, the greater the energy required to balance the effects engendered by steric repulsion. Further analysis of ΔE_{int} shows the relative contribution of the attractive ΔE_{oi} and ΔE_{elect} interactions. If the magnitude of the sum of the individual attractive contributions ($\Delta E_{elect} + \Delta E_{oi}$) is compared to the magnitude of the repulsive contribution (ΔE_{pauli}), we see that the attractive terms dominate the overall percentage of the total interaction as the EWD capacity of the para substituent increases. This makes sense in terms of steric interactions, because as the EWD capacity increases, the percentage contribution of the repulsive steric term slightly increases as well.

When the two attractive terms are examined individually it is found that the orbital interaction and electrostatic interaction terms are very close in importance. Overall, it was demonstrated that both attractive terms (ΔE_{oi} and ΔE_{elect}) contribute evenly to the bond formation energy, although there is an effect of the EWD ability of the olefin on the relative contribution of the covalent orbital interaction term (ΔE_{oi}). For instance, as the EWD ability of the olefin increases relative to styrene, the covalent orbital interaction (ΔE_{oi}) term is dominant and accounts for approximately 41-42 % of the attractive contribution (i.e. $\Delta E_{oi} + \Delta E_{elect}$) for transition metals of the [$Ni(CO)_3(\eta^2$-C_2H_3-C_6H_4-Y)] complex series, and 47-50 % for the [$M(CO)_x(\eta^2$-C_2H_3-C_6H_4-Y)] complexes. However, when the EWD capacity is decreased, the extent of the orbital interaction decreases and since the electrostatic interaction remains flat, then the electrostatic interaction (ΔE_{elect}) becomes the dominant term with only 39-40 % of the attractive interaction due to covalent orbital interactions for transition metals of the [$Ni(CO)_3$L-Y] complex series, and 44-47% for the [$M(CO)_x$L-Y] complex series. Interestingly, the magnitude of the repulsive energy term (ΔE_{pauli}) increases with the EWD ability of the olefin, i.e. it has the same trend as the attractive ΔE_{oi} term. This is likely a consequence of the stronger attraction between the olefin and the metal fragment. An olefin with a large EWD ability is able to get closer to the metal as manifested by shortened M-C_{olef} bond lengths (see Tables 5-7). As the olefin gets closer to the metal, there are larger repulsive forces acting between the two bonding fragments and thus the repulsive energy increases. The overall sum of the attractive and repulsive terms equals the total interaction energy (ΔE_{int}), which accounts for the net bonding energy between two reactants in a conformation that corresponds to the geometry they have in the complex.

Figures 61-65 illustrate the overall bond interaction energy (ΔE_{int}) BEDA component percent composition for each transition metal studied based on a quantitative measure of substituent effects. Graphs show the overall percent composition contributions to the interaction energy ΔE_{int} based on the absolute summation of the attractive orbital interaction ΔE_{oi}, attractive electrostatic interaction ΔE_{elect}, and Pauli repulsive interaction ΔE_{pauli} terms for each transition metal para substituted olefin complex. Figures 61-63 in particular are used as a means to compare the total ΔE_{int} BEDA percent composition distribution differences against substituent effects for the $[M(CO)_5(\eta^2\text{-}C_2H_3\text{-}C_6H_4\text{-}Y)]$ complex series. Figure 64-65 are used as a means to compare the overall ΔE_{int} BEDA percent composition distribution differences against substituent effects for the $[Fe(CO)_4(\eta^2\text{-}C_2H_3\text{-}C_6H_4\text{-}Y)]$ and $[Ni(CO)_3(\eta^2\text{-}C_2H_3\text{-}C_6H_4\text{-}Y)]$ complex series, respectively.

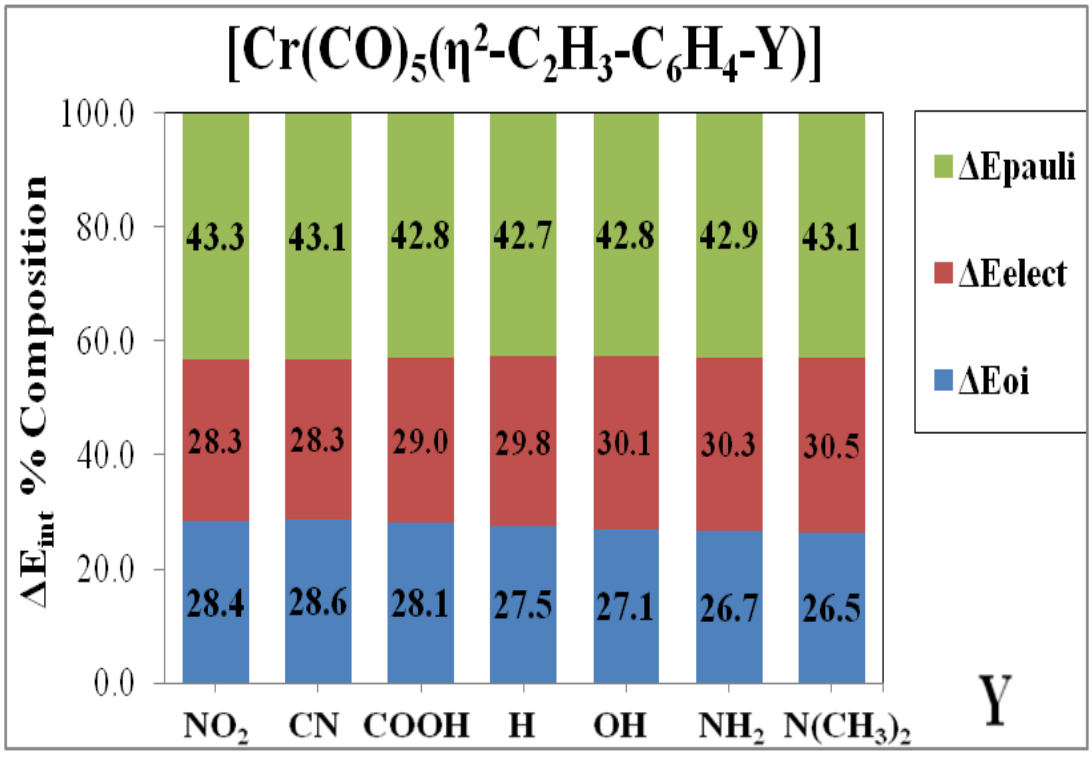

Figure 61. Graph of ΔE_{int} BEDA % composition**:** $[Cr(CO)_5L\text{-}Y]$ complex series.

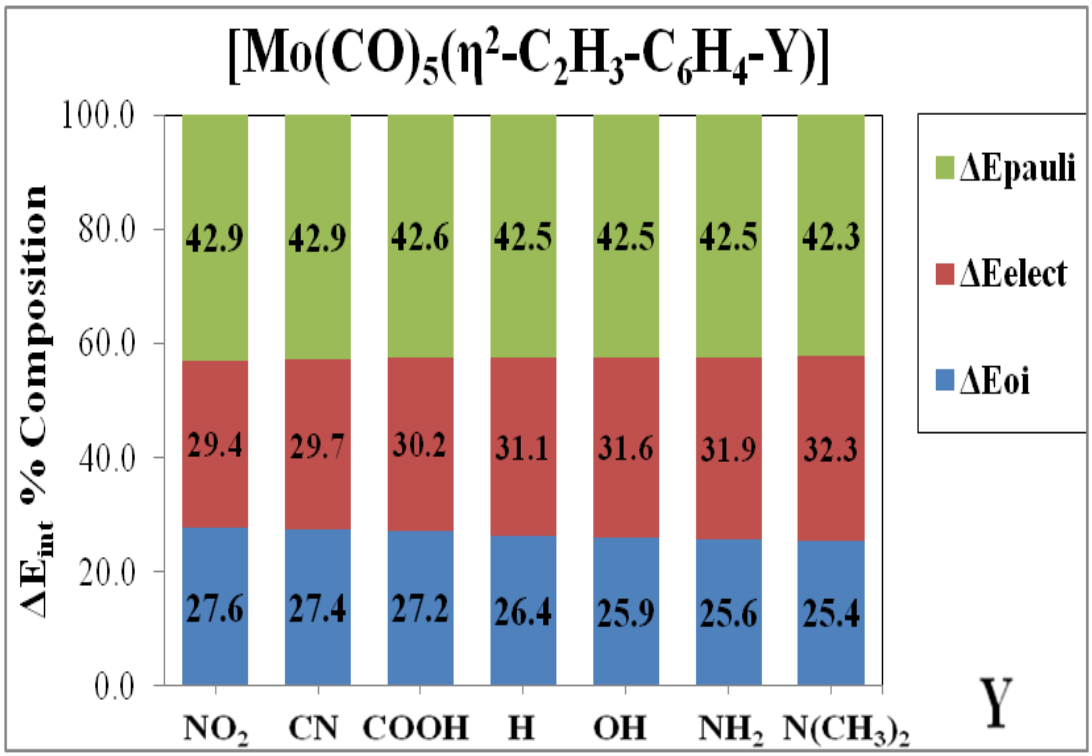

Figure 62. Graph of ΔE_{int} BEDA % composition: $[Mo(CO)_5L\text{-}Y]$ complex series.

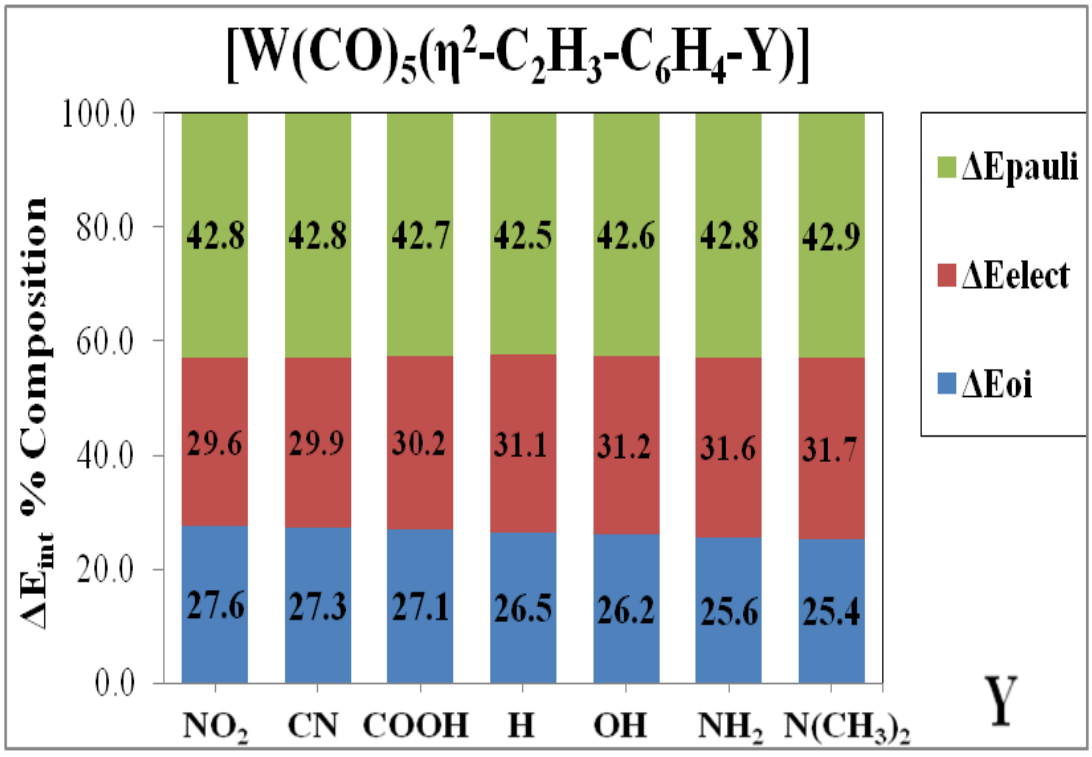

Figure 63. Graph of ΔE_{int} BEDA % composition: $[W(CO)_5L\text{-}Y]$ complex series.

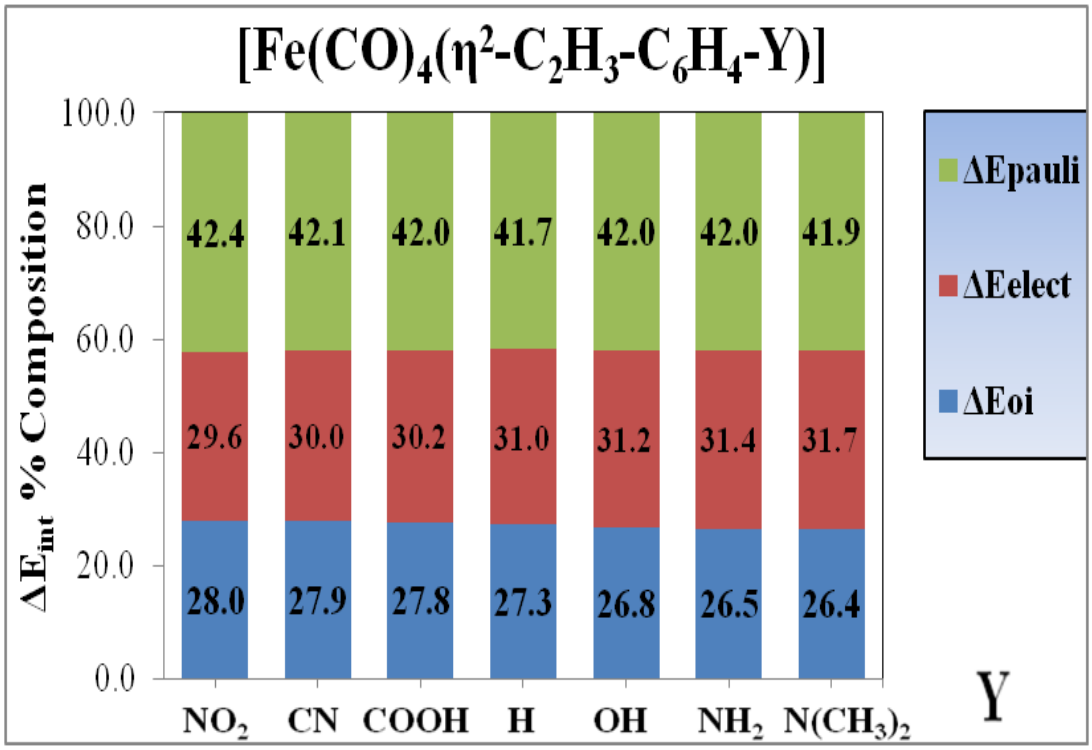

Figure 64. Graph of ΔE_{int} BEDA % composition**:** $[Fe(CO)_4L\text{-}Y]$ complex series.

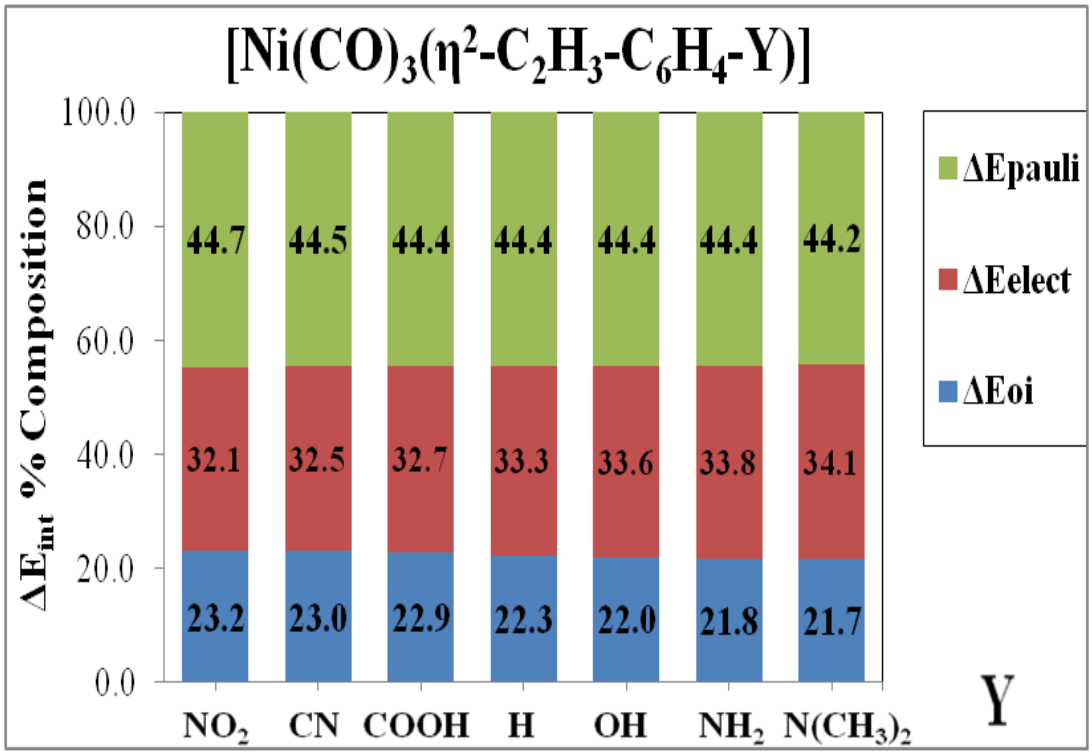

Figure 65. Graph of ΔE_{int} BEDA % composition: $[Ni(CO)_3L\text{-}Y]$ complex series.

Noticeable trends are evident, for instance the percentages of attractive covalent interaction ΔE_{oi} and electrostatic interactions ΔE_{elect} behave in opposition to one another with respect to an increase in the EWD capacity of the olefin system. This balancing act between the attractive terms ultimately causes the trend in the percentage of total repulsive energy to be rather flat across the ligand series. That is, notice that the total contribution of ΔE_{pauli} towards the absolute interaction energy is approximately 42-44 % overall, regardless of substituent effects or transition metal influence! It was found that the magnitude of the covalent attraction term ΔE_{oi} increases in proportion to an increase in the EWD ability of the para substituent; this is to be expected on the basis of former DCD implication. According to the common qualitative interpretation of the DCD model for metal-olefin binding, an increase in the EWD capability of the olefin should result in a stronger metal-olefin bond, because the back-bonding interaction is increased. One way to increase and tune the EWD ability of an olefin is by increasing the EWD capacity of the para substituent.

Qualitatively, ΔE_{oi} occupies approximately 21-28 % of the attractive contribution towards the total absolute magnitude of the bond interaction energy, whereas the electrostatic interaction (ΔE_{elect}) is the dominant term overall (comprising 28-34% of the attractive contribution towards the total ΔE_{int}). Notice that based on a range of percent contribution ΔE_{elect} and ΔE_{oi} seem to be most influenced by substituent effects relative to ΔE_{pauli}, which only varies by approximately 1 % across the ligand series for each metal. If the percent magnitude of the sum of attractive terms ($\Delta E_{elect} + \Delta E_{oi}$) is compared to the percent magnitude of the repulsive contribution (ΔE_{pauli}), we see that approximately 55-58 % of the total interaction energy is due to attraction.

Figures 66-72 show the general trends for the behavior of the overall interaction energy ΔE_{int} as a function of substituent effects Y. Figures 73-79 illustrate the general trends for the behavior of the overall metal-olefin bond formation energies ΔE as a function of substituent effects Y. Figures 80-86 show the general trends for the behavior of the reorganizational energy ΔE_{reorg} as a function of substituent effects Y. Figures 87-91 demonstrate the general trends for the overall BEDA distribution for each metal as a function of substituent effects Y. Figures 66, 73, and 80 in particular are used as a means to compare the overall $\Delta E_{int,}$ ΔE, and ΔE_{reorg} differences between each transition metal studied, respectively. Figures 92-96 demonstrate the overall bond formation energy ΔE BEDA component percent composition distribution for each transition metal studied based on a quantitative measure of substituent effects.

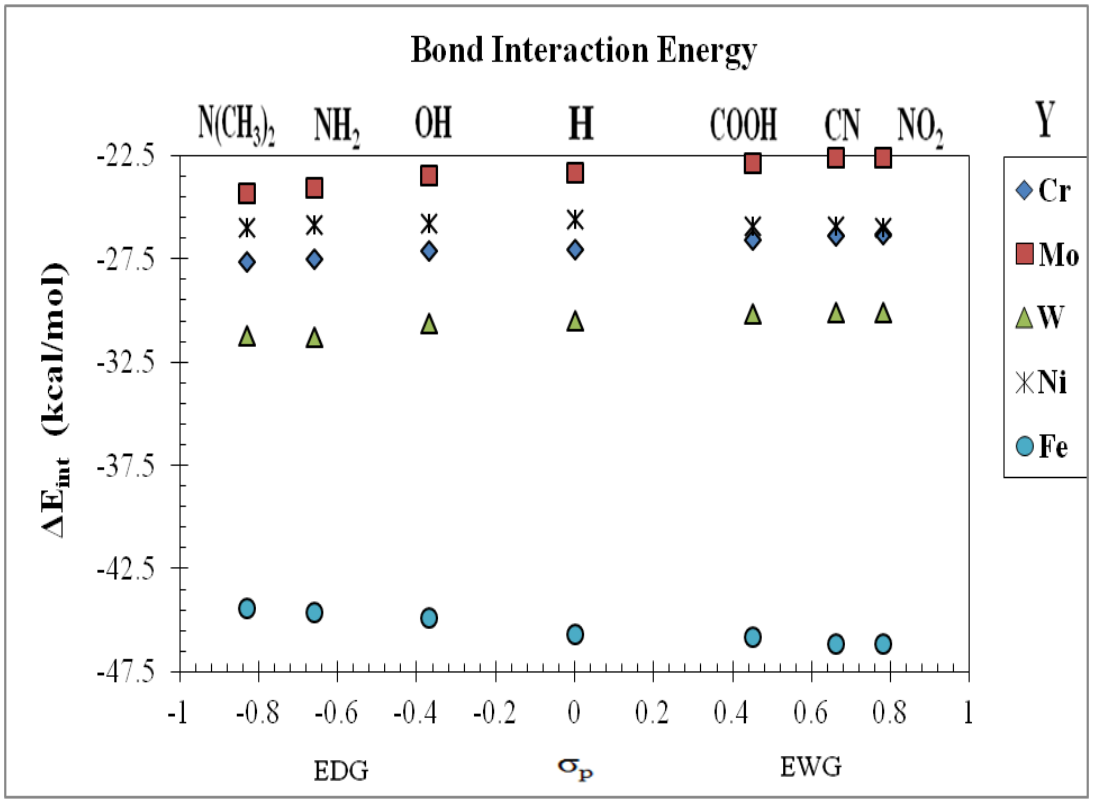

Figure 66. Graph of ΔE_{int} vs. σ_p for the $[M(CO)_xL\text{-}Y]$ complex series.

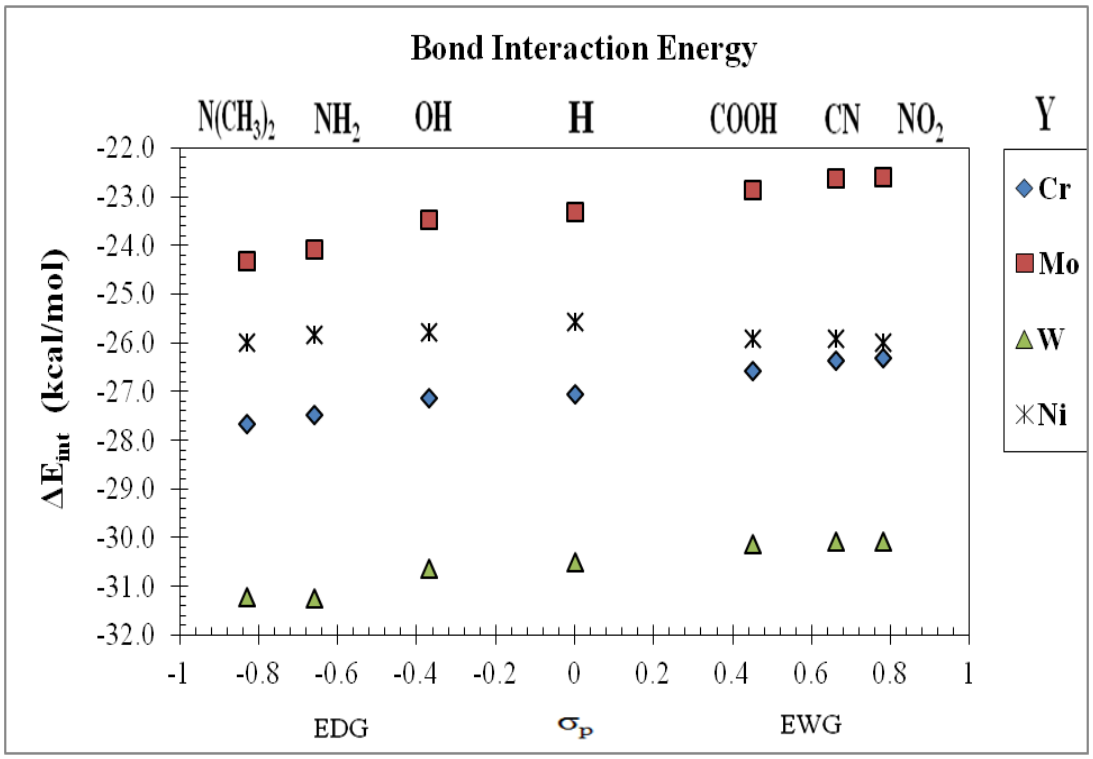

Figure 67. Graph of ΔE_{int} vs. σ_p for the $[M(CO)_xL\text{-}Y]$ complex series.

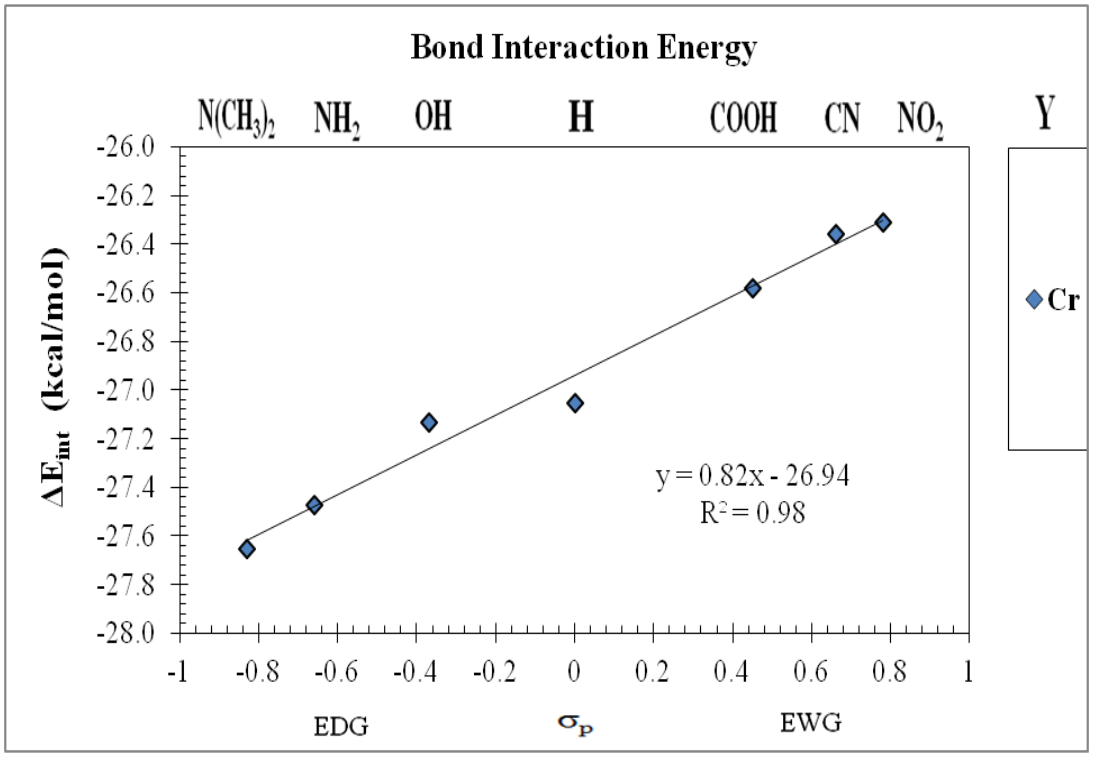

Figure 68: Graph of ΔE_{int} vs. σ_p for the $[Cr(CO)_5L\text{-}Y]$ complex series.

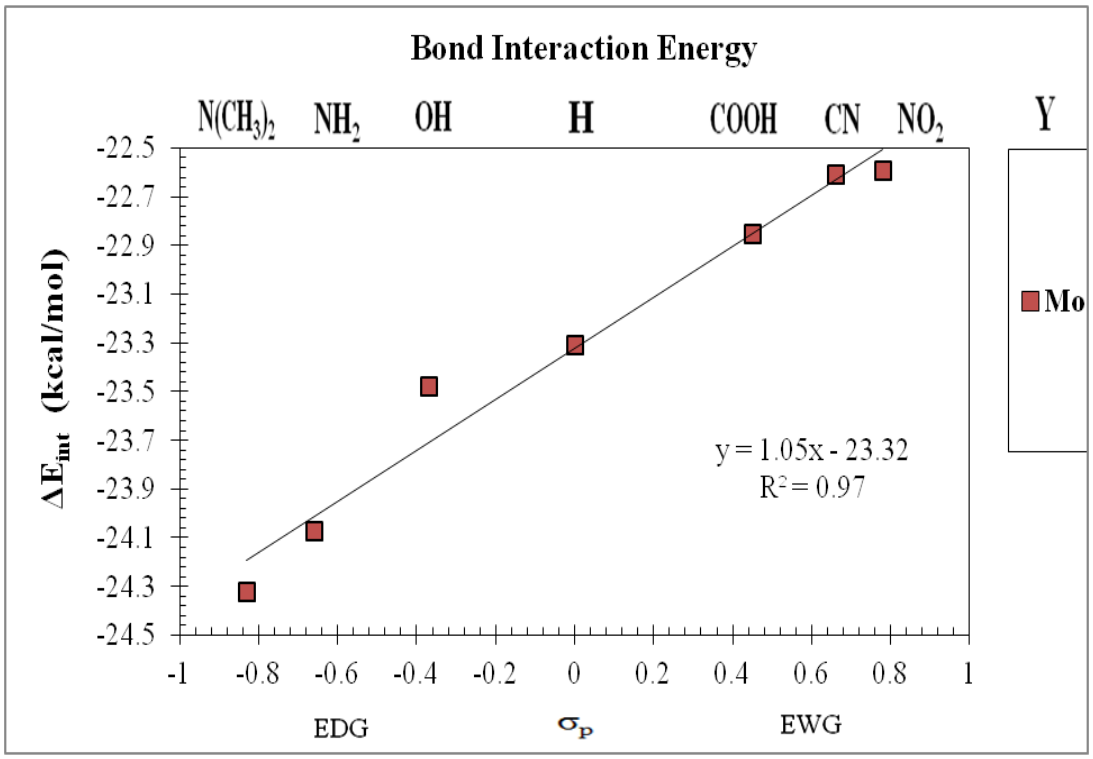

Figure 69. Graph of ΔE_{int} vs. σ_p for the $[Mo(CO)_5L\text{-}Y]$ complex series.

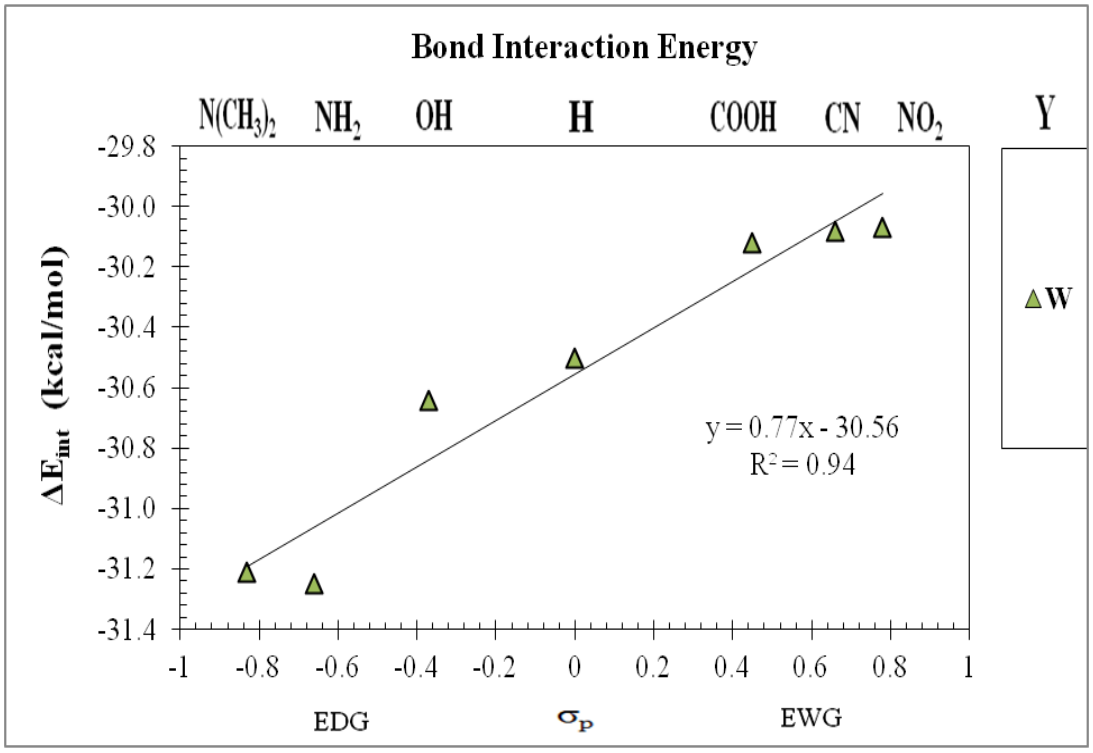

Figure 70. Graph of ΔE_{int} vs. σ_p for the $[W(CO)_5L\text{-}Y]$ complex series.

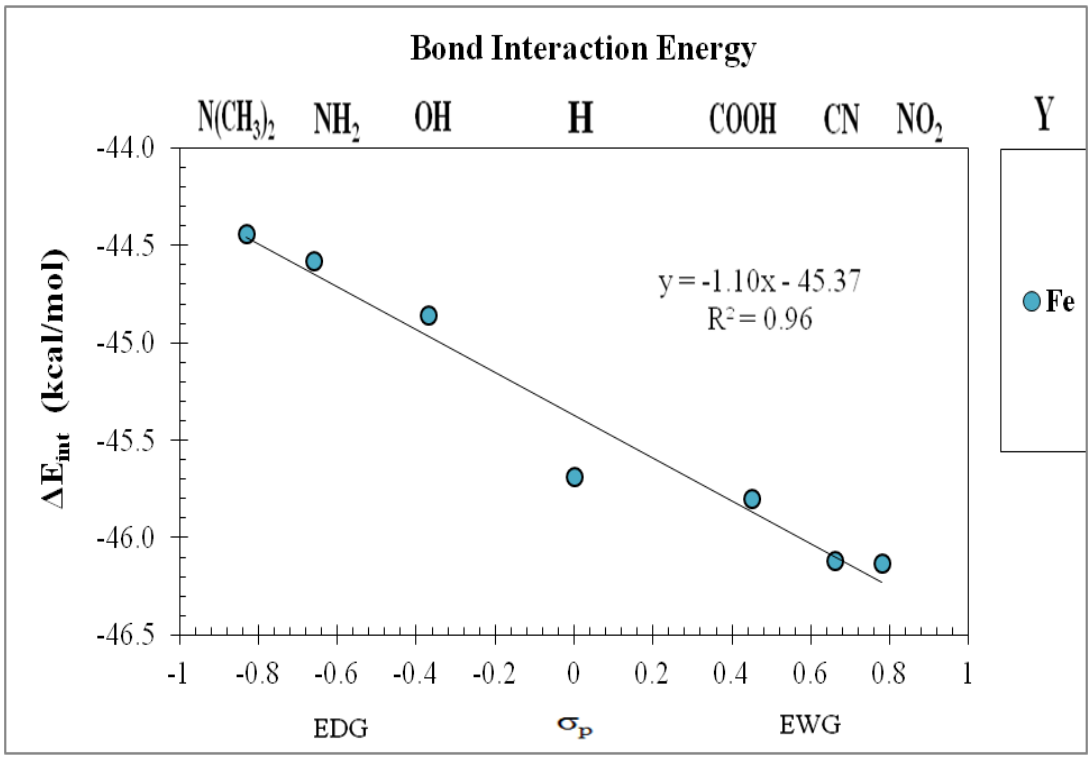

Figure 71. Graph of ΔE_{int} vs. σ_p for the [$Fe(CO)_4$L-Y] complex series.

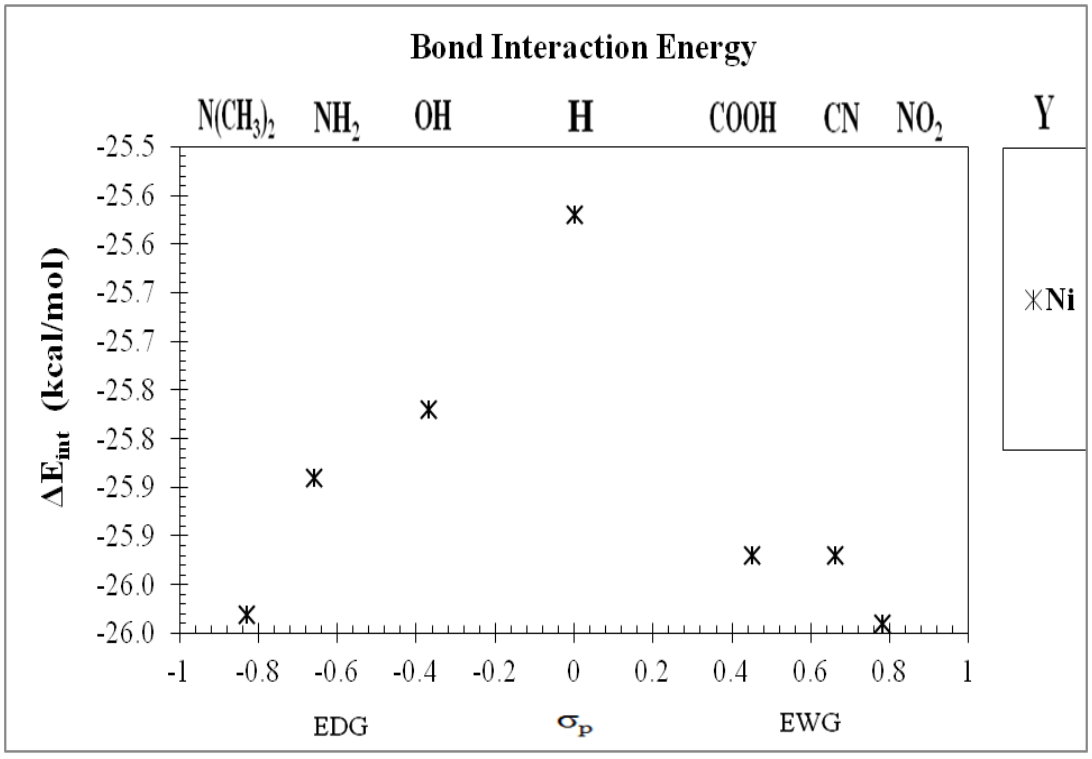

Figure 72. Graph of ΔE_{int} vs. σ_p for the [$Ni(CO)_3$L-Y] complex series.

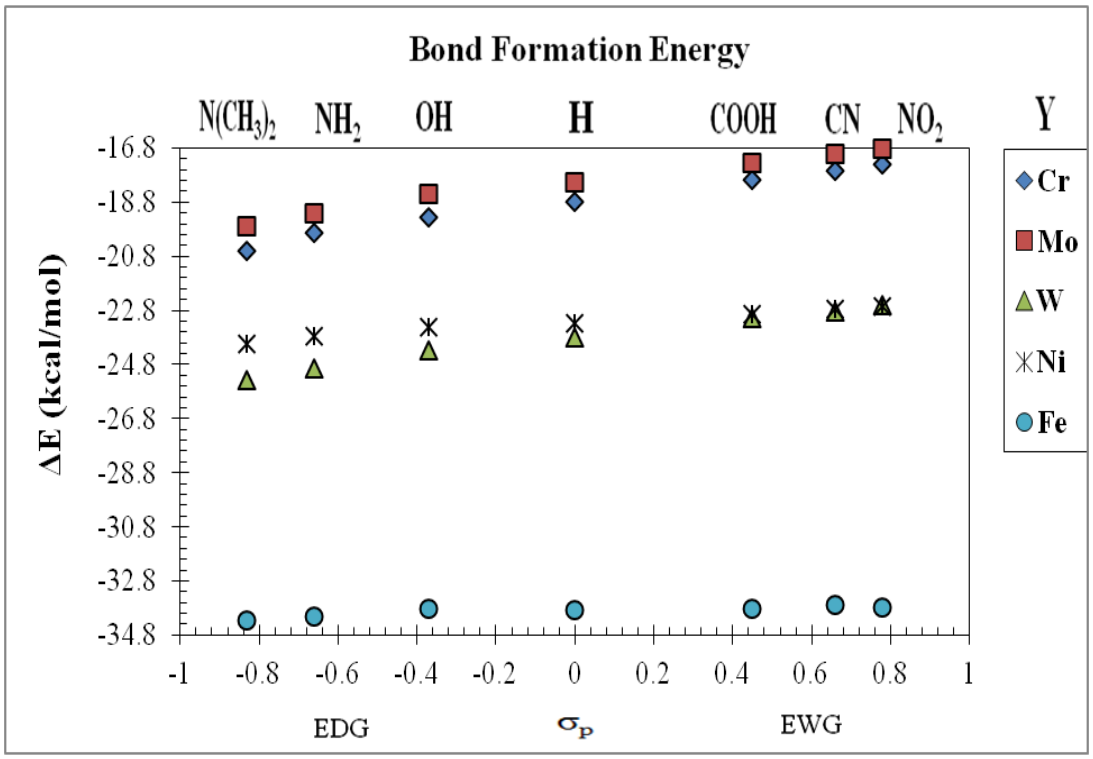

Figure 73. Graph of ΔE vs. σ_p for the [$M(CO)_xL$-Y] complex series.

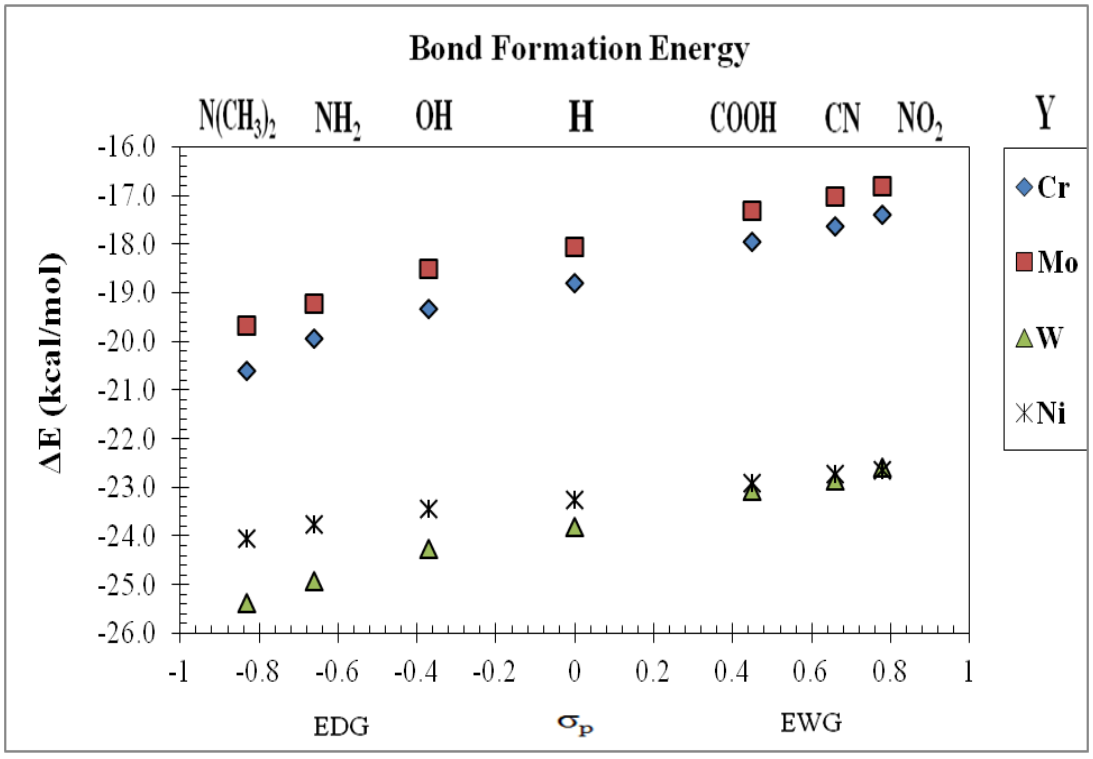

Figure 74. Graph of ΔE vs. σ_p for the [$M(CO)_xL$-Y] complex series.

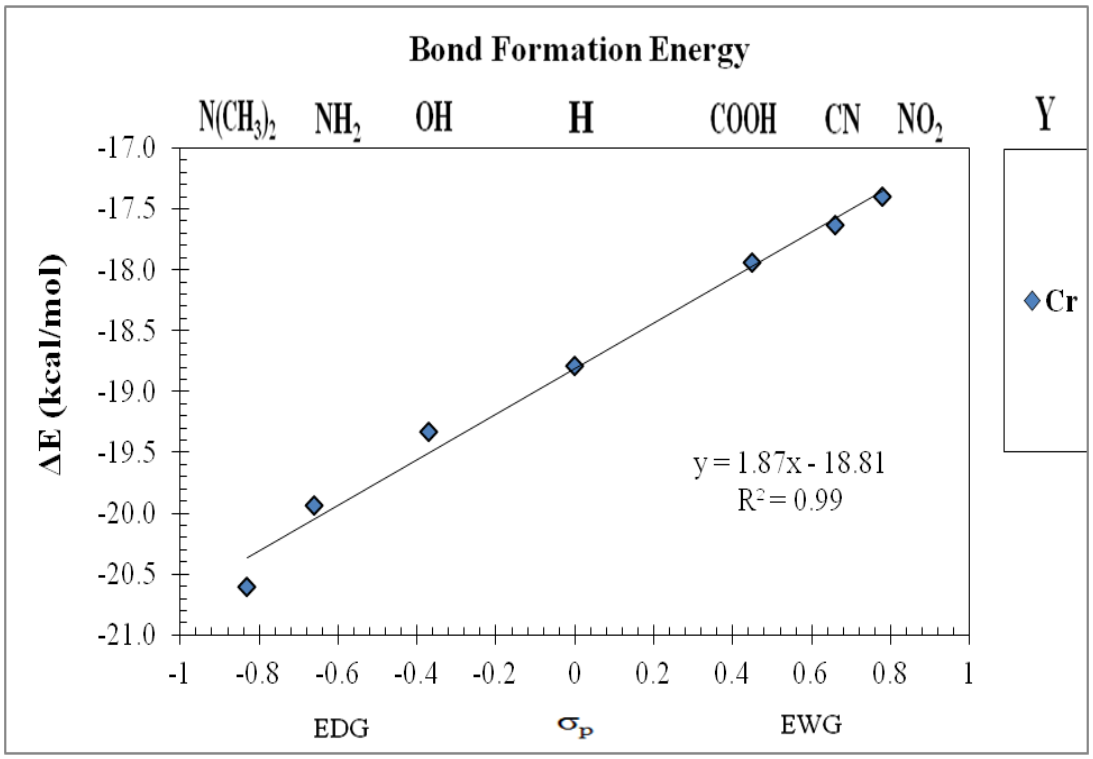

Figure 75. Graph of ΔE vs. σ_p for the [$Cr(CO)_5$L-Y] complex series.

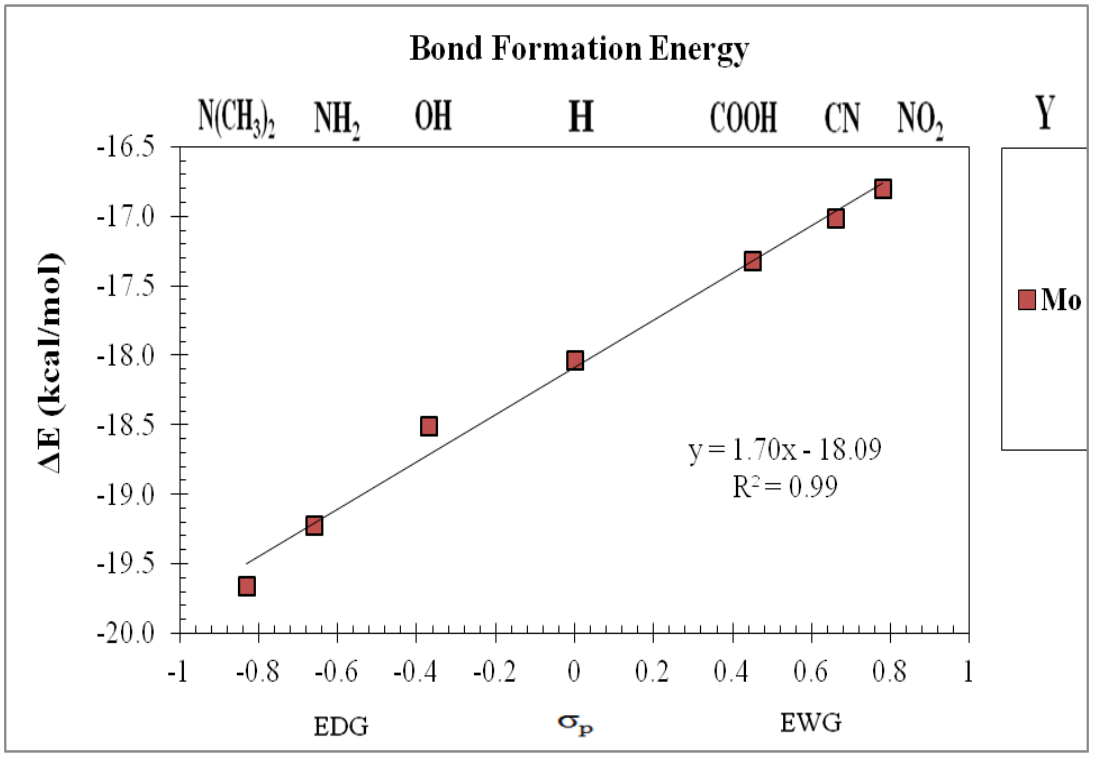

Figure 76: Graph of ΔE vs. σ_p for the [$Mo(CO)_5$L-Y] complex series.

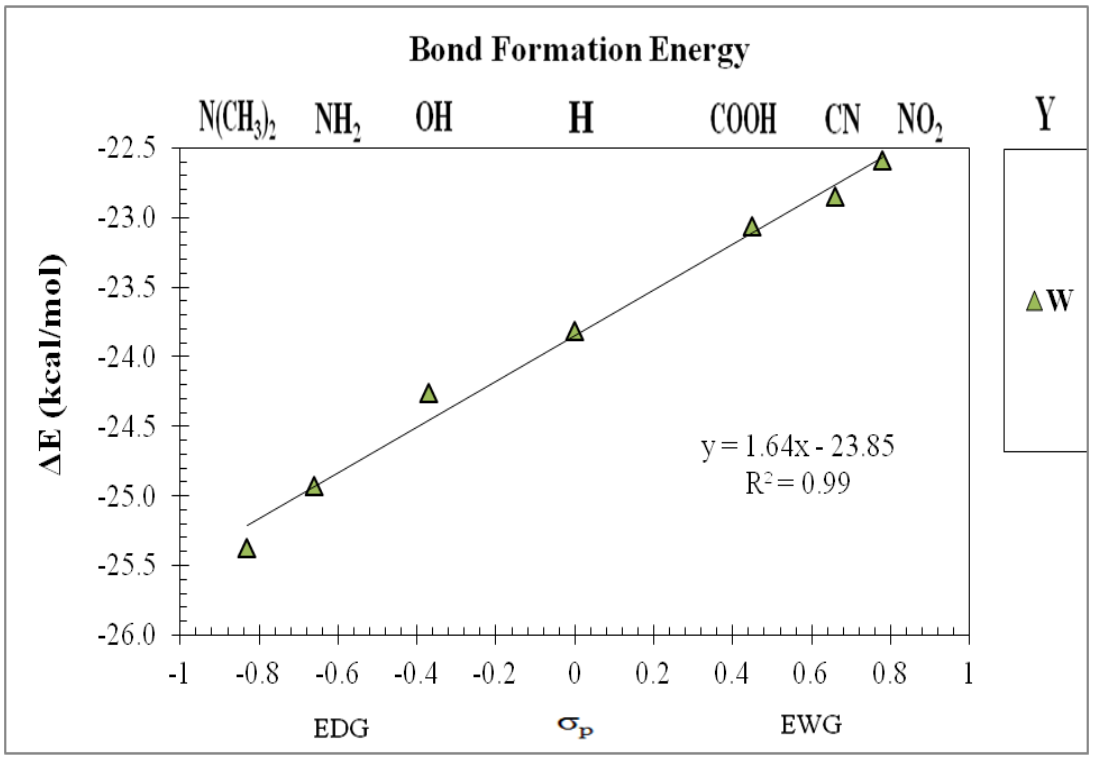

Figure 77. Graph of ΔE vs. σ_p for the [$W(CO)_5$L-Y] complex series.

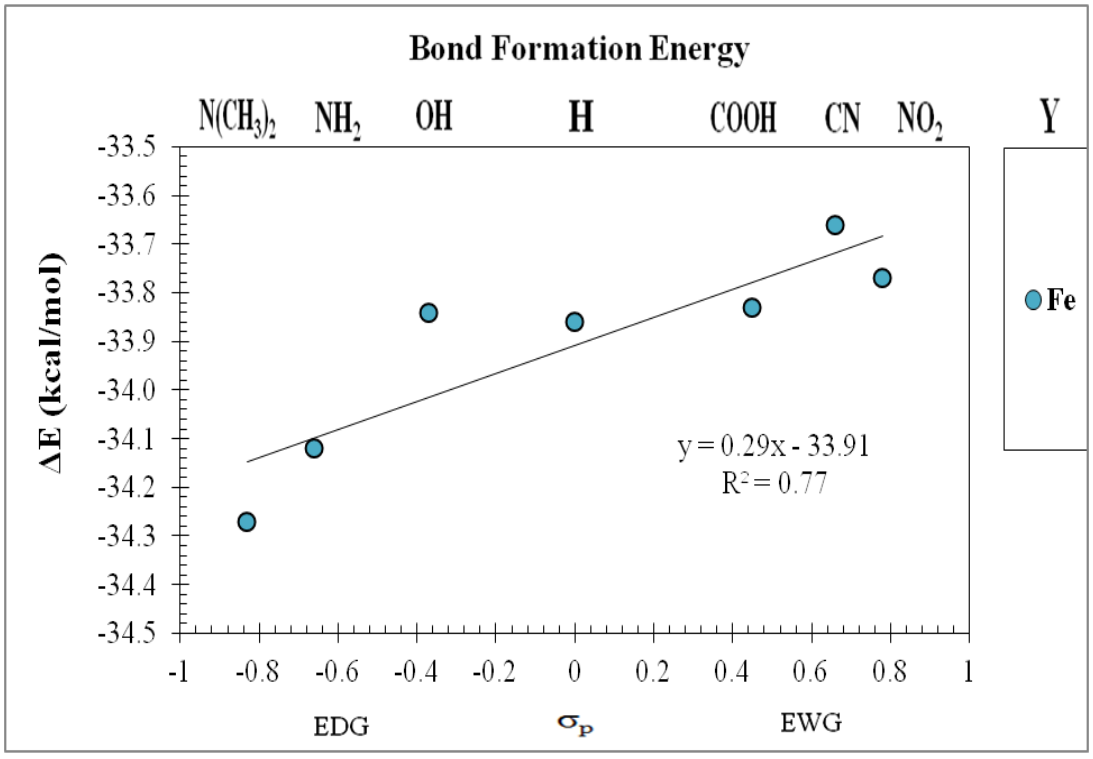

Figure 78. Graph of ΔE vs. σ_p for the [$Fe(CO)_4$L-Y] complex series.

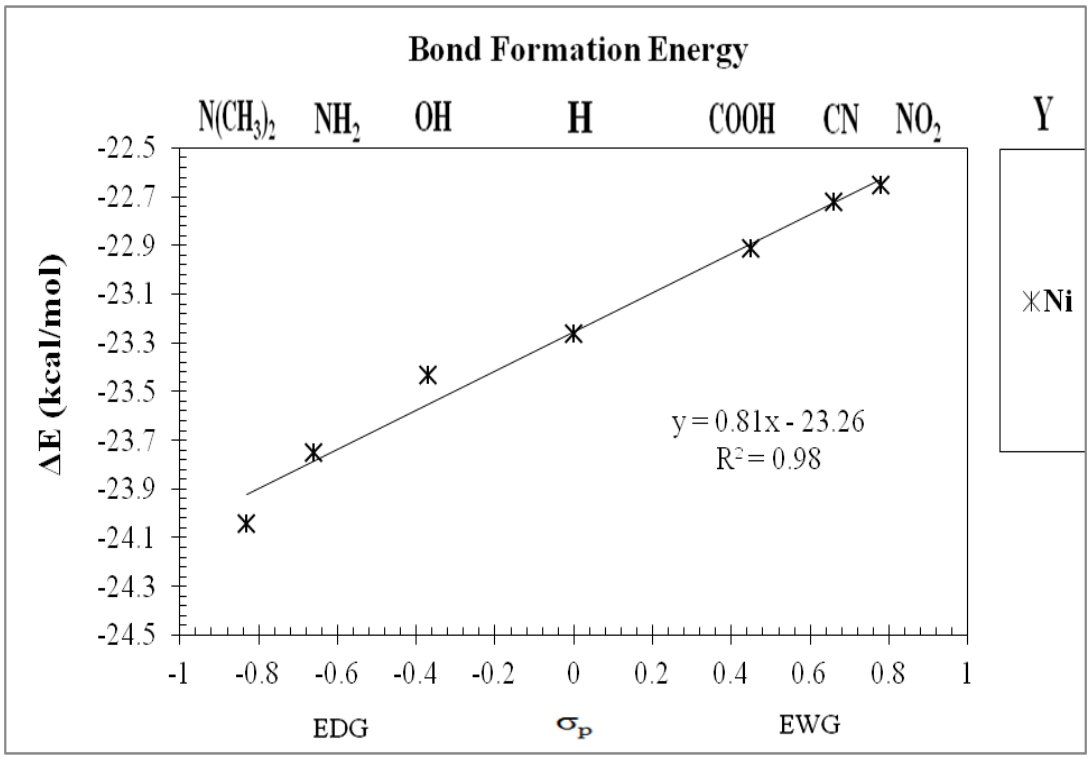

Figure 79. Graph of ΔE vs. σ_p for the [$Ni(CO)_3L$-Y] complex series.

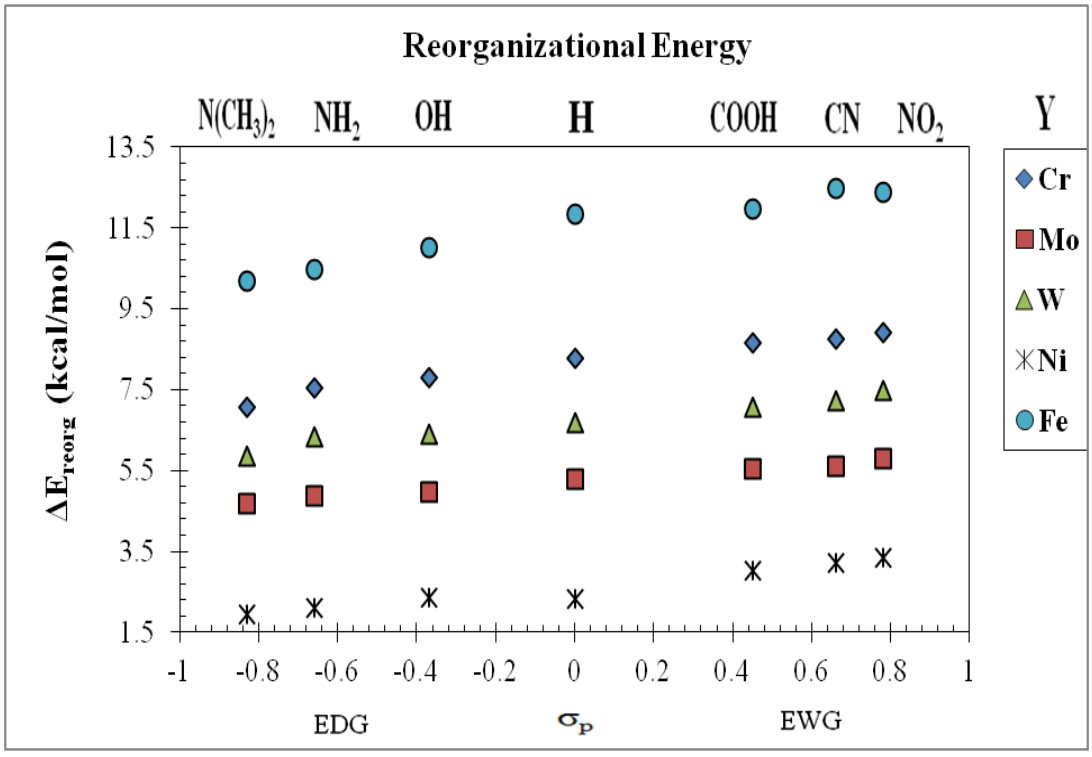

Figure 80. Graph of ΔE_{reorg} vs. σ_p for the [$M(CO)_xL$-Y] complex series.

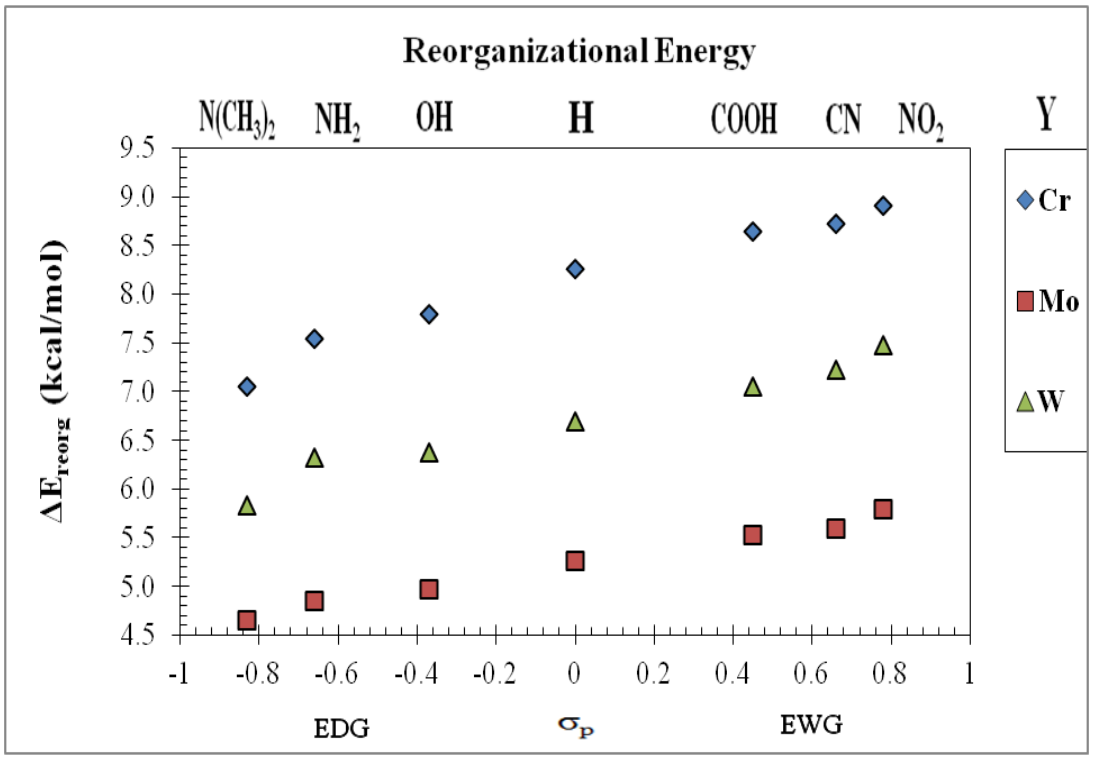

Figure 81. Graph of ΔE_{reorg} vs. σ_p for the $[M(CO)_xL\text{-}Y]$ complex series.

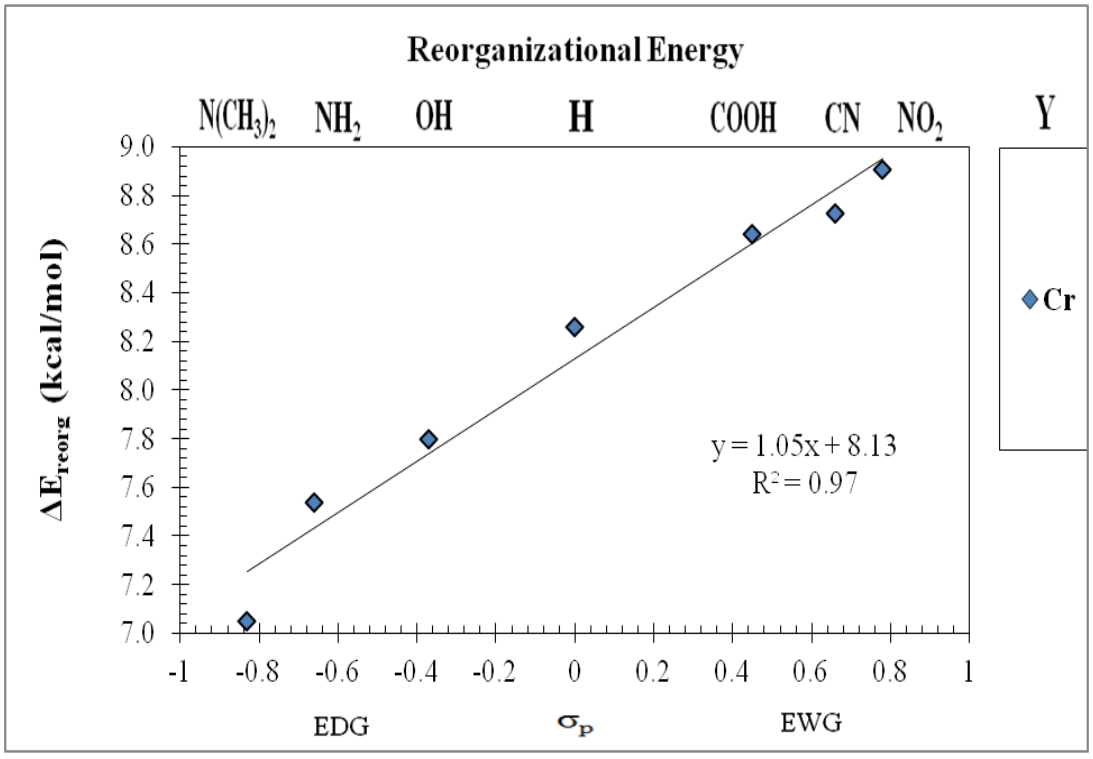

Figure 82. Graph of ΔE_{reorg} vs. σ_p for the $[Cr(CO)_5L\text{-}Y]$ complex series.

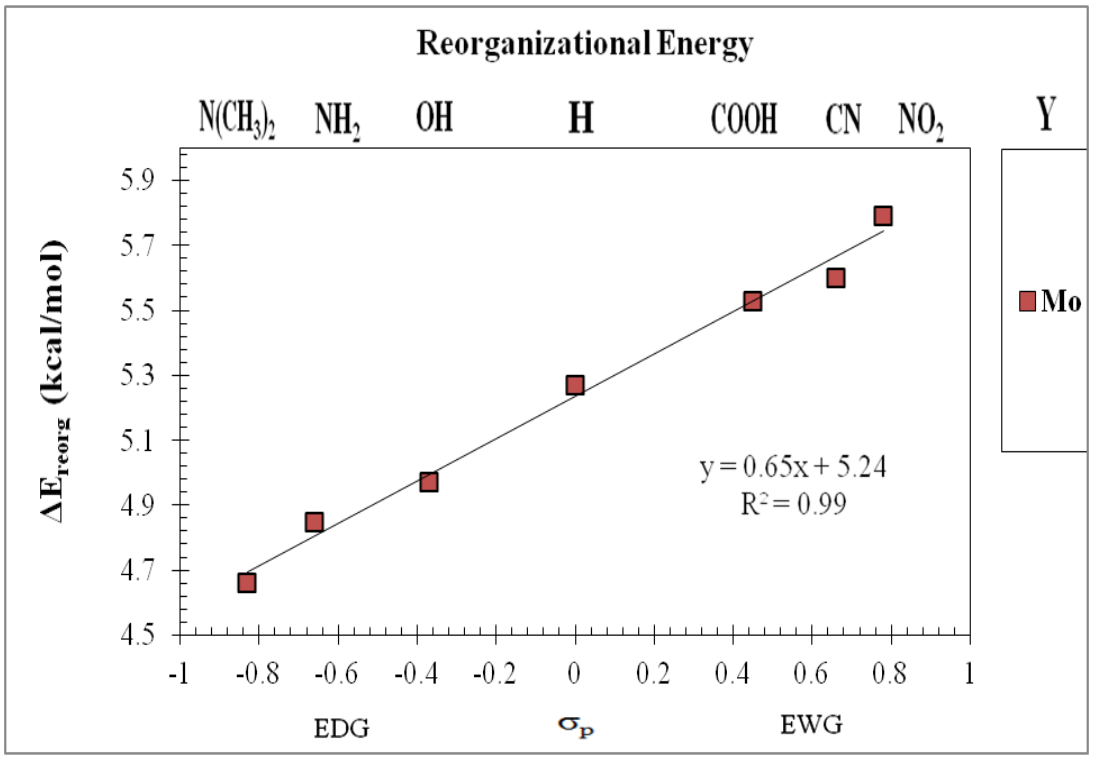

Figure 83. Graph of ΔE_{reorg} vs. σ_p for the $[Mo(CO)_5L\text{-}Y]$ complex series.

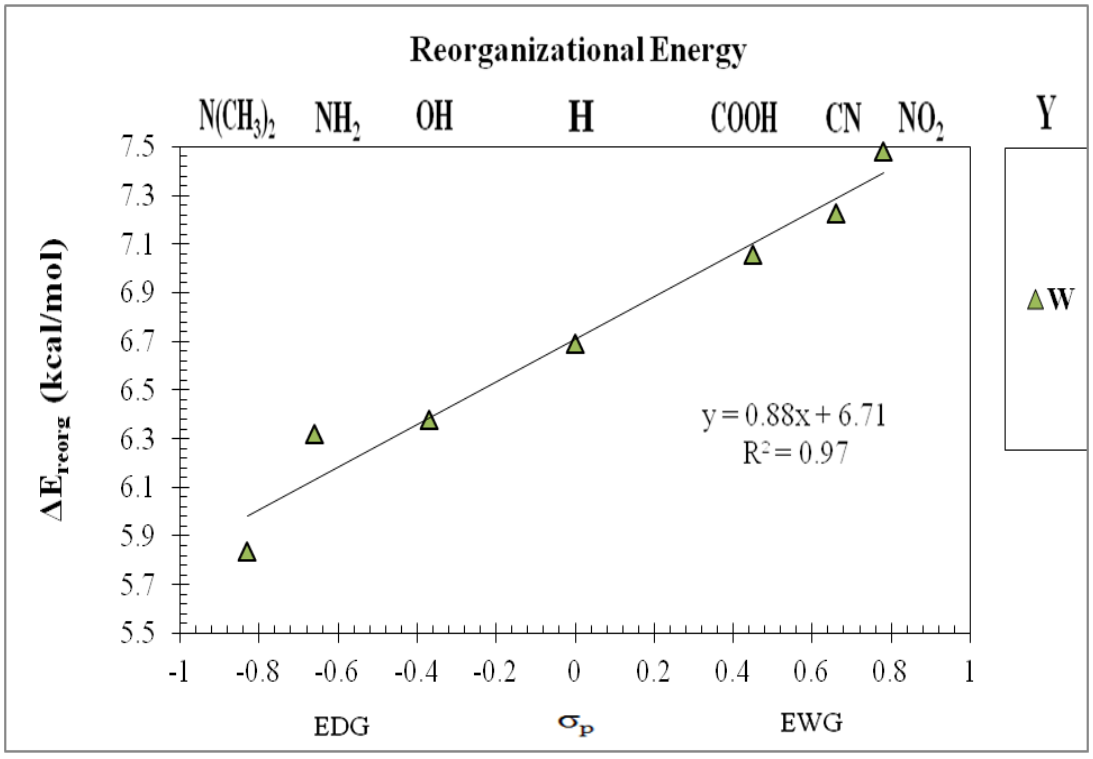

Figure 84. Graph of ΔE_{reorg} vs. σ_p for the $[W(CO)_5L\text{-}Y]$ complex series.

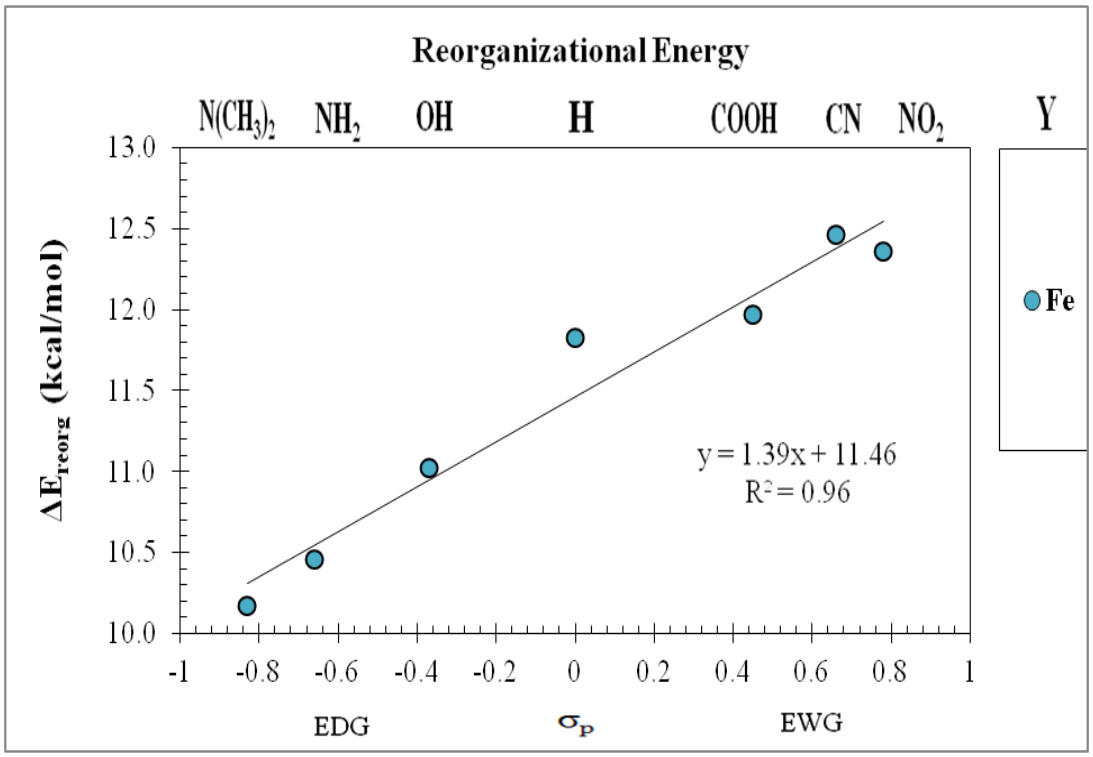

Figure 85. Graph of ΔE_{reorg} vs. σ_p for the $[Fe(CO)_4L\text{-}Y]$ complex series.

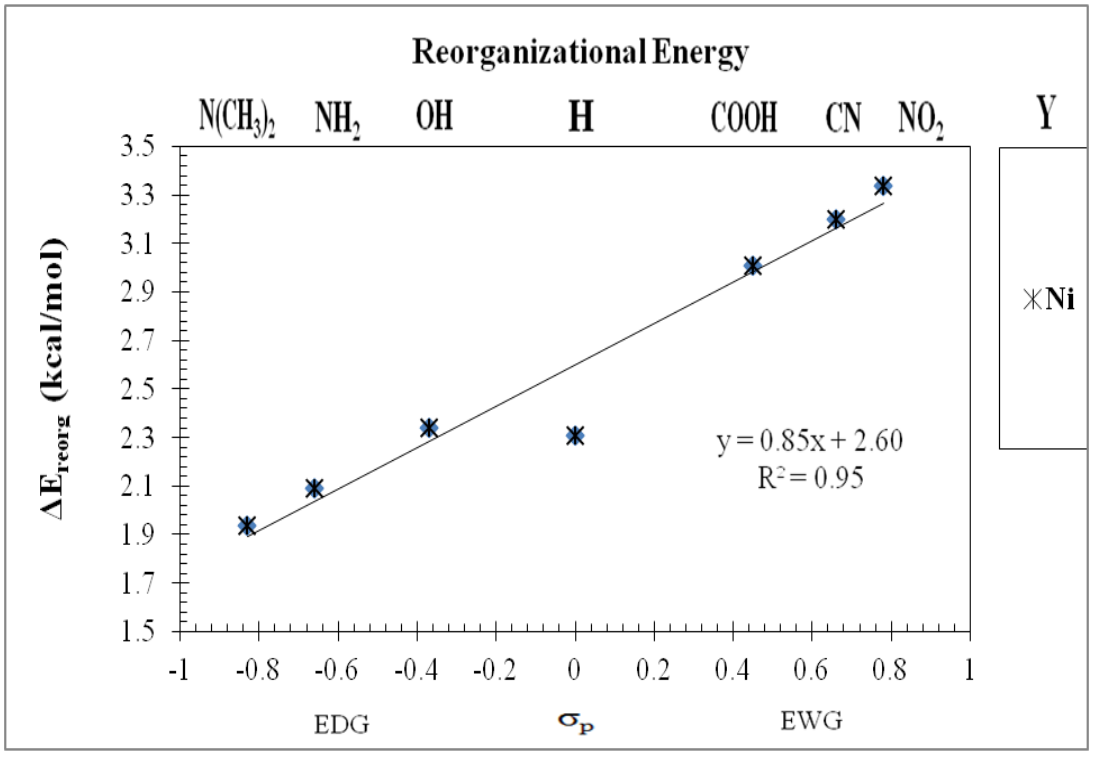

Figure 86. Graph of ΔE_{reorg} vs. σ_p for the $[Ni(CO)_3L\text{-}Y]$ complex series.

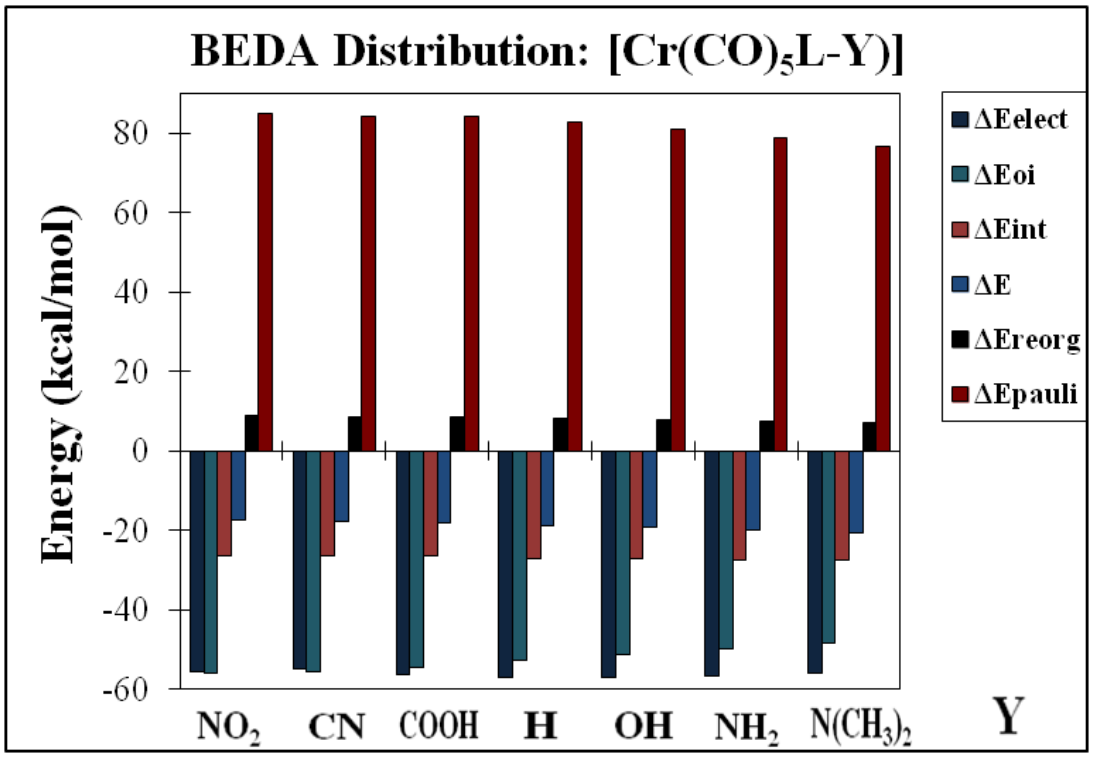

Figure 87. Graph of BEDA distribution: [$Cr(CO)_5$L-Y] complex series.

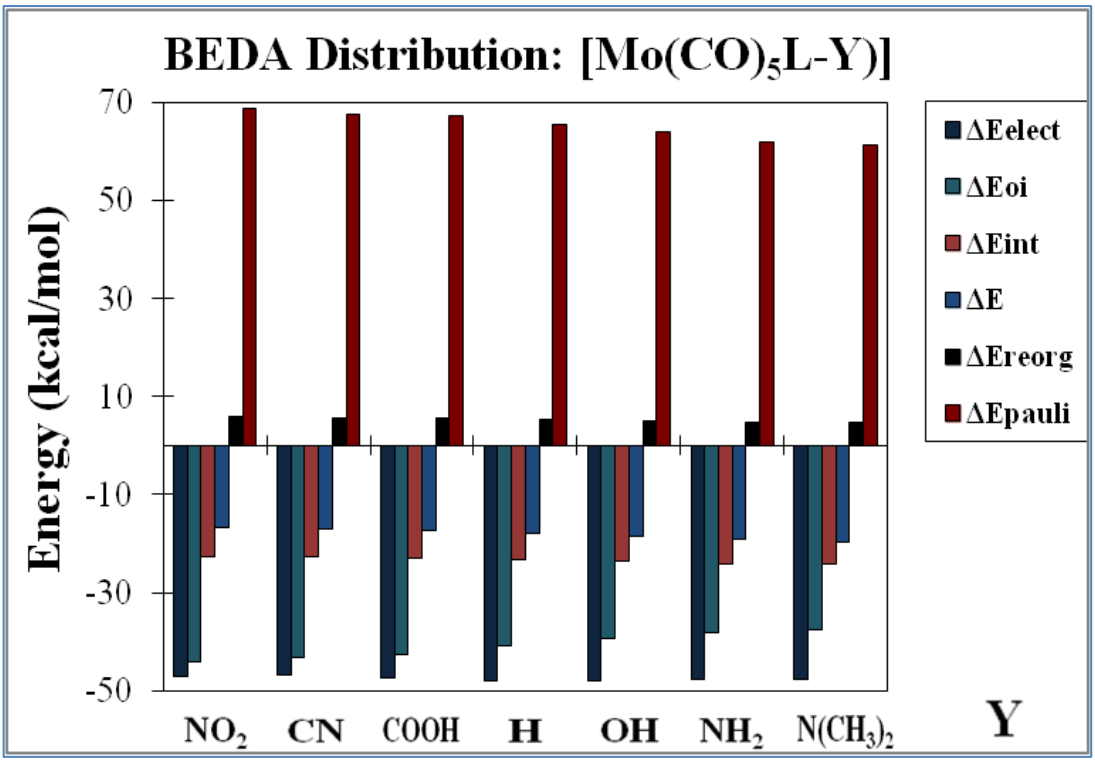

Figure 88. Graph of BEDA distribution: [$Mo(CO)_5$L-Y] complex series.

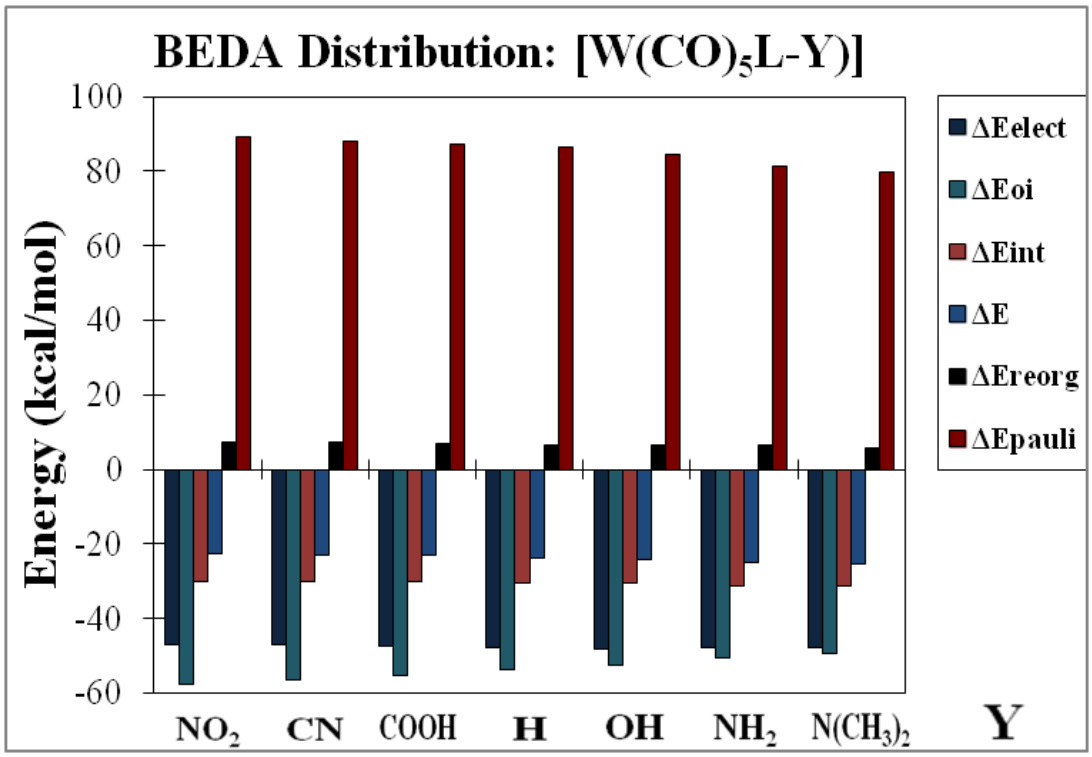

Figure 89. Graph of BEDA distribution: [$W(CO)_5$L-Y] complex series.

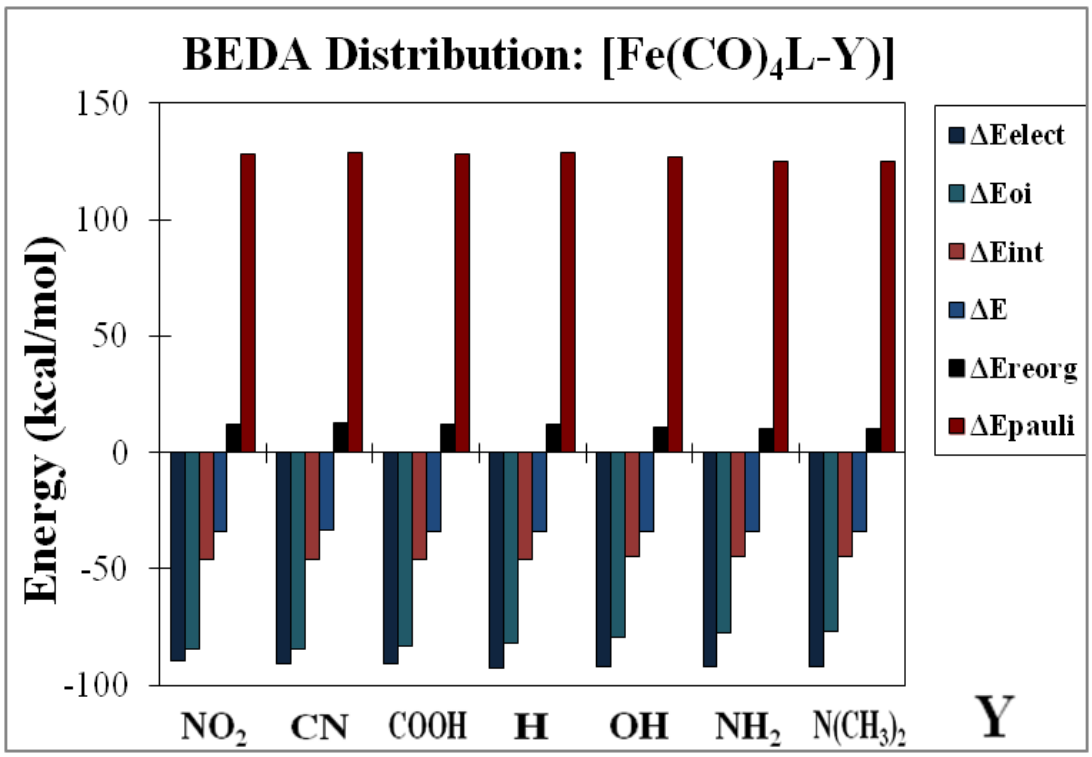

Figure 90. Graph of BEDA distribution: [$Fe(CO)_4$L-Y] complex series.

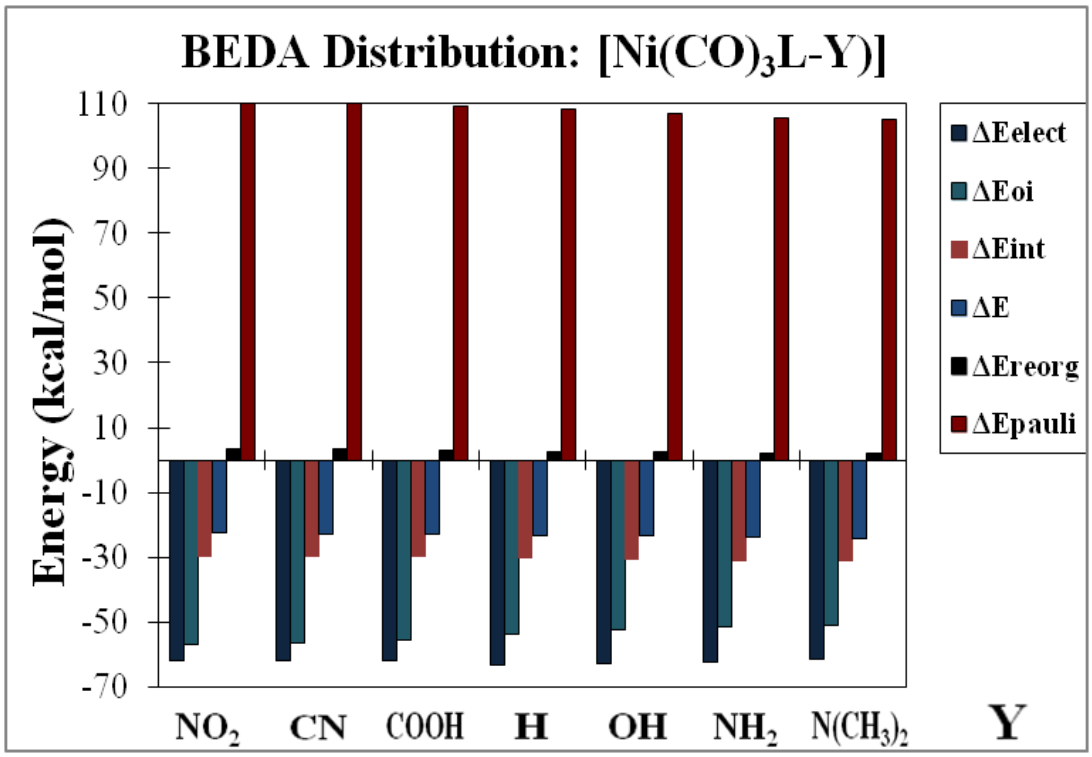

Figure 91. Graph of BEDA distribution: [$Ni(CO)_3$L-Y] complex series.

All plots suggest that the trend in energy distribution, based on ligand selection, should follow in the general order of stability: $N(CH_3)_2$ > NH_2 > OH > H > COOH > CN > NO_2. Figure 66 signifies the overall interaction energy trends between each transition metal studied, following in the general order of $Mo(CO)_5$ < $Cr(CO)_5$ < $Ni(CO)_3$ < $W(CO)_5$ < $Fe(CO)_4$. Figure 73 indicates the total bond formation energy trends between each transition metal studied, following in the general order of $Mo(CO)_5$ < $Cr(CO)_5$ < $Ni(CO)_3$ < $W(CO)_5$ < $Fe(CO)_4$. The reorganizational energy (ΔE_{reorg}) accounts for the energetic cost of the geometrical changes that occur in the $M(CO)_5$ fragment ($\Delta E_{reorg}(M(CO)_5)$) and the olefin ($\Delta E_{reorg}$(olefin)) as they interact to form the complex; following in the general order of $Ni(CO)_3$ < $Mo(CO)_5$ < $W(CO)_5$ < $Cr(CO)_5$ < $Fe(CO)_4$ as shown in Figure 80.

Figures 92-96 depict bond formation energy (ΔE) component percent distributions for each transition metal studied based on a quantitative measure of substituent effects. Graphs show individual percent contributions to the total bond formation energy ΔE based on the absolute summation of the relative magnitudes of the attractive orbital interaction ΔE_{oi}, attractive electrostatic interaction ΔE_{elect}, pauli repulsive interaction ΔE_{pauli}, and reorganizational energies ΔE_{reorg} for each transition metal para substituted olefin complex. Figures 92-94 compare the overall ΔE BEDA component percent distribution differences against substituent effects for the $[M(CO)_5(\eta^2\text{-}C_2H_3\text{-}C_6H_4\text{-}Y)]$ complex series. Figure 95-96 serve to compare the individual ΔE BEDA component percent distribution differences against substituent effects for the $[Fe(CO)_4(\eta^2\text{-}C_2H_3\text{-}C_6H_4\text{-}Y)]$ and $[Ni(CO)_3(\eta^2\text{-}C_2H_3\text{-}C_6H_4\text{-}Y)]$ complex series, respectively.

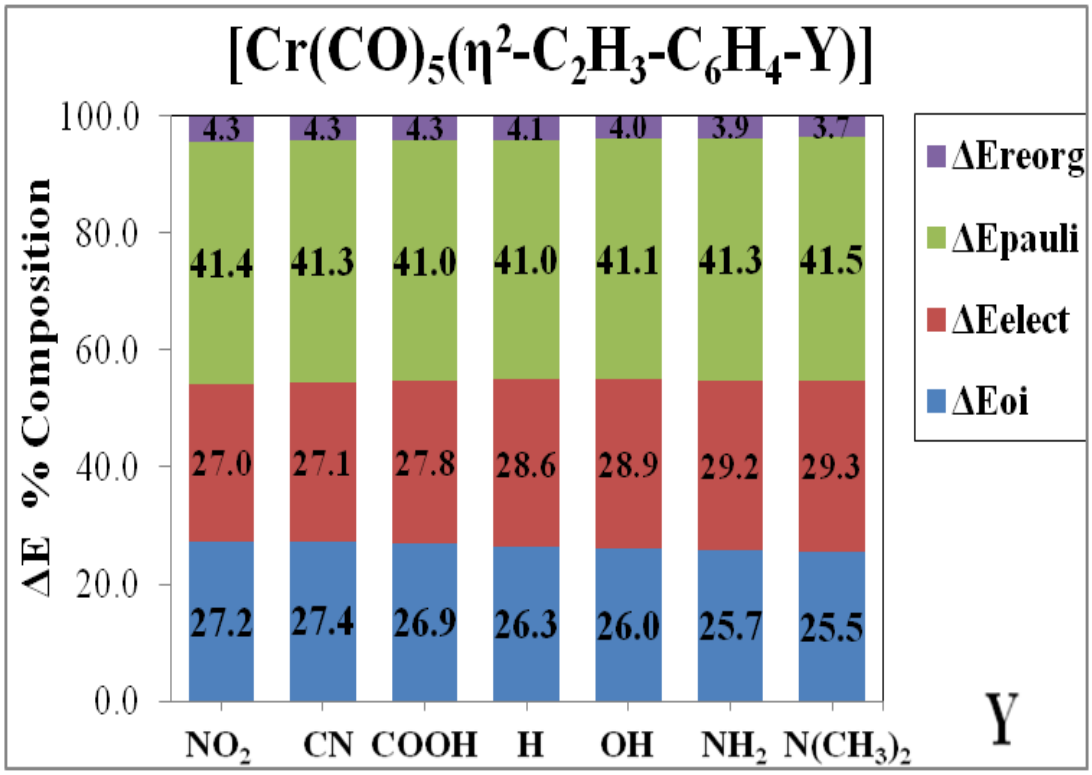

Figure 92. Graph of ΔE BEDA % composition: $[Cr(CO)_5L\text{-}Y]$ complex series.

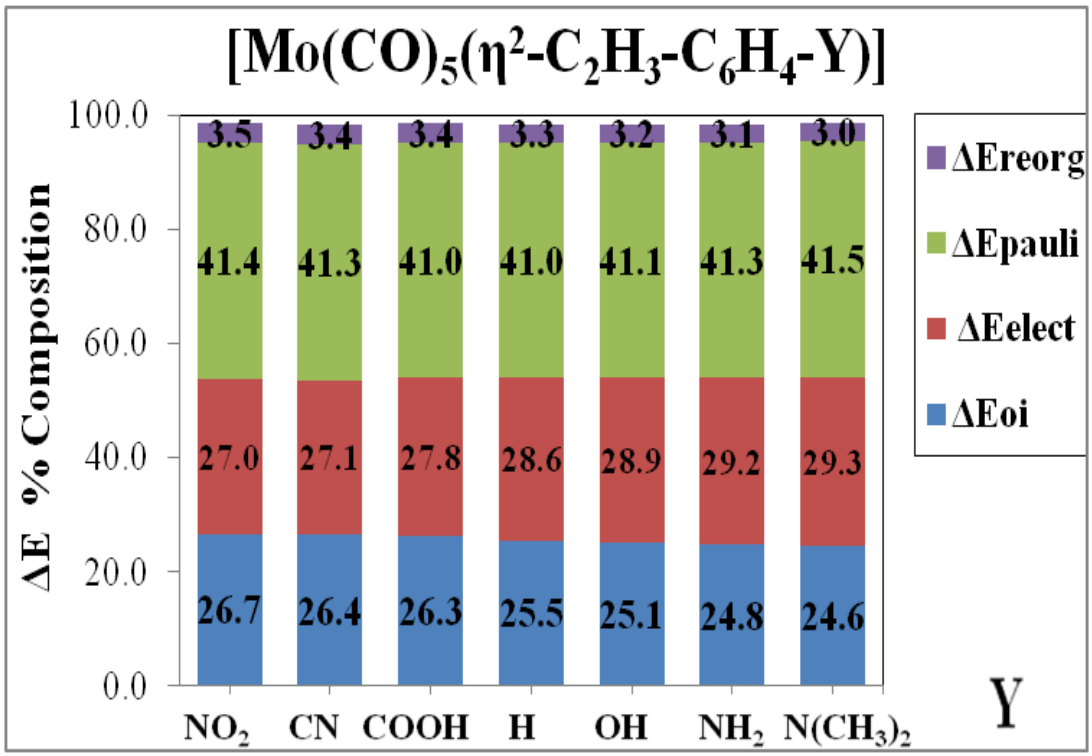

Figure 93. Graph of ΔE BEDA % composition: $[Mo(CO)_5L\text{-}Y]$ complex series.

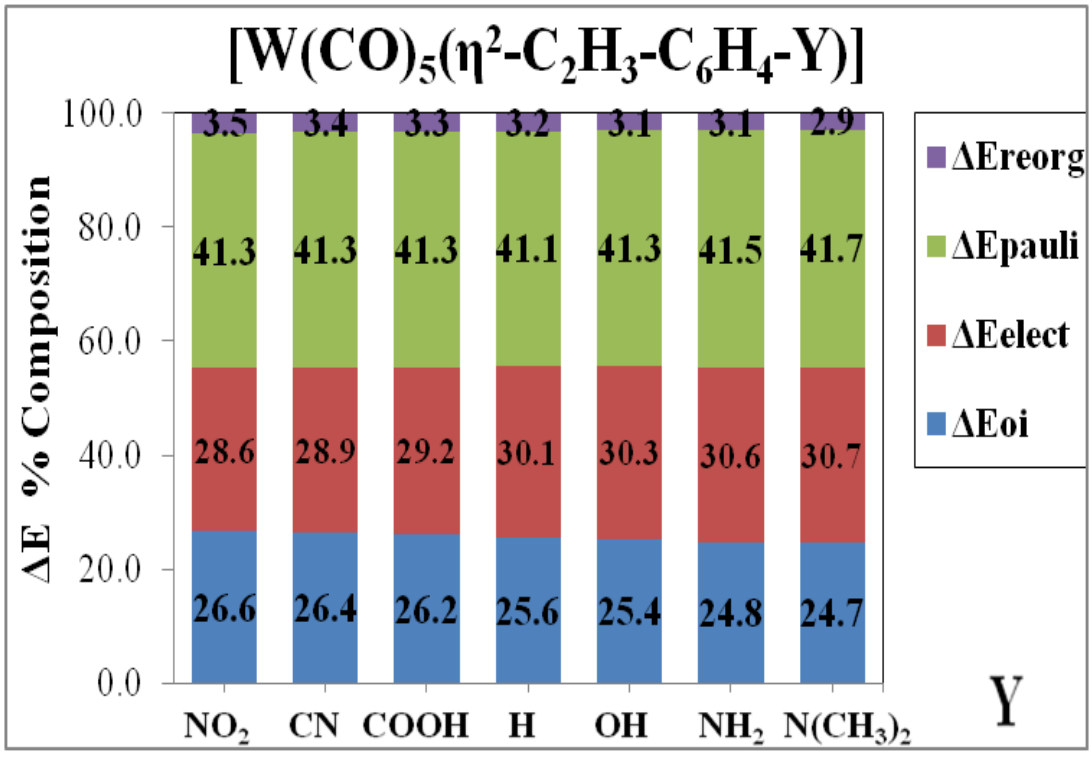

Figure 94. Graph of ΔE BEDA % composition: $[W(CO)_5L\text{-}Y]$ complex series.

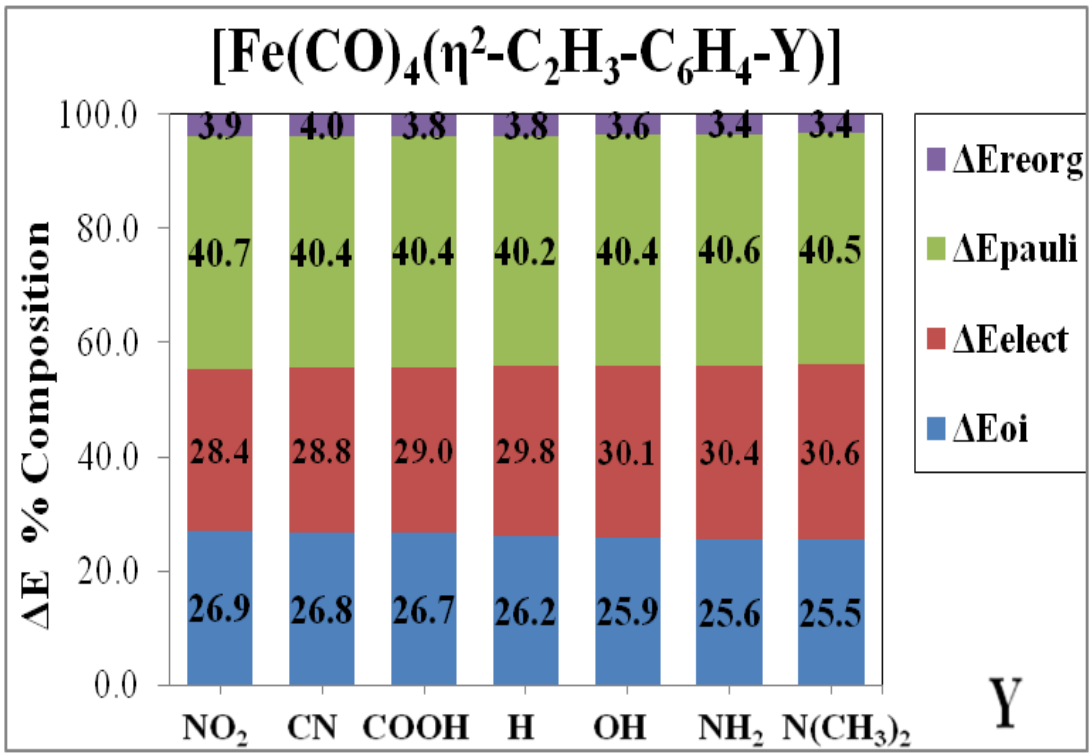

Figure 95. Graph of ΔE BEDA % composition: $[Fe(CO)_4L\text{-}Y]$ complex series.

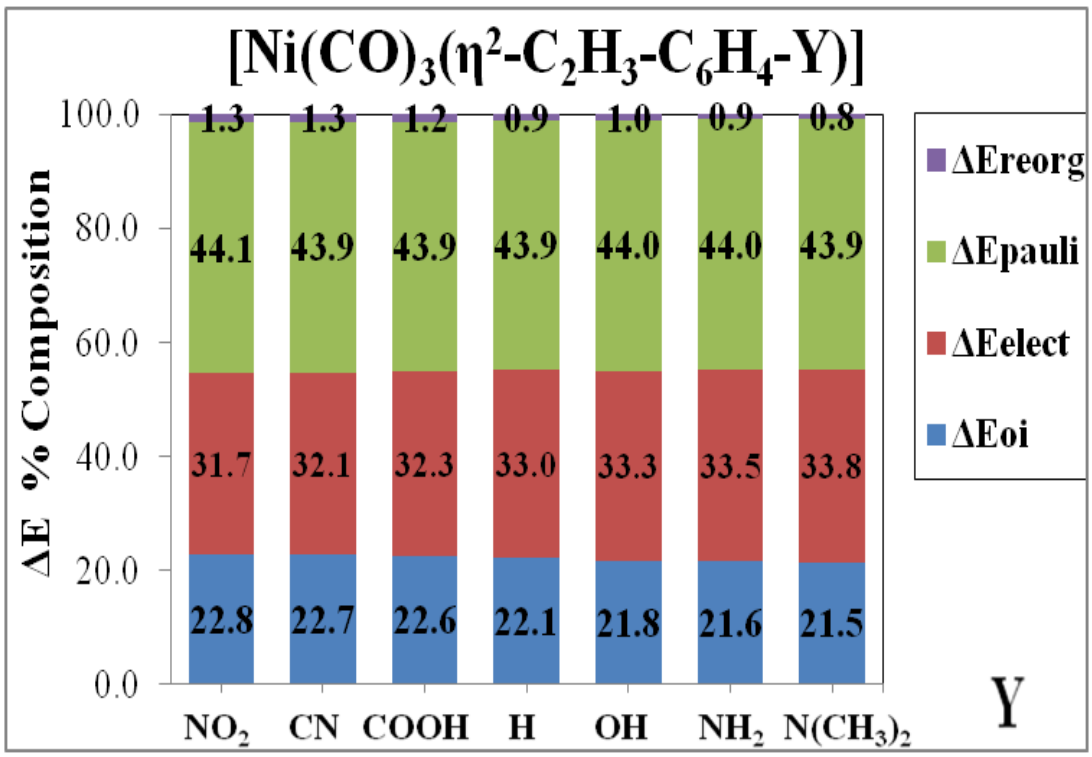

Figure 96. Graph of ΔE BEDA % composition: $[Ni(CO)_3L\text{-}Y]$ complex series.

Figures 92-96 serve to compare general trends in the overall bond formation energy (ΔE) based on a component percentage distribution for each transition metal studied. Noticeable trends are evident, for example the percentages of attractive covalent interaction ΔE_{oi} and electrostatic interactions ΔE_{elect} behave in similar fashion to the trends observed for $\Delta E_{int;}$ that is, in opposition of one another with respect to an increase in the EWD capacity of the olefin system. As before, this balancing act between the attractive terms ultimately causes the trend in the percentage of total repulsive energy to be rather flat across the ligand series. That is, notice that the total contribution of ΔE_{pauli} towards the absolute interaction energy is approximately 38-44 % overall, regardless of substituent effects or transition metal influence.

It was found that the magnitude of the covalent attraction term ΔE_{oi} increases in proportion to an increase in the EWD ability of the para substituent; this is to be expected on the basis of former DCD implications. Qualitatively, ΔE_{oi} occupies approximately 22-27 % of the attractive contribution towards the total absolute magnitude of the bond formation energy, whereas the electrostatic interaction (ΔE_{elect}) is the dominant term overall (comprising 27-34 % of the attractive contribution towards the total ΔE). Notice that based on a range of percent contribution ΔE_{elect} and ΔE_{oi} seem to be most influenced by substituent effects relative to ΔE_{pauli}, which only varies by approximately 1 % across the ligand series for each metal. If the percent magnitude of the sum of attractive terms ($\Delta E_{elect} + \Delta E_{oi}$) is compared to the percent magnitude of the repulsive contribution (ΔE_{pauli}), we see that approximately 54-56 % of the total interaction energy is due to attraction. Clearly, the contribution made by the ΔE_{reorg} term is quite insignificant relative to the overall magnitude of the interaction energy component.

In general, ΔE_{int} is not influenced much by the nature of substituent effects, ranging from 22-24, 26-28, 30-31, and 44-46 kcal/mol for $[Mo(CO)_5L\text{-}Y] < [Ni(CO)_3L\text{-}Y] < [Cr(CO)_5L\text{-}Y] < [W(CO)_5L\text{-}Y] < [Fe(CO)_4L\text{-}Y]$, respectively. Ultimately, DFT calculations indicate that the trend in metal-olefin bond formation energies are opposite to the electron-withdrawing ability of the olefin, which is counter to expectations based on the DCD model for metal-olefin bonding. Interestingly, the overall magnitudes of the attractive (ΔE_{oi}) and repulsive (ΔE_{pauli}) terms seem to increase with respect to an increase in the EWD potential of the para substituent at about the same rate. Since these trends are in opposition to one another and because the behavior of ΔE_{elect} is uninfluenced by substituent modification, this causes the trend in the total interaction energy to be rather flat across the ligand series. Another interesting observation is that the larger the steric term, the more an increase in the reorganizational trend (ΔE_{reorg}) across the series. Given that the bond formation energy is obtained by the combination of the interaction energy and the reorganizational energy, it can be concluded that the bond formation energy is influenced by the magnitude of the reorganizational energy; however, not to a substantial degree as the location of the effector group is well far from the bonding site. That is, the magnitude of the ΔE_{reorg} term accounts for less than ~5% the total composition of bond formation energy ΔE. Overall, the calculations from the energy decomposition analysis indicate that the trends in the total electronic interaction energy (ΔE_{int}, kcal/mol) decrease with an increase in the EWD capacity of the para substituent, for the $[Mo(CO)_5L\text{-}Y]$, $[Cr(CO)_5L\text{-}Y]$, and $[W(CO)_5L\text{-}Y]$ complex series. Clearly, this would suggest that metal-olefins of greater EWD capacity demonstrate a bonding energy contrary to what is expected based on former DCD implications.

The key attractive and repulsive interactions contributing to the bond formation energies were obtained from the BEDA. The strong interaction between olefins of greater EWD capacity and the metal carbonyl fragment is due to the large orbital interaction energy (ΔE_{oi}). The trend in this energy term is similar to the trend observed for ΔE_{pauli}. Further analysis of the interaction energy ΔE_{int} distribution trends indicate that the percent contribution of the ionic bonding component ΔE_{elect} to the total ΔE_{int} decreases as the olefinic EWD character increase, ranging from 31-28 %, respectively. When combined, the attractive terms ($\Delta E_{elect} + \Delta E_{oi}$) compose the percentage of overall attractive energy released during bond formation. Noticeable trends are evident, for instance the percentages of attractive covalent interaction ΔE_{oi} and electrostatic interactions ΔE_{elect} behave in opposition to one another with respect to an increase in the EWD capacity of the olefin system. This balancing act between the attractive terms ultimately causes the trend in the percentage of total repulsive energy to be rather flat across the ligand series. In general, the summation of the total magnitude for the combination of both attractive terms ($\Delta E_{elect} + \Delta E_{oi}$) is influenced by the electronic nature of the para substituent, as it increases with respect to an increase in the EWD ability of the olefin. However, when expressed as a percentage of the total bond formation energy composition the summation of these terms indicates a trend similar to the net bonding interaction energy, which is rather flat. Interestingly, the amount of steric repulsion towards the net bonding interaction energy is also influenced by the electronic nature of substituent effects in a similar fashion. This may suggest an imperative nature of balance between the attractive and repulsive terms towards formation of the metal-olefin bond, which is manifested in a rather flat trend for the net bonding interaction energy term (ΔE_{int}).

Metal-olefin bond energy decomposition analyses provide much greater insight into the contradiction between calculated bond formation energies and the expectation based on a MO analysis and the DCD model. A most important result which comes out of the decomposition analysis of the metal-olefin bond formation energy is that *if only the orbital interaction energy* (ΔE_{oi}) *were considered, all the EWD olefins would be more strongly bound to* $M(CO)_x$ *than styrene*. One primary finding of this particular study shows that as the EWD capacity of the para substituent increases, the metal to olefin bond formation energy decreases. In the context of the DCD model, an increase in the back-bonding ability of the olefin should result in the formation of more stable complexes. However, our results actually indicate that the opposite occurs as manifested by a reduction in overall bond strength. In addition, although the energetic cost due to molecular reorganization of the reacting moieties can be an important factor in predicting the total metal-olefin bond formation energy, this contribution has typically been neglected in considerations of BDEs in organometallic complexes.[1,26, 63-65] Another intriguing observation from these calculations is that the metal-olefin bond lengths do not correlate directly with the bond energy for all the complexes being studied. This is likely a consequence of the stronger attraction between the olefin and the metal fragment. An olefin with a large EWD ability is able to get closer to the metal as manifested by the M-C_{olefin} bond lengths (see Tables 5-7), further resulting in an increase in the repulsive energy term as the EWD effect increases. Thus, typical expectations regarding bond energy bond-order correlations are not valid for this series of complexes and, more importantly, it is clear that predictions of relative bond energy based on relative bond lengths could be inaccurate.

There are some differences in the metal complexes to be noticed. For instance, the BEDA analyses indicate that the EWD ligands are the ones that interact the most with the metal, followed by the neutral styrene and electron donating ligands as reflected from the orbital interaction (ΔE_{oi}) energies. This order is also congruent with the MO analysis which indicates that the EWD ligands back-bond better with a given metal because they demonstrate a smaller energy gap. All systems studied contribute similarly into the σ interaction, with preference towards the effector of greatest electron donating capacity. The stronger attractive interaction of the EWD ligand draws it closer to the metal (bond length is shorter) which also accounts for a larger Pauli (steric) orbital repulsion.

In prior discussions, it has been shown that geometrical changes in the olefin accounts for 75-85% of the total reorganizational energy; thus, we can deduce that the conformational changes that occur in the olefin are mostly responsible for the trend seen for the bond dissociation energy.[1] The main geometrical changes occurring are related to the change in orbital hybridization as a result of the metal-olefin σ and π interactions and are manifested in the elongation of the olefinic C=C bond and the pyramidalization angle. The changes that occur in the geometry of the olefin correlate very well to the changes that are observed in reorganizational energy. As the EWD potential of the para effector is increased, the C=C bond lengthens mostly because of the increase in the electron population of the π^* orbitals in the olefin from the back-bonding interaction with the metal. It is also evident that the change in the pyramidalization angle is increasing as well with respect to an increase in the EWD capacity of the olefin. This is a result of a greater change in hybridization of the olefinic carbons toward a more sp^3 like molecular orbital induced by the changes in electron population.

In this thesis, the relative effect of the influence of the group 6 triad transition metal (M= Cr, Mo, W) down a group for the complex $[M(CO)_5(\eta^2\text{-}C_2H_3\text{-}C_6H_4\text{-}Y)]$ olefin series has been gauged. We were also able to measure and compare metal-olefin bond energies for the $[Fe(CO)_4(\eta^2\text{-}C_2H_3\text{-}C_6H_4\text{-}Y)]$ and $[Ni(CO)_3(\eta^2\text{-}C_2H_3\text{-}C_6H_4\text{-}Y)]$ complex series. Nickel(0) is a d^8 electron metal, which can be compared with the d^5 group 6 triad. The iron complexes are d^6 and will provide a direct comparison to the nickel styrene complexes. It is evident that the $[Fe(CO)_4(\eta^2\text{-}C_2H_3\text{-}C_6H_4\text{-}Y)]$ complex series forms the most stable metal-olefin bond. The strongest alkene-metal bonds occur with third row metals (as with almost all ligands) and when one can get more π-backbonding to occur. The amount of π-backbonding depends strongly on how electron-rich the metal center is and whether or not there are electron-withdrawing groups on the alkene to make it a better acceptor ligand.

In extreme cases, if the metal is electron-rich enough and if there are strong electron-withdrawing groups on the olefin, a metala-cyclopropane structure may suit a better description. The metal-olefin system can now be considered as an η^2 structure. In this η^2 structure, the C atoms of the alkene rehybridize close to sp^3. In this bonding mode, there are two σ bonds to the metal center and the Dewar-Chatt-Duncanson model no longer applies. These two extremes are often referred to as X type and L type ligands. In both cases the ligand is considered as a 2e donor in the covalent model. Factors favoring X_2-type binding are strong donor ligands, a net negative charge on the complex, and low-oxidation state metals. In regards of chemical reactivity differences between the bonding types: L-type, the alkene is electron deficient and prone to attack by nucleophiles; whereas, X_2-type: the carbons are carbanion-like -and prone to attack by electrophiles.

What do these results tell us about the DCD model and its validity? They validate what Cedeño and Weitz had previously implied.[1] The DCD model is founded on covalent orbital interaction and may be utilized to predict qualitative metal-olefin bonding properties as long as such interaction does not involve energetically expensive events such as strong steric interactions and large geometrical reorganizations of the binding fragments. As expected our results validate and support the qualitative predictions of the DCD model if one were to neglect the effects of sterics and reorganization. An increase in the electron-withdrawing ability of the olefin increases the extent of back-bonding which in turns increases the attractive covalent interaction energy. However, the decomposition analyses make it clear that the attractive orbital interactions (σ and π), which are central to the DCD model, are only one component of the complex interaction between an olefin and a metal.

Thus, the prediction of metal-olefin bond strengths and interactions requires a model that rationalizes the contribution of all components in a quantitative manner. For instance, this study shows that even though attractive orbital interactions between metal (M = Ni, Fe, Cr, Mo and W) carbonyl fragments $M(CO)_x$ and the olefin increase as the olefin becomes more electron withdrawing, this bond-favoring trend is counterbalanced by the pauli (steric) repulsion energy, which also increases as with respect to an increase in the EWD ability of the para substituent. Furthermore, reorganizational energies, which inherently originate from the metal-olefin bonding interaction, play a determining role in the measurable bond strength. As shown in this and previous studies, the magnitude of the reorganizational energy may offset much of the energy gained by attractive metal-olefin interactions.

Hammett Plots of Metal-Olefin Bond Formation Rates

Density functional theory has been applied to describe electronic substituent effects, especially in the pursuit of linear relationships similar to those observed from the Hammett correlations on *Linear Free Energy Relationships* (LFERs). Correlations between the rate constants and the ρ parameters of the para substituents were explored by plotting Log(K_Y/K_H) values against a series of Hammett substituent constants based on substituent effects (σ_p).[70] The olefin ligand (L = η^2-C_2H_3-C_6H_4-Y) series evaluated in this study consisted of styrene and styrene analogs, electronically modified at the para position. The original basis for this selection was inspired by Louis Hammett's correlations on LFER and their applications in elucidating reaction mechanisms.

In context the application outlined herein, consider a particular metal-olefin reaction between two substrates. We might carry out a series of reactions by varying one of the reactants slightly, for example by examining para modified styrene analogs relative to styrene. We might expect that the position of the equilibrium between reactants and products, will change as we change the reactant in this way. If the same series of changes in conditions affects a second reaction equilibrium in exactly the same way as it affected the first reaction, then we may say that there exists a linear free energy relationship between the two sets of effects. Since logK_H is directly related to the standard free energy change accompanying the formation/dissociation equilibrium for metal-styrene coordination, and logK_Y is directly related to the standard free energy changes accompanying the formation/dissociation equilibrium of the para-substituted styrene analog series, the substituent constant is then actually related to the difference in the free energy changes for the two formation processes as: $\Delta G^{\ddagger} = \Delta G_Y - \Delta G_H$.

Traditionally, a Hammett analysis employs the use of LFERs as a means to compare the logarithm of a reaction rate or equilibrium constant of two different reactions of the same overall class in order to understand the mechanism of the reaction or to determine a quantitative measure of substituent effects.[70] Linear free energy treatments using the same substituent constants have been applied to rate constants and can provide valuable mechanistic information about the extent of charge build up at the transition state of the rate determining step.[84-85] Many LFERs exist with variations in the systems they are intended to describe. In 2004, a study by the Hartwig group employed the use of the original Hammett σ_p constants as a means to rationalize and explain the rates of reductive elimination for electronically modified bis-aryl platinum complexes.[86]

In more recent literature, it has been demonstrated that computational methods may be used broadly to accurately determine the effect of substituents on reaction rates and equilibria.[86-87] The use of Hammett's correlations on the LFER complements our DFT studies by providing quantitative insight into how substituent modification at the para position Y on styrene and styrene analogs affects the overall equilibrium of metal-olefin bond formation and dissociation. The lack of an extended database of experimental and its related computational data has precluded the extension of some of the correlations presented herein this thesis into a more generalized form that may allow us to make predictions of logarithmic rate formation constants relative to the dissociation of substituted benzoic acids in H_2O at 25^oC. Although there may be some inherent error associated within current theoretical methods used for free energy calculations based on energy of solvation approximations, a trend-wise analysis should provide a little more insight into the mechanistic nature elucidating metal-olefin bond formation.

From the free energy calculations obtained in using DFT, metal-olefin bond formation/dissociation equilibrium constants were extrapolated based on the difference in the standard free energy changes (ΔG_H) accompanying transition metal-styrene coordination **[**$M(CO)_xL$-H**],** and the standard free energy changes (ΔG_Y) accompanying the formation reaction for a given para substituted styrene analog in the series **[**$M(CO)_xL$-Y**]**. That is, Log (K_Y/K_H) determinations were indirectly acquired by taking the difference between ΔG_Y and ΔG_H for a given reaction accordingly to Eq. (17):

$$\text{Log}\,(K_Y/K_H) = \Delta G_Y - \Delta G_H = \Delta G^{\ddagger} \qquad (17)$$

Once the equilibrium constants for a set of substituents were calculated, information was then derived regarding the sensitivity ρ of other reactions to substituent effects relative to the standard reaction (i.e. styrene) in the pursuit of linear relationships similar to those observed from the Hammett correlations based on LFERs. This was done by plotting Log(K_Y/K_H) against various Hammett substituent constants based on the ionization of benzoic acid and benzoic acid derivatives (σ_p).[75]The σ_p parameter represents the substituent constant as calculated previously for the dissociation of benzoic acid and benzoic acid derivatives in solution and serves as a quantitative reference for drawing a correlation between metal-olefin bond formation reaction rates and substituent effects in order to provide further insight into the very nature of transition metal-olefin chemistry. The Hammett Postulate asserts that these same substituents will have effects upon the equilibrium or rate constants for any other reaction which parallels those in styrene metal-olefin bond formation and can be mathematically modeled according to the Hammett Equation, Eq. (18):

$$\text{Log}(K_Y/K_H) = \rho\,\sigma_p \qquad (18)$$

In principle, all reactions that correlate to the Hammett equation will use the same set of substituent constants. That is, a structural modification will produce a proportional change in reaction rate based on the σ_p values. Further derivation of the Hammett correlations based on LFERs would then assert that changes in structure produce proportional changes in $\Delta G^{\ddagger}$ with accord to Eq. (19):

$$-\Delta G^{\ddagger}/(2.303\ RT) = \mathrm{Log}(K_Y/K_H) = \rho\ \sigma_p \qquad (19)$$

where, ΔG_H and 2.303 RT are held constant (R = 0.001987 kcal/K· mol, T = 298.15 K). The proportionality constant (i.e., the slope of the line) ρ, will vary with the particular reaction under study, but its overall magnitude reveals the degree of sensitivity the reaction has to substituent effects.

The sign and absolute magnitude of the ρ value determined from a Hammett plot give information about charge development at the transition state. A value of ρ = 0 implies that substituents have no electronic effect on the equilibrium, and thus no inductive effects affect the equilibrium. Large absolute values of ρ mean that substituents influence the equilibrium greatly, and thus inductive effects are large and influenced significantly by substituent effects. The overall magnitude of the sign of ρ tells whether a positive or negative charge is being developed during the reaction. A positive ρ value means that electron density is increased (negative charge is being produced); whereas, a negative ρ value means that electron deficiency is being produced (often a positive charge) during the reaction. If ρ > 1, the reaction is said to be more sensitive to the nature of substituent effects relative to the dissociation of benzoic acid in solution.[75] Values of $\Delta G^{\ddagger}$ and $\mathrm{Log}(K_Y/K_H)$ for the formation of the $[M(CO)_xL\text{-}Y]$ complex series are listed in Tables 16 and 17; σ_p values were attained from Reference 75.

TABLE 16: LFERs Data for the [$M(CO)_5$L-Y] Complex Series.

$M(CO)_5$-L- Y	$\Delta G^{\ddagger}$ [a]	σ_p [b]	$Log(K_Y/K_H)$
$Cr(CO)_5L$- NO_2	1.81	0.78	-1.33
$Cr(CO)_5L$- CN	1.46	0.66	-1.07
$Cr(CO)_5L$- COOH	1.12	0.45	-0.82
$Cr(CO)_5L$- COH	1.16	0.42	-0.85
$Cr(CO)_5L$- CF_3	1.22	0.54	-0.90
$Cr(CO)_5L$- $OCOCH_3$	1.20	0.31	-0.88
$Cr(CO)_5L$- H	0.00	-0.01	0.00
$Cr(CO)_5L$- CH_3	-0.29	-0.17	0.21
$Cr(CO)_5L$- $C(CH_3)_3$	-0.37	-0.20	0.27
$Cr(CO)_5L$- OH	-0.54	-0.37	0.40
$Cr(CO)_5L$- OCH_3	-0.43	-0.27	0.32
$Cr(CO)_5L$- $OC(CH_3)_3$	-0.34	*n/a*	0.25
$Cr(CO)_5L$- NH_2	-1.21	-0.66	0.89
$Cr(CO)_5L$- $N(CH_3)_2$	-1.60	-0.83	1.17
$Mo(CO)_5L$- NO_2	1.92	0.78	-1.40
$Mo(CO)_5L$- CN	1.54	0.66	-1.13
$Mo(CO)_5L$- COOH	1.24	0.45	-0.91
$Mo(CO)_5L$- COH	1.24	0.42	-0.91
$Mo(CO)_5L$- CF_3	1.37	0.54	-1.00
$Mo(CO)_5L$- $OCOCH_3$	1.37	0.31	-1.01
$Mo(CO)_5L$- H	0.00	-0.01	0.00
$Mo(CO)_5L$- CH_3	-0.17	-0.17	0.12
$Mo(CO)_5L$- $C(CH_3)_3$	0.27	-0.20	-0.20
$Mo(CO)_5L$- OH	-0.36	-0.37	0.26
$Mo(CO)_5L$- OCH_3	-0.35	-0.27	0.26
$Mo(CO)_5L$- $OC(CH_3)_3$	-0.58	*n/a*	0.43
$Mo(CO)_5L$- NH_2	-1.21	-0.66	0.88
$Mo(CO)_5L$- $N(CH_3)_2$	-1.13	-0.83	0.83
$W(CO)_5L$- NO_2	1.82	0.78	-1.33
$W(CO)_5L$- CN	1.51	0.66	-1.10
$W(CO)_5L$- COOH	1.23	0.45	-0.90
$W(CO)_5L$- COH	1.28	0.42	-0.94
$W(CO)_5L$- CF_3	1.36	0.54	-0.99
$W(CO)_5L$- $OCOCH_3$	1.31	0.31	-0.96
$W(CO)_5L$- H	0.00	-0.01	0.00
$W(CO)_5L$- CH_3	-0.20	-0.17	0.15
$W(CO)_5L$- $C(CH_3)_3$	0.43	-0.20	-0.32
$W(CO)_5L$- OH	-0.51	-0.37	0.37
$W(CO)_5L$- OCH_3	-0.19	-0.27	0.14
$W(CO)_5L$- $OC(CH_3)_3$	-0.05	*n/a*	0.04
$W(CO)_5L$- NH_2	-1.38	-0.66	1.01
$W(CO)_5L$- $N(CH_3)_2$	-1.22	-0.83	0.90

a) All reported values are in kcal/mol. *b)* σ_p values were attained from *Ref*erence *75.*

TABLE 17: LFERs Data for the [$M(CO)_xL$-Y] Complex Series.

$M(CO)_xL$- Y	$\Delta G^{\ddagger}$ [a]	σ_p [b]	$\text{Log}(K_Y/K_H)$
$Fe(CO)_4L$- NO_2	0.56	0.78	-0.41
$Fe(CO)_4L$- CN	0.46	0.66	-0.34
$Fe(CO)_4L$- COOH	0.35	0.45	-0.26
$Fe(CO)_4L$- COH	0.39	0.42	-0.29
$Fe(CO)_4L$- CF_3	0.51	0.54	-0.38
Fe $(CO)_4L$- $OCOCH_3$	0.96	0.31	-0.70
Fe $(CO)_4L$- H	0.00	-0.01	0.00
Fe $(CO)_4L$- CH_3	-0.05	-0.17	0.04
Fe $(CO)_4L$- $C(CH_3)_3$	0.13	-0.20	-0.10
Fe $(CO)_4L$- OH	0.10	-0.37	-0.07
Fe $(CO)_4L$- OCH_3	0.35	-0.27	-0.25
Fe $(CO)_4L$- $OC(CH_3)_3$	0.30	*n/a*	-0.22
Fe $(CO)_4L$- NH_2	-0.28	-0.66	0.21
Fe $(CO)_4L$- $N(CH_3)_2$	-0.08	-0.83	0.06
$Ni(CO)_3L$- NO_2	0.97	0.78	-0.71
$Ni(CO)_3L$- CN	0.79	0.66	-0.58
$Ni(CO)_3L$- COOH	0.67	0.45	-0.49
$Ni(CO)_3L$- COH	0.60	0.42	-0.44
$Ni(CO)_3L$- CF_3	0.79	0.54	-0.58
$Ni(CO)_3L$- $OCOCH_3$	0.90	0.31	-0.66
$Ni(CO)_3L$- H	0.00	-0.01	0.00
$Ni(CO)_3L$- CH_3	-0.18	-0.17	0.13
$Ni(CO)_3L$- $C(CH_3)_3$	-0.27	-0.20	0.20
$Ni(CO)_3L$- OH	-0.21	-0.37	0.16
$Ni(CO)_3L$- OCH_3	0.10	-0.27	-0.07
$Ni(CO)_3L$- $OC(CH_3)_3$	-0.12	*n/a*	0.09
$Ni(CO)_3L$- NH_2	-0.44	-0.66	0.32
$Ni(CO)_3L$- $N(CH_3)_2$	-0.45	-0.83	0.33

a) All reported values are in kcal/mol. *b)* σ_p values were attained from *Ref*erence *75.*

Figures 97-101 show the general trends obtained following Linear Free Energy Relationship (LFER) analyses for the [$M(CO)_xL$-Y] complex series. Using Hammett's original correlations on LFERs, we were ultimately able to establish a mathematical relationship between the electronic nature of substituent effects and logarithmic metal-olefin bond formation/dissociation equilibrium constants. The substituent constant σ_p serves as a measure of the total polar electronic effect exerted by para substituent modification Y (relative to no substituent) on the reaction center of a given complex.

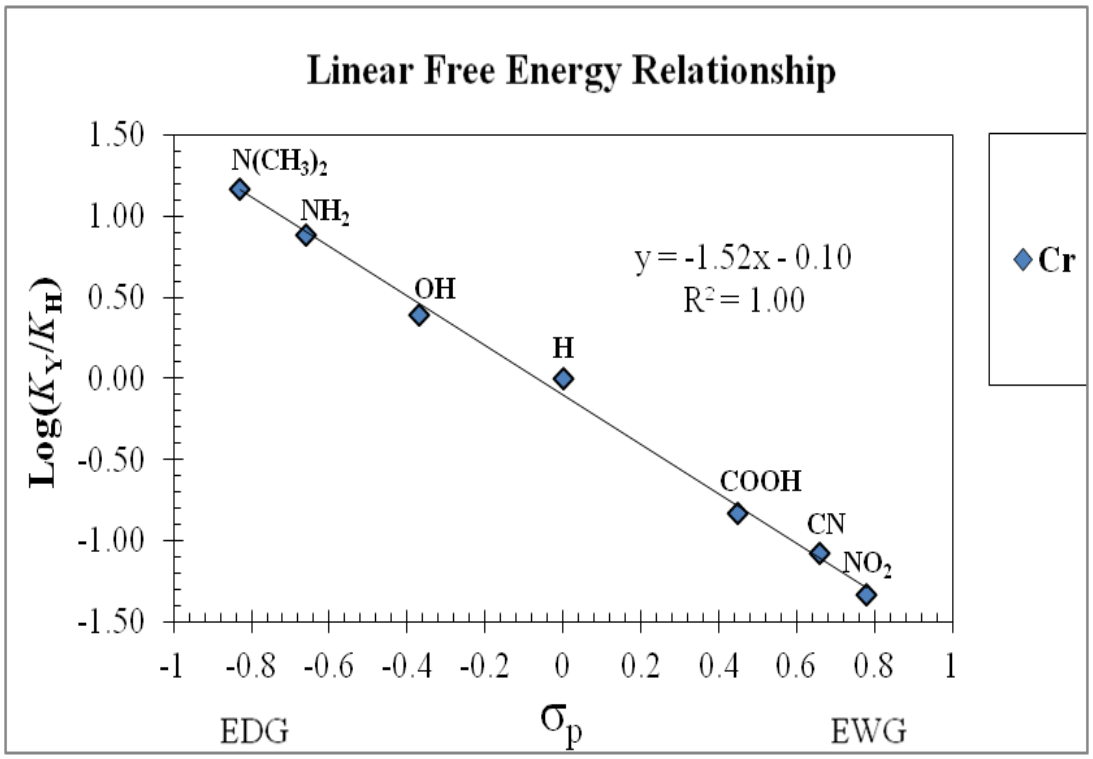

Figure 97. Hammett plot of the LFER for the $[Cr(CO)_5L\text{-}Y]$ complex series.

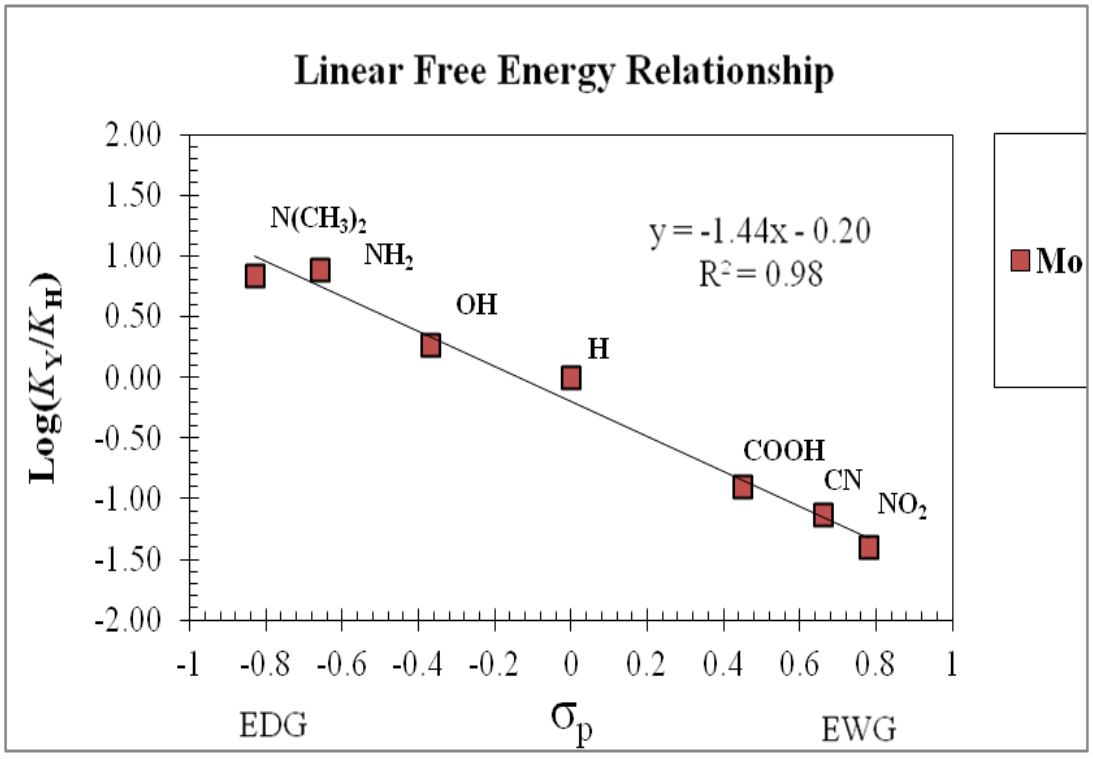

Figure 98. Hammett plot of the LFER for the $[Mo(CO)_5L\text{-}Y]$ complex series.

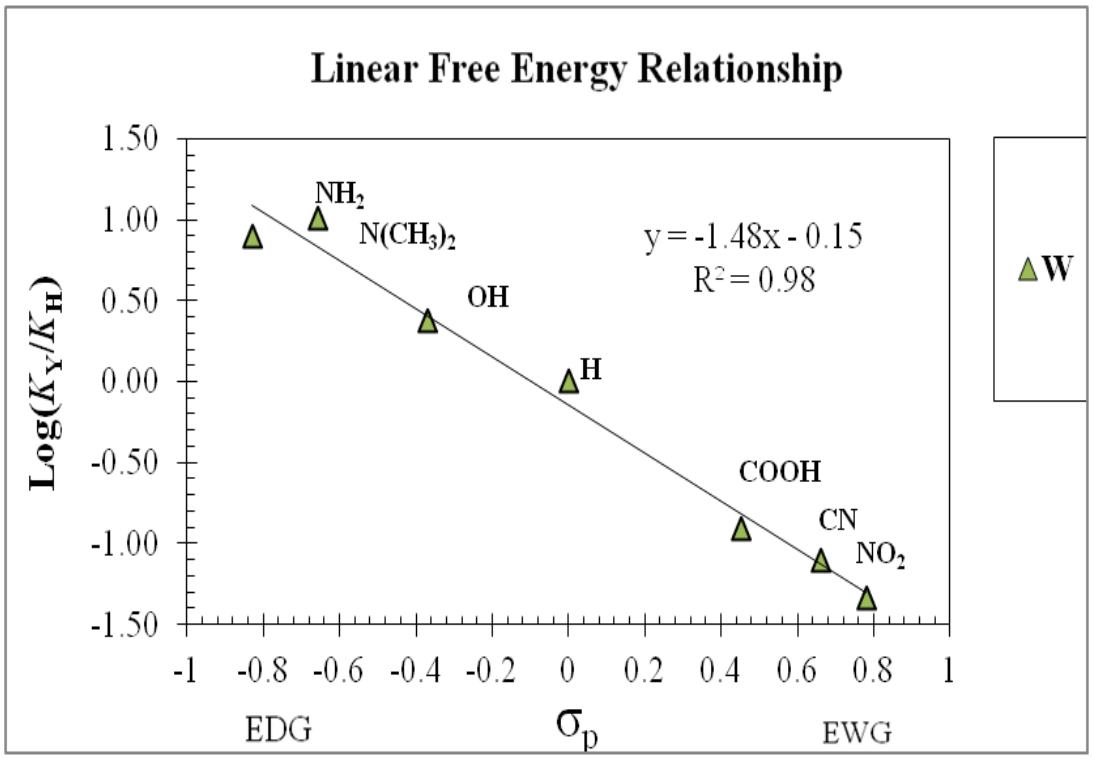

Figure 99. Hammett plot of the LFER for the $[W(CO)_5L\text{-}Y]$ complex series.

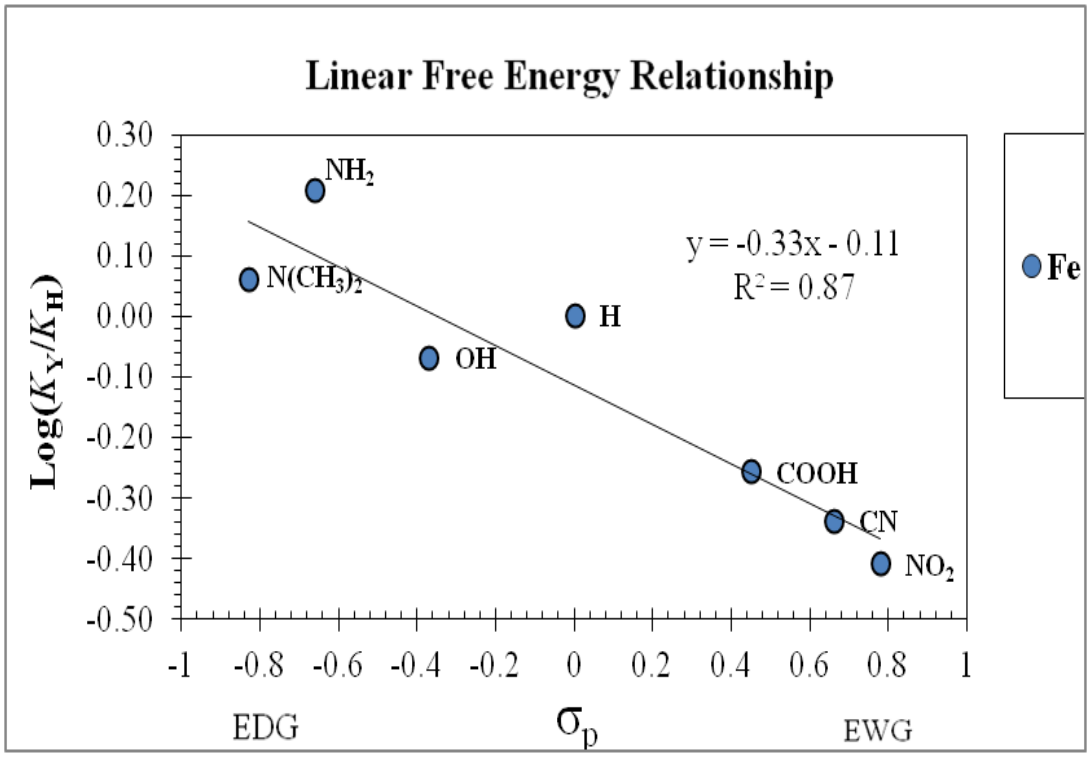

Figure 100. Hammett plot of the LFER for the $[Fe(CO)_4L\text{-}Y]$ complex series.

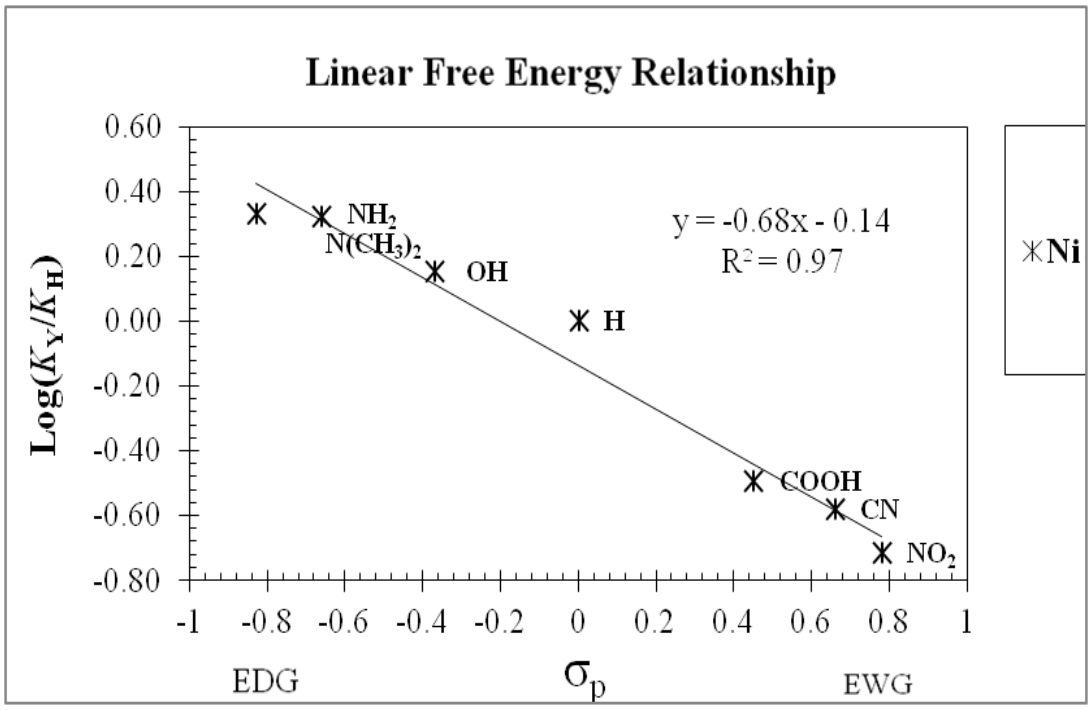

Figure 101. Hammett plot of the LFER for the [Ni(CO)$_3$L-Y] complex series.

Interestingly, it was found that as the magnitude of the σ_p term increases in proportion to an increase in the EWD ability of the olefin, the overall magnitude of Log (K_Y/K_H) decreases; following in general order of $N(CH_3)_2$ < NH_2 < OH < H < COOH < CN < NO_2. Thus, as the EWD capacity of the olefin increases, an overall reduction in the Log (K_Y/K_H) term would then suggest that the NO_2 substituent opposes the nature of charge advent during formation of the complex. Based on Hammett's correlations, a negative ρ value indicates that electron deficiency is being produced (often a positive charge) during the reaction. Thus, clearly our results indicate the development of a positive charge as the metal-olefin bond is being formed. Perhaps, a buildup of positive charge near the reaction center could help corroborate the metal-olefin bond formation energy trends observed from our BEDA calculations and possibly be used to justify the paradox nature between DCD expectation and experimental observation.

Plots of Log (K_Y/K_H) vs. the Hammett substituent constant (σ_{para}) of Y in $[M(CO)_xL\text{-}Y]$ are presented in Figures 97-101. In general, these results demonstrate a linear free energy relationship, with a ρ coefficient of -1.52, - 1.44, - 1.48, -0.33, and -0.68 for Cr, Mo, W, Fe, and Ni, respectively. A $\rho < 1$ indicates a reaction which is less sensitive to the nature of substituent effects. Perhaps this would suggest a reaction which develops less positive charge near the reaction center as a result of the π-backbonding interaction. That is, because Fe and Ni have more electrons available for the backbonding interaction, the overall charge built up near the reaction center during complex formation is lessened relative to that of the group six transition triad series. More significantly, the y-intercept obtained in the present work of ≤ 0.2 is rather close to zero, as might be expected for any Hammett-type plot.[88]

The calculated equilibrium constant for metal-olefin bond formation from the para-dimethylamino substituted chromium pentacarbonyl complex was 15 times larger than that for formation from the para-nitro chromium pentacarbonyl complex. Based on electronic effects, the general order of stability was Y: $N(CH_3)_2 > NH_2 > OCH_3 > OH > C(CH_3)_3 > CH_3 > H > OCOCH_3 > COH > COOH > CF_3 > CN > NO_2$. Overall, two trends were found to affect the equilibrium of metal-olefin bond formation reactions. Ultimately, complexes with aryl groups containing more electron-donating substituents undergo bond formation stronger than complexes with aryl groups containing more electron-withdrawing substituents, and complexes containing electron rich metal centers were less susceptible towards complex stabilization via substituent effects. Based on the metallic influence of ρ towards metal-olefin bond formation, the overall order of sensitivity was M: Cr > W > Mo > Ni > Fe.

CHAPTER IV

CONCLUSIONS

Metal-olefin bond formation energies have been calculated for the transition metal (M = Ni, Fe, Cr, Mo and W) complex series [$M(CO)_xL$-Y] in order to compare general bonding trends. One qualitative interpretation of the DCD model implies that the metal-olefin bond energy should increase in proportion to an increase in the electron-withdrawing ability of the para substituent. However, the trend in calculated bond formation energies in our studies were found to demonstrate that, contrary to the DCD bonding model, as electron-withdrawing nature of the para substituent increase, the strength of the metal-olefin interaction diminishes.

Bond energy decomposition analyses demonstrate that if covalent orbital interactions were the unique contributor to the stability of a metal-olefin bond, then bond formation energies would follow the trend expected from the DCD model. However, our DFT calculations indicate that attractive electrostatic and covalent (orbital) interactions are actually offset by the Pauli (steric) repulsion between the occupied orbitals of the reactants in such a way that the total interaction energy is almost independent of the electronic nature of the para substituent. Our results also indicate that the conformational changes in the olefin resulting from stronger covalent bonding interactions increase with respect to an increase in the EWD capacity of the para substituent on the olefin; however, these conformational changes have an energetic cost (reorganizational energy).

In summary, an increase in the electron-withdrawing ability of the olefin increases the strength of the attractive covalent interaction as predicted correctly by the DCD model; however, both steric interactions and reorganizational energies also increase in detriment to the overall metal-olefin bond strength. In other words, the reorganizational energy offsets much of the available attractive metal-olefin interaction energy for bonding. Since steric interactions and reorganizational energies are not included in the original DCD model formulations, their inclusion and rationalization should lead us to formulate an extended DCD model that would allow us to predict metal-olefin bond strengths and interactions in a more quantitative manner. Density functional theory has also been applied to describe electronic substituent effects, especially in the pursuit of linear relationships similar to those observed from the Hammett correlations based on *Linear Free Energy Relationships*.

Plots of Log (K/K_H) vs. various Hammett parameters based on ionization of benzoic acids (σ_p) indicate that metal-olefin bond formation occurs more favorably in complexes with more electron-donating capacity for the $[Cr(CO)_5L\text{-}Y]$, $[Mo(CO)_5L\text{-}Y]$, and $[W(CO)_5L\text{-}Y]$ complex series, whereas formation for the $[Fe(CO)_4L\text{-}Y]$ and$[Ni(CO)_3L\text{-}Y]$ complex series were much less sensitive to substituent effects based on acquired reaction constants ρ. Overall, we have shown that bond formation from complexes with more electron-withdrawing capacity is less stable than for olefin complexes of greater electron donating character based on overall reactivity and theoretical free energy change calculations. From the LFERs provided in this study, our results may suggest the advent of a positive charge being developed near the reaction center in the bond formation process.

Transition metals which are more electron rich near the metal center have a greater potential for backbonding and thus, perhaps can reduce the overall advent of charge formed during metal-olefin bond formation. Reduction of this charge has shown to induce less dependence towards substituent stabilization, as was the case for the $[Fe(CO)_4L\text{-}Y]$ and $[Ni(CO)_3L\text{-}Y]$ complex series. This is supported by flat bond formation energy trends across the entire substituent series for these metals relative to the observed slopes of the group six transition triad (M = Cr, Mo, and W); refer to Figures 73-79. It must be noted that the trend for the iron complex series was not reported due to a low correlation value, however, it is approximately similar to the slope of the $[Ni(CO)_3L\text{-}Y]$ complex series. Clearly, transition metal influence on the π-backbonding interaction is greatest for the iron complex series.

Overall, the research proposed here represents a viable systematic study of metal-olefin bond strengths as a function of the electronic effects engendered by substituent modification, and nature of the metal and its other coordinating ligands. Assuming a trend-wise reliability in the computations obtained using DFT methods, a full bond energy decomposition analysis provided further insight into the quantitative correlations between electronic, steric, and reorganizational effects and the structural nature of the metal-olefin complex. Ultimately, we hope that these correlations will lead us to a more quantitative model for meta-olefin bonding that extends to the traditional DCD model. An interesting application of this model would be towards the predication of the thermodynamic and kinetic viability of chemical reactions in which the metal-olefin bond plays an essential role; in particular, polystyrene polymerization reactions.

REFERENCES

(1)Schlappi, D. N.; Cedeño, D. L. Metal-Olefin Bond Energies in $M(CO)_5(C_2H_{4-n}Cl_n)$ M = Cr, Mo, W; n = 0-4: Electron-Withdrawing Olefins Do Not Increase the Bond Strength. *J. Phys. Chem. A* **2009**, *113*, 9692-9699.

(2) Kazlauskas, R. J.; Wrighton, M. S. Photochemistry of Metal Carbonyl Alkyls. Study of Thermal .Beta.-Hydrogen Transfer in Photogenerated, 16-Valence-Electron Alkyldicarbonylcyclopentadienylmolybdenum and -Tungsten Complexes**.** *J. Am. Chem. Soc.* **1982**, *104*, 6005-6015.

(3) Miller, M. E.; Grant, E. R. Relaxation Kinetics in the Homogeneous Gas-Phase Photocatalytic Hydrogenation of Ethylene by $Fe(CO)_4(C_2H_4)$**.** *J. Am. Chem. Soc.* **1984**, *106*, 4635-4636.

(4) Wuu, Y. M.; Bentsen, J. G.; Brinkley, C. G.; Wrighton, M. S. Photochemical Formation of Mononuclear Bis- and Tris(ethylene) Complexes from Irradiation of Iron Pentacarbonyl or Triruthenium Dodecacarbonyl: Species involved in Catalytic Alkene Isomerization**.** *Inorg. Chem.* **1987**, *26*, 530-540.

(5) Barnhardt, T. M.; McMahon, R. J. Kinetic Generation of Cis Cyclopentadienyl(dicarbonyl)rhenium Dihydride from the Reaction of $(C_5H_5)Re(CO)_2(\mu\text{-}H)Pt(H)(PPh_3)_2$ with Diphenylacetylene. *J. Am. Chem. Soc.* **1992**, *114*, 5434-5439.

(6) Maxwell, J. L.; Brown, K. C.; Bartley, D. W.; Kodadek, T. Mechanism of the Rhodium Porphyrin-Catalyzed Cyclopropanation of Alkenes. *Science* **1992**, *256*, 1544-1547.

(7) Willis, M. C., Transition Metal Catalyzed Alkene and Alkyne Hydroacylation, *Chem. Rev.* **2010**, *110*, 725-748.

(8) Nakamura, I.; Yamamoto, Y. Transition-Metal-Catalyzed Reactions in Heterocyclic Synthesis. *Chem. Rev.* **2004**, *104*, 2127-2198.

(9) Trnka, T. N.; Grubbs, R. H. The Development of $L_2X_2R{=}CHR$ Olefin Metathesis Catalysts: An Organometallic Success Story. *Chem. Inform.* **2001**, *34*, 18-29.

(10) Baird, M. C. Carbocationic Alkene Polymerizations Initiated by Organotransition Metal Complexes: An Alternative, Unusual Role for Soluble Ziegler-Natta Catalysts. *Chem. Inform.* **2000**, *100*, 1471-1478.

(11) Boffa, L. S.; Novak, B. M. Copolymerization of Polar Monomers with Olefins Using Transition-Metal Complexes. *Chem. Rev.* **2000**, *100*, 1479-1493.

(12) Mingos, D. M. P. A Historical Perspective on Dewar's Landmark Contribution to Organometallic Chemistry. *J. Organomet. Chem.* **2001**, *635*, 1-8.

(13) Frenking, G. Understanding the Nature of the Bonding in Transition Metal Complexes: from Dewar's Molecular Orbital Model to an Energy Partitioning Analysis of the Metal–Ligand Bond. . *J. Organomet. Chem.* **2001**, *635*, 9-23.

(14) Winterton, N. Some Notes on the Early Development of Models of Bonding in Olefin-Metal Complexes. In *Modern Coordination Chemistry*, Leigh, G. J.; Winterton, N. Eds., 2002; pp 103-110.

(15) Frenking, G. The Dewar-Chatt-Duncanson Bonding Model of Transition Metal-Olefin Complexes Examined by Modern Quantum Chemical Methods. In *Modern Coordination Chemistry*, Leigh, G. J.; Winterton, N. Eds., **2002**, 111-122.

(16) Dewar, M. J. S. A Review of the π-complex Theory. *Bulletin of the Chemical Society of France* **1951**, *18*, 71-79.

(17) Chatt, J.; Duncanson, L. A. Olefin Coordination Compounds. III. Infrared Spectra and Structure: Attempted Preparation of Acetylene Compounds. *J. Chem. Soc.* **1953**, 2939-2947.

(18) Crabtree, R. H. *The Organometallic Chemistry of Transition Metals*; Wiley: New York, 1986; pp 107.

(19) Pruchnick, F. P. *Organometallic Chemistry of the Transition Elements*; Plenum: New York, 1990; pp 343.

(20) Crabtree, R. H. *The Organometallic Chemistry of Transition Metals*, 3rd ed.; Wiley: New York, 2001; pp 116.

(21) (a) Nunzi, F.; Sgamelotti, A.; Re, N.; Floriani, C. A Density Functional Study of $[M(PH_3)_2(\eta^2\text{-}C_2X_4)]$ Alkene Complexes for the Group 10 Metals Ni, Pd, Pt: The Effect of Electron-Attracting Substituents. *J. Chem. Soc., Dalton Trans.* **1999**, 3487-3491. (b) Uddin, J.; Dapprich, S.; Frenking, G.; Yates, B. F. Nature of the Metal-Alkene Bond in Platinum Complexes of Strained Olefins. *Organometallics* **1999**, *18*, 457-465.

(22) Cedeño, D. L.; Weitz, E.; Bérces, A. Bonding Interactions in Olefin (C_2X_4, X = H, F, Cl, Br, I, CN) Iron Tetracarbonyl Complexes: Role of the Deformation Energy in Bonding and Reactivity. *J. Phys. Chem. A* **2001,** *105*, 8077-8085.

(23) Schlappi, D. N.; Cedeño, D. L. Electron-Withdrawing Effects on Metal-Olefin Bond Strengths in $Ni(PH_3)_2(CO)(C_2X_nH_{4-n})$, X = F, Cl; *n* = 0-4: A DFT Study. *J. Phys. Chem. A* **2003**, *107*, 8763-8773.

(24) Cedeño, D. L.; Weitz, E. Experimental Determination of the Cr-C_2Cl_4 Bond Dissociation Enthalpy in $Cr(CO)_5(C_2Cl_4)$: Quantifying Metal-Olefin Bonding Interactions. *J. Am. Chem. Soc*. **2001**, *123*, 12857-12865.

(25) Muhammad, S.; Kyran, S. J.; Raju, R.K.; Brothers, E. N.; Darensbourg, D. J.; Bengali, A. A. Time-Resolved Infrared Spectroscopy Studies of Olefin Binding in Photogenerated CpRu(CO)X (X = Cl, I) Transients. *Organometallics* **2012**, *31*, 3972-3979.

(26) Welch, J. A.; Peters, K. S.; Vaida, V. Medium Effects on the Photodissociation of Hexacarbonylchromium ($Cr(CO)_6$). *J. Phys. Chem.* **1982**, *86*, 1941-1947.

(27) Baerends, E. J.; Rosa, A. Metal–CO Photodissociation in Transition Metal Complexes: The Role of Ligand-Field and Charge-Transfer Excited States in the Photochemical Dissociation of Metal–Ligand Bonds. *Coordination Chemistry Reviews* **1998**, *177*, 97-125.

(28) Cedeño, D. L.; Sniatynsky, R. Metal-Olefin Interactions in $M(CO)_5$(cycloolefin) (M = Cr, Mo, W; Cycloolefin = Cyclopropene to Cyclooctene): Strain Relief and Metal-Olefin Bond Strength. *Organometallics* **2005**, *24*, 3882-3890.

(29) Schultz, N. E.; Zhao, Y.; Truhlar, D. G. Density Functionals for Inorganometallic and Organometallic Chemistry. *J. Phys. Chem. A* **2005**, *109*, 11127-11143.

(30) Sniatynsky, R.; Cedeño, D. L. A Density Functional Theory Benchmark of the Formation Enthalpy and First CO Dissociation Enthalpy of Hexacarbonyl Complexes of Chromium, Molybdenum, and Tungsten. *J. Mol. Struct.* **2004**, *711*, 123-131.

(31) Hehre, Warren. J. "*A Guide to Molecular Mechanics and Quantum Chemical Calculations*", Wavefunction, Irvine, CA, 2003; pp 30.

(32) ADF2004.01 and ADF2008.01; SCM, Theoretical Chemistry, Vrije Universiteit, Amsterdam, The Netherlands; http://www.scm.com.

(33) Bickelhaupt, F. M.; Nibbering, N. M.; van Wezenbeek, E. M.; Baerends, E. J. Central Bond in the Three CN• Dimers NC-CN, CN-CN, CN-NC: Electron Pair Bonding and Pauli Repulsion Effects. *J. Phys. Chem. A* **1992**, *96*, 4864-4873.

(34) Ziegler, T.; Rauk, A. A Theoretical Study of the Ethylene-Metal Bond in Complexes between Cu^{+}, Ag^{+}, Au^{+}, Pt^{0}, or Pt^{2+} and Ethylene, based on the Hartree-Fock-Slater Transition-State Method. *Inorg. Chem.* **1979**, *18*, 1558-1565.

(35) Ziegler, T.; Rauk, A. CO, CS, N_2, PF_3 and $CNCH_3$ as σ Donors and π Acceptors. A Theoretical Study by the Hartree-Fock-Slater Transition State Method. *Inorg. Chem.* **1979**, *18*, 1755-1759.

(36) Bickelhaupt, F. M.; Nibbering, N. M.; van Wezenbeek, E. M.; Baerends, E. J. Central Bond in the Three CN• Dimers NC-CN, CN-CN, CN-NC: Electron Pair Bonding and Pauli Repulsion Effects. *J. Phys. Chem. A* **1992**, *96*, 4864-4873.

(37) Velde, G.; Bickelhaupt, F. M.; van Gisbergen, S. J. A.; Fonseca Guerra, C.; Baerends, E. J.; Snijders, J. G.; Ziegler, T. Chemistry with ADF. *J. Comput. Chem.* **2001**, *22*, 931-967.

(38) Cedeño, D.L.; Weitz, E. An Experimental Determination of the Cr-DMB (DMB = 3,3-Dimethyl-1-butene) Bond Energy in $Cr(CO)_5$(DMB): Effects of Alkyl Substitution on Chromium-Olefin Bond Energies in $Cr(CO)_5$(olefin) Complexes. *J. Phys. Chem. A* **2002,** *106*, 4651-4660.

(39) Thomas, I. R.; Bruno, I. J.; Cole, J. C.; Macrae, C. F.; Pidcock, E.; Wood, P. A. WebCSD: the online portal to the Cambridge Structural Database. *J. Appl. Cryst.* **2010**, *43*, 362-366.

(40) Thayer, J. S. Historical Origins of Organometallic Chemistry. Part I, Zeise's Salt**.** *J. Chem. Ed.* **1969**, *7*, 442-443.

(41) Black, M.; Mais R. H. B.; Owston, P. G. The Crystal and Molecular Structure of Zeise's salt, $KPtCl_3$•C_2H_4•H_2O. *Acta Crystallogr. B* **1969,** *9*, 1753-1759.

(42) Seyferth, D. $[(C_2H_4)PtC1_3]^{-}$, the Anion of Zeise's Salt, $K[(C_2H_4)PtC1_3]$·H_20. *Organometalics* **2001**, *20*, 2-6.

(43) Wunderlich, J. A.; Mellor, D. P. A Note on the Crystal Structure of Zeise's Salt. *Acta Crystallogr.* **1954**, *7***,** 130-131.

(44) Wunderlich, J. A.; Mellor, D. P. A Correction and a Supplement to a Note on the Crystal Structure of Zeise's Salt. *Acta Crystallogr.* **1955**, *8***,** 57-58.

(45) Bartell, L. S.; Roth, E. A**.;** Hollowell, C. D.; Kuchitsu, K.; Young, J. E. Electron-Diffraction Study of the Structures of C_2H_4 and C_2D_4. *J. Chem. Phys.* **1965**, *42*, 2683-2686.

(46) Otto, S.; Roodt, A.; Elding, L. I. Bridge-splitting kinetics, equilibria and Structures of Trans-Biscyclooctene Complexes of Platinum(II). *Dalton Trans*. **2003**, 2519-2525.

(47) Love, R. A.; Koetzle, T. A.; Williams, G. J. B.; Andrews, L. C.; Bau, R. Neutron Diffraction Study of the Structure of Zeise's Salt, $KPtC1_3(C_2H_4)\cdot H_2O$. *Inorg. Chem*. **1975**, *14*, 2653-2656.

(48) Crabtree, R. H. *The Organometallic Chemistry of Transition Metals*, 4th ed.; Wiley: New York, 2005; pp 126.

(49) Elschenbroich, C., Salzer, A., *Organometallics: A Concise Introduction*, 1st ed.; VCH: Weinheim, 1989; pp 252.

(50) Tolman, C. A. Olefin Complexes of Nickel(0). III. Formation Constants of (Olefin) Bis(tri-o-tolyl phosphite)Nickel Complexes. *J. Am. Chem. Soc*. **1974**, *96*, 2780-2789.

(51) Ittel, S. D. Electron Donor-Acceptor Properties in the Bonding of Olefins and Other Unsaturated Molecules to Zerovalent Nickel. *Inorg. Chem*. **1977**, *16*, 2589-2597.

(52) Ziegler, T. The 1994 Alcan Award Lecture. Density Functional Theory as a Practical Tool in Studies of Organometallic Energetics and Kinetics. Beating the Heavy Metal Blues with DFT. *Can. J. Phys.* **1995**, *73*, 743-761.

(53) Cedeño, D. L.; Sniatynsky, R. Metal-Olefin Interactions in $M(CO)_5$(cycloolefin) (M = Cr, Mo, W; Cycloolefin = Cyclopropene to Cyclooctene): Strain Relief and Metal-Olefin Bond Strength. *Organometallics* **2005**, *24*, 3882-3890.

(54) (a) Schrock, R. R. Recent Advances in Olefin Metathesis by Molybdenum and Tungsten Imido Alkylidene Complexes. *J. Mol. Catal. A*: *Chem.* **2004**, *213*, 21-30. (b) Schrock, R. R. High Oxidation State Multiple Metal-Carbon Bonds. *Chem. Rev*. **2002**, *102*, 145-179.

(55) Schultz, N. E.; Zhao, Y.; Truhlar, D. G. Density Functionals for Inorganometallic and Organometallic Chemistry. *J. Chem. Phys. A* **2005**, *109*, 11127-11143.

(56) Ehlers, A. W.; Frenking, G. Structures and Bond Energies of the Transition-Metal Carbonyls $M(CO)_5$ (M = Fe, Ru, Os) and $M(CO)_4$ (M = Ni, Pd, Pt). *Organometallics* **1995**, *14*, 423-426.

(57) Ehlers, A. W.; Frenking, G. Structures and Bond Energies of the Transition Metal Hexacarbonyls $M(CO)_6$ (M = Cr, Mo, W). A Theoretical Study. *J. Am. Chem. Soc.* **1994**, *116*, 1514-1520.

(58) Spartan Modeling Software V4.1.2; Wavefunction Inc.: 2014.

(59) Slater, J. C. *Quantum Theory of Molecules and Solids, Vol. 4: The Self-Consistent Field for Molecules and Solids*; McGraw-Hill: New York, 1974; pp 176.

(60) Vosko, S. H.; Wilk, L.; Nusair, M. Accurate Spin-Dependent Electron Liquid Correlation Energies for Local Spin Density Calculations: A Critical Analysis. *Can. J. Phys.* **1980**, *58*, 1200-1211.

(61) Becke, A. D. Density-Functional Exchange-Energy Approximation with Correct Asymptotic Behavior. *Phys. Re*V. *A.* **1988**, *38*, 3098-3100.

(62) Perdew, J. P. Density-Functional Approximation for the Correlation Energy of the Inhomogeneous Electron Gas. *Phys. Re*V. *B.* **1986**, *33*, 8822–8824.

(63) Hay, P. J.; Wadt, W. R. *Ab initio* Effective Core Potentials for Molecular Calculations. Potentials for Main Group Elements Na to Bi. *J. Chem. Phys.* **1985**, *82*, 299-310.

(64) (a) Ditchfield, R.; Hehre, W. J.; Pople, J. A. Self-Consistent Molecular-Orbital Methods. IX. An Extended Gaussian-Type Basis for Molecular-Orbital Studies of Organic Molecules. *J. Chem. Phys.* **1971**, *54*, 724-728. (b) Hehre, W. J.; Pople, J. A. Self-Consistent Molecular Orbital Methods. XIII. An Extended Gaussian Type Basis for Boron. *J. Chem. Phys.* **1972**, *56*, 4233-4234. (c) Binkley, J. S.; Pople, J. A. Self-Consistent Molecular Orbital Methods. XIX. Split Valence Gaussian-type Basis Sets for Beryllium. *J. Chem. Phys.* **1977**, *66*, 879-880. (d) Hariharan, P. C.; Pople, J. A. The Influence of Polarization Functions on Molecular Orbital Hydrogenation Energies. *Theor. Chim. Acta*. **1973**, *28*, 213-222. (e) Hehre, W. J.; Ditchfield, R.; Pople, J. A. Self-Consistent Molecular Orbital Methods. XII. Further Extensions of Gaussian-Type Basis Sets for Use in Molecular Orbital Studies of Organic Molecules. *J. Chem. Phys.* **1972**, *56*, 2257-2261. (f) Francl, M. M.; Pietro, W. J.; Hehre, W. J.; Binkley, J. S.; Gordon, M. S.; DeFrees, D. J.; Pople, J. A. Self-Consistent Molecular Orbital Methods. XXIII. A Polarization-Type Basis Set for Second-Row Elements. *J. Chem. Phys.* **1982**, *77*, 3653-3665.

(65) Deakyne, C. A.; Liebman, J. F. In *Encyclopedia of Computational Chemistry*; Schleyer, P. v. R., Allinger, N. R., Clark, T., Gasteiger, J., Kollman, P. A., Schaefer, H. F., III., Schreiner, P. R., Eds.; Wiley: Chichester, U.K., 1998; Vol. 2, pp 1439.

(66) Boerrigter, G. V.; Baerends, E. J. Three-Dimensional Numerical Integration for Electronic Structure Calculations. *J. Quantum Chem.* **1988**, *33*, 87-113.

(67) Bickelhaupt, F. M.; Nibbering, N. M.; van Wezenbeek, E. M.; Baerends, E. J. Central Bond in the Three $CN^{\bullet}$ Dimers NC–CN, CN–CN and CN–NC: Electron Pair Bonding and Pauli Repulsion Effects *J. Phys. Chem*. **1992**, *96*, 4864-4873.

(68) Mulliken, R. S. Electronic Population Analysis on LCAO-MO Molecular Wave Functions. *J. Chem. Phys.* **1955**, *48*, 1833-1841.

(69) Isaacs, N. *Physical Organic Chemistry*; Wiley: New York, 1995; pp 36.

(70) Hammett, L. P. The Effect of Structure upon the Reactions of Organic Compounds. Benzene Derivatives. *J. Am. Chem. Soc.* **1937**, *59*, 96-103.

(71) Jaffe, H. H. A Reëxamination of the Hammett Equation. *Chem. Rev.* **1953**, *53*, 191-261.

(72) Lowry, T. H.; Schuller Richardson, K. *Mechanism and Theory in Organic Chemistry*; Harper and Row: New York, 1987; pp 143-159.

(73) Exner, O. *The Hammett Equation*. In Advances in Linear Free Energy Relationships; Chapman, N. B. and Shorter, J., Eds.; Plenum Press: London, 1972; pp 1-10.

(74) March, J. *Advanced Organic Chemistry*; Wiley: New York, 2001; pp 368-375.

(75) Taft, R.W.; Leo, A.; Hansch. A Survey of Hammett Substituent Constants and Resonance and Field Parameters. *Chem. Rev.* **1991**, *91*, 165-195.

(76) Wells, P.R. *Linear Free Energy Relationships*; Academic Press, New York, 1968; pp 12-13.

(77) Cedeño, D.L.; Weitz, E. An Experimental Determination of the Cr-DMB (DMB = 3,3-Dimethyl-1-butene) Bond Energy in $Cr(CO)_5$(DMB): Effects of Alkyl Substitution on Chromium-Olefin Bond Energies in $Cr(CO)_5$(olefin) Complexes. *J. Phys. Chem. A* **2002,** *106*, 4651-4660.

(78) R.N. Perutz, R.N.; Turner, J. Photochemistry of the Group VI Hexacarbonyls in Low-Temperature Matrices. II. Infrared Spectra and Structures of Carbon-13 Monoxide-Enriched Hexacarbonyls and Pentacarbonyls of Chromium, Molybdenum, and Tungsten. *J. Inorg. Chem.* **1975**, *14*, 262-270.

(79) Darensbourg, D. J.; Nelson, H. H., III.; Hyde, C. L. Detailed Analysis of the Carbonyl Stretching Vibrations in Axial and Equatorial Substituted Iron Carbonyl Compounds. Absolute Infrared Intensities and Force Constants of the Carbonyl Ligands. *Inorg. Chem.* **1974**, *13*, 2135-2145.

(80) Wilson, S. T.; Coville, N. J.; Shapely, J. R.; Osborn, J. A. Rapid Intramolecular Rearrangements in Pentacoordinate Transition Metal Compounds. V. Coupling of Olefin Rotation and Berry Pseudorotation in Tetracarbonyliron-Olefin Complexes. *J. Am. Chem. Soc.* **1974**, *96*, 4038-4040.

(81) Davis, M. I.; Speed, C. S. Gas-Phase Electron Diffraction Studies of some Iron Carbonyl Complexes. *J. Organomet. Chem.* **1970**, *21*, 401-413.

(82) Beagley, B.; Schmidling, D. G.; Cruickshank, D. W. The Molecular Structure of $C_2F_4Fe(CO)_3$, by Gas-Phase Electron Diffraction. *J. Acta Crystallogr.* **1973**, *B29*, 1499-1504.

(83) (a) Rossi, A. R.; Hoffmann, R. Transition Metal Pentacoordination. *Inorg. Chem.* **1975**, *14*, 365-374. (b) Elian, M.; Hoffmann, R. Bonding capabilities of transition metal carbonyl fragments. *Inorg. Chem.* **1975**, *14*, 1058-1076.

(84) Mullins, R.J.; Vedernikov, A.; Viswanathan, R. Competition Experiments as a Means of Evaluating Linear Free Energy Relationships. *J. Chem. Educ.* **2004**, *81*, 1357-1361.

(85) Wiberg, K.B. Substituent Effects on the Acidity of Weak Acids; Calculated Gas Phase Acidities of Substituted Benzoic Acids. *J. Org. Chem.* **2002**, *67*, 4787–4794.

86) Hartwig, J. F.; Shekhar, S. Distinct Electronic Effects on Reductive Eliminations of Symmetrical and Unsymmetrical Bis-Aryl Platinum Complexes. *J. Am. Chem. Soc.* **2004**, *126*, 13016-13027.

(87) Zeigler, B. E.; McMahon, T. B. Computational Analysis of Substituent Effects and Hammett Constants for the Ionization of Gas Phase Acids. *Computational and Theoretical Chemistry* **2013**, *1008*, 46–51.

(88) Burch, M. R. (2010). The HyperTexts. Albert Einstein Poetry. http://www.thehypertexts.com/Albert%20Einstein%20Poet%20Poetry%20Poems%20Pictures%20Bio.htm. (Accessed, September 1st, 2015).

APPENDIX

"RESEARCH," A POEM BY ALBERT EINSTEIN [88]

"I used to go away for weeks in a state of confusion.
Now I think and think for months and years.
Ninety-nine times, the conclusion is false.
The hundredth time I am right.
But I never think of the future—
that comes soon enough.

Learn from yesterday,
live for today,
hope for tomorrow.
The important thing is never
to stop questioning.
Never lose a holy curiosity.

It is a miracle that curiosity
survives formal education
and yet it is the supreme art
of the teacher to awaken joy
in creative expression
and knowledge.

Still, it sometimes seems
that "education" is what remains
after one has forgotten
everything he learned in school,
and the only thing that interferes
with my learning is my education.

But always remember that all that is valuable in human society
depends upon the opportunity for development accorded the individual!

If you are out to describe the truth,
leave elegance to the tailor . . .
and yet
if you can't explain it simply,
you don't understand it.
Still, if we knew what it was we were doing,
it wouldn't be called "*research*,"
would it?"

- Albert Einstein